

University of Warwick institutional repository: <http://go.warwick.ac.uk/wrap>

**A Thesis Submitted for the Degree of PhD at the University of Warwick**

<http://go.warwick.ac.uk/wrap/71413>

This thesis is made available online and is protected by original copyright.

Please scroll down to view the document itself.

Please refer to the repository record for this item for information to help you to cite it. Our policy information is available from the repository home page.

ANISOTROPIC SURFACE WAVES AND INSTABILITIES

UNDER A VERTICAL ELECTROMAGNETIC FORCE

by

I.S. Robinson, M.A.

A Ph.D Thesis submitted to the University of Warwick, 1973.

**BEST COPY**

**AVAILABLE**

Poor text in the original  
thesis.

Some text bound close to  
the spine.

Some images distorted

## ABSTRACT

This thesis describes theoretical and experimental research into the anisotropic waves and instabilities which can be produced at the surface of a conducting fluid, or at the interface between a conducting and non-conducting fluid, when the conductor is subject to a vertical electromagnetic force due to the imposition of a horizontal magnetic field and an electric current.

The basic theory of M.H.D. anisotropic surface waves is expanded to include the effect of surface tension, viscosity, and a two-fluid interface. Polar plots of phase and group velocity and lines of constant phase are presented for sets of experimentally feasible parameters. The nature of the anisotropy is discussed.

The problems of reflection and refraction, the initial impulse problem and the 'ship-wave' and 'fish-line' problems, as applied to anisotropic surface waves, are solved using methods of wave-crest kinematics.

The requirements of a rig to demonstrate the anisotropic waves in the laboratory are discussed. Two different rigs are described. One using mercury produces inconclusive results. The other using electrolyte covered by organic solvents clearly demonstrates the existence of anisotropic waves, giving qualitative agreement with the theoretical predictions.

As background to the theoretical study of the M.H.D. Rayleigh-Taylor instability, the influence of  $\mathbf{j} \times \mathbf{B}$  forces on free surface shapes is examined. Variants of the instability itself are analysed, and it appears that some interesting instability motions may exist. The variation of orientation of the instability with the electromagnetic parameters is determined.

Experiments and experimental techniques to demonstrate some of the predicted instabilities are described. A novel, large amplitude 'bridge' instability is recorded, and excellent agreement with theory is obtained in an orientation experiment.

CONTENTS

LIST OF FIGURES

NOMENCLATURE

ACKNOWLEDGEMENTS

1. INTRODUCTION

1.1. The Nature and Scope of the Research

1.2. The Evolution of the Research

1.3. Layout of Thesis

2. ANISOTROPIC SURFACE WAVES UNDER A VERTICAL  $j \times B$  FORCE

2.1 Introduction to the Problem

2.1.1. Outline of chapter contents

2.1.2. Basic assumptions and approximations made

2.2 Previous Work

2.2.1. General literature

2.2.2. The basic dispersion relation (Shercliff, 1969)

2.2.3. Predicted results

2.3 Adaptation of Theory for Practical Situation

2.3.1. Waves at a two-fluid interface

2.3.2. The effect of surface tension

2.3.3. The effect of viscosity

2.4 Theoretical Predictions

2.4.1. Note about phase and group velocity and lines of constant phase

2.4.2. Computational methods

2.5 Further Basic Considerations of Anisotropic Surface Waves

2.5.1. Discussion on the nature of the anisotropy

2.5.2. The orientation of the anisotropy

3. THE ANISOTROPIC DISPERSION OF SURFACE WAVES APPLIED TO VARIOUS WAVE PHENOMENA

3.1 Basis of the Chapter

3.1.1. Introduction to chapter

3.1.2. Assumptions

- 3.1.3. Brief review of methods of dealing with wave systems
- 3.2 Reflection of Anisotropic Surface Waves
  - 3.2.1. The problem stated
  - 3.2.2. Graphical method
  - 3.2.3. Analytical method
- 3.3 The Initial Value Problem
  - 3.3.1. Analytical solution
  - 3.3.2. Computational results
- 3.4 The Refraction of Anisotropic Surface Waves
  - 3.4.1. The problem stated
  - 3.4.2. The analytical solution
  - 3.4.3. The numerical solution
- 3.5 The Kelvin Ship-Wave Problem
  - 3.5.1. The problem stated
  - 3.5.2. Kelvin's method
  - 3.5.3. Ursell's method
  - 3.5.4. Theoretical M.H.D. ship wave patterns
  - 3.5.5. With surface tension included - the 'fish-line' problem
- 4. EXPERIMENTAL PRODUCTION OF ANISOTROPIC SURFACE WAVES
  - 4.1 The Basic Problem
    - 4.1.1. The nature and scope of the problem
    - 4.1.2. The basic alternative systems
  - 4.2 Preliminary Experiments using Mercury
    - 4.2.1. Introduction
    - 4.2.2. The experimental equipment
    - 4.2.3. Observations and conclusions
  - 4.3 Experimental Rig for use with Electrolytes
    - 4.3.1. The fluids used
    - 4.3.2. The scale of the experiments
    - 4.3.3. The magnet

- 4.3.4. The electric current supply
- 4.3.5. The wave tanks
- 4.3.6. Wave generation equipment
- 4.3.7. Wave observation
- 4.4. Point Source Experiments
- 4.5. Line Source Experiments
- 4.6. Experiments to show up other Anisotropic Surface Wave Phenomena
  - 4.6.1. Introduction
  - 4.6.2. Refraction experiments
  - 4.6.3. Reflection experiments

5. VARIATIONS OF THE M.H.D. RAYLEIGH-TAYLOR INSTABILITY

- 5.1. Basis of Chapter
  - 5.1.1. Introduction
  - 5.1.2. Other work on the M.H.D. Rayleigh-Taylor instability
  - 5.1.3. The irrotationality condition
- 5.2. The  $\mathbf{j} \times \mathbf{B}$  Force and the Shape of a Fluid Surface
  - 5.2.1. The need to consider the problem
  - 5.2.2. The effect of conservative  $\mathbf{j} \times \mathbf{B}$  force upon surface shape
  - 5.2.3. The effect of rotational  $\mathbf{j} \times \mathbf{B}$  forces
  - 5.2.4. The effect of a disturbed surface on the  $\mathbf{j} \times \mathbf{B}$  configuration
  - 5.2.5. The effect of surface tension in the presence of  $\mathbf{j} \times \mathbf{B}$  forces
- 5.3. Variations of the M.H.D. Rayleigh-Taylor Instability
  - 5.3.1. Solving the basic configuration
  - 5.3.2. Variation of current density in the current direction
  - 5.3.3. Variation of current density in the vertical direction
  - 5.3.4. Variation of magnetic field in the vertical direction
  - 5.3.5. Variations of electric field with time
- 5.4. The Effect of Varying the Orientations of  $\mathbf{E}$  and  $\mathbf{B}$

6. EXPERIMENTAL WORK RELATING TO THE M.H.D. RAYLEIGH-TAYLOR INSTABILITY

6.1 Introduction

6.2 General Experimental Considerations

6.2.1. Choice of working fluid

6.2.2. Magnetic field

6.2.3. Containing vessels and scale of experiments

6.2.4. Current supply

6.2.5. Depth probes

6.3 The Effect of Teepol on the Surface Tension

6.4 Experiments to investigate the Rayleigh-Taylor Instability  
when  $\frac{\partial \rho}{\partial x} \neq 0$

6.4.1. Small amplitude

6.4.2. Large amplitude motion

6.5 The effect of B Varying with Height

6.6 The dependence of Instability mode Orientation with the  
Relative Orientation of Magnetic Field and Current Density

7. CONCLUSIONS AND SUGGESTIONS FOR FURTHER WORK

8. REFERENCES

APPENDIX

Listings of Computer Programmes used.

LIST OF FIGURES

- 2.1 Notation of wave analysis
- 2.2 Shercliff's dispersion plots
- 2.3 Construction for constant phase lines
- 2.4 Dispersion plots (Mercury)
- 2.5 Dispersion plots (two-fluid interface with Teepol)
- 2.6 Dispersion plots (two-fluid interface without Teepol)
- 2.7 Long wave dispersion plots
- 2.8 Wavenumber, frequency relationships
- 2.9 Anisotropy ratio-frequency dependence
- 2.10 Phase-velocity, wavenumber relationship
- 2.11 Notation for Section 2.5.2.
- 2.12 Variation of orientation of anisotropy with  $\beta$
- 2.13 To illustrate the resolving effect of the wave on  $j$  and  $B$
  
- 3.1 Reflection construction - anisotropic waves
- 3.2 Reflection construction - isotropic waves
- 3.3 Reflection function  $F v n$ ,  $0 - 90^\circ$
- 3.4 Typical reflection characteristic, from fig. 3.3.
- 3.5  $F v n$ ,  $0 - 180^\circ$
- 3.6 To illustrate the meaning of  $n > 90^\circ$
- 3.7 Notation for analytical solution of reflection problem
- 3.8 Computed reflection characteristics
- 3.9 Wave reflection pattern when  $r > 90^\circ$
- 3.10 Wave pattern after initial disturbance - ignoring surface tension
- 3.11 Computed constant phase lines after initial disturbance - mercury
- 3.12 Detail of fig. 3.11 (c)
- 3.13 Layout of a typical situation where refraction could occur

- 3.14 Notation for refraction problem
- 3.15 Notation of numerical solution, line source
- 3.16 Computed plots of group rays, line source, linear variation of  $\chi$
- 3.17 Computed plots of group rays, line source, quadratic variation of  $\chi$
- 3.18 Computed plots of group rays, point source
- 3.19 Lamb's typical ship wave pattern
- 3.20 Notation for Lamb's method
- 3.21 Notation for Ursell's method
- 3.22 To illustrate method of plotting lines of constant phase
- 3.23 Typical M.H.D. anisotropic ship wave patterns,  $\alpha = 0, 90^\circ$
- 3.24 Typical M.H.D. anisotropic ship wave patterns,  $\alpha = -15^\circ, +15^\circ, 30^\circ, 45^\circ, 60^\circ, 75^\circ$ ,
- 3.25 Total anisotropic ship-wave pattern to be expected.
- 3.26 Computed wave crest patterns for the fish-line problem
  
- 4.1 Photograph - Tank for mercury experiments
- 4.2 Photograph - General view of equipment for mercury experiments
- 4.3 Optical path for wave observation in mercury experiments
- 4.4 Photograph - Typical wave pattern observed in mercury experiments
- 4.5 Photograph - General view of ancillary equipment
- 4.6 Photograph - View of Helmholtz Coil magnet
- 4.7 Magnet conductor section
- 4.8 Photograph - Flow monitor
- 4.9 Magnet protection electrical circuits
- 4.10 Magnet calibration curve
- 4.11 Axial field plot
- 4.12 Transverse field plot
- 4.13 Stray field round the magnet
- 4.14 Photograph - Main wave tank

- 4.15 Sketch of details of large tank
- 4.16 Photograph - Large tank in position
- 4.17 Photograph - Smaller tank
- 4.18 Photograph - Overall view of equipment
- 4.19 Photograph - Plungers used to produce waves
- 4.20 Expected flow produced by disturbed surface
- 4.21 Photographs - Anisotropic waves from a point source
- 4.22 Photographs - Waves from a line source
- 4.23 Anisotropy ratio plotted against the parameter  $\frac{jB}{\Delta\rho g}$
- 4.24 Photographs - Waves from a line source, different orientations
- 4.25 Wavelength ratio plotted against orientation
- 4.26 Sketch of false floor for wave refraction experiment
- 4.27 Photographs - Wave refraction
- 4.28 Photograph - attempted wave reflection
  
- 5.1 General notation for m.h.d. Rayleigh Taylor problem
- 5.2 The effect of inclined B upon surface inclination, notation
- 5.3 Variation of surface inclination with magnetic field inclination
- 5.4 Plane of instability when heavier fluid is lifted above lighter fluid by  $\underline{j} \times \underline{B}$  force
- 5.5 Comparison of menisci for different  $\underline{j} \times \underline{B}$  forces
- 5.6 Comparison of menisci for different liquids
- 5.7 Typical tank configuration for  $\frac{\partial j}{\partial x} \neq 0$
- 5.8 Predicted surface profile for  $\frac{\partial j}{\partial x} \neq 0$
- 5.9 Mathieu function stability diagram
- 5.10  $jB_{\min}$  to produce instability for a given  $\beta$
  
- 6.1 Photograph - General view of instability measuring rig
- 6.2 Calibration of capacitive probe

- 6.3 Photograph - depth probes
- 6.4 Circuit for resistance probes
- 6.5 Typical calibration curve for resistance probe
- 6.6 Circuit for T-probe
- 6.7 Photographs - Effect of Teepol on meniscus
- 6.8 Surface profiles plotted using resistance probe
- 6.9 Photograph -  $\frac{\partial j}{\partial x} \neq 0$  instability in large tank
- 6.10 Photographs - Sequence to show 'bridge' instability
- 6.11 Photographs - Interfacial instability when  $\frac{\partial B}{\partial z} \neq 0$
- 6.12 Photographs - Effect of magnetic field alone on fluids of different  $\mu$
- 6.13 Photographs - Typical photographs from orientation experiment
- 6.14 Plotted results of orientation experiment.

TABLES

- 4.1 Relative magnitude of terms in dispersion equation (2.34) involving viscosity.

NOMENCLATURE

Other symbols used occasionally will be defined as used.

<u>B</u>	Magnetic field strength
c	Phase velocity of waves
C	Group velocity of waves
g	acceleration due to gravity
h	depth of fluid
<u>i</u>	unit vector in the vertically upwards direction
i, j	Variables defining <sup>points</sup> in the numerical solutions of § 3.4
<u>i</u>	Electric current density
<u>k, k</u>	Wavenumber, wavenumber vector
M	$\frac{\mu_2 - \mu_1}{\rho_2 - \rho_1}$ - a type of dynamical viscosity term
n	Instability time constant or frequency (chapter 5)
n	Co-ordinate axis normal to a given surface
p	Pressure in fluid
p	Point in a numerical solution
P	Stress (normal and shear)
s	Co-ordinate axis lying along a given surface
t	Time
u, U	Speed of travelling disturbance
<u>v</u>	Fluid velocity
X	Dummy variable in computations for shallow fluids
x, y	Horizontal co-ordinate axes
z	Vertical co-ordinate axis
$\alpha, \bar{\alpha}$	Surface tension
$\alpha$	Angle between 'mirror' and <u>B</u> direction in § 3.2
$\alpha$	Angle between 'ship' direction and <u>B</u> in § 3.5

$\beta$	Angle between $\underline{j}$ and $\underline{B}$ if not assumed as $90^\circ$
$\beta$	Angle used in ship wave solution, for § 3.5.2 see fig(3.20), for § 3.5.3 and 3.5.5. see fig(3.21)
$\Delta$	The difference in the value of a parameter across an interface.
$\delta$	Dirac's delta function
$\epsilon$	A small quantity
$\eta, z_0$	Surface or interface level
$\theta$	Angle between $\underline{k}$ and $\underline{B}$
$\theta$	Angle $\underline{B}$ makes with horizontal in § 5.2.2
$\lambda$	Wavelength
$\mu$	Viscosity
$\mu$	Magnetic Permeability in § 5.3.4
$\nu$	Kinematic viscosity
$\nu_M$	$\frac{\mu_1 + \mu_2}{\rho_1 + \rho_2}$ - a type of kinematic viscosity term
$\rho$	Density of fluid
$\Sigma$	Summation symbol
$\sigma$	Frequency
$\sigma$	Fluid conductivity in § 5.2.4
$\phi$	Velocity potential in the wave solution
$\phi$	Phase function (chapter 3)
$\phi$	Surface angle to the horizontal in § 5.2.2
$\phi$	$\tan^{-1} \frac{C}{C_k}$ in § 2.4.2
$\chi$	" in § 3.5
$\psi$	Part of velocity 'potential' term in viscous waves solution
$\underline{\omega}$	Vorticity
$\omega$	Frequency

Subscripts :-

- $i, j$  denote co-ordinate directions in vector differential expressions
- $k$  denotes wavenumber direction
- $n$  denotes normal to wave crest (ch 2)
- $n$  denotes normal to surface (ch 5)
- $p, q$  denote directions parallel and normal to the 'mirror' respectively in § 3.2
- $s$  denotes along wave crest (ch 2)
- $s$  denotes in plane of surface (ch 5)
- $\alpha$  denotes all relevant co-ordinate directions in summation terms
- $\theta$  normal to wavenumber direction
- $0$  indicates value of parameter at surface or interface
- $1$  denotes  $\underline{j}$  direction in § 3.4
- $2$  denotes  $\underline{B}$  direction in § 3.4
- $1$  value of parameter in upper (non-conducting) fluid
- $2$  value of parameter in lower (conducting) fluid

ACKNOWLEDGEMENTS

I wish to express my thanks to all those who have contributed to the development of the work described here, and towards the production of the thesis itself.

In particular I must thank Professor J.A. Shercliff, my supervisor, who first suggested the subject of M.H.D. anisotropic surface waves as a topic for research, and who has guided and encouraged me throughout. Thanks are also due to Dr. C.J. Alty for help with practical arrangements in the laboratory.

Mr. P. Worsnop of U.K.A.E.A., Culham, supervised the design and construction of the Helmholtz Coils described in Chapter 4.

Various members of the workshop staff in the Warwick University engineering department helped to build the equipment described in the thesis. However, in this respect I owe the biggest debt of gratitude to Mr. Alf. Webb who not only helped to make the equipment work smoothly through his skill and effort but also encouraged me to persevere with the experimental work until success was achieved. The cheerful assistance of Mr. Colin Major in developing the equipment, and of Mr. Alec Ross must also be acknowledged.

I thank Mr. Colin Lovatt for help in processing the photographic records of wave patterns. Thanks must also go to Miss E. Peatman who willingly and patiently typed this thesis.

The work was carried out whilst I was on a research studentship from the Science Research Council, whom I thank for financial support.

Finally, I want to thank my wife, who helped in drawing diagrams and other editorial work on the thesis, for her patient encouragement and support throughout all this work.

## 1. INTRODUCTION

### 1.1. The Nature and Scope of the Research

Problems in magnetohydrodynamics (M.H.D.) can be loosely divided into three types; those of kinematic M.H.D. where the motion of a conducting fluid which influences the electromagnetic parameters is given ab initio, and essentially the solution is merely an exercise in electromagnetic field theory; those where the problem is basically one of fluid mechanics, with the Lorentz ( $\underline{j} \times \underline{B}$ ) force, imposed and invariant from the start, acting as one more (albeit possibly rotational) force acting on the fluid along with pressure gradients, gravity etc.; and those which exhibit a true M.H.D. coupling where the fluid mechanical and electromagnetic equations are interrelated and cannot be solved independently. The research presented in this thesis is basically to do with problems of the second type, although in fact the phenomena described could not occur were it not for a particular mechanism whereby the fluid mechanical parameters feed back to influence the electromagnetic ones.

The subject is the study of the waves, instability, and the stationary profile of the surface, or interface with an insulating liquid, of a conducting fluid which is subject to an imposed magnetic field and carries an imposed electric current, such that the resultant  $\underline{j} \times \underline{B}$  force is irrotational. To the extent that current and field are both imposed, the problem is of the second category, but the particular coupling effect referred to above is that the current always tends to "fill" the conducting fluid, and so at the surface of the fluid it is always to be found parallel to the surface.

In this way the fluid motion, or more strictly the motion of the liquid surface, is able to influence the electromagnetic forces, and the result is strong anisotropy in the wave dispersion and instabilities.

The basic phenomenon of anisotropy in the above circumstances has already been reported by Shercliff (1969) in the case of waves, and in instabilities by Lemaire (1963) and others. The original theoretical work in this thesis has been to examine some of the implications which this anisotropy has beyond the simplest cases already solved. Thus a number of classical surface wave phenomena have been applied to the case of anisotropic surface waves, with interesting results. In the stability problem an attempt has been made to study the effect of small variations in the configuration of electromagnetic parameters upon the instability motions, with the result that novel instability modes have been discovered.

The experimental work has been to demonstrate the anisotropy, which has not been done before, to show its influence on other wave phenomena, and to discover what effect it has on various configurations of instability.

#### 1.2. The Evolution of the Research

The whole of the work reported here grew out of an initial attempt to demonstrate experimentally the existence of anisotropic surface waves. It soon became apparent that further theoretical work needed to be done to predict accurately the practical possibilities. It was at an early stage, too, that an unintended instability in the mercury experiments focussed attention upon the stability question.

Most of the work has as its goal the academic aim to inquire, learn and verify; it is not related very closely to current technological needs, but since M.H.D. is a relatively new, and still largely uncharted subject, it was thought well worthwhile to explore this corner of it relating to free surfaces and interfaces under imposed  $\underline{j} \times \underline{B}$  forces. As far as is known, the phenomena under investigation do not occur naturally in the universe.

In the instability work in particular, although the results are presented in a logical sequence, it would be false to pretend that the particular problems dealt with were in practice posed, solved, and experimentally verified, in that order. Rather, only when the instability mechanisms were better understood through a combination of theoretical study and experimental work, and the answers effectively obtained, could the questions be posed in the way set out in chapter 5. Thus the overall philosophy with which the research was approached was one of going step by step, asking questions and finding answers as the understanding grew, rather than starting with the research mapped out from the beginning. The interplay between experimental and theoretical work has fostered this approach, which is somewhat unusual in M.H.D., a subject in which it is not often easy to match experimental and theoretical progress and let each influence the other.

One practical aim which does lie behind the wave experiments, although not developed as yet, is that of using the anisotropic surface wave system as a visual demonstration, even a teaching aid,

for the general study of anisotropic waves in physics. It was this aim which prompted the theoretical study of the application of the anisotropic dispersion relation to classical surface wave problems, since these could be the very things used to visually demonstrate the sometimes unexpected properties of anisotropic waves.

Finally, it is worth recording that a ten month delay in the delivery of the central piece of equipment, the large Helmholtz coil magnet system, has seriously limited the progress in experimentally demonstrating all the wave phenomena it was hoped to show.

### 1.3. Layout of Thesis

The thesis is in two broad sections, chapters 2, 3 and 4 on anisotropic surface waves, and chapters 5 and 6 on the M.H.D. Rayleigh-Taylor instability and related problems.

Chapter 2 is a detailed study of the basic anisotropic wave problem, as a preliminary to the experiments, and so contains some of the work already done by Shercliff, as a basis, but the rest is original, computing and plotting theoretical dispersions involving surface tension, the solution involving viscosity, and discussion on the nature of the anisotropy.

Chapter 3 moves on to deal in more general terms with the application of the anisotropic dispersion to classical wave problems, and is more an exercise in kinematic wave theory than M.H.D.

There is a review of methods of wave kinematics developed by others, and then these methods are applied successively to

(a) the reflection of anisotropic surface waves,

(b) the initial value problem applied to anisotropic surface waves

i.e. the pattern of waves to be found a given time after an instantaneous point impulse or point surface displacement,

(c) the refraction of waves due to  $\underline{j}$  varying in a plane normal to  $\underline{B}$ , and

(d) the problem of finding the pattern of waves when a disturbance moves steadily across the surface - the "ship wave" problem, or when account is taken of surface tension, the "fish line" problem.

Chapter 4 describes the experimental work to demonstrate the existence of anisotropic surface waves, and to show some of the phenomena of chapter 3. This covers the consideration of possible experimental approaches and choice of suitable parameters, the design and operation of equipment, and the results obtained.

Chapter 5 covers the theoretical aspects of the work on the Rayleigh-Taylor instability, with a section on the effect of  $\underline{j} \times \underline{B}$  forces on the shape of stable liquid surfaces, a brief resumé of the simple M.H.D. instability case already solved, and then investigation into the effect on the instability of varying  $\underline{j}$  and  $\underline{B}$  whilst still maintaining irrotationality.

In chapter 6, the experimental work on instabilities is detailed, including a description of the equipment, the development of surface-height sensing probes, and a novel large-amplitude instability which was discovered, as well as attempting to verify the phenomena predicted in chapter 5.

Finally, brief conclusions are drawn in chapter 7, along with suggestions for further work.

Where possible figures are bound next to the relevant pages of script. Some information, not considered relevant to the main text, is relegated to the appendices, notably specification of

computer programmes ;

which are simply copied out. Since the programmes were merely used as tools to solve lengthy equations, both directly and numerically, and to plot out results, no attempt has been made to describe their operation except the numerical plotting of group rays in chapter 3, since computing at this level cannot be considered an end in itself, but merely a means of solving problems it would be otherwise time consuming to solve by hand.

## 2. ANISOTROPIC SURFACE WAVES UNDER A VERTICAL $j \times B$ FORCE

### 2.1. Introduction to the Problem

#### 2.1.1. Outline of chapter contents

In this chapter, the basic theory of anisotropic surface waves in a conducting liquid is examined. When a horizontal magnetic field and horizontal electric current are imposed on an electrically conducting liquid, producing a vertical electromagnetic force, waves on the surface of the fluid, which must be excited by external means, propagate at different speeds in different directions. The foundation of this theory is the work of Shercliff (1969), the salient features of which are outlined for completeness in 2.2. since they form the basis of the rest of the original work relating to the anisotropic surface waves.

In 2.3 the analysis has been extended to cope more realistically with experimental conditions. Theoretical predictions are obtained from a dispersion relation for waves at the interface between two liquids, with surface tension taken fully into account and an attempt has been made to analyse the effect of viscosity in both liquids.

In 2.4 the computational solution is described and polar plots of phase and group velocity and lines of constant phase are presented, along with a discussion of their implications.

In 2.5 the fundamental nature of the anisotropic effect is discussed, in an attempt to isolate the true M.H.D. aspect of the phenomenon. Finally, the effect is considered of varying the angle between the imposed magnetic field and electric current directions, for the practically possible case involving surface tension.

The aim of the work in this chapter has been to take the theoretical base of Shercliff, and modify and present it in a form relevant to the problem of producing anisotropic waves experimentally.

### 2.1.2. Basic assumptions and approximations made

These are the same as those made in Shercliff (1969).

Small amplitude waves are considered in every case so that only the linear terms of the hydrodynamic perturbation equations are necessary.

The magnetic field is imposed horizontally and is supposed steady and uniform throughout and the electric current due to an applied D.C. electric field is assumed to be horizontal and of uniform density throughout the conducting fluid in the undisturbed state. Thus the liquid surface is normally at rest horizontally under gravity and vertical irrotational  $\underline{j} \times \underline{B}$  forces.

The magnetic induction due to the imposed currents is assumed negligible compared with the applied field, and induced currents due to wave motion in the presence of the magnetic field are also neglected. These assumptions will be justified later in chapter 4.

In general when the surface is disturbed vertically the distortion of the current density field will give rise to rotational  $\underline{j} \times \underline{B}$  forces but we shall assume the waves to be of small enough amplitude for this to be ignored.

## 2.2. Previous Work

### 2.2.1. General Literature

Melcher (1963) gives a fairly comprehensive description of field coupled M.H.D. surface waves which in some cases are anisotropic but those are a different phenomenon from the one under consideration here, being for cases where the electric and magnetic fields are not effectively independent, and are an integral part of the wave propagating mechanism.

There is an extensive literature about ordinary hydrodynamic surface waves e.g. Lamb (1932), Stoker (1957).

2.2.2. The basic dispersion relation (Shercliff. 1969)

Using the notation of Fig. 2.1. we consider a plane wave train of frequency  $\omega$  with normal in the  $n$  direction, troughs and crests in the  $s$  direction.  $j_s$ , the component of imposed current in the  $s$  direction will not be perturbed by the waves whereas  $j_n$  is perturbed in the  $z, n$  plane, and in fact in this plane, the current at the surface follows the surface profile. Thus it follows that  $\text{curl}(\underline{j} \times \underline{B})$ , ( $= (\underline{B} \cdot \text{grad}) \underline{j}$  since  $\text{div} \underline{j} = 0$  and  $\underline{B}$  is uniform) has zero  $s$  component. Now the linearized perturbation equation of motion is:-

$$\rho \frac{\partial \underline{v}}{\partial t} + \text{grad } p = \underline{j} \times \underline{B} - \rho g \underline{i} \quad \dots 2.1$$

neglecting viscosity, with all variables harmonic functions of time  $\underline{i}$  is a unit vector in the  $+z$  direction.

Taking the curl of (2.1) gives

$$\rho \frac{\partial \underline{\omega}}{\partial t} = \text{curl } \underline{j} \times \underline{B} \quad \text{which has no } s \text{ component, and so}$$

$$\frac{\partial \omega_s}{\partial t} = 0 \text{ which requires } \omega_s = 0 \text{ if } \omega_s \text{ is a harmonic function of time.}$$

Therefore it is possible to define a velocity potential

$\phi(z, n, t)$  for the irrotational flow in the  $z, n$  plane.

Now  $\underline{j} \times \underline{B}$  in (2.1) may be expressed as  $-j_s B_n \underline{i} + \underline{j}' \times \underline{B}_s + \underline{j}' \times \underline{B}_n$

where  $\underline{j}'$  is the current vector in the  $z, n$  plane.  $\underline{j}' \times \underline{B}_n$  acting horizontally may be neglected as small in this small amplitude approximation, whilst it should be noted that  $\underline{j}' \times \underline{B}_s$  will be in the  $z, n$  plane, and at the surface will always be normal to the surface.

Thus (2.1) may be expressed as :-

$$\text{grad} \left( \rho \frac{\partial \phi}{\partial t} + p + (\rho g + j_s B_n) z \right) = \underline{j}' \times \underline{B}_s \quad \dots 2.2$$

If this is integrated along the surface  $z = z_0$ ,  $\underline{j}' \times \underline{B}_s$

contributes nothing, and if the ambient pressure above the surface

be taken as zero:-  $\rho \frac{\partial \phi}{\partial t} + p + (\rho g + j_s B_n) z_0 = F(t) = 0$



with  $Z_0 = \sum e^{i(\omega t - kn)}$  and hence all the variables are harmonic functions of  $n$ .

For surface tension  $\alpha$ , at the surface,  $p = -\alpha \frac{\partial^2 Z_0}{\partial n^2} = k^2 \alpha Z_0$  to a first approximation.

Hence, at  $z = 0$  (applying the classic linearization process such that all variables are the same at  $z = 0$  as at  $z = z_0$ )

$$\rho \frac{\partial \phi}{\partial t} + (k^2 \alpha + \rho g + j_s B_n) Z_0 = 0 \quad \dots 2.3$$

(2.3) is effectively the boundary condition on pressure at the surface.

The motion of the fluid as a whole is defined also by the two-dimensional Laplacian  $\nabla^2 \phi = 0$ , ....2.4

since we assume incompressibility, and by the boundary conditions:-

$$v_z = \frac{\partial \phi}{\partial z} = \frac{\partial z_0}{\partial t} \quad \text{at } z = 0 \quad \dots 2.5$$

and  $\frac{\partial \phi}{\partial z} = 0$  at  $z = -h$  ....2.6

in a bounded fluid of depth  $h$ .

(2.4), (2.5) and (2.6) require a form:-

$$\phi = \left( \frac{i\omega \xi}{k} \right) e^{i(\omega t - kn)} \left\{ \sinh kz + \coth kh \cosh kz \right\} \quad \dots 2.7$$

For (2.3) also to be satisfied, a constraint relating  $\omega$  and  $k$  is required, and this is the dispersion relation.

Substituting (2.7) in (2.3) gives :-

$$\rho \omega^2 = k \tanh kh (k^2 \alpha + \rho g + j_s B_n) \quad \dots 2.8$$

N.B. A somewhat different approach to solving for the dispersion relation may be found in chapter 5 where the stability equation is effectively the same as the dispersion relation.

Thus it can be clearly seen that of the field and current components, only  $j_s$  and  $B_n$  affect the dispersion relation. This

produces anisotropy of wave propagation, since the magnitude of  $j_s B_n$  varies with the orientation of the wave number direction  $\hat{k}$  relative to the imposed  $\underline{j}$  and  $\underline{B}$  fields, and given that  $\omega$  is fixed there is directional variation of  $|\underline{k}|$

### 2.2.3. Predicted results

Shercliff went on to evaluate the sort of results to be expected from the dispersion relation (2.8) in both the case of "surface" waves on a deep fluid, where the wavelength is short compared with the depth; and "long" waves in shallow fluid, where the depth is small compared with the wavelength, and vertical accelerations can be ignored; i.e.  $\tanh kh = 1$ , and  $\tanh kh = kh$  respectively.

Taking  $\gamma = \frac{jB}{\rho g}$  as a dimensionless parameter indicating the relative strengths of  $\underline{j} \times \underline{B}$  and gravity forces, and ignoring surface tension to simplify the calculations; and considering the case where  $\underline{j}$  and  $\underline{B}$  are imposed mutually at right angles, to produce  $\underline{j} \times \underline{B}$  upwards, equ. (2.8) reduces to:-

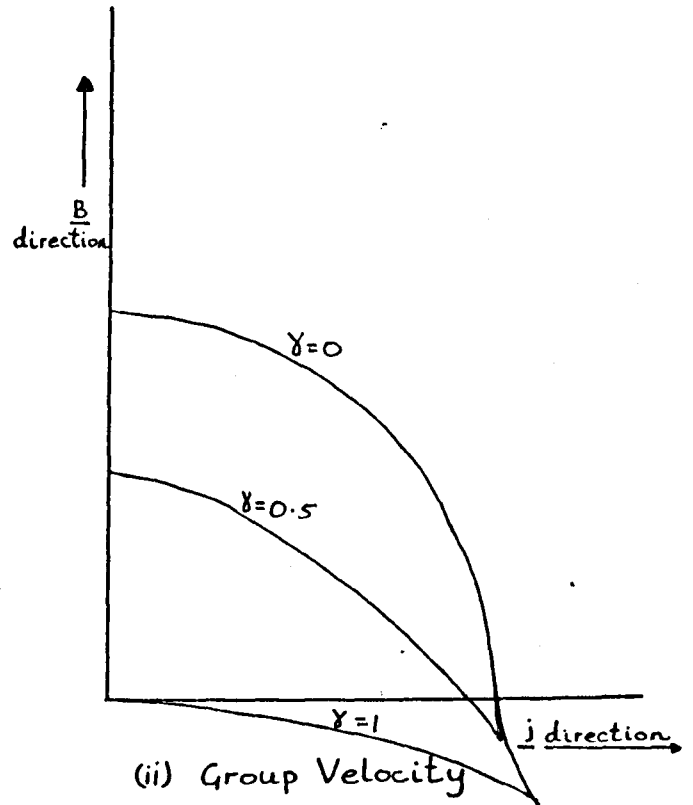
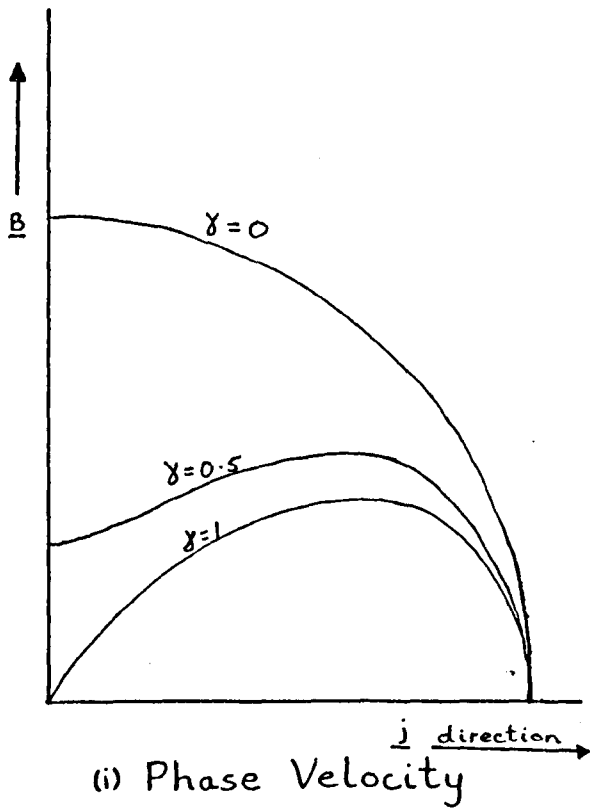
$$\omega^2 = gk (1 - \gamma \cos^2 \theta) \quad \text{for surface waves and} \quad \dots 2.9a$$

$$\omega^2 = k^2 hg (1 - \gamma \cos^2 \theta) \quad \text{for long waves,} \quad \dots 2.9b$$

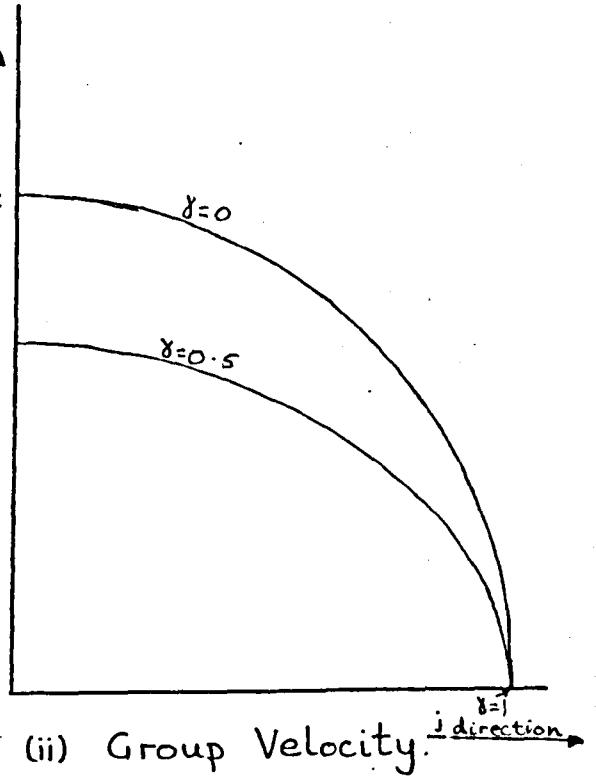
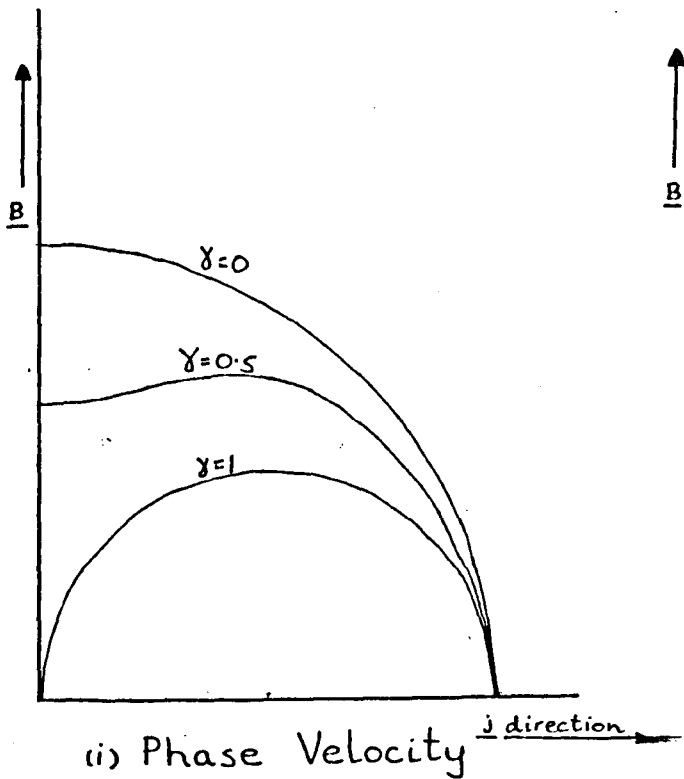
where  $\theta$  is the angle between the  $\underline{k}$  and  $\underline{B}$  directions.

This configuration of imposed fields produces the greatest degree of anisotropy, although there is a stability limit of  $\gamma < 1$  if the net force on the fluid is not to be upwards, causing the Rayleigh-Taylor instability to occur.

Shercliff presented the anisotropy visually in polar plots of phase and group velocity, (see 2.4.1. and 3.1.3.) and these are shown in fig. (2.2), adjusted to suit the particular case of the configuration of imposed fields stated above. Only one quadrant



a) surface waves



b) long waves

FIG.2.2. SHERCLIFF'S DISPERSION PLOTS

(To show shape only - not to a particular scale.)

is drawn, and the complete picture is obtained by reflection in both axes. The salient features to note as characteristic of the dispersion are that waves propagating in the  $j$  direction are unaffected by the  $j \times B$  force, whilst those in the  $B$  direction are most affected, to the degree that when  $\gamma = +1$  the waves will not propagate at all. For waves in other directions, the effect is somewhere between the two extremes, and of great interest is the fact that the phase and group velocity are not in the same direction.

Lines of constant phase due to a continuously oscillating point source, i.e. the trough and crest pattern which would be observed in an experimental situation, are identical in shape to the polar plot of group velocity for the dispersion relations specified by eq. (2.9). \*

## 2.3 Adaptation of Theory for Practical Situation

### 2.3.1. Waves at a two fluid interface

Now the first aim of this project was to demonstrate experimentally that the anisotropy of M.H.D. surface waves exists at all, and to do this I had to determine how to show up the anisotropy to best advantage. From some of the practical considerations to be found in chapter 4, it became clear that probably the best way to obtain suitable waves was at the interface between two liquids of very similar densities, one electrically conducting, the other not. Using these, the gravity force influencing the waves could be reduced by an order of magnitude, making it practically possible for the  $j \times B$  force to "compete" with the gravity force.

In this case, the dispersion relation is obtained assuming the anisotropic effect of  $j \times B$  as discussed above, simply adding the  $j B \cos^2 \theta$  term where appropriate to Lamb's analysis (Lamb 1932 Art. 2.31) and it is supposed therefore that  $j$  and  $B$

\* N.B. The plane wave dispersion relation 2.9. is valid for waves from a point source only when the radius of curvature of the wave crest is large compared with the wavelength.

are applied mutually at right angles and that  $\underline{j} \times \underline{B}$  acts upwards, and  $\theta$  is then the angle between the wave direction and the magnetic field.

If subscript (1) denotes the upper non conducting fluid, and (2) denotes the lower conducting fluid, the analysis is as follows:-

$$\left. \begin{array}{l} \text{In the upper fluid, } \nabla^2 \phi_1 = 0 \\ \text{In the lower fluid, } \nabla^2 \phi_2 = 0 \end{array} \right\} \begin{array}{l} \text{In a vertical plane containing} \\ \text{the wave number vector} \end{array} \quad \dots 2.10$$

$\phi$  being a two dimensional velocity potential, as we saw in Shercliff's analysis.

The equation of motion is:-

$$\text{grad} \left( \rho_1 \frac{\partial \phi}{\partial t} + p_1 + \rho_1 g z \right) = 0 \quad \dots 2.11a$$

$$\text{grad} \left( \rho_2 \frac{\partial \phi}{\partial t} + p_2 + [\rho_2 g - j B \omega^2 \theta] z \right) = \underline{j} \times \underline{B}_s \quad \dots 2.11b$$

At the interface,  $\underline{j} \times \underline{B}$  is always normal, so integrating (2.11b) along the interface  $z = z_0$  gives :-

$$\rho_2 \left( \frac{\partial \phi}{\partial t} \right)_{z=z_0} + p_2 + (\rho_2 g - j B \cos^2 \theta) z_0 = 0 \quad \dots 2.12$$

$$\text{and (2.11a) gives } \rho_1 \left( \frac{\partial \phi}{\partial t} \right)_{z=z_0} + p_1 + \rho_1 g z_0 = 0 \quad \dots 2.13$$

Now the interfacial condition on pressure at  $z = 0$  is:-

$$p_2 = p_1 - \alpha \frac{\partial^2 z_0}{\partial n^2} \quad \dots 2.14$$

∴ from (2.12), (2.13) and (2.14)

$$\rho_2 \left( \frac{\partial \phi}{\partial t} \right)_{z=z_0} + (\rho_2 g - j B \cos^2 \theta) z_0 = \rho_1 \left( \frac{\partial \phi}{\partial t} \right)_{z=z_0} + \rho_1 g z_0 + \alpha \frac{\partial^2 z_0}{\partial n^2} \dots 2.15$$

$$\text{But } \left( \frac{\partial \phi}{\partial z} \right)_{z=z_0} = \left( \frac{\partial \phi}{\partial z} \right)_{z=z_0} = \frac{\partial z_0}{\partial t} \quad \dots 2.16$$

$$\text{Now if the interface } z_0 = \xi e^{i(\omega t - k \cdot n)} \quad \dots 2.17$$

(2.10) can be solved using (2.16) and (2.17), with the boundary conditions  $\frac{\partial \phi_1}{\partial z} = 0$  at  $z = +h_1$  and  $\frac{\partial \phi_2}{\partial z} = 0$  at  $z = -h_2$  for fluids of depth  $h_1$  and  $h_2$ .

$$\text{Thus } \phi_1 = \frac{i\omega\epsilon}{k} e^{i(\omega t - \underline{k} \cdot \underline{n})} \left\{ \sinh kz - \coth kh_1 \cosh kz_1 \right\}$$

$$\phi_2 = \frac{i\omega\epsilon}{k} e^{i(\omega t - \underline{k} \cdot \underline{n})} \left\{ \sinh kz + \coth kh_2 \cosh kz_2 \right\} \quad \dots 2.18$$

For (2.18) to be compatible with the boundary condition on pressure, (2.15), the constraint necessary is the dispersion relation  $\omega = f(k)$  obtained by substituting (2.18) in (2.15) and assuming that  $\left( \frac{\partial \phi}{\partial t} \right)_{z=z_0} = \left( \frac{\partial \phi}{\partial t} \right)_{z=0}$

Hence:-

$$(\rho_1 \coth kh_1 + \rho_2 \coth kh_2) \omega^2 = k \left\{ (\rho_2 - \rho_1)g - jB \cos^2 \theta + \alpha k^2 \right\} \quad \dots 2.19$$

From this it can be seen that the two fluid case is essentially the same as that of the surface waves on a single fluid in contact with vacuum or gas, since had we introduced  $\underline{j} \times \underline{B}$  acting downwards in the upper field, with the lower fluid non-conducting, the dispersion relation would have been identical (showing that the anisotropy term  $j B \cos^2 \theta$  is independent of the actual fluid parameters used).

The final choice of experimental parameters is discussed in chapter 4, but it is worth noting here that the degree of anisotropy obtainable will depend upon the right hand side of (2.19), in particular the ratio :-

$$\left\{ (\rho_2 - \rho_1)g + \alpha k^2 - jB \right\} : \left\{ (\rho_2 - \rho_1)g + \alpha k^2 \right\}$$

Comparing this with the single fluid case it can be seen that if  $(\rho_2 - \rho_1)$  is made very small,  $j B$  can compete with it all the more easily, though of course  $j B$  must not exceed  $(\rho_2 - \rho_1)g$  or else the Rayleigh-Taylor instability occurs. Whereas in the single fluid case negative  $j B$  (i.e. downward acting  $\underline{j} \times \underline{B}$ ) produced anisotropy an order of magnitude less severe than for the

upward force, here, if  $(\rho_2 - \rho_1)g$  is an order of magnitude less than  $j B$ , as is possible by almost equalising the two densities, then a large degree of anisotropy is obtainable with a downward  $j \times B$  too, with no problem of instability. Certainly the possibility of varying the magnitude of the term  $(\rho_2 - \rho_1)$  offers more scope for obtaining suitable experimental parameters.

### 2.3.2. The effect of surface tension

Shercliff, to show up the basic phenomenon to best advantage, and for ease of manipulation chose to ignore surface tension effects in plotting the sort of shapes of wave pattern to be expected (fig. 2.2). Whilst this is justified for that reason, it is misleading when approaching the problem of actually generating such shapes in practice. One might initially assume that given a large enough space dimension, waves of sufficiently long wavelengths could be produced for surface tension effects to be of no practical significance. However in the extreme cases of anisotropy the theory predicts zero or nearly zero wavelength in the directions where the  $j \times B$  force has most effect. So that however long the usual wavelength of the system is, there would always be present some wavelength short enough to be affected by surface tension. However small surface tension is, the more severe anisotropy could not be achieved in practice for this reason.

Looking at eq. (2.19), it is the size of the  $\alpha k^2$  term compared with  $(\rho_2 - \rho_1)g - jB \cos^2 \theta$  which determines the extent to which surface tension is important, but of course  $k$  itself is the dependent variable in this equation for most situations (i.e. where  $\omega$  is imposed by exciting at a given frequency), (For resonance experiments,  $k$  is fixed and  $\omega$  is the dependent variable and solution is much easier). Since  $k$  also appears explicitly on the left hand side of eq. (2.19) it is not directly

possible to determine the overall effect which surface tension does have on the pattern by simply introducing some sort of correcting factor. In fact it is true to say that here is a fluid mechanics problem where the exclusion of surface tension from the analysis has a qualitative as well as quantitative effect. Thus eq. (2.19) must be solved as it stands, and this is done in 2.4.

### 2.3.3. The effect of Viscosity

Since in the search for suitable experimental liquids a number of otherwise possibly useful ones had a viscosity an order of magnitude higher than water, which is usually considered inviscid for surface wave propagation problems, it was thought necessary to determine by analysis what effect, if any, viscosity has on the anisotropy. Moreover, in the two-fluid case, the wavelength for a given frequency is less than for the free-surface case, and it is not immediately obvious whether this would result in more or less damping of energy by viscosity, whilst there is also the effect of shear stresses at the interface to be taken into account.

As far as could be determined, the problem of solving the wave equation, with viscous effects, for the interface between two liquids, has not been tackled in the literature and so it is set out below, using Lamb's analysis for the free surface case as a guide (Lamb 1932 § 349).

The axis notation is as shown in fig. 2.1, subscript 1 for upper parameters and variables, 2 for lower.

The equations of motion in the  $z, n$  plane are:-

$$\frac{\partial \underline{u}_1}{\partial t} + \frac{1}{\rho_1} \text{grad } p_1 = -g \underline{i} + \nu_1 \nabla^2 \underline{u}_1 \quad \dots 2.20a$$

and

$$\frac{\partial \underline{u}_2}{\partial t} + \frac{1}{\rho_2} \text{grad } p_2 = -(g + \frac{jB}{\rho_2} \cos^2 \theta) \underline{i} + \nu_2 \nabla^2 \underline{u}_2 \quad \dots 2.20b$$

and  $\text{div. } \underline{u}_1 = \text{div. } \underline{u}_2 = 0$  ... 2.21

where the vectors are two dimensional with  $z, n$  components.

(2.20) and (2.21) are satisfied by

$$u_{\alpha n} = -\frac{\partial \phi_\alpha}{\partial n} - \frac{\partial \psi_\alpha}{\partial z}, \quad u_{\alpha z} = -\frac{\partial \phi_\alpha}{\partial z} + \frac{\partial \psi_\alpha}{\partial n} \quad [\alpha=1,2] \quad \dots 2.22$$

with  $\nabla^2 \phi = 0, \quad \frac{\partial \psi_\alpha}{\partial t} = \nu_\alpha \nabla^2 \psi$  where  $\nabla^2$

is a two dimensional Laplacian operator, ... 2.23

with  $\frac{p_1}{\rho_1} = \frac{\partial \phi_1}{\partial t} - gz$  ... 2.24a

and  $\frac{p_2}{\rho_2} = \frac{\partial \phi_2}{\partial t} - (g + \frac{jB}{\rho_2} \cos^2 \theta)z$  ... 2.24b

On assuming the variables to vary as  $e^{ikn + \sigma t}$

the solutions of (2.23) are :-

$$\left. \begin{aligned} \phi_1 &= (A_1 e^{-kz} + B_1 e^{kz}) e^{ikn + \sigma t} \\ \psi_1 &= (C_1 e^{-m_1 z} + D_1 e^{m_1 z}) e^{ikn + \sigma t} \end{aligned} \right\} z > 0$$

$$\left. \begin{aligned} \phi_2 &= (A_2 e^{kz} + B_2 e^{-kz}) e^{ikn + \sigma t} \\ \psi_2 &= (C_2 e^{m_2 z} + D_2 e^{-m_2 z}) e^{ikn + \sigma t} \end{aligned} \right\} z < 0$$

... 2.25

where  $m_\alpha^2 = k^2 + \frac{\sigma}{\nu_\alpha}$  ... 2.26

If the fluids have infinite height and depth (for simplicit y)

then one boundary condition is for zero motion at  $z = \pm \infty$

Hence  $B_1 = B_2 = 0$ , and provided  $m_\alpha$  has its real part positive,

$D_1 = D_2 = 0$ .

Substituting (2.25) in (2.22) gives

$$\left. \begin{aligned} u_{n1} &= -(ikA_1 e^{-kz} - m_1 C_1 e^{-m_1 z}) e^{ikn + \sigma t} \\ u_{z1} &= +(kA_1 e^{-kz} + ik C_1 e^{-m_1 z}) e^{ikn + \sigma t} \\ u_{n2} &= -(ikA_2 e^{kz} + m_2 C_2 e^{m_2 z}) e^{ikn + \sigma t} \\ u_{z2} &= -(kA_2 e^{kz} - ik C_2 e^{m_2 z}) e^{ikn + \sigma t} \end{aligned} \right\} \dots 2.27$$

If  $z = \eta$  denote the interface, with  $\eta = 0$  the undisturbed level, then  $\frac{\partial \eta}{\partial t} = u_{z1} = u_{z2}$  at the interface, is another boundary condition, and the small amplitude approximation is made that

$$\frac{\partial \eta}{\partial t} = (u_{z1})_{z=0} = (u_{z2})_{z=0}$$

Hence  $\eta = \frac{k}{\sigma} (A_1 + i C_1) e^{ikn + \sigma t} = -\frac{k}{\sigma} (A_2 - i C_2) e^{ikn + \sigma t} \dots 2.28$

The other boundary conditions are those due to normal and shear stresses, viz :-  $P_{22z} - P_{12z} = \alpha \frac{\partial^2 \eta}{\partial n^2}$

and  $P_{2nz} = P_{1nz}$ , where  $\alpha$  is surface tension  $\dots 2.29$

But  $P_{\alpha 2z} = -p_\alpha + 2\mu_\alpha \frac{\partial u_{\alpha z}}{\partial z}$  and  $P_{\alpha nz} = \mu_\alpha \left( \frac{\partial u_{z\alpha}}{\partial n} + \frac{\partial u_{n\alpha}}{\partial z} \right) \dots 2.30$

Substituting for  $p_\alpha$  from (2.24) at  $z = \eta$ , with  $\phi$  at  $z = 0$  from (2.25), and substituting for  $\frac{\partial u_{n\alpha}}{\partial z}$ ,  $\frac{\partial u_{z\alpha}}{\partial z}$ ,  $\frac{\partial u_{z\alpha}}{\partial n}$

from (2.27) gives

$$\begin{aligned} P_{12z} / \rho_1 &= [-\sigma + \frac{gk}{\sigma} - 2\nu_1 k^2] A_1 + [g \frac{k}{\sigma} - 2\nu_1 k m_1] i C_1 \\ P_{22z} / \rho_2 &= [-\sigma - (g + j B \cos^2 \theta) \frac{k}{\sigma} - 2\nu_2 k^2] A_2 + [(g + j B \cos^2 \theta) \frac{k}{\sigma} + 2\nu_2 k m_2] i C_2 \\ P_{1nz} &= \mu_1 [2 i k^2 A_1 - (k^2 + m_1^2) C_1] \\ P_{2nz} &= \mu_2 [-2 i k^2 A_2 - (k^2 + m_2^2) C_2] \end{aligned} \dots 2.31$$

(2.31) in (2.29) gives, with  $j B \cos^2 \theta = \Gamma$ ,  $A_1 = -A_2$ ,  $C_1 = C_2$  from (2.28)

$$\begin{aligned} &\{ (\rho_2 + \rho_1) \sigma + [(\rho_2 - \rho_1) g + \Gamma] \frac{k}{\sigma} + (\mu_2 + \mu_1) 2k^2 + \frac{\alpha k^3}{\sigma} \} A_1 \\ &+ \{ (\rho_2 - \rho_1) g \frac{k}{\sigma} + \Gamma \frac{k}{\sigma} + 2k(\mu_2 m_2 + \mu_1 m_1) + \frac{\alpha k^3}{\sigma} \} i C_1 = 0 \dots 2.32 \end{aligned}$$

$$\text{and } (\mu_1 - \mu_2) 2ik^2 A_1 + \{(\mu_2 - \mu_1) 2k^2 + (\rho_2 - \rho_1) \sigma\} C_1 = 0 \quad \dots 2.33$$

Combining (2.32) and (2.33) to eliminate  $A_1$  and  $C_1$  we have

$$(\rho_2 + \rho_1) \sigma (\mu_2 - \mu_1) 2k^2 + (\mu_2^2 - \mu_1^2) 4k^4 + (\rho_2^2 - \rho_1^2) \sigma^2 + (\rho_2 - \rho_1)^2 gk + (\rho_2 - \rho_1) \Gamma k + (\rho_2 - \rho_1) (\mu_2 + \mu_1) 2k^2 \sigma + \alpha k^3 (\rho_2 - \rho_1) = 4k^3 (\mu_2 m_2 + \mu_1 m_1) (\mu_2 - \mu_1)$$

After rearranging, with  $M = \frac{\mu_2 - \mu_1}{\rho_2 - \rho_1}$  ,  $\frac{\mu_2 + \mu_1}{\rho_2 + \rho_1} = \nu_M$

and  $\frac{(\rho_2 - \rho_1) gk + \Gamma k + \alpha k^3}{\rho_2 + \rho_1} = \omega^2$  (the frequency without viscosity for the given wave number  $k$ )

$$\underline{(M + \nu_M) 2k^2 \sigma + \sigma^2 + 4k^4 M \nu_M + \omega^2 = 4k^3 (\mu_2 m_2 + \mu_1 m_1) \frac{M}{(\rho_1 + \rho_2)}} \quad \dots 2.34$$

This is the dispersion relation.

The simplest case is when  $\mu_1 = \mu_2$  ,  $M = 0$

$$\text{Then } \sigma^2 + \omega^2 + \nu_M 2k^2 \sigma = 0$$

$$\therefore \sigma = -k^2 \nu_M \pm \sqrt{k^4 \nu_M^2 - \omega^2} \quad \dots 2.35$$

This case gives at least an approximate guide to the sort of behaviour to be expected in the more general case.

For the present, what matters is the extent to which the viscosity alters the wavelength for a given frequency, as this would alter the anisotropy, and also the magnitude of the wave damping. Both effects depend upon the size of the term  $k^2 \nu_M$

The former effect is negligible for  $\omega^2 \gg k^4 \nu_M^2$  whence  $\sigma = -k^2 \nu_M + i\omega$  , since the term  $i\omega$  , which contains the anisotropy, dominates the magnitude of  $\sigma$ .

The effect of having two fluids is to increase  $k$  for a given  $\omega$  , and this therefore increases the relative strength of

the viscous term, which effectively sets a limit on the closeness to which the liquid densities may usefully be matched. Similarly, in the case of an upward force ( $\Gamma$ -ve), the usefulness of increasing the magnitude of  $\Gamma$  is limited, since  $k$  is thereby increased in one direction, increasing the influence of viscosity in that direction. However, with a downward force, if the frequency is unaffected by viscosity in the o.h.d. case it will be unaffected in the M.H.D. case. For an upward force, it is worth noting that the viscous term will increase as the square of the anisotropy ratio between smallest and largest wave numbers encountered, so that  $k^4 \nu_M^2$  could possibly increase by two orders of magnitude. This suggests that viscosity may not be negligible even with the use of fluids such as water normally considered inviscid for wave propagation purposes, and certainly discourages the use of more viscous liquids. The limiting effects of viscosity on the size of frequency and wavelength to be used in practical cases will be considered in chapter 4.

The general interpretation and solution of eq. (2.34) is more complex, since after substitution for  $m$ , a polynomial of order 8 in  $\sigma$  is encountered. It is interesting to note that the consideration of two fluids has the effect, via the right hand side of (2.34) of doubling the order of the equation. In practice, some of the terms may well be negligible compared with others, and in chapter 4 the equation will be examined with pertinent values inserted.

Thus although (2.34) does not readily give a clear idea of what happens when viscosity dominates, (i.e. when the problem is no longer a true wave motion problem, having odd order terms in  $\sigma$  comparable in magnitude to even order terms), it does enable the

results of an inviscid solution to be tested as to the validity of the inviscid assumption.

## 2.4 Theoretical Predictions

### 2.4.1. Note about phase and group velocity and lines of constant phase

Since we are dealing with anisotropic waves, dispersive with respect to direction as well as frequency, distinction must be made between polar plots of phase and group velocity and lines of constant phase (at unit time after that phase has left a point source), whereas in an isotropic system all would give polar plots that were circles, although possibly of different size. The dispersion relation so far has been expressed in the polar  $k$  plane, i.e.

$\omega = f(k, \theta)$  where  $k$  is the wave number of wave crests lying normal to the  $\theta$  direction. In this situation the phase velocity  $c = \frac{\omega}{k}$ , the speed of wave crests, is in the  $\theta$  direction. The group velocity, which may be thought of as the speed and direction of a packet of waves with a given  $k$  and  $\omega$  or equivalently as the speed of propagation of energy contained in a given  $\omega, k$  mode, has components for a given  $k$  both parallel and perpendicular to  $\theta$ . These are  $C_k = \left(\frac{\partial \omega}{\partial k}\right)_\theta$  and  $C_\theta = \frac{1}{k} \left(\frac{\partial \omega}{\partial \theta}\right)_k$  :- Shercliff (1970).

$c$  and  $C = \sqrt{C_k^2 + C_\theta^2}$  are conveniently displayed in polar plots.

However, for direct comparison with a visual observation of the waves in practice, the most suitable theoretical parameter to plot is the line of constant phase. This is the locus of all points having the same phase, and in the case of a wave system excited at the origin at uniform frequency (a situation easily realisable in practice) such lines define the shape of troughs and crests at any distance from the origin (once the starting transients have been allowed to damp out of the field of view). In our dispersion

relation including surface tension,  $k \neq F(\theta) G(\omega)$  so that, referring to Shercliff (1970), the lines of constant phase are not the same shape as the polar plot of group velocity. This is because the vector representing the constant phase curve bears a ratio to the group velocity vector which varies with the wave number direction. The line of constant phase may be plotted graphically by constructing the envelope of normals to the extremity of the wave number vector  $\underline{k}$ , but to be able to draw the lines by computer, the further fact is needed that such normals touch the lines of constant phase at a point whose direction from the origin is that of the group velocity corresponding to  $\underline{k}$ .

#### 2.4.2. Computational methods

To explore the experimental possibilities, it was decided to solve eq. (2.19) to determine what degree of anisotropy would be available from different experimental parameters.

##### a) Waves in a deep fluid

When  $h$  is greater than half a wavelength;

$$h > \frac{\lambda}{2}, \quad kh > \pi, \quad | < \coth kh | \approx 1$$

$$\text{and we may take } \omega^2 = \left[ (\rho_2 - \rho_1)g - jB \cos^2 \theta + \alpha k^2 \right] \frac{k}{(\rho_1 + \rho_2)}$$

For  $\omega$  fixed, this turns out to be a cubic in  $k$ , or after

$$\text{rearrangement, in } c, \text{ i.e. } c^3 - \frac{(\rho_2 - \rho_1)g}{(\rho_1 + \rho_2)\omega} c^2 - jB \cos^2 \theta - \frac{\alpha \omega}{\rho_1 + \rho_2} = 0$$

The computer was used to solve this for the range of  $0 < \theta < \frac{\pi}{2}$

for varying values of  $\omega$ ,  $jB$ ,  $\rho_1$ ,  $\rho_2$  and  $\alpha$ ,

and this range gives all the results by reflection in the  $\theta = 0$

and  $\frac{\pi}{2}$  axes. Details of the programme are given in the appendix.

The group velocity was then calculated directly from

$$c_k = \frac{(\rho_2 - \rho_1)g - jB \cos^2 \theta}{2\omega(\rho_1 + \rho_2)} + \frac{3\alpha\omega}{2c^2(\rho_1 + \rho_2)}$$

$$\text{and } c_\theta = \frac{jB \sin 2\theta}{2\omega(\rho_1 + \rho_2)}$$

The group velocity, then, is in a direction  $\theta + \phi$  to the B direction, where  $\phi = \tan^{-1} \left( \frac{C_o}{C_k} \right)$ .

The lines of constant phase were then obtained as follows.

If their locus be  $(x_3, y_3)$ , at such a time and distance scale that  $(x_3, y_3)$  is the locus of the perpendiculars from the position vectors c (i.e. unit time after the phase in question left the origin), and if the locus of c be  $(x_1, y_1)$ , then  $x_3 = x_1 - c \tan \phi \sin \theta$  and  $y_3 = y_1 + c \tan \phi \cos \theta$ . See fig. (2.3).

b) Long waves in shallow fluid

When  $h$  is small  $c/f \lambda$ , i.e.  $kh \ll 1$

then  $\tanh kh \approx kh$

for  $h_1$  and  $h_2$  both small,

∴ (2.19) reduces to  $\omega^2 = [(\rho_2 - \rho_1)g - jB \cos^2 \theta + \alpha k^2] \frac{k^2 h_2 h_1}{\rho_1 h_2 + \rho_2 h_1}$

which is more easily soluble - a quadratic in  $k^2$ , but again the computer was used to obtain a series of theoretical predictions.

See appendix .

c) One fluid shallow, the other deep

This is the most complex case where, for  $h_2$  small and  $h_1$  large  $c/f \lambda$ , (2.19) becomes  $\omega^2 = [(\rho_2 - \rho_1)g - jB \cos^2 \theta + \alpha k^2] \frac{k^2 h_2}{\rho_1 k h_2 + \rho_2}$ , a quartic in  $k$ .

but it may reasonably be approximated to

$\omega^2 = [(\rho_2 - \rho_1)g - jB \cos^2 \theta + \alpha k^2] \frac{k^2 h_2}{\rho_2}$  which is now again a quadratic in  $k^2$ .

b) and c) can then be combined into one computation solution

using a variable  $X = \frac{h_1 h_2}{\rho_1 h_2 + \rho_2 h_1}$ ,  $\frac{h_2}{\rho_2}$  or  $\frac{h_1}{\rho_1}$ .

depending on the situation being considered.

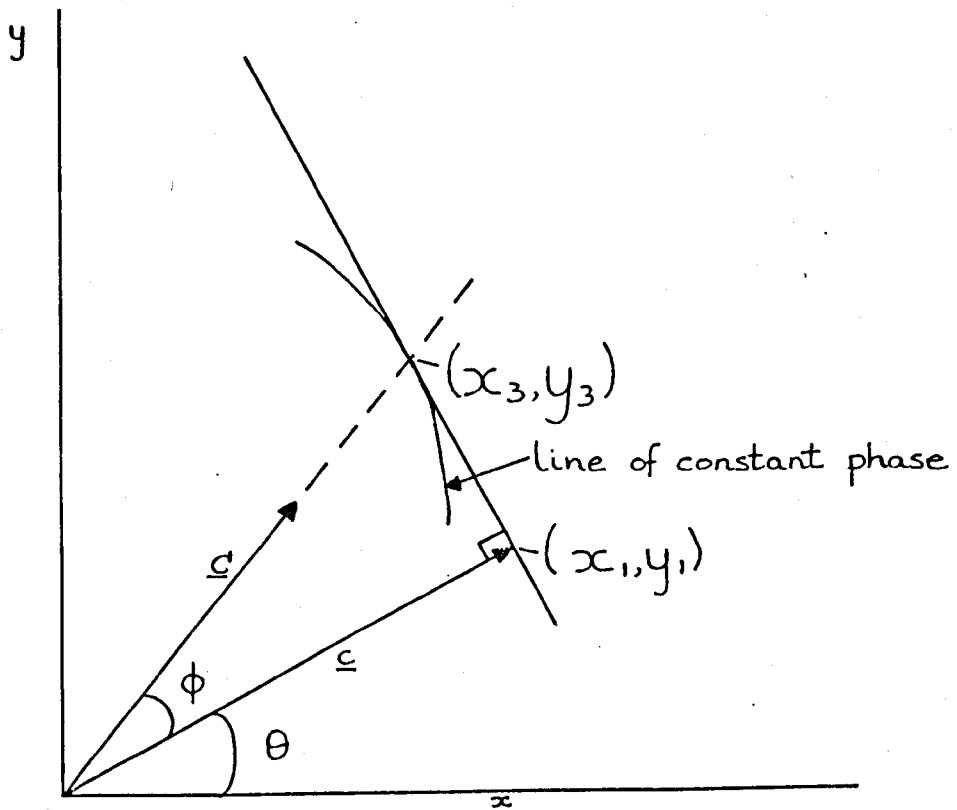


FIG. 2.3. CONSTRUCTION FOR CONSTANT  
 PHASE LINES

$$\text{Hence } c^4 - c^2 [(\rho_2 - \rho_1)g - jB \cos^2 \theta]X - \alpha \omega^2 X = 0$$

$$\therefore c = \sqrt{\left\{ \frac{1}{2} [(\rho_2 - \rho_1)g - jB \cos^2 \theta]X + \frac{1}{2} \sqrt{[(\rho_2 - \rho_1)g - jB \cos^2 \theta]^2 X^2 + 4\alpha \omega^2 X} \right\}}$$

$$C_k = [(\rho_2 - \rho_1)g - jB \cos^2 \theta + 4\alpha k^2] \frac{kX}{2\omega}$$

$$\text{and } C_\theta = jB \sin 2\theta \frac{kX}{2\omega}$$

The lines of constant phase are plotted as for a).

The resulting plots are shown in figs. 2.4 - 2.7 for the case of mercury with a free surface, and that of a conducting liquid of S.G. 1.100 covered by a non-conducting liquid of S.G. 1.080. The surface tension for mercury was taken as 0.5 N/m and for the other case 0.04 N/m and 0.004 N/m were chosen to represent a possible range of practically realisable values, the latter case being where a detergent, Teepol, has been added to the conducting liquid.

The magnetic field was set at 0.2 Wb/m<sup>2</sup>, and the current density, for the mercury at 5 x 10<sup>5</sup> A/m<sup>2</sup> (giving  $\frac{jB}{\rho g} \approx 0.8$  and for the other case at 1000 A/m<sup>2</sup> giving  $\frac{jB}{(\rho_2 - \rho_1)g} \approx 1.02$  which, though nominally unstable, is in fact stabilized by the surface tension for the frequencies used.

It can be seen that the phase velocity results are of the same sort of shape as for the ideal case, but the degree of anisotropy is markedly reduced, and the group velocity curve, where  $\theta + \phi > 90^\circ$ , is of a different shape, whereas the constant phase lines for this case still show the same cusped shape.

There is a marked variation of pattern with frequency, and it is instructive to draw a graph of  $k$  v  $\omega$  for the cases where  $\theta = 0$  and  $90^\circ$  (i.e. with full  $\underline{j} \times \underline{B}$  effect and zero effect) and also for the  $\underline{j} \times \underline{B}$  acting downwards case. These curves are shown in fig. 2.8. They show most clearly the effect which the surface tension has of reducing the degree of anisotropy, and

FIG. 2.4. DISPERSION PLOTS  
(MERCURY).

Surface tension 0.5 N/m  
Specific gravity 13.6.

$$\gamma \left( \frac{jB}{\rho g} \right) = 0.8$$

(i) Phase Velocity

frequency in c/s  
U Upward force  
D Downward force

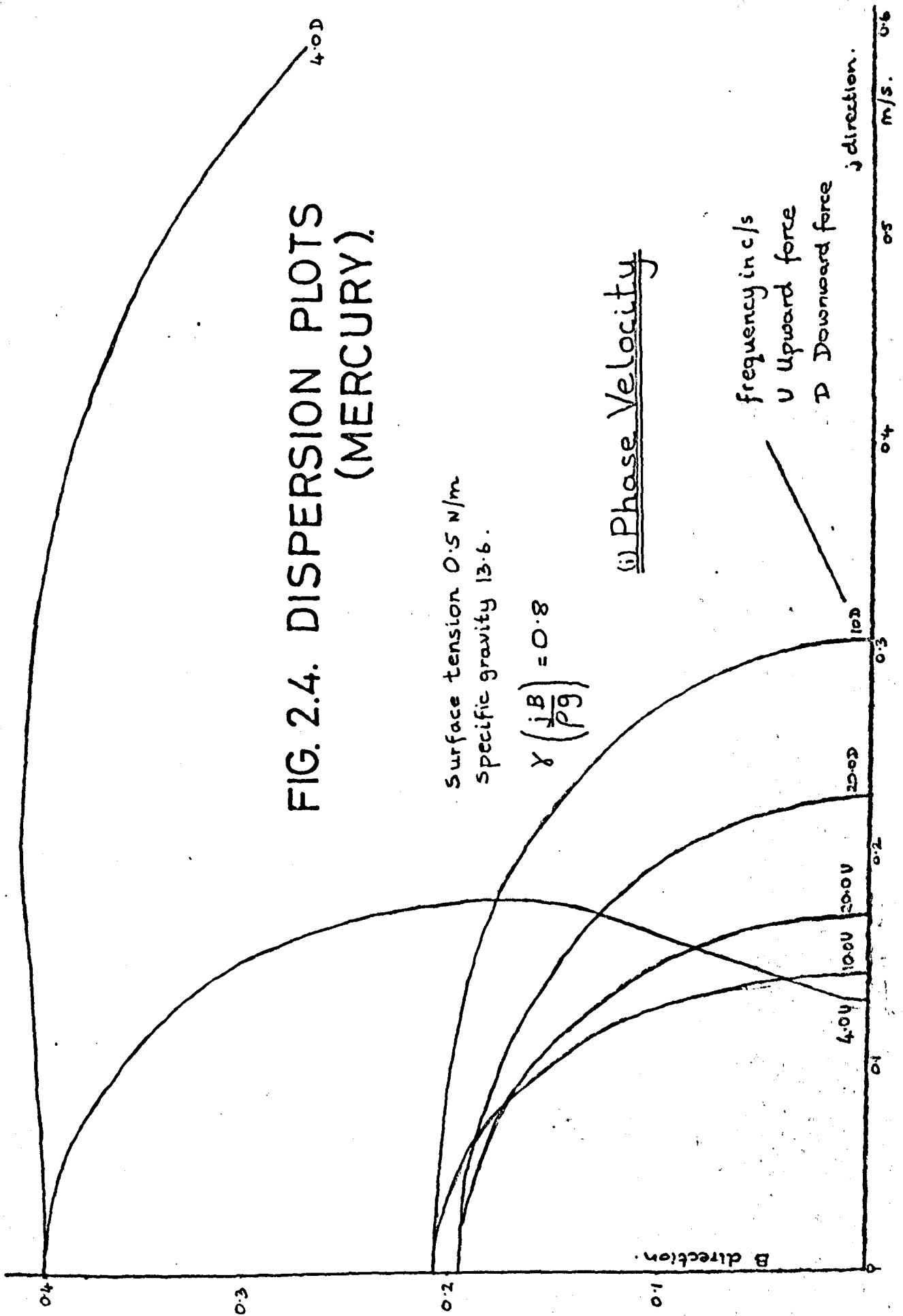


Fig. 2.4 (ii) Group Velocity.

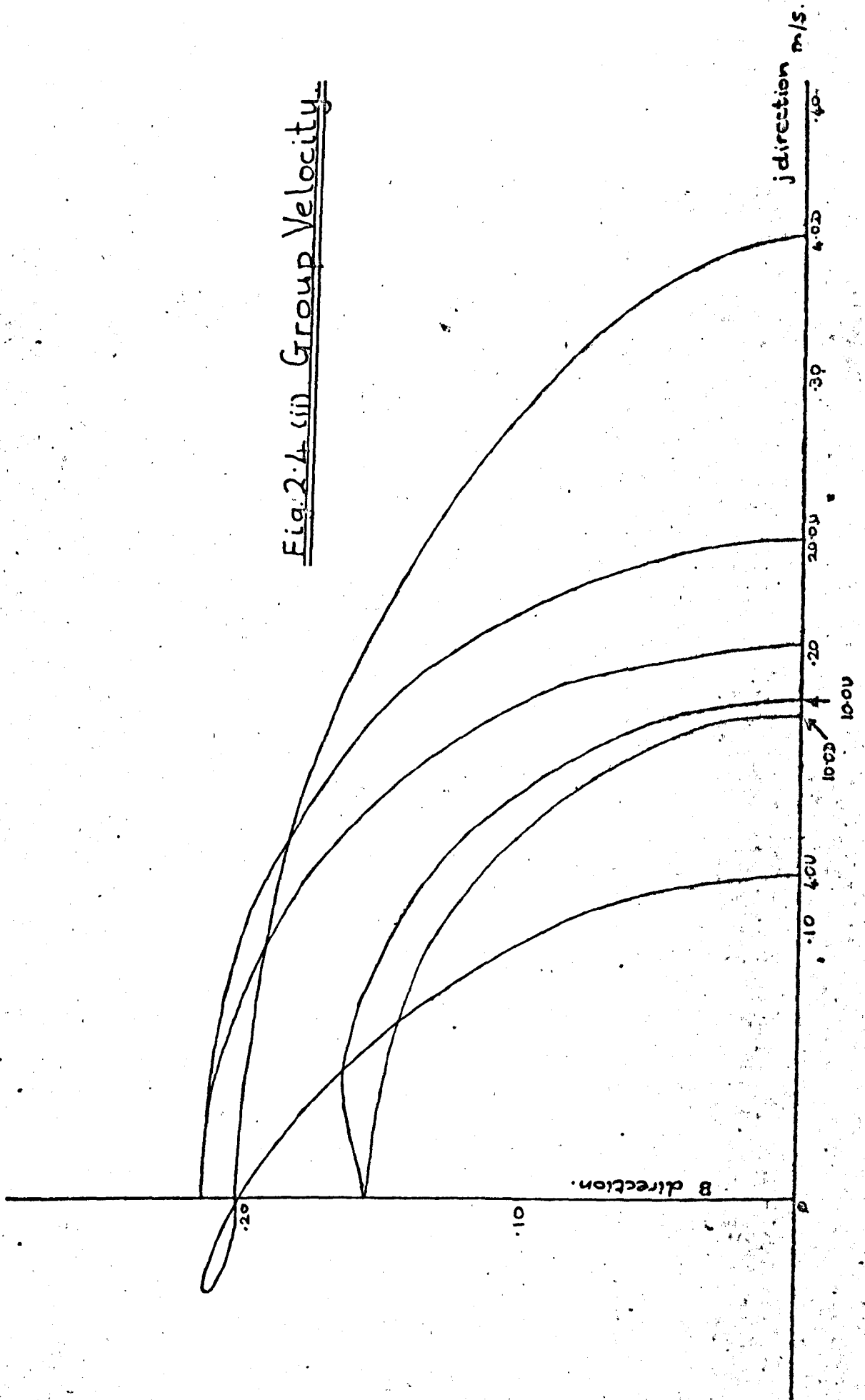


FIG. 2.1. (iii) Lines of Constant

Phase

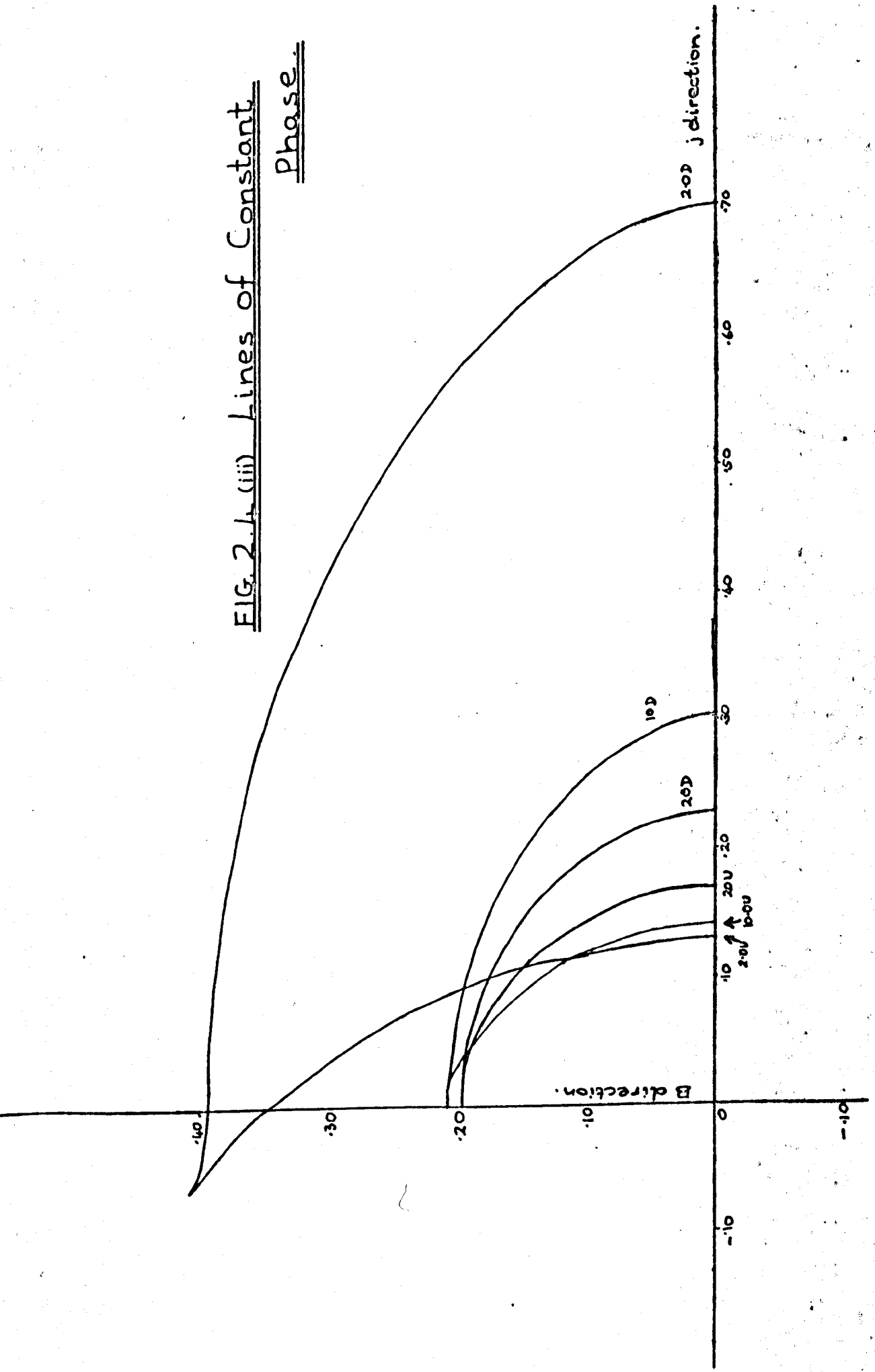


FIG. 2.5. DISPERSION PLOTS (TWO-FLUID INTERFACE WITH TEEPOL).

(i) Phase Velocity

S.G. upper = 1.08

S.G. lower = 1.10

surface tension = 0.004 N/m

$j = 100 \text{ m} / \text{s} / \text{gcm}$

$B = 0.2 \text{ Wt} / \text{m}^2$

frequency in c/s

U = upwards force

D = downwards.

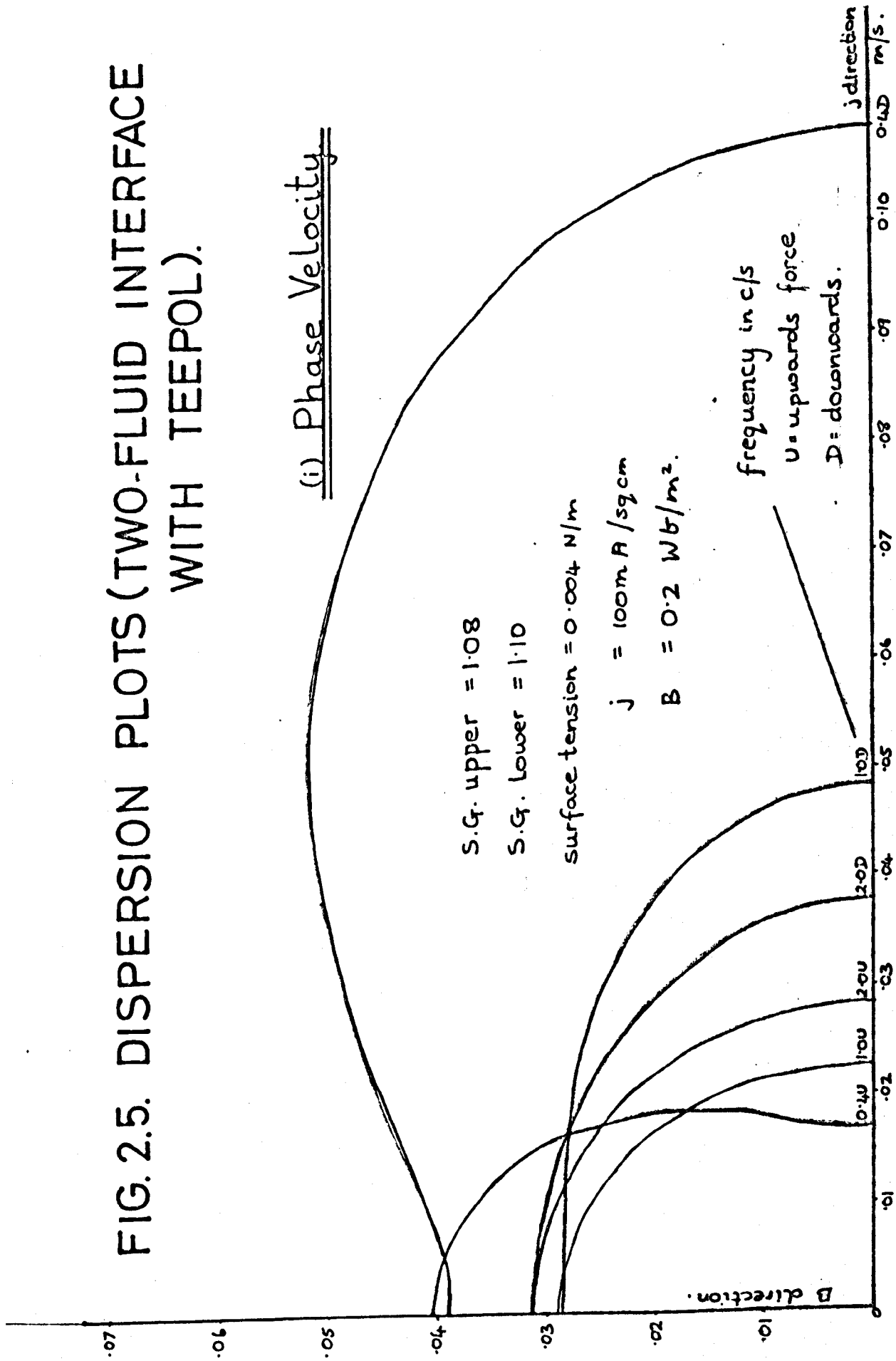


FIG. 2.5 (ii) Group Velocity

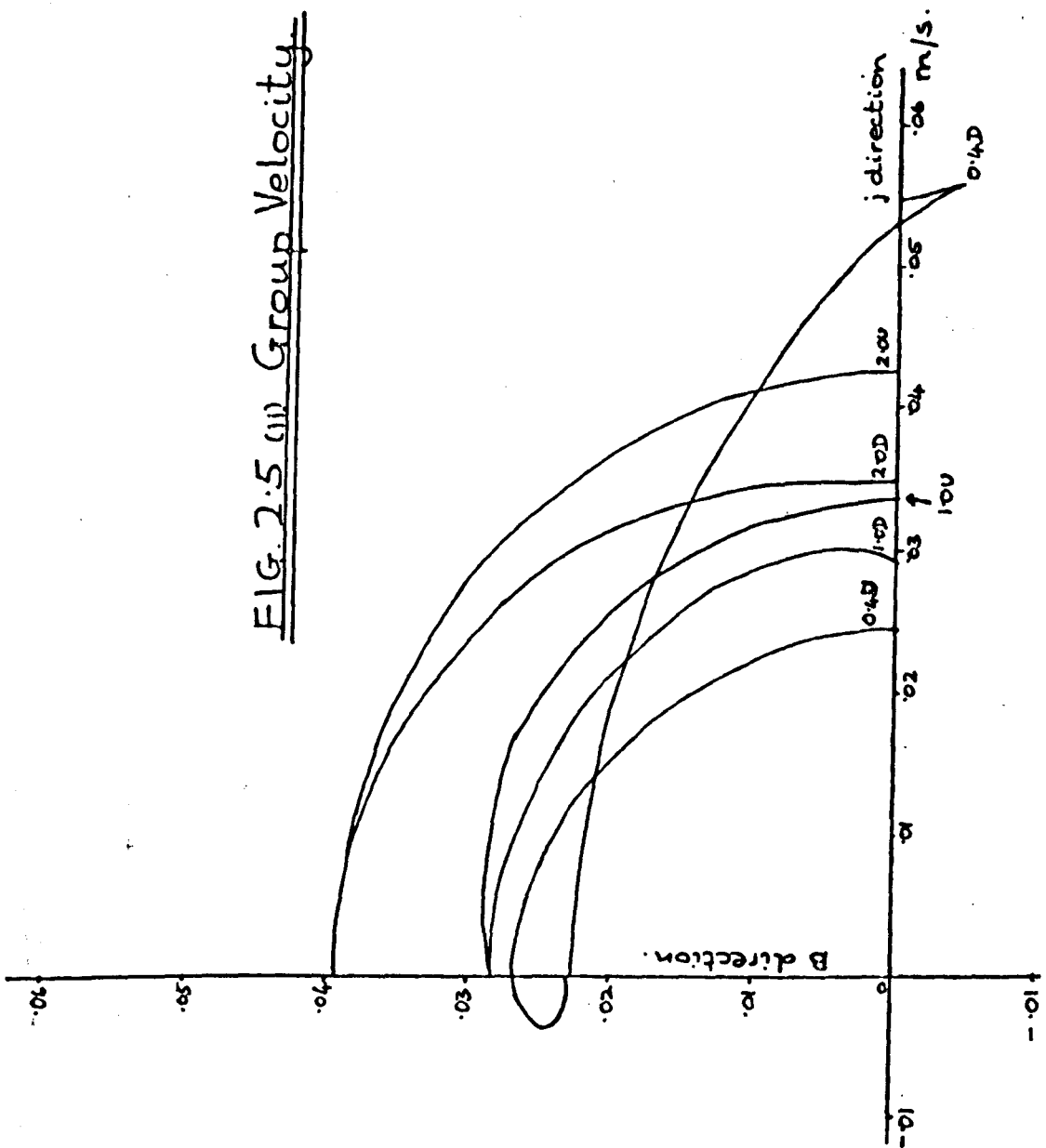


FIG. 2.5 (iii) Constant Phase Lines.

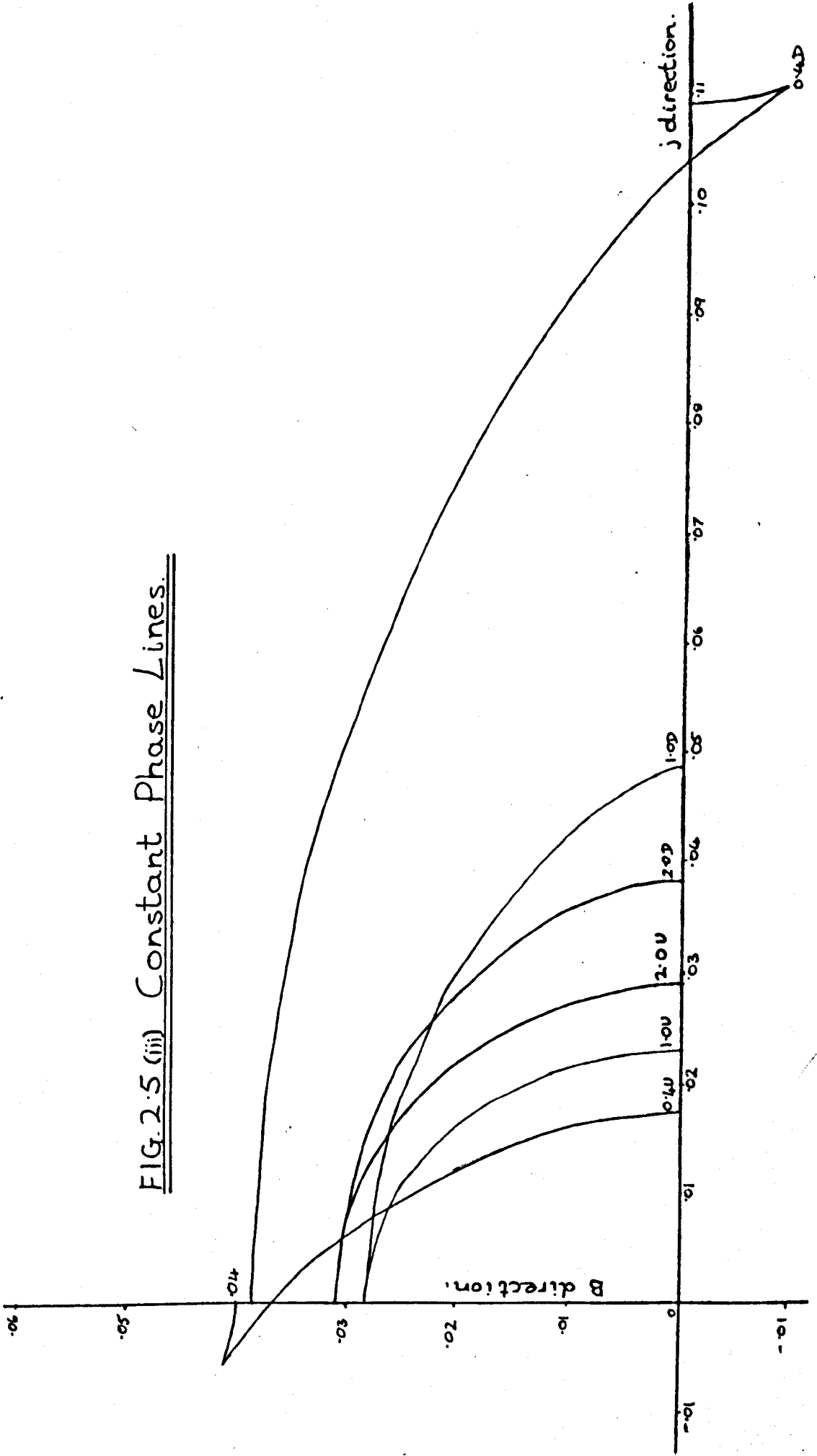


FIG. 2.6. DISPERSION PLOTS  
(TWO FLUIDS WITHOUT TEEPOL).

parameters as for 2.5 except  
surface tension = 0.04 n/m

(i) Phase Velocity.

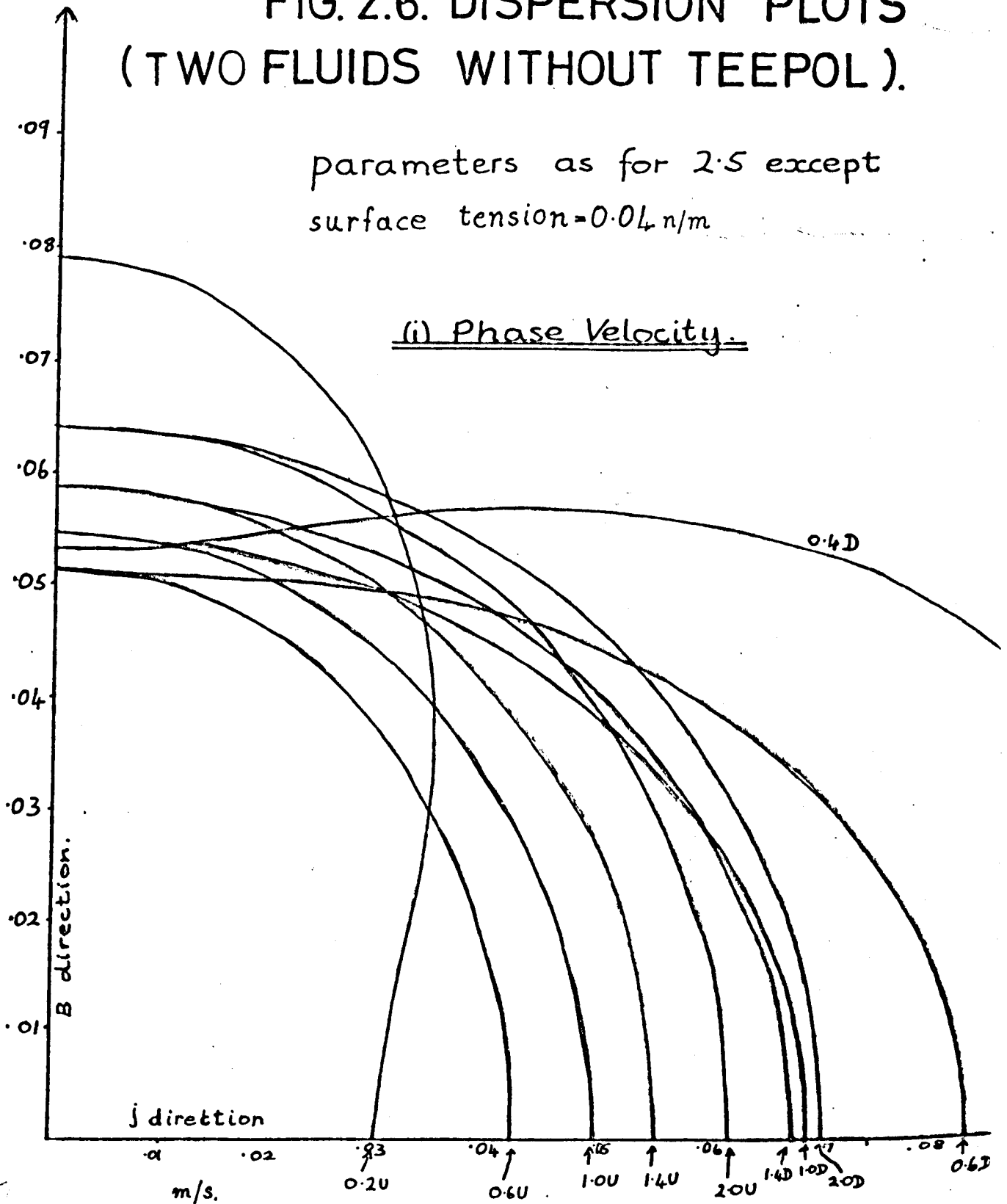


FIG. 2.6(ii) Group Velocity.

Group Vel. = .04  
 $\gamma = 0.368$

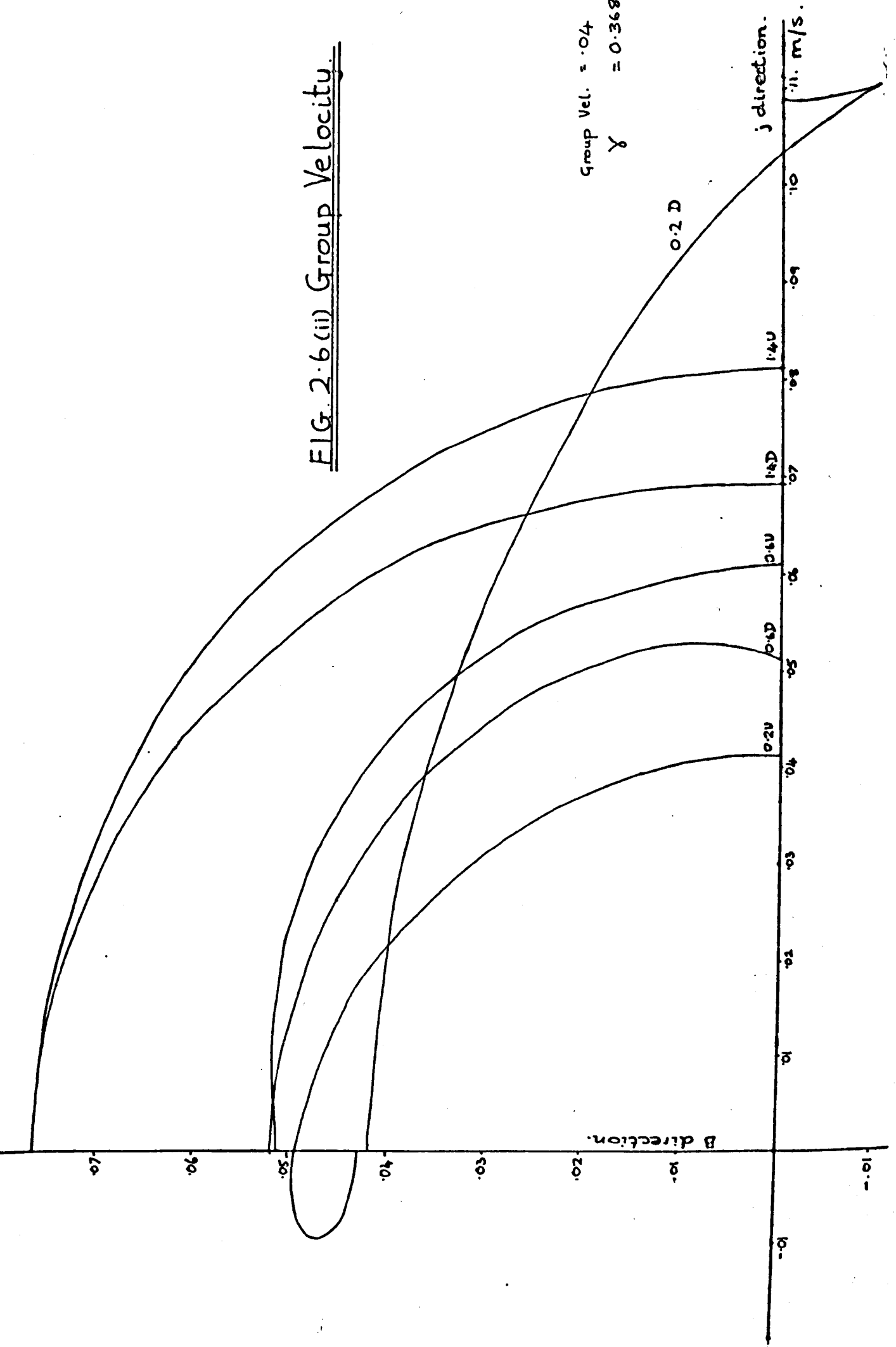


FIG. 2.6.(iii) Constant Phase Lines.

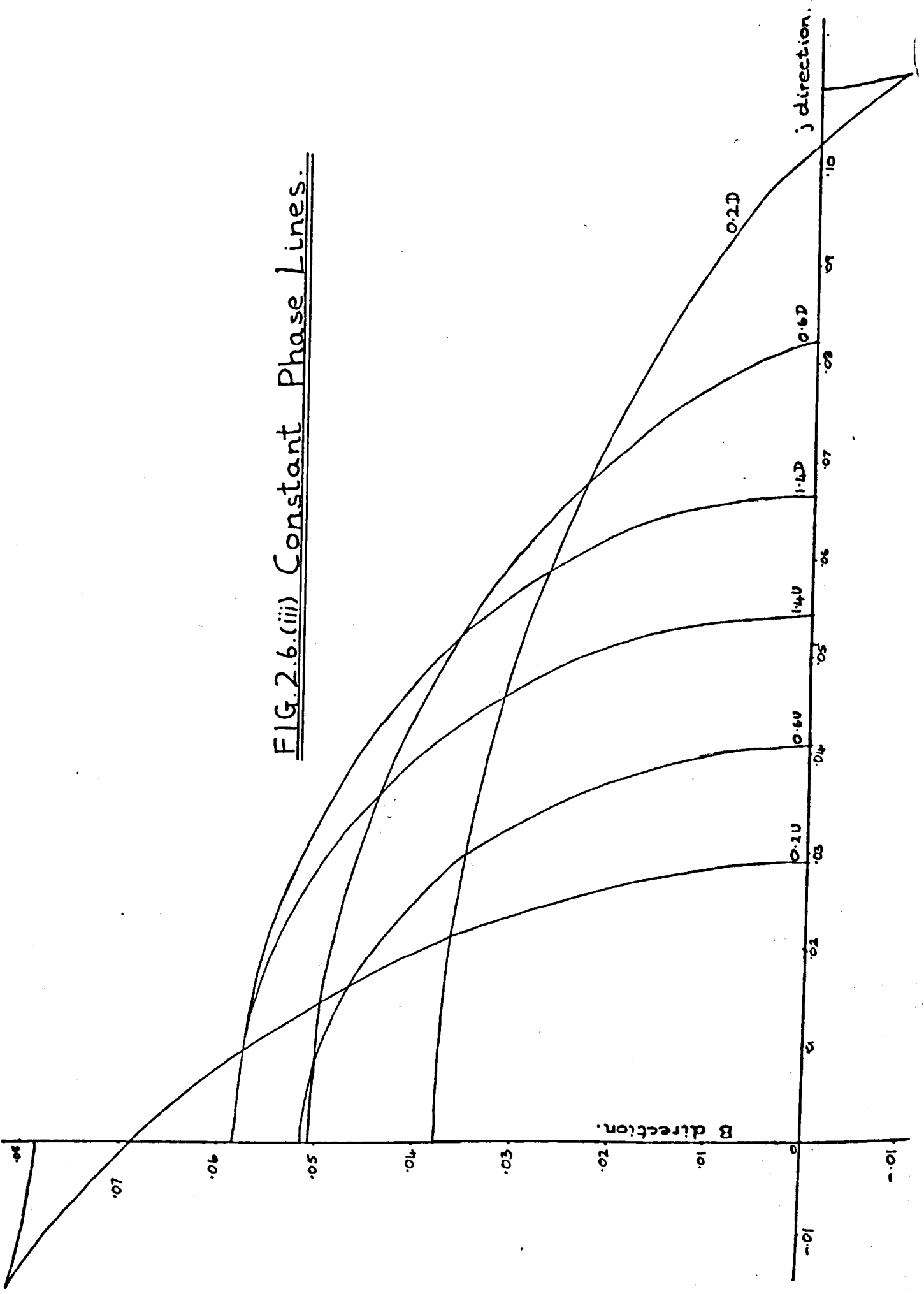


FIG. 2.7. LONG WAVE DISPERSION PLOTS.

(i) Phase Velocity.

Surface tension =  $0.004 \text{ N/m}$

Lower S.G. = 1.101      frequency =  $\frac{1}{2} \text{ c/s}$

Upper S.G. = 1.090

$B = 0.2 \text{ Wb/m}^2$

$j = 100 \text{ nA/cm}$

①  $H_1 = 200 \text{ mm.}$

$H_2 = \text{large}$   
Downward force

②  $H_1 = 2.0 \text{ mm.}$

Downward

$H_2 = 2.0 \text{ mm.}$

③  $H_1 = 2.0 \text{ mm.}$

Upward

$H_2 = 2.0 \text{ mm.}$

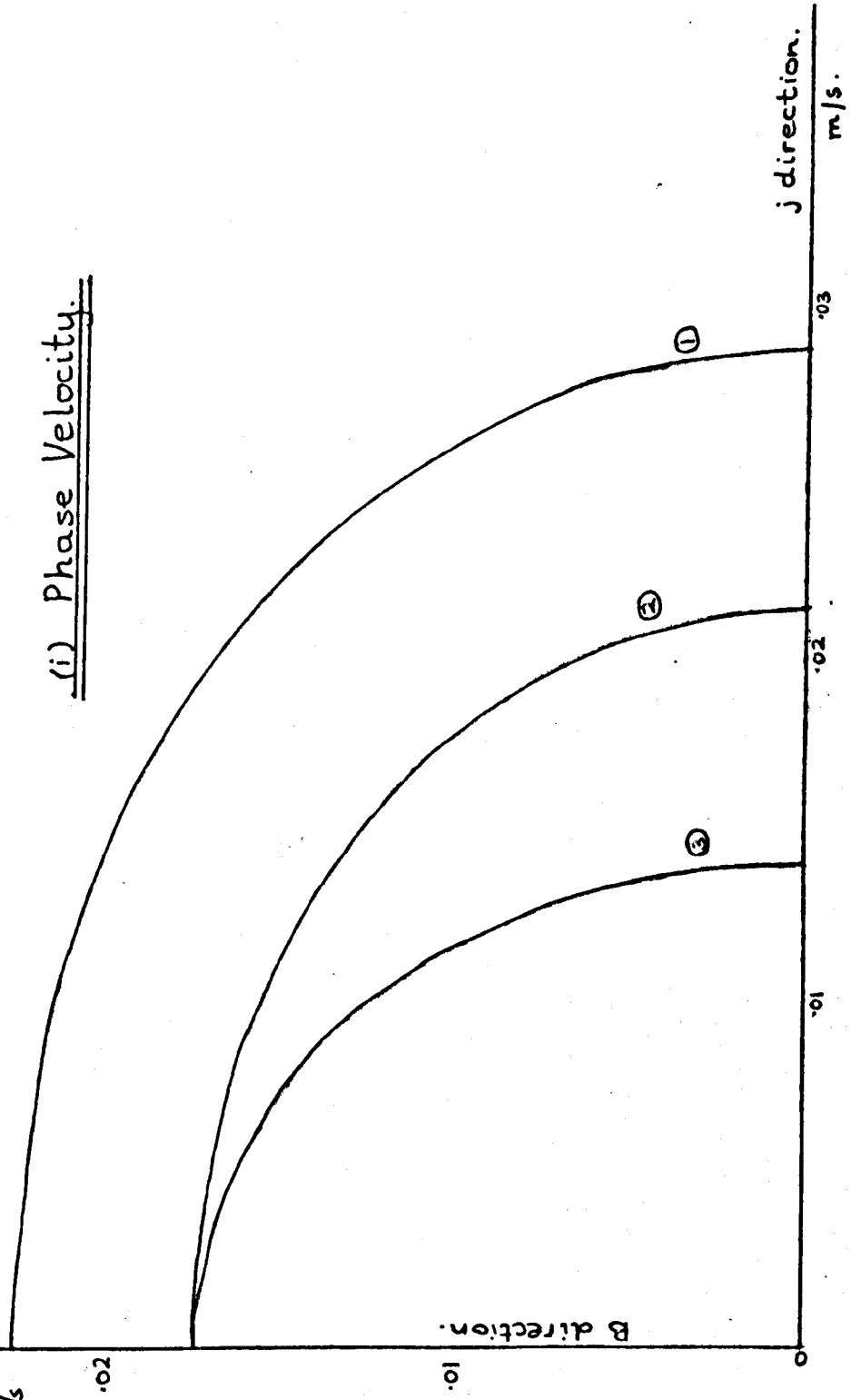


FIG. 2.7 (ii) Group Velocity.

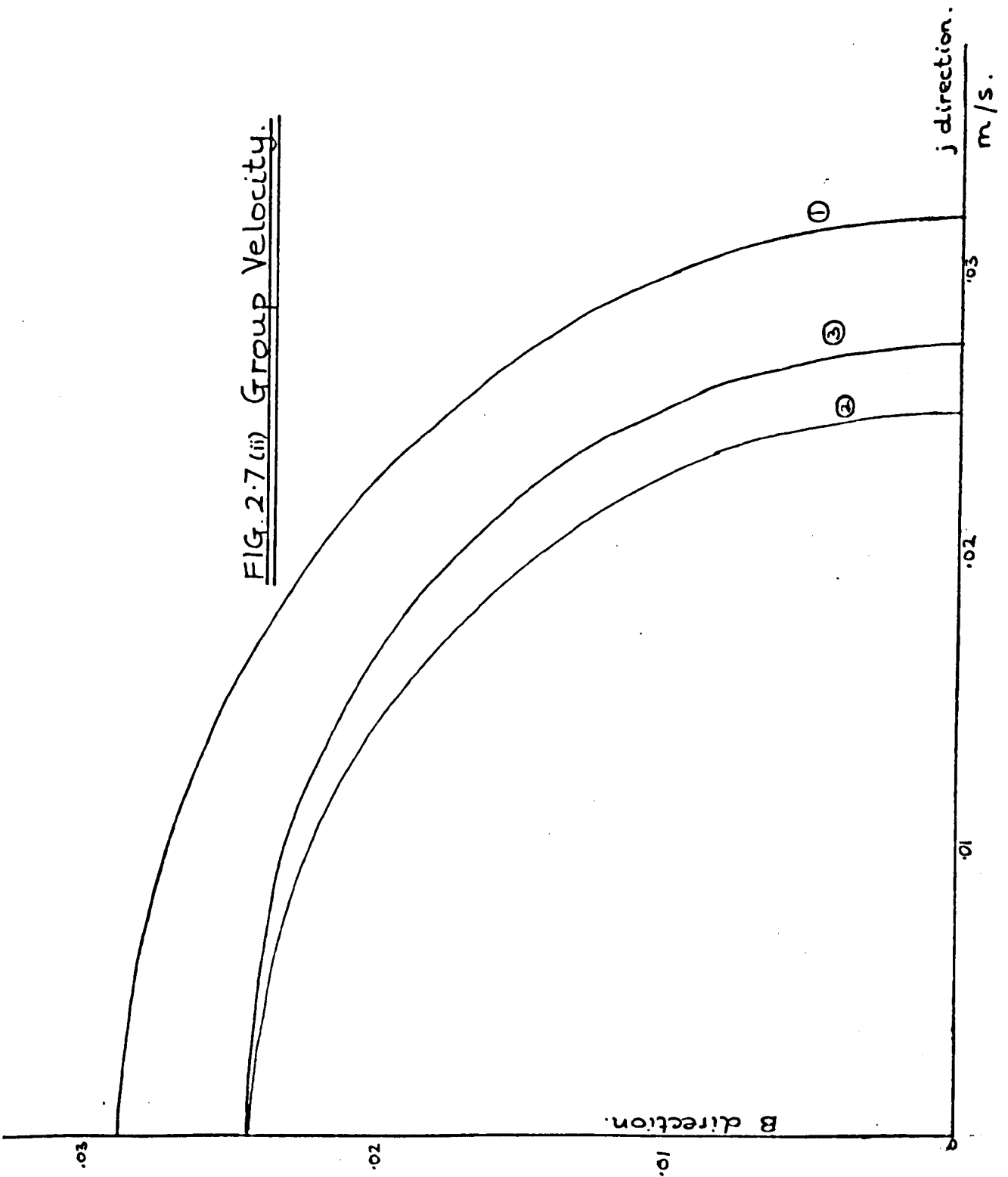
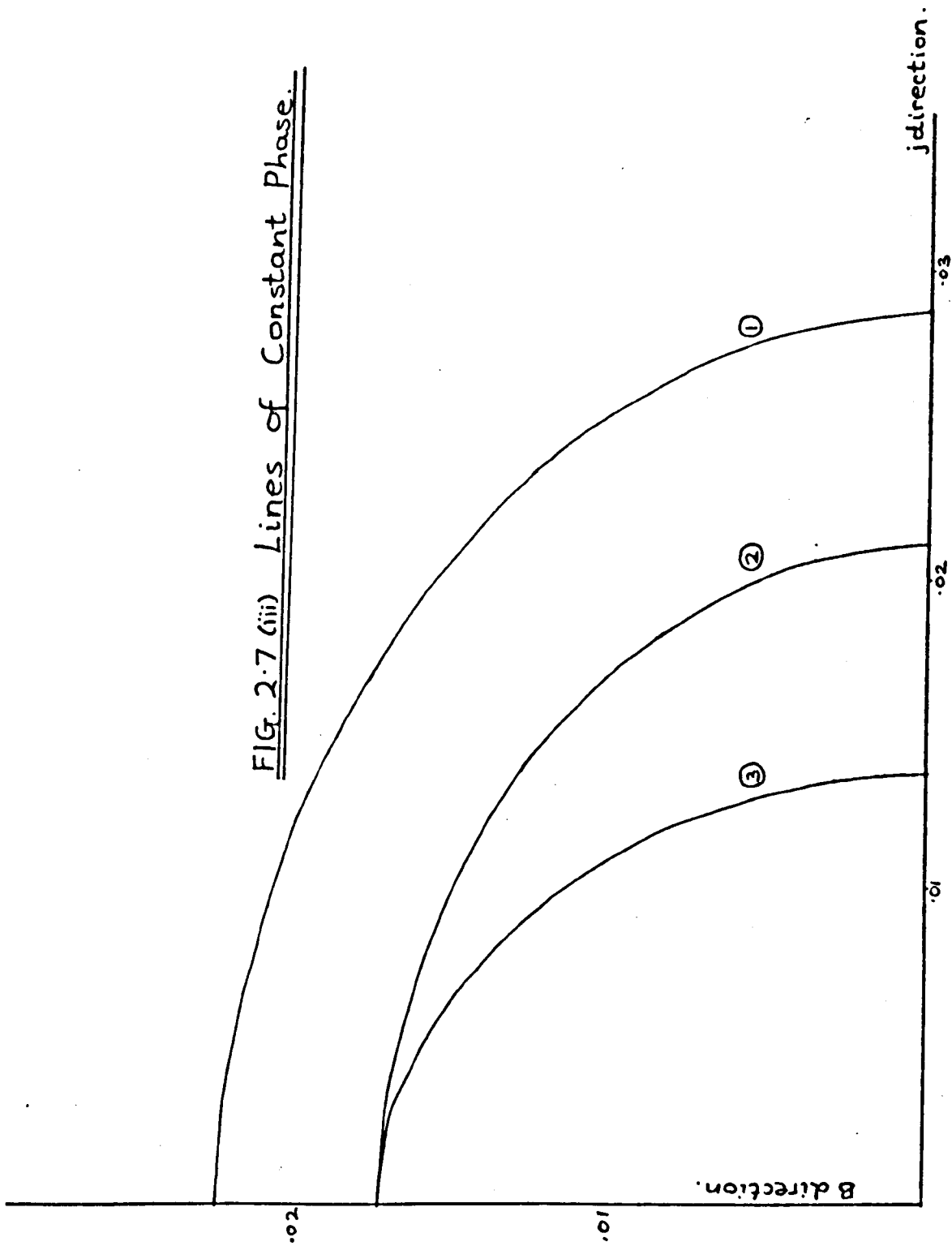


FIG. 2.7 (iii) Lines of Constant Phase.



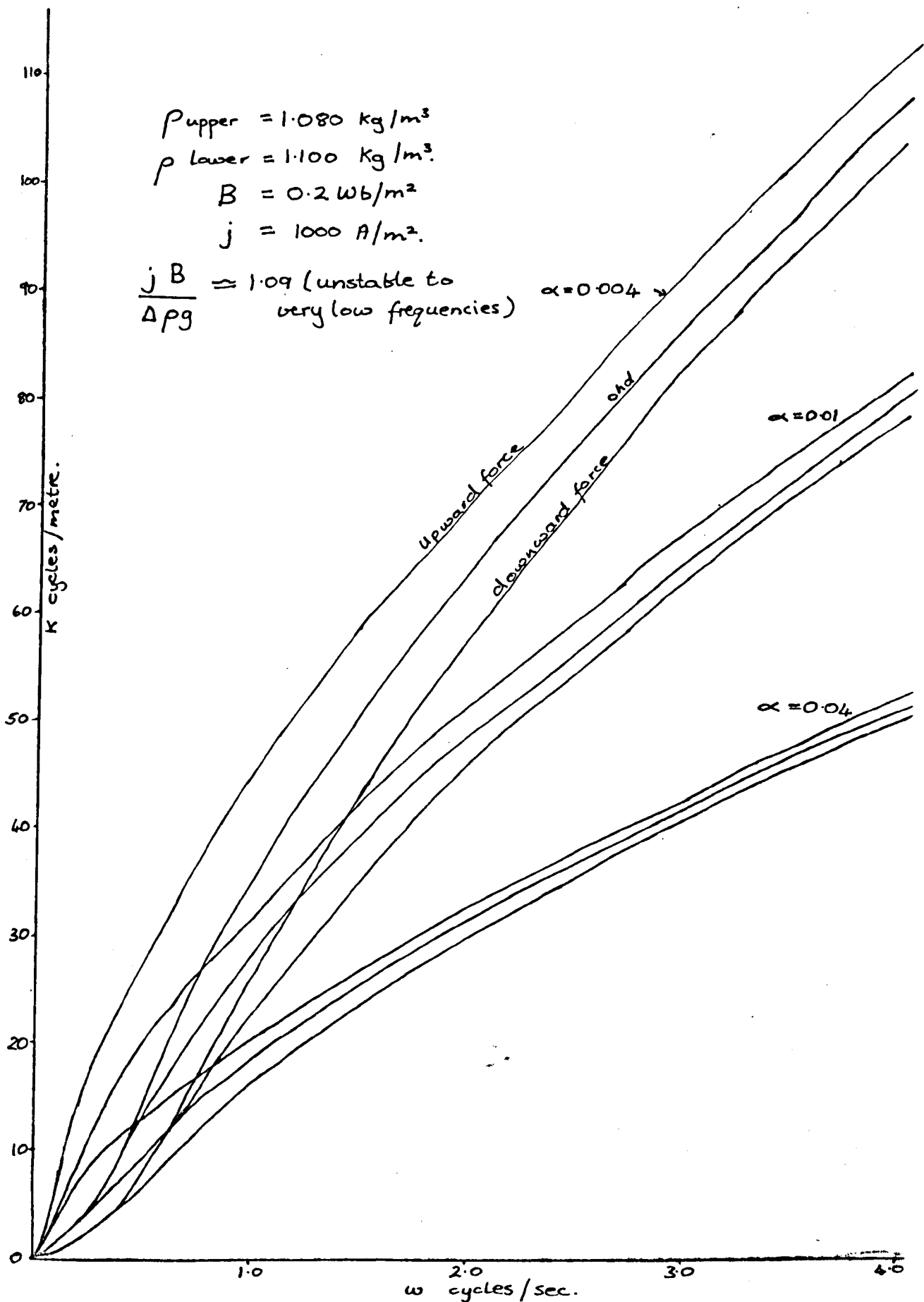


FIG. 2.8. WAVENUMBER, FREQUENCY RELATIONSHIP.

provide a useful guide for the selection of experimental parameters, as will be discussed in chapter 4.

The degree of anisotropy may be loosely defined by the ratio  $\left(\frac{k_{\max}}{k_{\min}}\right)$  and this plotted against  $\omega$  for a given  $\alpha$ , as in

fig. (2.9), shows clearly the frequency range below which surface tension effects are not too predominant.

As a further indication of the influence of surface tension, the plot of  $c$  against  $k$  (fig.2.10), and in particular the value of  $\omega$  and  $k$  for  $c_{\min}$  can be of help in choosing experimental parameters.

#### 2.5.1 Discussion on the nature of the anisotropy

The plotted results of the previous section show up the marked anisotropy of wave propagation which arises from the  $jB \cos^2 \theta$  term of (2.19). If the mathematics is traced back, it can be seen that the physical origin of the anisotropy is the action of the electromagnetic parameters on the pressure boundary condition in the fluid. Effectively  $\underline{j} \times \underline{B}$  acts as a 'gravity' force when the fluid is at rest and the surface flat. In the presence of waves, the  $\underline{j} \times \underline{B}$  force due to the current component parallel to the wave troughs and crests continues to act as a vertical body force, helping or hindering the gravity force and so influencing wave propagation, whereas the  $\underline{j} \times \underline{B}$  force due to current normal to troughs and crests is always normal to the surface, unable to exert a restoring or destabilising influence on the surface shape.

Thus if we are looking for the kernel of the M.H.D. effect, where fluid mechanical and electromagnetic parameters interact to produce a true M.H.D. phenomenon, it is in the boundary condition on current, which keeps the current always parallel to the surface so that waves in different directions "feel" different  $\underline{j} \times \underline{B}$  forces.

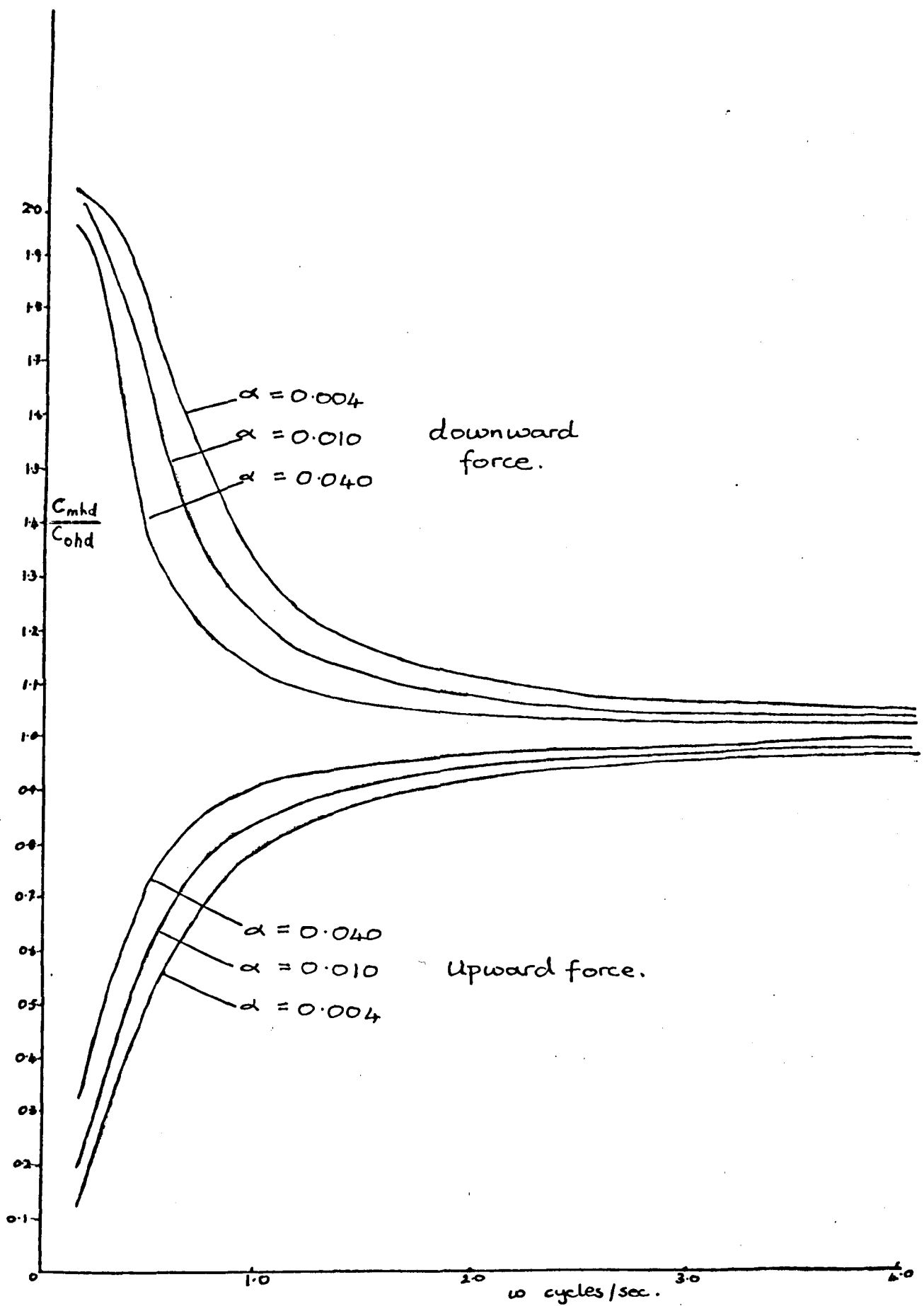


FIG.2.9. ANISOTROPY RATIO-FREQUENCY  
DEPENDENCE

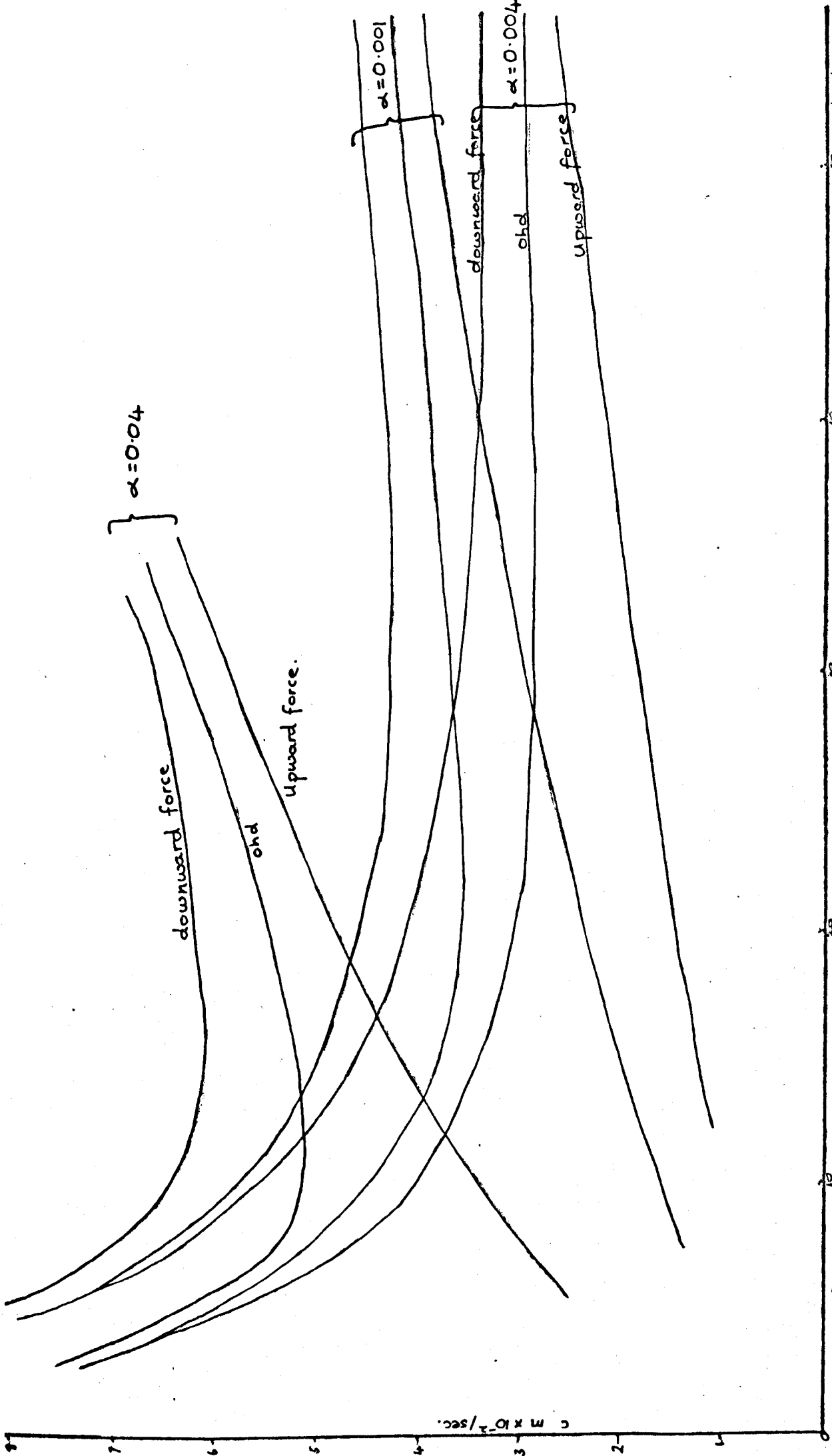


FIG. 2.10. PHASE VELOCITY-WAVENUMBER RELATIONSHIP.

i.e. the fluid pressure which balances the  $\underline{j} \times \underline{B}$  force varies with the wave direction. Otherwise the mechanism of wave propagation is a purely fluid mechanical action. This is by contrast to magneto-acoustic waves where there is true M.H.D. 'coupling' and anisotropy is governed by the magnetic field direction.

Also this anisotropic wave system can be contrasted with most others encountered in physics in that the medium of wave propagation itself is not anisotropic as is the case e.g. with light in an anisotropic crystal, or vibration in anisotropically transmitting materials. The anisotropy is effectively imposed by external parameters, and thus there is in this system a potential for variation of the dispersion relation by simply changing the magnitude and direction of the imposed field and current, providing a flexibility which could make it valuable in the investigation and demonstration of general anisotropic wave phenomena.

#### 2.5.2. The orientation of the anisotropy

So far we have considered only the simplest cases with  $\underline{j}$  and  $\underline{B}$  imposed at right angles to one another such that the  $\underline{j} \times \underline{B}$  force in the undisturbed field is upwards. Shercliff's analysis is generalized for any relative directions of  $\underline{j}$  and  $\underline{B}$ , and his polar plots of phase velocity etc., are expressed in this generalized way, showing that when surface tension is ignored, it is possible in principle to produce the same wave patterns whatever the angle between  $\underline{j}$  and  $\underline{B}$ , but the orientation of the patterns will vary, and the magnitude of  $\underline{j}$  and  $\underline{B}$  must be adjusted.

To express this in a way which will relate directly with section 2.3 (i.e. the adaptation of the theory to the practical situation), it is instructive to substitute  $j_s B_n$  for  $-jB \cos^2 \theta$

in (2.19), which then becomes the general case, and to consider the variation of  $j_s B_n$  with  $\theta$  (still defined as the angle  $k$  makes with  $\underline{B}$ ) for different  $\beta$  (the angle between  $\underline{j}$  and  $\underline{B}$ ) see fig. (2.11).

$$\begin{aligned} \text{Now } j_s B_n &= j B \sin(\beta - \theta) \cos \theta = jB (\sin \beta \cos^2 \theta - \cos \beta \sin \theta \cos \theta) \\ &= \frac{jB}{2} [\sin \beta + \sin(\beta - 2\theta)] \end{aligned} \quad \dots 2.36$$

Thus when  $\beta = +\frac{3\pi}{2}$ ,  $j_s B_n = -jB \cos^2 \theta$  as in (2.19)

Now as  $\theta$  is varied,  $j_s B_n$  varies from a maximum when

$\theta = \frac{\beta}{2} - \frac{\pi}{4}$  and  $\frac{\beta}{2} + \frac{3\pi}{4}$  to a minimum when  $\theta = \frac{\beta}{2} + \frac{\pi}{4}$  and  $\frac{\beta}{2} - \frac{5\pi}{4}$ , and the difference between maximum and minimum values is always  $jB$ . As  $\beta$  is varied, the mean of  $j_s B_n$  over all  $\theta$  varies as  $\sin \beta$ .

As was seen in (2.4) the degree of anisotropy may be represented by  $\left(\frac{k_{\max}}{k_{\min}}\right)$  for a given frequency. In Shercliff's case ignoring surface tension this is very much dependent upon  $\beta$ , for a given  $jB$ , since the absolute value of  $j_s B_n$  is important in the dispersion relation, and anisotropy is most readily obtained for  $\beta = \frac{3\pi}{2}$  i.e. when  $j$  and  $B$  are perpendicular and  $\underline{j} \times \underline{B}$  acts upwards. But in the practical case where the surface tension term in (2.19) is of the same order as the others, then:-

$$\begin{aligned} \frac{k_{\max}}{k_{\min}} &= \frac{(\rho_2 - \rho_1)g + (j_s B_n)_{\max} + \alpha k_{\text{mean}}^2}{(\rho_2 - \rho_1)g + (j_s B_n)_{\min} + \alpha k_{\text{mean}}^2} \\ &= \frac{(\rho_2 - \rho_1)g + (j_s B_n)_{\text{mean}} + \frac{jB}{2} + \alpha k_{\text{mean}}^2}{(\rho_2 - \rho_1)g + (j_s B_n)_{\text{mean}} - \frac{jB}{2} + \alpha k_{\text{mean}}^2} \end{aligned}$$

and though  $(j_s B_n)_{\text{mean}}$  can vary from  $+\frac{jB}{2}$  to  $-\frac{jB}{2}$  depending on  $\beta$ , this will not have a very marked effect on the anisotropy ratio.

Fig. (2.9) shows the anisotropy ratio  $\frac{k_{\max}}{k_{\min}}$  plotted against frequency for upward and downward  $\underline{j} \times \underline{B}$  ( $\beta = -\frac{\pi}{2}$  and  $+\frac{\pi}{2}$ )

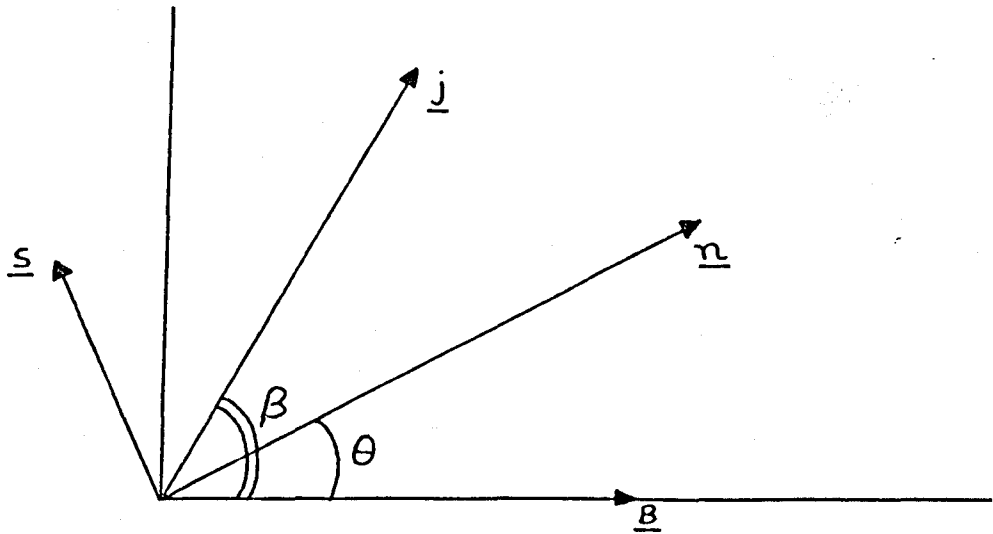


FIG. 2.11. NOTATION FOR SECTION 2.52.

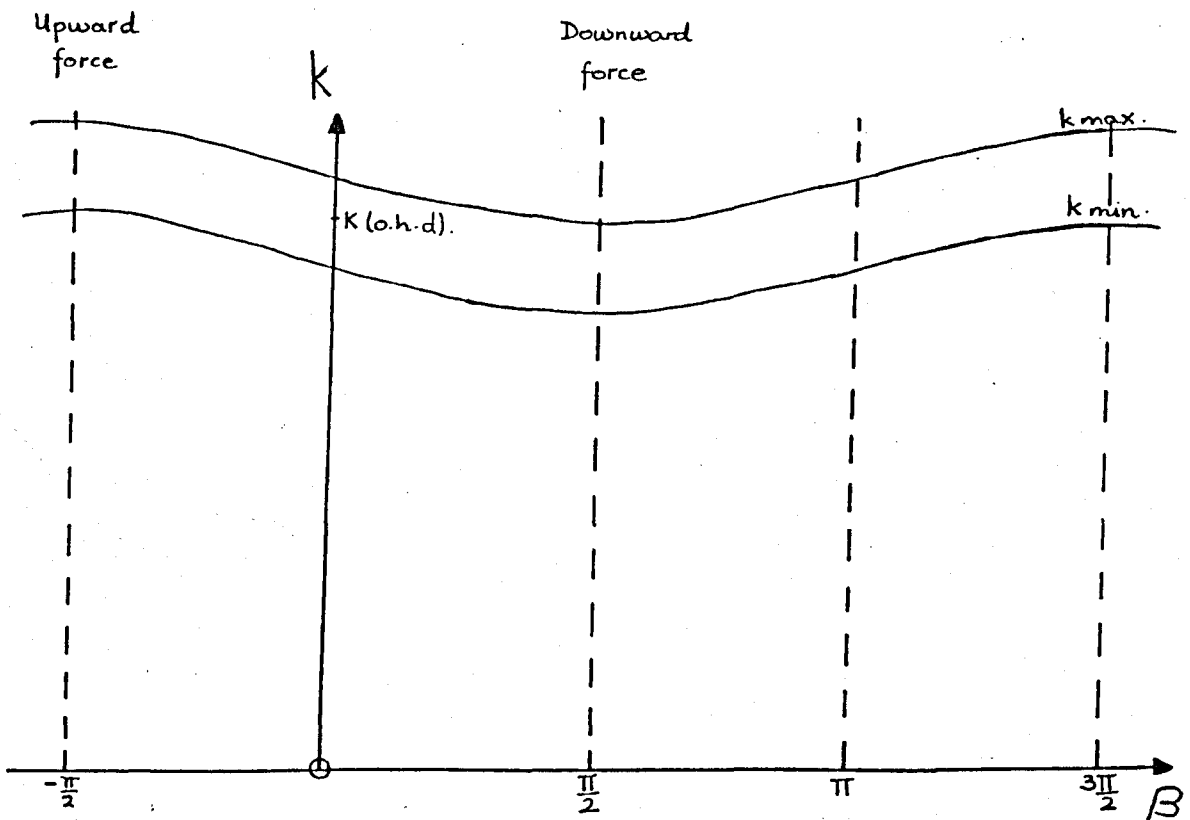
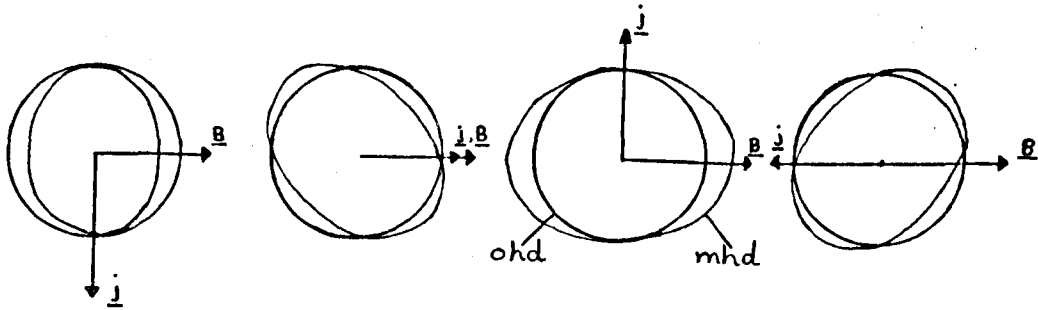


FIG. 2.12. VARIATION OF ORIENTATION OF ANISOTROPY WITH  $\beta$

for the two fluid case considered in (4.2). Hence if  $\beta$  be varied from  $-\frac{\pi}{2}$  to  $\frac{\pi}{2}$ , the pattern of waves would remain approximately the same shape, but rotate through  $\frac{\pi}{2}$  in the opposite direction to  $\beta$  from having  $k_{\min}$  in the  $\theta = \frac{\pi}{2}$  direction to  $k_{\min}$  in the  $\theta = 0$  direction, see fig. (2.12).

This brings to light the interesting cases of  $\beta = 0, \pi$  which although included in the Shercliff results and (in the instability case) in Murty (1961), are worth commenting on here. Mathematically they are quite straightforward, but physically they represent the cases where  $\underline{j}$  and  $\underline{B}$  are parallel or antiparallel and there is no  $\underline{j} \times \underline{B}$  force in the undisturbed state.

Wave numbers normal or parallel to  $\underline{j}$  and  $\underline{B}$  experience no influence from  $\underline{j}$  and  $\underline{B}$  at all, but all others do, the most marked effect being at  $\frac{\pi}{4}$  and  $\frac{3\pi}{4}$  to  $\underline{j}$  and  $\underline{B}$ . According to the assumptions governing the whole theory, any deviation of current other than in the vertical plane is negligible in its effect on  $\underline{j} \times \underline{B}$  forces, so that the only  $\underline{j} \times \underline{B}$  forces actually acting are in a horizontal direction, normal to  $\underline{j}$  and  $\underline{B}$ . But the waves propagate as if under a vertical body force of  $\frac{\underline{j} \times \underline{B}}{2}$  either added to or acting against gravity. Effectively, (see fig.2.13) the waves resolve the  $\underline{j}$  and  $\underline{B}$  into  $(j_s, j_n)$  and  $(B_s, B_n)$  having  $\underline{j} \times \underline{B}$  components  $j_s B_n$  downwards and  $j_n B_s$  upwards, a net force of zero. But because the wave motion is sensitive only to  $j_s$ , the  $j_s B_n$  force is effectively felt whereas the  $j_n B_s$  force is not and the anisotropy of wave motion follows, another example of the interesting nature of the phenomenon.

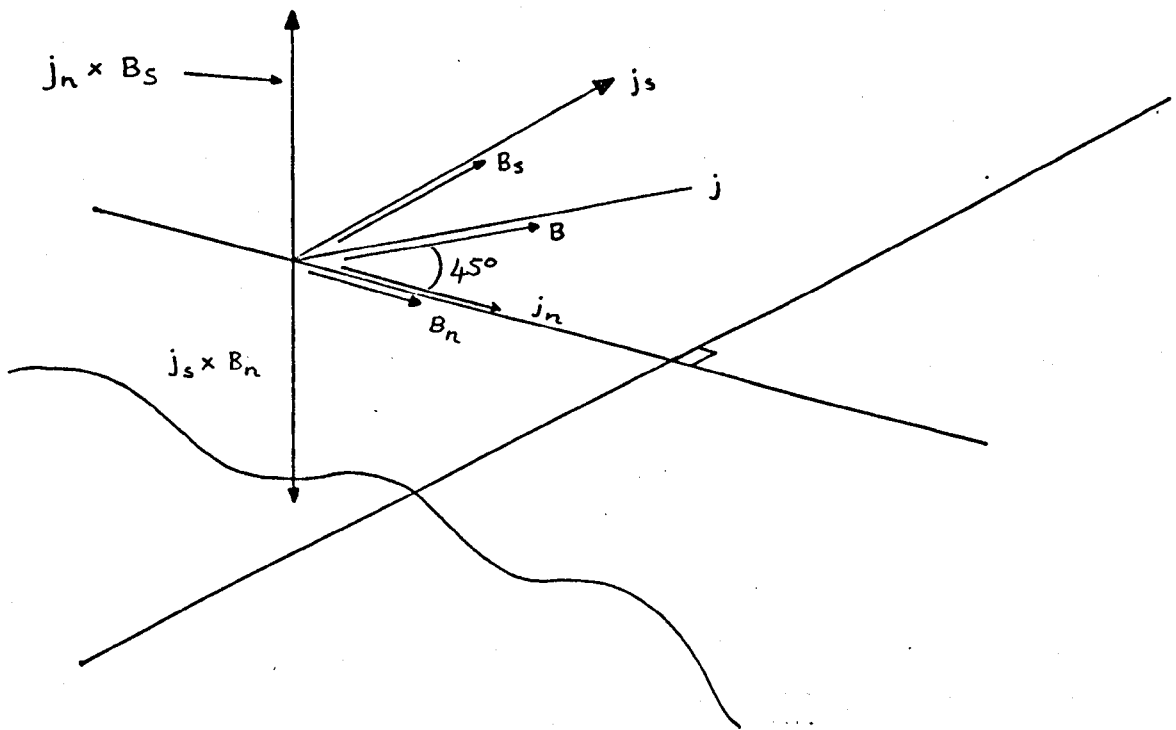


FIG. 2.13. TO ILLUSTRATE THE RESOLVING EFFECT OF THE WAVE ON  $j$  AND  $B$

3. THE ANISOTROPIC DISPERSION OF SURFACE WAVES APPLIED  
TO VARIOUS WAVE PHENOMENA

3.1.1. Introduction

Having established the theoretical basis for the existence of M.H.D. anisotropic surface waves, it is interesting to consider how the anisotropic dispersion affects some basic phenomena of surface waves, viz:- reflection, refraction, the initial impulse problem and the ship-wave problem. By removing some of the simplicity of the situation, adding the anisotropic term to the dispersion encourages a more fundamental study of the phenomenon itself, as in the case of reflection of plane waves at a plane wall, and at the same time provides a relatively simple, two dimensional wave system upon which to demonstrate the properties of anisotropic waves, the general results of which may be applicable to the three dimensional anisotropic wave systems encountered in other branches of physics. There is the further attraction that whilst the latter cannot readily, if at all, be directly observed by the naked eye, the phenomena relating to our anisotropic surface waves should be capable of being verified experimentally to some extent. Thus whilst it may seem to be only of academic interest to consider the "ship-wave" problem, or the initial disturbance problem referred to our wave system, that is no reason for avoiding these interesting exercises which may well help in the understanding of more complex and practically useful anisotropic wave systems.

3.1.2. Assumptions

To simplify the mathematics where necessary we shall consider the case where surface tension is ignored. This has the effect of showing up the phenomena to an extent which would not be

expected to be obtainable in laboratory experiments, but the theoretical results should be of the same general nature as the practically realisable ones.

It has been assumed that the conditions necessary for production of the M.H.D. anisotropic waves can be met. Effectively, the M.H.D. effects are used merely as a tool for producing an anisotropic wave system, and do not in themselves contribute in any other way to the phenomena under consideration, except in the case of refraction due to varying current density (see below). Thus we ignore the distortion of current due to a 'ship' or wave producing disturbance; in the initial disturbance problem we ignore any distortion of current, producing rotational forces, due to the small radius and large amplitude of wave crests close to the source, since the principle of stationary phase used tends to be erroneous in the region close to the source anyway; and we leave to the practical section the question of providing a 'reflecting wall' which is permeable and indeed invisible to the electromagnetic parameters i.e. which reflects the waves without affecting the imposed  $\underline{j} \times \underline{B}$  force. (This theoretical approach would seem to be justified in the light of the discussion of the nature of the anisotropy in (2.5) ).

### 3.1.3. Brief review of methods of dealing with wave systems

In chapter 2, reference has been freely made to such quantities as phase velocity, group velocity and lines of constant phase, and brief definitions have been given. Essentially we have been thinking purely in terms of plane wave systems—even the ideas about lines of constant phase, themselves not plane waves, derived from plane wave theory. This would be sufficient to solve the

reflection characteristics problem, but to gain more insight into the problem of energy reflection, and to solve the further problems posed in this chapter, it is necessary to refer to more complex and generalised methods of analysing wave systems which can be used to treat our anisotropic waves. These themselves are approximations of the complete mathematical formulation. We shall look at two general approaches since these will be used later on.

First is the principle of stationary phase, developed by Kelvin and Lamb (1932). The wave system is represented in the form of an equation for one of the variables, in this particular case  $\eta$  the surface elevation would be appropriate.

$$\eta = \sum_{\alpha} \int_{-\infty}^{+\infty} f(k) \exp \{i(k_{\alpha} x_{\alpha} - \omega t)\} dk_{\alpha} \quad \dots 3.1$$

$\alpha = 1, 2$  (represents the different co-ordinate axes, and obeys ~~the summation convention.~~

$\omega$  is a real function of  $k_{\alpha}$ , such that (3.1) satisfies the governing wave equation.  $k_{\alpha}$  at the moment is simply an arbitrary variable in the number of dimensions we are considering. The problem is to evaluate the integral when  $t$  and  $x_{\alpha}$  are large, given an initial condition over a limited region of  $\underline{x}$ .

It turns out that the main contribution to the integral of (3.1) for a particular interval  $k + \delta k$  is when  $(k_{\alpha} x_{\alpha} - \omega t)$  is constant in the interval, i.e. the "phase is stationary". Hence it becomes meaningful to talk of  $k_{\alpha}$  as a wave number to be found in the  $x_{\alpha}$  space where  $k_{\alpha} x_{\alpha} - \omega t$  is constant, and the idea of a group velocity arises because where the phase is stationary :-

$$\frac{\partial}{\partial k_{\alpha}} (k_{\alpha} x_{\alpha} - \omega t) = 0 \quad \text{i.e.} \quad \frac{dx_{\alpha}}{dt} = \frac{\partial \omega}{\partial k_{\alpha}}$$

So that if we travel in the  $(\underline{x}, t)$  space such that  $\frac{dx_{\alpha}}{dt} = \frac{\partial \omega}{\partial k_{\alpha}}$

i.e. at the group velocity, then that value of  $\underline{k}$  which contributes most to the integral of (3.1) at that particular  $(\underline{x}, t)$  remains constant. The amplitudes of waves can be obtained by this method, using the theory of Fourier integrals and it can be shown that energy travels with the group velocity.

Nonetheless to apply the method as it stands to each problem encountered would be very tedious and difficult, especially where  $\omega$  is a function of direction as well as magnitude of the wave vector  $\underline{k}$ , or even of  $\underline{x}$  also in the case of non-homogeneous dispersive media.

A much simpler approach is that of wave crest kinematics (Lighthill (1964), Whitham (1961), Hayes (1970)). At its simplest this is basic geometrical optics, but to apply it to dispersive systems needs some justification. Lighthill (1964) develops the theory from the principle of stationary phase above, and Whitham (1961) does so implicitly. He defines a phase function  $\phi(\underline{x}, t)$ , such that lines of constant phase are given by,  $\phi(\underline{x}, t)$  is constant. He then defines frequency and wave number as

$$\omega = -\frac{\partial \phi}{\partial t}, \quad \underline{k} = \nabla \phi \quad \dots 3.2$$

As Whitham points out, the existence of  $\phi$  gives a precise meaning to the idea of conservation of waves even where wave crests are not easily defined. This is crucial since it enables the ideas of wave crest kinematics to be extended to dispersive systems.

The phase velocity  $\underline{c} = \frac{\partial \phi}{\partial t} \hat{\underline{k}} / |\nabla \phi|$  where  $\hat{\underline{k}}$  is a unit vector in the  $\underline{k}$  direction.

$$(3.2) \rightarrow \frac{\partial \underline{k}}{\partial t} + \nabla \omega = 0 \quad \dots 3.3$$

which in effect states the conservation of waves. The particular medium and type of waves in question governs the form of the dispersion relation,  $\omega = f(\underline{k})$  .

Thus substituting for  $\omega$  in (3.3) we have

...3.4

$$\frac{\partial k_i}{\partial t} + C_j \frac{\partial k_j}{\partial x_i} = 0 \quad \text{where } C_j = \frac{\partial f}{\partial k_j},$$

the group velocity. Now as  $\underline{k} = \nabla \phi$ ,  $\text{curl } \underline{k} = 0$

i.e.  $\frac{\partial k_j}{\partial x_i} = \frac{\partial k_i}{\partial x_j}$

$$\therefore \frac{\partial k_i}{\partial t} + C_j \frac{\partial k_i}{\partial x_j} = 0 \quad \dots 3.5$$

which states that on a characteristic curve in  $(\underline{x}, t)$  space such that  $\frac{\partial x_j}{\partial t} = C_j$ ,  $\underline{k}$  remains constant.

Whitham then goes on to show, as does Lighthill in a fuller explanation, that for a non homogeneous medium defined by

$$\omega = f(\underline{k}, \underline{x}) \quad \dots 3.6$$

if the characteristic lines in  $(\underline{x}, t)$  space governed

by  $\frac{\partial f}{\partial k_i} = \frac{dx_i}{dt} \quad \dots 3.7$

are followed, then  $\underline{k}$  varies along these group lines as

$$\frac{dk_i}{dt} = - \frac{\partial f}{\partial x_i} \quad \dots 3.8$$

although  $\omega$  remains constant along these rays. Strictly this is limited to slightly non-homogeneous media, where the variation of dispersive properties throughout the medium is not such as would prevent the application of the principle of stationary phase in the fuller mathematical solution of the integral equations. Lighthill demonstrates that as for the homogeneous case, energy of a given wave packet is propagated along the characteristic rays.

For the homogeneous case,  $\underline{k}$  is constant along  $\frac{d\underline{x}}{dt} = \underline{C}$ , and as  $\underline{C}$  is a function of  $\underline{k}$  only, it must be constant in magnitude and direction, i.e. group velocity rays are straight lines. In the non-homogeneous case,  $\underline{k}$  varies along  $\frac{d\underline{x}}{dt} = \underline{C}$ , which is now a function of  $\underline{x}$  as well as  $\underline{k}$ , so that in general a group velocity ray is curved.

Thus if the initial distribution of  $\underline{k}$ , and the dispersion

relation  $\omega = f(\underline{k}, \underline{x})$  are known, the kinematic properties of the wave system at a subsequent time and place can be found, as the problems tackled later in the chapter will demonstrate.

Having found the kinematic properties, the amplitudes of disturbances can be calculated from consideration of energy conservation along the group rays, assuming - as does the whole theory - that the media are non-dissipative. To facilitate calculation of wave intensity or amplitude, Hayes (1970) has developed alternative equations to the ones above, but in the rest of this chapter no further mention will be made of amplitude since the anisotropic wave system furnishes a wealth of interesting phenomena in the kinematic properties alone.

Thus far, the problem has been posed as one of solving for  $\underline{w}$ , and to plot lines of constant phase (i.e. the trough and crest pattern actually observed), where these are not obvious from the solution for  $\underline{k}$ , recourse must be made to equ.(3.2). Most recently, however, Hunter (1972) has shown how  $\phi$  is directly related to the space co-ordinates, enabling a direct calculation of  $\phi$  without having to integrate the  $\underline{k}$  field. This method is used to advantage in the solution of the initial value problem.

### 3.2. Reflection of Anisotropic Surface Waves

#### 3.2.1. The problem stated

When plane waves of any sort meet a boundary where all or part of their energy is not absorbed but reflected, it might be expected that they will obey the usual reflection law, i.e. the angle of incidence will equal the angle of reflection. This is true however, only when the waves are isotropic in propagation. The problem then is how to characterize the reflection of waves which propagate anisotropically, i.e. to obtain the relationship

between incident and reflected angle of plane wave fronts for different orientations of the reflector to a characteristic direction of the anisotropic system. In our case this direction has been arbitrarily chosen as that of maximum phase velocity which, in the  $\underline{j}$  perpendicular to  $\underline{B}$  situation, is the  $\underline{B}$  direction. Also of interest is to determine how the energy of the waves is reflected, as characterised by the relationship between incident and reflected group velocity directions. First an intuitive method using the polar plot of phase velocity was tried.

### 3.2.2. Graphical method

This method shows up clearly how it is that the waves are reflected off the "mirror" at a different angle to their incidence. It is based on the Huygen's wavelet idea of reflection being due to the sum effect of an infinite number of sources along the line of the mirror, each in phase with the incident wave at that point.

In fig. (3.1),  $A_1 A_2$  represents a section of an infinitely long plane wave crest whose normal is incident at angle  $i$  with the "mirror".  $A_1 B_1 C_1 D_1$  and  $A_2 B_2 C_2 D_2$  represent particular 'rays' (normal to the crests and hence in the direction of phase velocity). Now if the polar plot of phase velocity be drawn in, with centre at  $B_1$ , where ray 1 strikes the mirror, and to such a scale that  $A_1$  lies on the plot, then  $A_1 B_1$  represents the distance travelled by the wave crest in the incident direction in unit time.

Now if ray 2 is drawn at such a distance from ray 1 that  $B_2$  (opposite  $B_1$ ) to  $C_2$  (where ray 2 strikes the mirror) is equal to  $A_1 B_1$ , then the wave crest must take unit time to travel from  $B_2$  to  $C_2$ . During this time  $B_1$  has acted as a secondary source, and can be imagined to have sent out a wave whose crest will have reached the given locus of phase velocity when ray 2 has reached  $C_2$ .

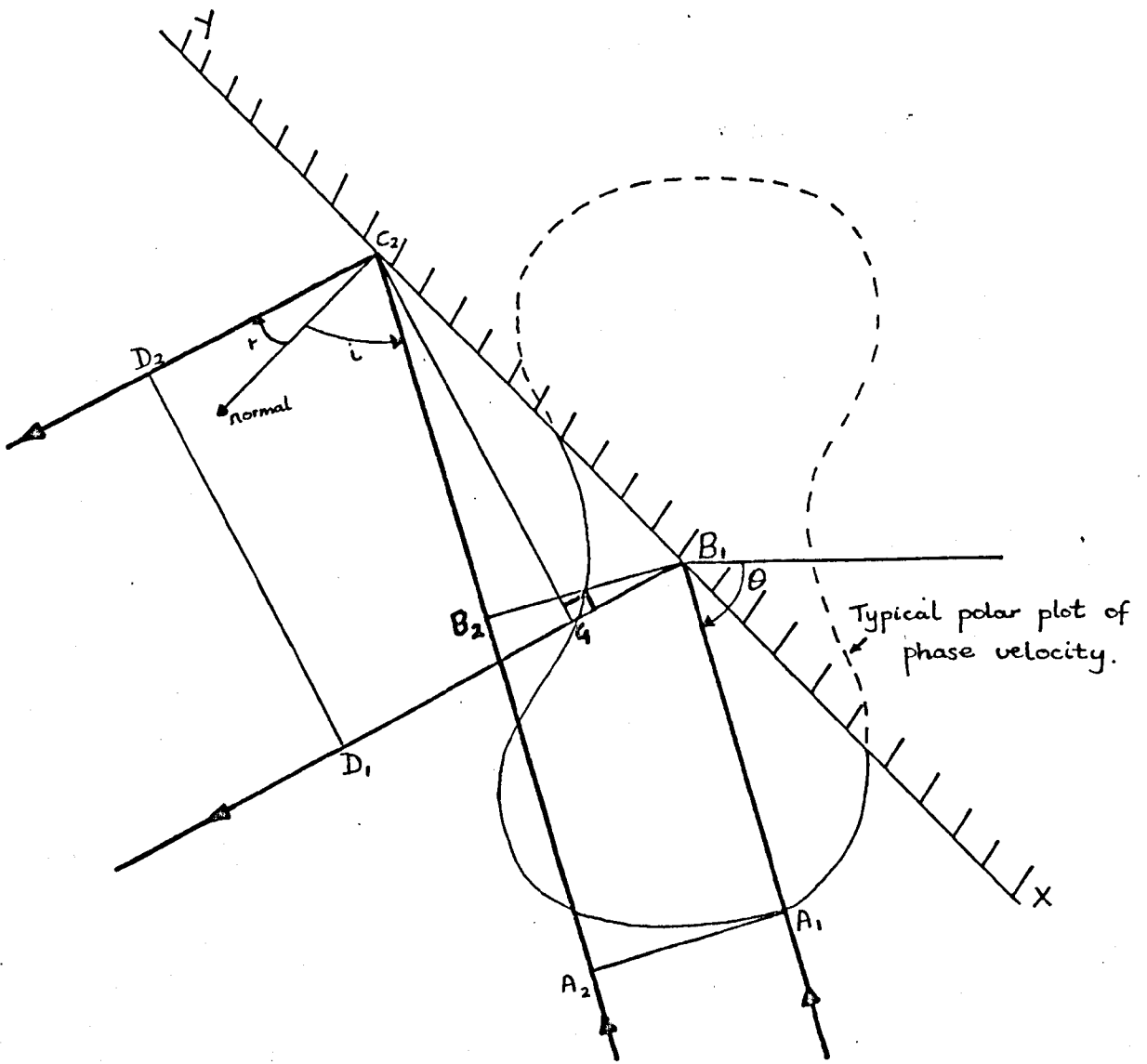


FIG. 3.1. REFLECTION, CONSTRUCTION, ANISOTROPIC WAVES

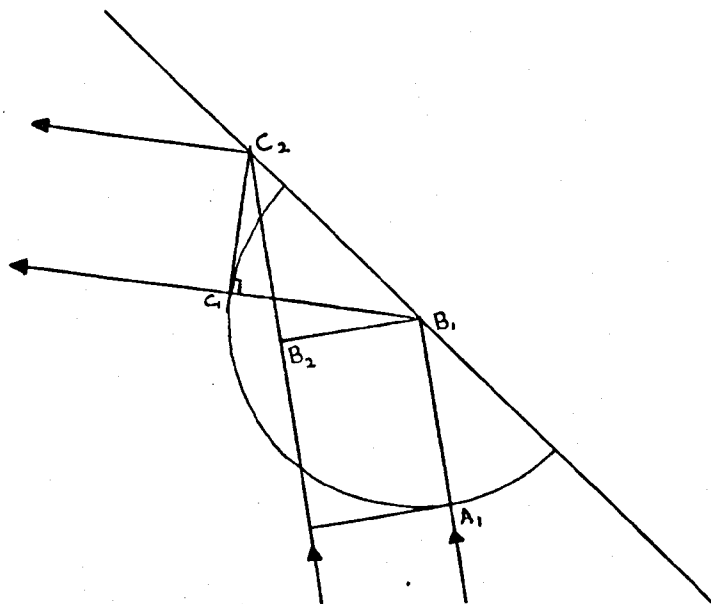


FIG. 3.2. REFLECTION CONSTRUCTION ISOTROPIC WAVES

However, since all the points between  $B_1$  and  $C_2$  and  $B_1$  and  $X$  will have acted in a similar way, there will be interference, and only those parts of the crest will reinforce which lie on a line passing through  $C_2$ , thus forming the reflected wave crest. Thus the graphical construction is to find that point  $C$ , on the phase velocity locus such that  $\angle B_1 C_1 C_2$  is a right angle.  $C_1 C_2$  then represents the reflected wave crest at reflected angle  $r$ .

If the phase velocity locus is a circle, as in isotropic waves, then fig. (3.2) shows clearly that the reflected angle will equal the incident since  $\triangle B_2 C_2 B_1 \equiv \triangle C_1 B_1 C_2$ , but fig. (3.1) shows equally clearly that this is not in general the case for anisotropic waves, except where there is symmetry, with the mirror along the major or minor axis of the phase velocity locus or else when the incident ray is normal to the mirror.

To save solving by drawing out the construction for each different angle of incidence, the method can be expressed trigonometrically.

As we have seen,  $\overline{A_1 B_1} = \overline{B_2 C_2} = c_i$  the incident phase velocity

$$\angle B_2 B_1 C_2 = i$$

$$\angle C_1 C_2 B_1 = r$$

and  $\overline{B_1 C_1} = c_r$

$$\therefore \overline{B_1 C_2} = \frac{c_i}{\sin i} = \frac{c_r}{\sin r}$$

It is interesting to compare this result with that for refraction in geometrical optics. Now  $c = f(\theta)$  <sup>where  $\theta$</sup>  is the orientation of the phase velocity to the magnetic field direction and  $f$  is determined by the dispersion relation.

$$\theta_i = \alpha + \frac{\pi}{2} - i \text{ and } \theta_r = \alpha + \frac{\pi}{2} + r$$

but  $i$  and  $r$  are clearly reversible.

∴ the condition that  $n_1$ ,  $n_2$  are corresponding incident/reflected angles or vice versa is that :-

$$F_1 \equiv \frac{f\left(\alpha + \frac{\pi}{2} - n_1\right)}{\sin n_1} = \frac{f\left(\alpha + \frac{\pi}{2} + n_2\right)}{\sin n_2} \equiv F_2$$

$$0 < n \leq \frac{\pi}{2}$$

so that if  $\frac{f\left(\alpha + \frac{\pi}{2} \pm n\right)}{\sin n}$  obtained from the computed solutions

for  $c(\theta)$ , be plotted against  $n$ , the abscissae of points on the two curves having the same ordinates are the corresponding values  $n_1, n_2$ . Fig. (3.3) is a typical curve and from it the incident versus reflection angle characteristic may be plotted, in fig. (3.4).

This shows clearly that as  $n_1$  varies from 0 to  $90^\circ$ ,  $n_2$  varies from 0 to angle  $n_{\text{crit}}$  less than  $90^\circ$ . Now if we take  $n_1$  as being  $i$  there is a range of  $r$  which is from 0 to angles less than  $90^\circ$ , but if we take  $n_2$  as  $i$  then there is an angle  $i = n_{\text{crit}}$  at which  $r$  is  $90^\circ$ , and when  $i$  is increased beyond  $n_{\text{crit}}$  it is not immediately clear what happens to  $r$ . There is an analogy here with the critical angle encountered in total internal reflection in optics, but in this case there is no alternative means whereby the energy may propagate away from the reflector. Fig. (3.5) represents a typical  $F$  v  $n$  curve taken over  $0 < n < 180^\circ$ , and it is seen to be symmetrical about  $n = 90^\circ$ .

Thus, if we take  $n_2$  as being the incident angle, when  $n_2 = a$ ,  $n_1$  is  $90^\circ$  and ordinary reflection is just possible. When  $n_2 = b$ , the corresponding  $n_1$  is  $d$  or  $e$ , and there is another possible  $n_1 = c$  having the same  $F$ .

Now a value of  $90^\circ < n_1 < 180^\circ$ , is in fact meaningful if thought of as a value of  $n_2 = 180^\circ - n_1$  (see fig. 3.6). Thus

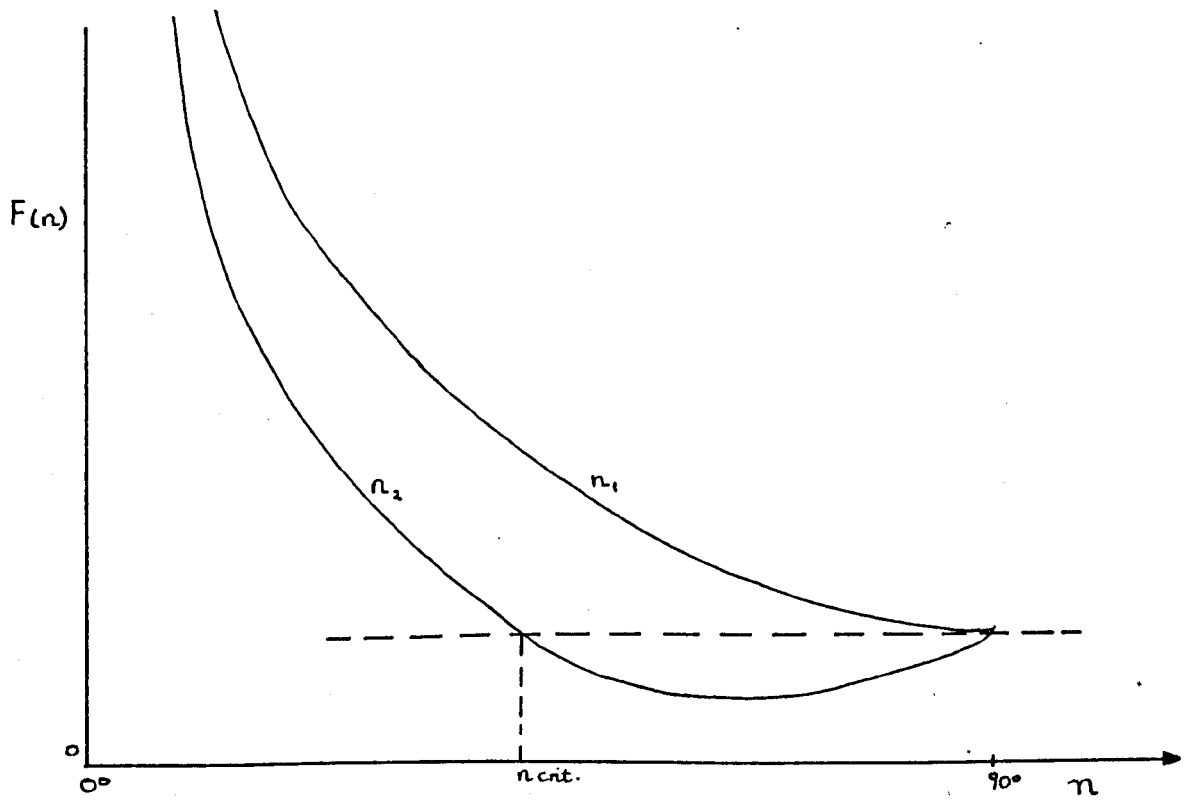


FIG. 3.3. PLOT OF F AGAINST  $n$   $0-90^\circ$

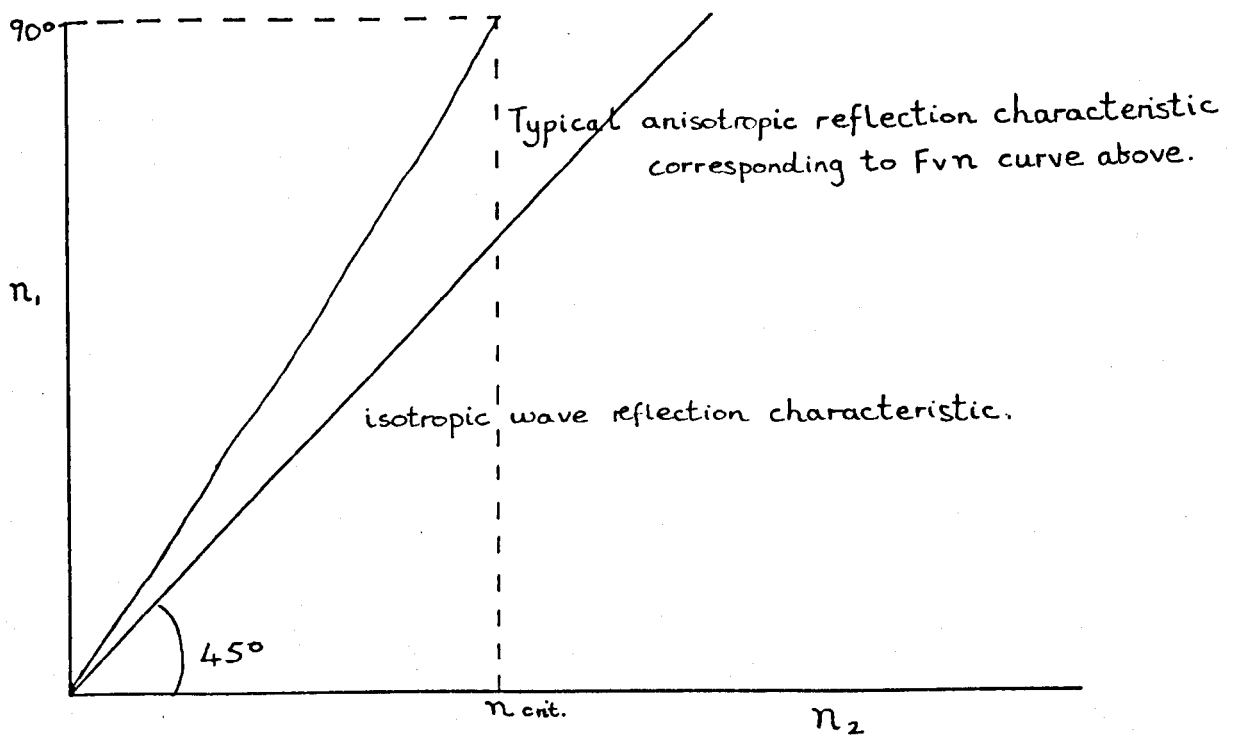


FIG. 3.4. TYPICAL REFLECTION CHARACTERISTIC FROM FIG. 3.3.

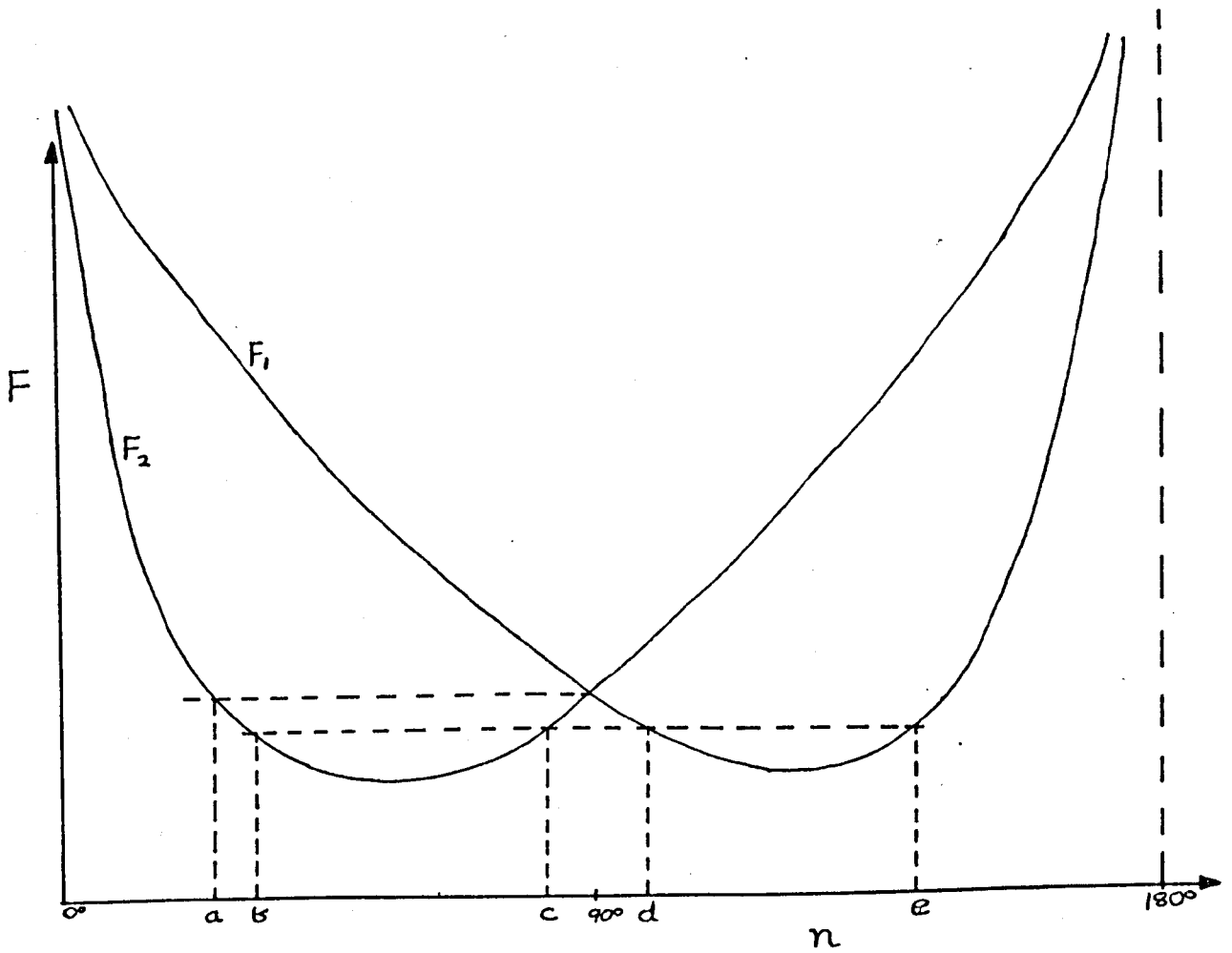


FIG.3.5. PLOT OF  $F$  AGAINST  $n$ ,  $0-180^\circ$

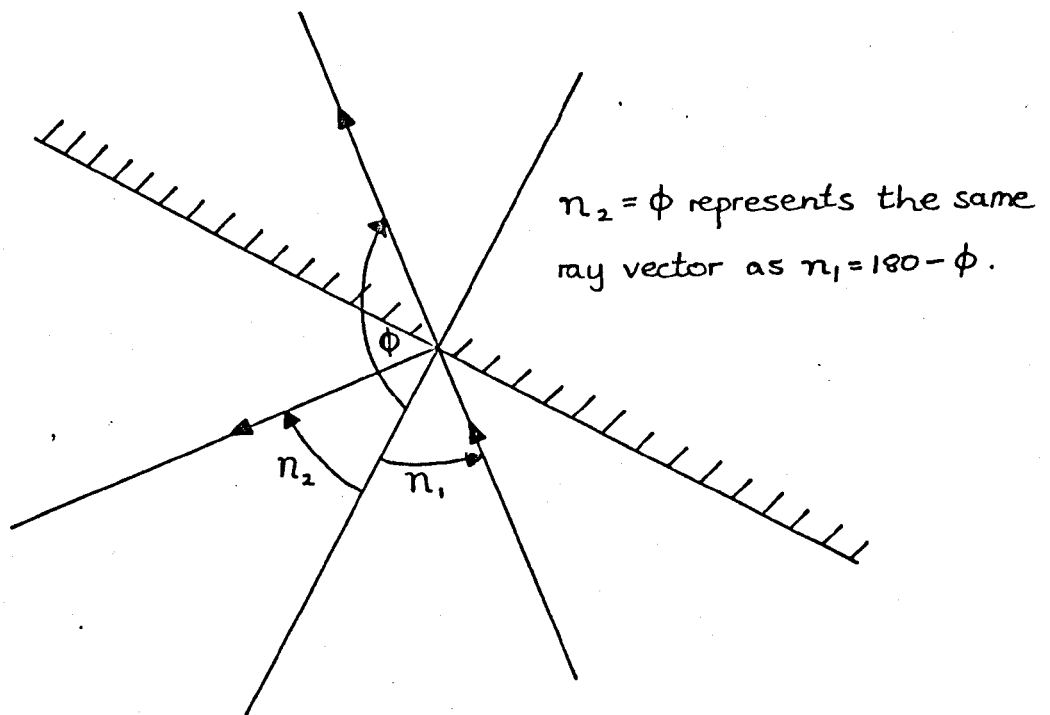


FIG. 3.6. TO ILLUSTRATE THE MEANING OF  $n > 90^\circ$ .

$n_1 = d$  is equivalent to  $n_2 = c$  and  $n_1 = e$  equivalent to  $n_2 = b$ . This would suggest therefore that the "reflected" ray compatible with a ray incident at angle  $b$ , is in fact another incident ray, incident at angle  $c$ .

This is conceivably possible when it is remembered that for anisotropic waves the phase and group velocities are not parallel, and it is the group velocity which governs the reflection of energy.

However, it did not seem possible using a graphical method to determine incident and reflected angle relationships for the group velocity, and so it was decided to try to solve the problem completely analytically, so that phase and group velocity reflection characteristics could be determined in one operation on the computer. This is to be found in the next section, and sheds some light on the anomalies which have appeared above.

### 3.2.3. Analytical method

The method above is rather cumbersome, involving as it does obtaining results from an intermediate graph, but it does illustrate well how the non-symmetrical reflection arises from the anisotropic dispersion.

It is possible, as suggested above, to solve the problem completely analytically, given the dispersion relation, and this method could be used for obtaining the reflection characteristics of any anisotropically propagating two dimensional wave medium. (In three dimensions the incident group and phase velocities need not be in the same plane as the reflected group and phase velocity, and the extra degree of freedom allows the possibility of wave systems splitting on reflection into two normally plane polarised waves each having their own phase and group velocity).

The key to this approach is the appreciation that the component of the wave number vector parallel to the mirror is the

same for both reflected and incident waves. This is obvious from the fact that the parallel components of incident and reflected waves coincide at the mirror itself.

Then, mathematically if the dispersion relation is represented in terms of  $k_q$  and  $k_p$  normal and parallel to the mirror (see fig.3.7) all that remains to be done is, given  $k_p$  and  $\omega$  to solve for  $k_q$ . Those solutions with no imaginary part will represent the possible  $k_q$  and normally there will be two, one positive and the other usually negative representing the incident and reflected waves though more than two is not impossible, which would indicate more than one possible reflected wave. Thus, the whole solution can be computed, along with group velocity for incident and reflected rays, and the reflection characteristics of both phase and group velocity can be plotted directly. We take (2.14) as the dispersion relation, so that the results will be applicable to the practicably realisable case.

$$\omega^2 = \frac{[(\rho_1 - \rho_2)g + jB \cos^2 \theta + \alpha k^2] k}{(\rho_1 + \rho_2)}$$

in  $k_p, k_q$  space, this becomes

$$\omega^2 = \left[ (\rho_1 - \rho_2)g + jB \frac{(k_p \cos \alpha - k_q \sin \alpha)^2}{k^2} + \bar{\alpha} k^2 \right] \frac{k}{(\rho_1 + \rho_2)}$$

where  $k = \sqrt{k_p^2 + k_q^2}$  and surface tension is now represented by  $\bar{\alpha}$ .

This may finally be represented as a polynomial in  $k_q$  :-

$$\sum_{n=0}^8 b_n k_q^n = 0$$

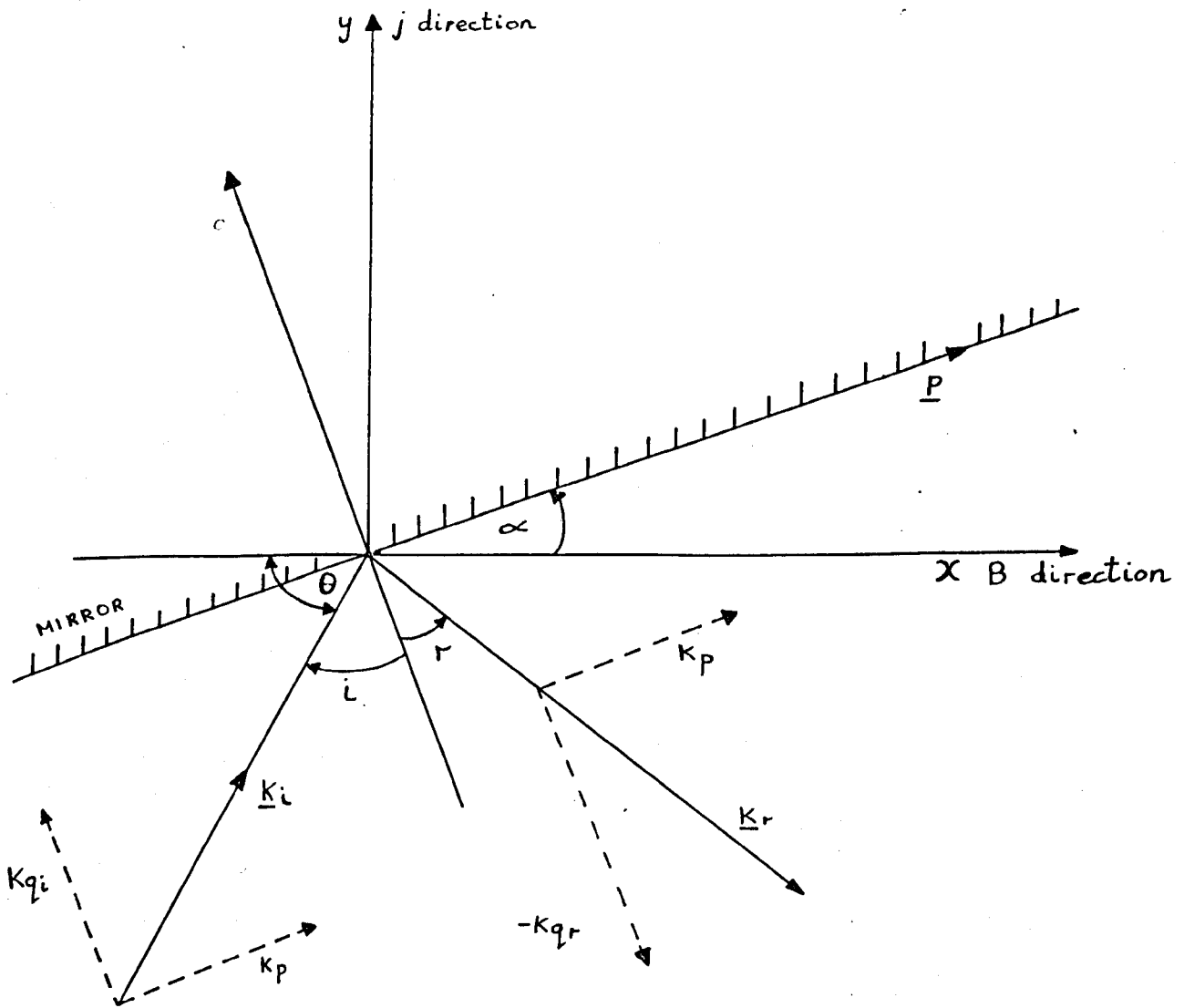


FIG.3.7. NOTATION FOR ANALYTICAL SOLUTION OF REFLECTION PROBLEM

where,

$$b_8 = z_8$$

$$b_7 = 0$$

$$b_6 = 4z_8 k_p^2 + z_6 + z_{42}$$

$$b_5 = z_{41}$$

$$b_4 = 6z_8 k_p^4 + 3z_6 k_p^2 + z_4 + 2z_{42} k_p^2 + z_{22} + j^2 B^2 \sin^4 \alpha$$

$$b_3 = 2z_{41} k_p^2 + z_{21} - 4j^2 B^2 \cos \alpha \sin^3 \alpha k_p$$

$$b_2 = 4z_8 k_p^6 + 3z_6 k_p^4 + 2z_4 k_p^2 + z_{42} k_p^4 + z_2 + z_{22} k_p^2 + 6j^2 B^2 k_p^2 \cos^2 \alpha \sin^2 \alpha$$

$$b_1 = z_{41} k_p^4 + z_{21} k_p^2 - 4j^2 B^2 k_p^3 \cos^3 \alpha \sin \alpha$$

$$b_0 = z_8 k_p^8 + z_6 k_p^6 + z_4 k_p^4 + z_2 k_p^2 + j^2 B^2 k_p^4 \cos^4 \alpha$$

where,

$$z_8 = \bar{\alpha}^2$$

$$z_6 = 2\bar{\alpha} (\rho_1 - \rho_2) g$$

$$z_4 = 2\bar{\alpha} j B k_p^2 \cos^2 \alpha + (\rho_1 - \rho_2)^2 g^2$$

$$z_{41} = -4\bar{\alpha} j B k_p \cos \alpha \sin \alpha$$

$$z_{42} = 2\bar{\alpha} j B \sin^2 \alpha$$

$$z_2 = 2j B g (\rho_1 - \rho_2) k_p^2 \cos^2 \alpha - \omega^4 (\rho_1 + \rho_2)^2$$

$$z_{21} = -4j B g (\rho_1 - \rho_2) k_p \cos \alpha \sin \alpha$$

$$z_{22} = 2j B g (\rho_1 - \rho_2) \sin^2 \alpha$$

The programme used to solve this polynomial will be found in the Appendix.

The programme produces theoretical results in the form of reflection characteristics for wave number vector and group velocity, based on a range of wave number vector incident angles from  $-90^\circ$  to  $+90^\circ$  in  $5^\circ$  steps.

Typical reflection characteristics are shown in fig. (3.8) (c) and (d) corresponding to an experimentally feasible case, and (a) and (b) a more extreme case where surface tension has been ignored to amplify the effect of anisotropy upon the reflection.

The wave number characteristics all pass through the origin, but only for  $\alpha = 0^\circ$  and  $\pm 90^\circ$  are the normal laws of reflection obeyed. There is symmetry about the line  $i = -r$ , for both wave number and group velocity vectors, and the characteristic for  $-\alpha$  is the mirror image of that for  $+\alpha$  in the line  $i = r$ .

It is clear that for  $\alpha$  +ve,  $r$  is sometimes greater than  $90^\circ$  when  $i$  is less, and for  $\alpha$  negative  $-r > 90^\circ$  for  $-i < 90^\circ$ . In some of these cases the corresponding group velocity incident and reflection angles are greater than  $90^\circ$ , representing an impossible situation, and for these the points have not been connected by lines, but there are other cases where the group velocity  $i$  and  $r$  are less than  $90^\circ$ . i.e. it is possible to construct a case where the reflected wave crests look as though they approach the wall. If we then attempt to construct the sort of wave pattern that might be expected between two group velocity rays, fig. (3.9) is the result. Thus given sufficient time, a wide wave train incident on a mirror would result in two interfering wave trains filling the space, but any slight disturbance at a point would be reflected along the group velocity rays.

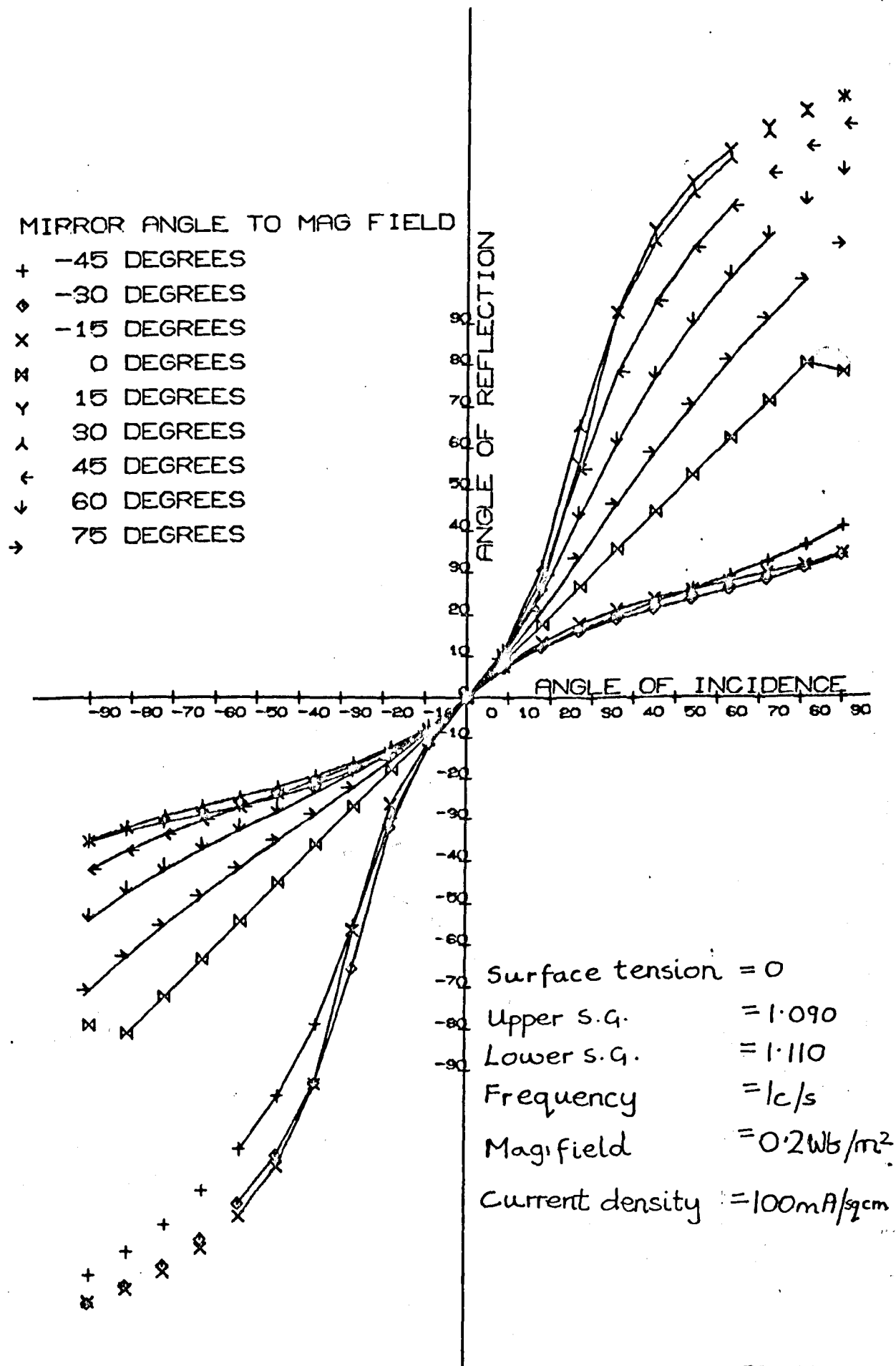


FIG. 3.8.(a) PHASE VELOCITY REFLECTION CHARACTERISTICS.

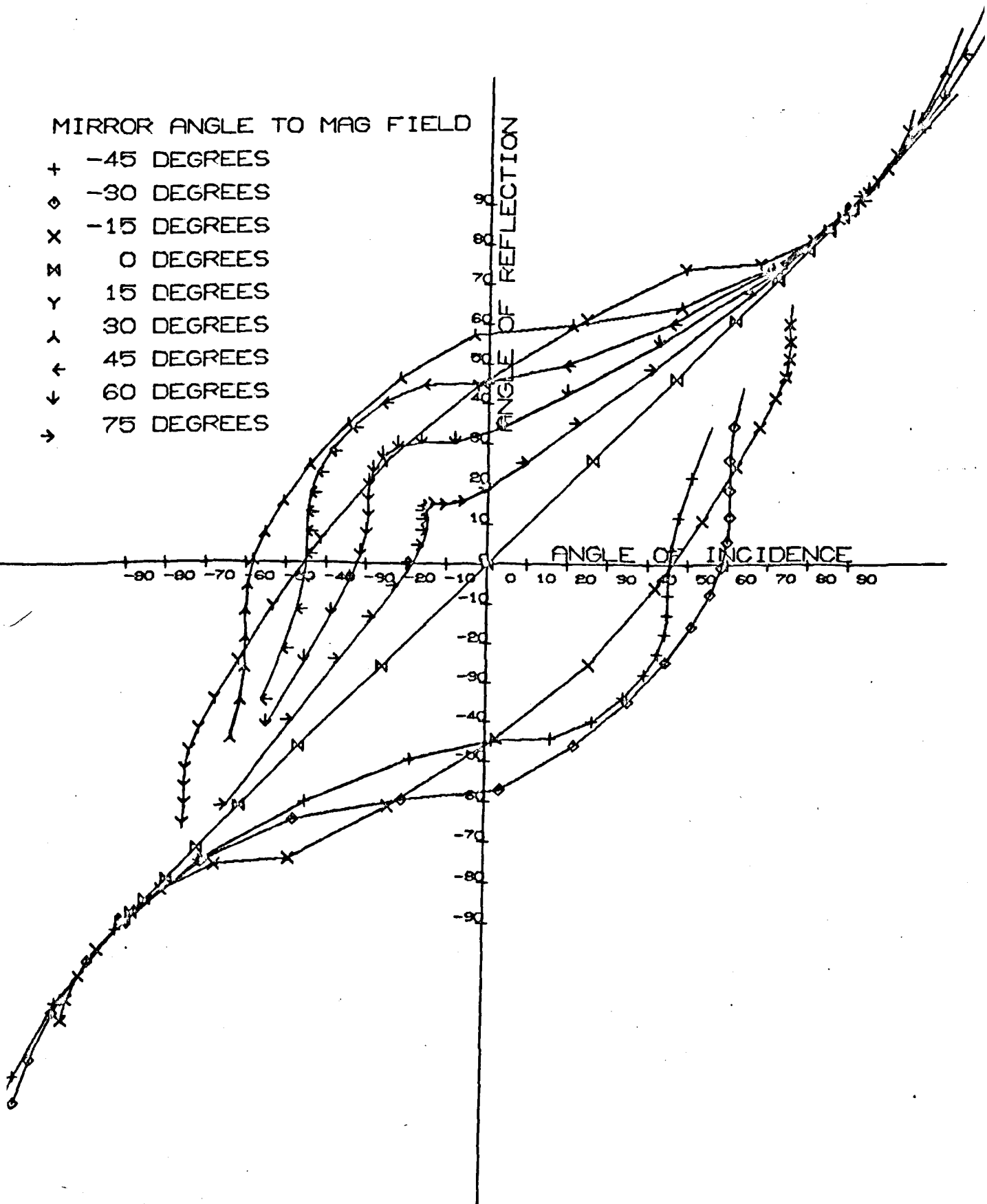
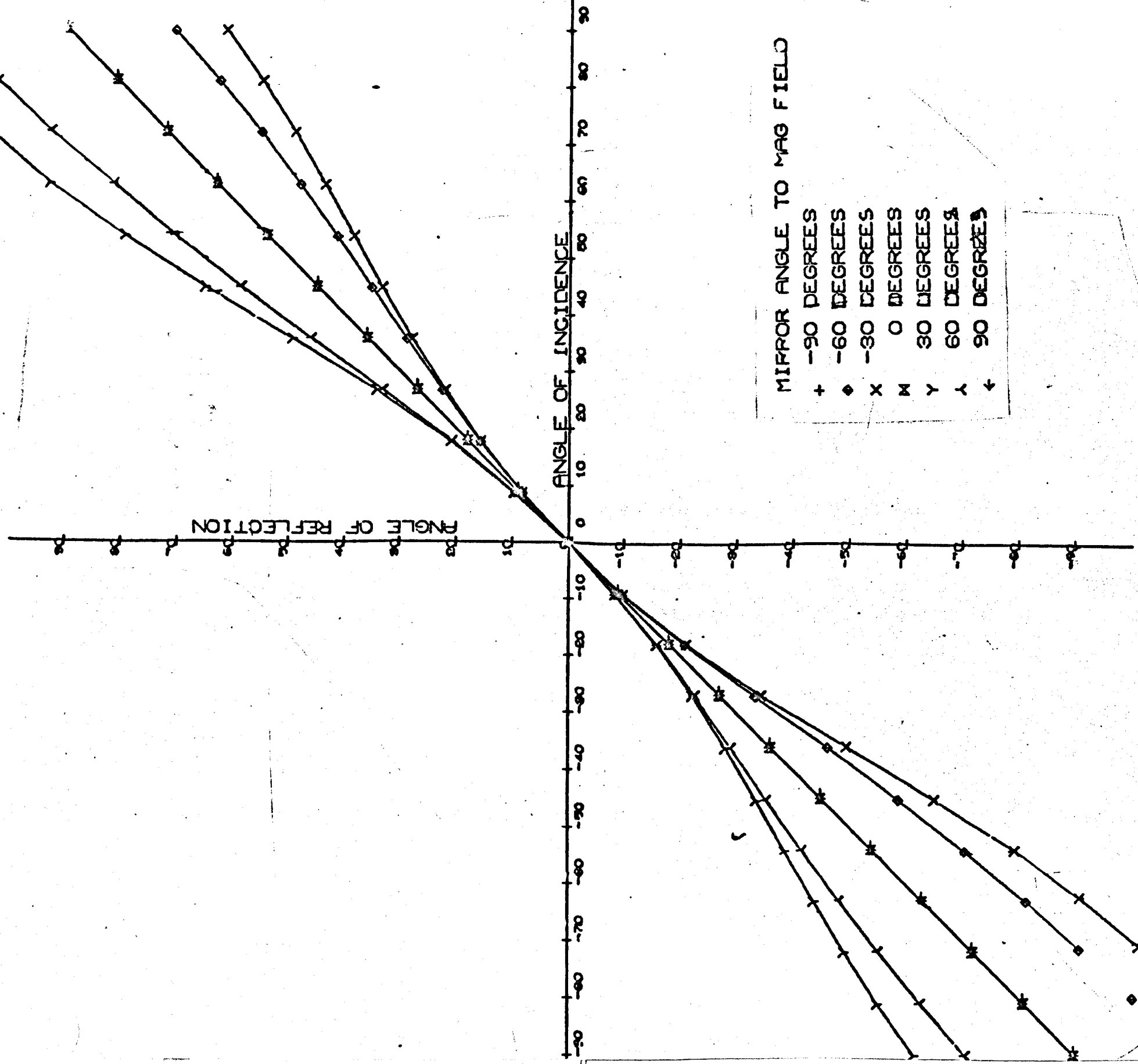


FIG. 38.(b). GROUP VELOCITY REFLECTION CHARACTERISTICS, PARAMETERS as for 3.8(a).



$\alpha = 0.004$  1.110 1.080  
 0.111 0.101  
 $100 \text{ N/A}^2/\text{m}^2$  0.2  $\text{Wb/m}^2$   $\omega = 1 \text{ c/s}$   
 3.8

FIG 3.8(c). As 3.8(a) except  $\alpha = 0.004 \text{ N/m}$ .

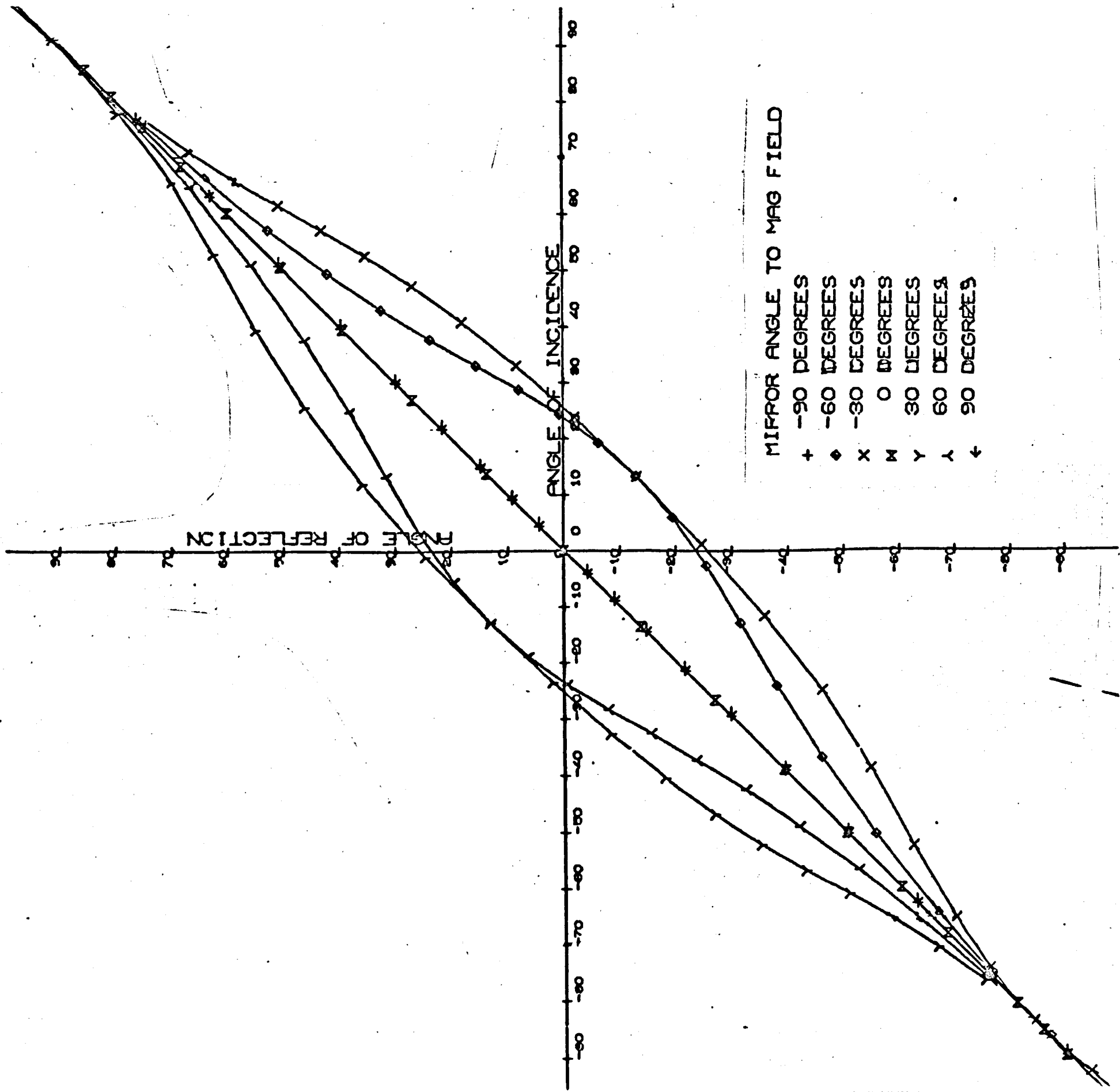
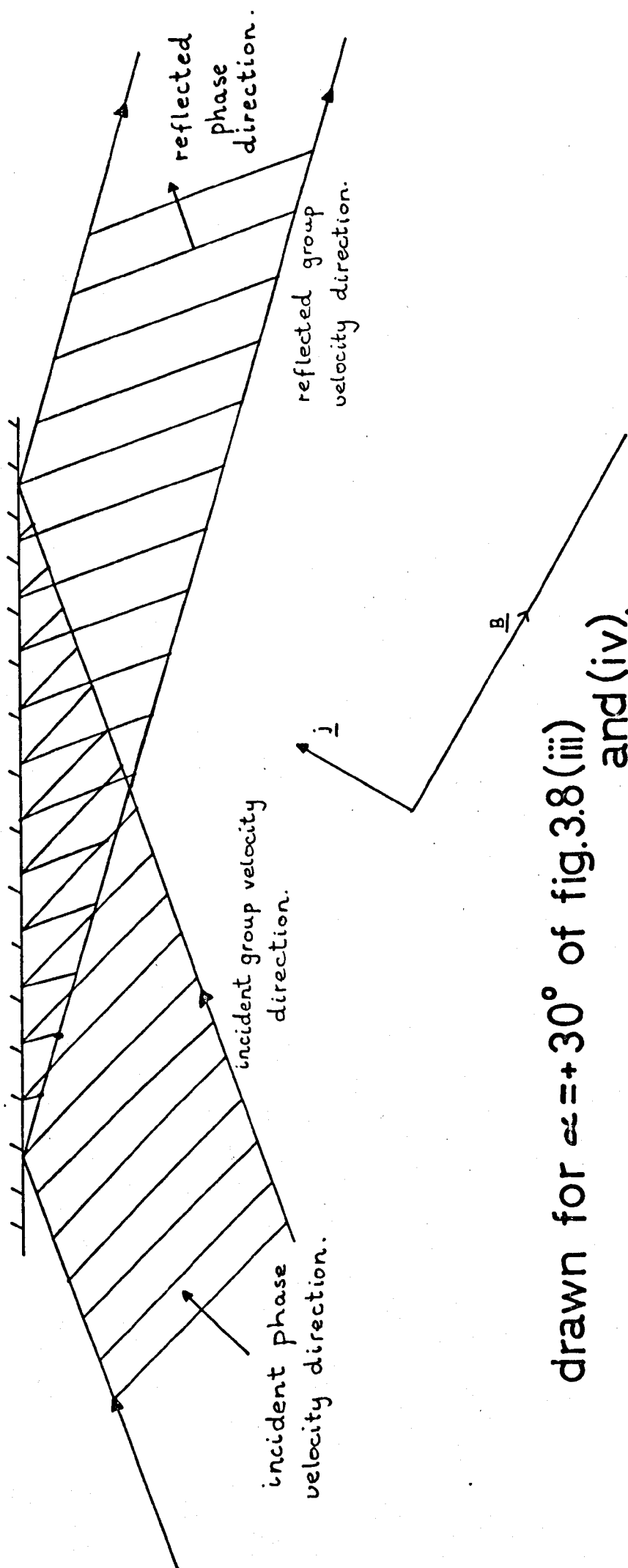


FIG 3.8(d) As 3.8(b) except  
 $\alpha = 0.004 \text{ N/m}$ .



drawn for  $\alpha = +30^\circ$  of fig. 3.8 (iii) and (iv).

FIG. 3.9. WAVE REFLECTION PATTERN WHEN  $r > 90^\circ$ .

If the group velocity characteristics are studied, some interesting points emerge. Firstly for  $|i| = 90^\circ$ ,  $|r| = 90^\circ$  and for  $|i| < 90^\circ$ ,  $|r| < 90^\circ$ . This would be expected from energy considerations, but answers any questions of an anomaly raised in (3.2.1), i.e. all wave energy incident in a given direction has a corresponding reflection direction.

But it can be seen that a lot of points lie in the second and fourth quadrant of the graph, i.e. there is a range of wave number directions for each where the energy is reflected back on the same side of the normal as it is incident. Moreover, in case (b), the square shape of the  $\alpha = 45^\circ, 60^\circ, 75^\circ$  characteristics shows that there is a range of wave numbers where the reflected direction is fairly constant for various incident directions, and another range where small changes in incident direction produce large changes in reflected direction.

Here it has been shown, in theory at least, that these anisotropic surface waves are capable of exhibiting reflection behaviour very different from what is normally suspected of waves. If these phenomena could be demonstrated experimentally, they could provide a useful illustration of the reflection behaviour encountered in other forms of anisotropic waves, such as the behaviour of the 'e' ray in a medium doubly refractive to light rays.

### 3.3. The Initial Value Problem

#### 3.3.1. Analytical solution

This is the problem, given an initial point elevation or impulse at a surface, of determining the subsequent elevation of the whole surface. The ordinary hydrodynamic (O.H.D.) case was

first solved by Cauchy and Poisson and a complete solution of the two dimensional solution using Fourier integrals is to be found in Lamb (238, 239). Stoker (1957) shows how this can be extended to the three dimensional cylindrically symmetrical case, where Bessel functions become a characteristic part of the solution.

However, for the case of anisotropic surface waves, there is no cylindrical symmetry, and  $\nabla^2 \phi = 0$  must be solved in cylindrical polar co-ordinates where  $\frac{\partial^2 \phi}{\partial \theta^2} \neq 0$ . The general solution therefore seemed beyond the scope of this thesis, but it was nonetheless thought worthwhile to attempt to solve the kinematic problem i.e. to plot the shape of the wave pattern at any time without knowing the amplitude.

In the O.H.D. case, after the initial impulse, waves with an infinite range of wave numbers propagate out from the origin, each wave number having the particular frequency required by the dispersion relation, and the energy contained in that wave number travelling with the appropriate group velocity. In the case of simple surface waves, without surface tension, the troughs and crests accelerate away from the source so that at a fixed time the wave number decreases away from the source, and at a fixed place the wave number increases with time.

The kinematic problem is easily solved for the O.H.D. case either by directly applying the principle of stationary phase or using the principle of wave crest kinematics, so that at time  $t$  and distance  $r$  from the origin, waves will be found with wave number  $k$  and frequency  $\omega$  such that  $\omega^2 = gk$  and  $\frac{\partial \omega}{\partial k} = \frac{g}{2\omega} = \frac{r}{t}$

For the M.H.D. surface waves, ignoring surface tension, the problem is almost trivial since the polar plots of group velocity and lines of constant phase are identical and the same for all

frequency. Therefore, the pattern of waves (troughs and crests) to be expected after time  $t$  would be as shown in fig. (3.10), being the pattern of fig. (2.1) repeated concentrically in differing magnitudes such that along the direction where  $\mathbf{j} \times \mathbf{B}$  has no effect, the distribution of wave numbers obeys  $\omega^2 = gk$ ,  $\frac{g}{2\omega} = \frac{r}{t}$ . In the more extreme cases of anisotropy, there will be triangular regions where interference occurs between three different wave numbers at each point.

However, it has already been shown in chapter 2 that for the experimental scale being used, it is impossible to ignore surface tension effects. When they are included, not only is the polar plot of group velocity different from that of the locus of constant phase but it varies with frequency. Thus whilst it is possible to deduce directly from the knowledge of the group velocity as a function of wave number the exact position of wave energy of a given wave number vector, at a given time after the initial elevation, it is not possible to plot lines of constant phase directly from this. In principle it is possible, given the knowledge of  $\mathbf{k}$  everywhere at a given time to obtain the phase  $\phi$  from  $\mathbf{k} = \text{grad}\phi$ , and thence to plot lines of constant phase. But the problem is ill-posed for computational methods, since it is not possible with the methods already developed in chapter 2 for solving the dispersion relation, to set the group velocity magnitude and direction and from it deduce the relevant wave number vector, as would be necessary to obtain  $\mathbf{k}$  at fixed mesh points in a numerical solution. Moreover, since  $\mathbf{k}$  could be double or treble valued in some regions  $\phi$  would be likewise, and this would be difficult, though not impossible to cope with by the method of integrating  $\mathbf{k}$ .

However, the recent work of Hunter (1972), developing the

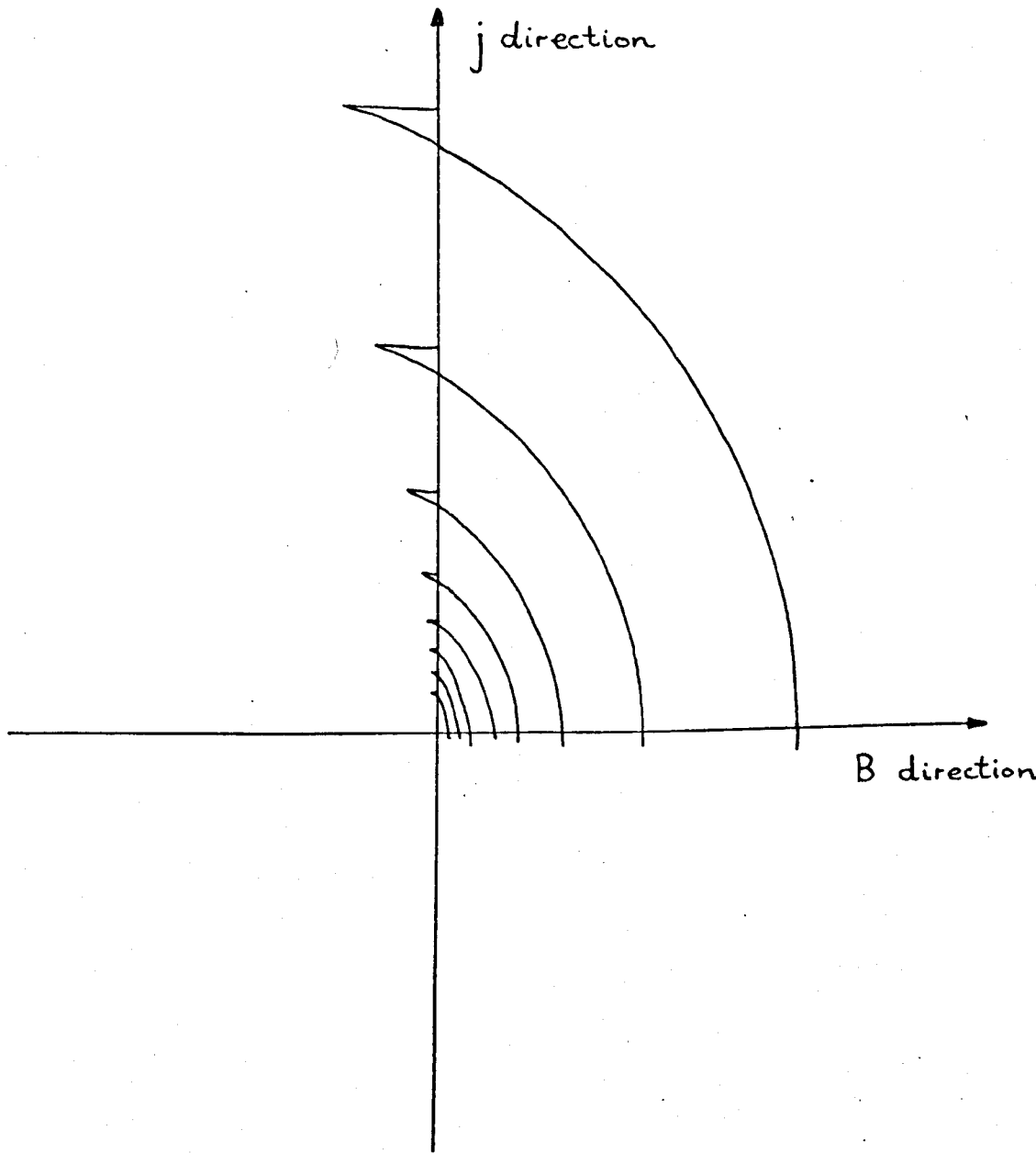


FIG. 3.10. WAVE PATTERN AFTER INITIAL  
DISTURBANCE - IGNORING SURFACE  
TENSION

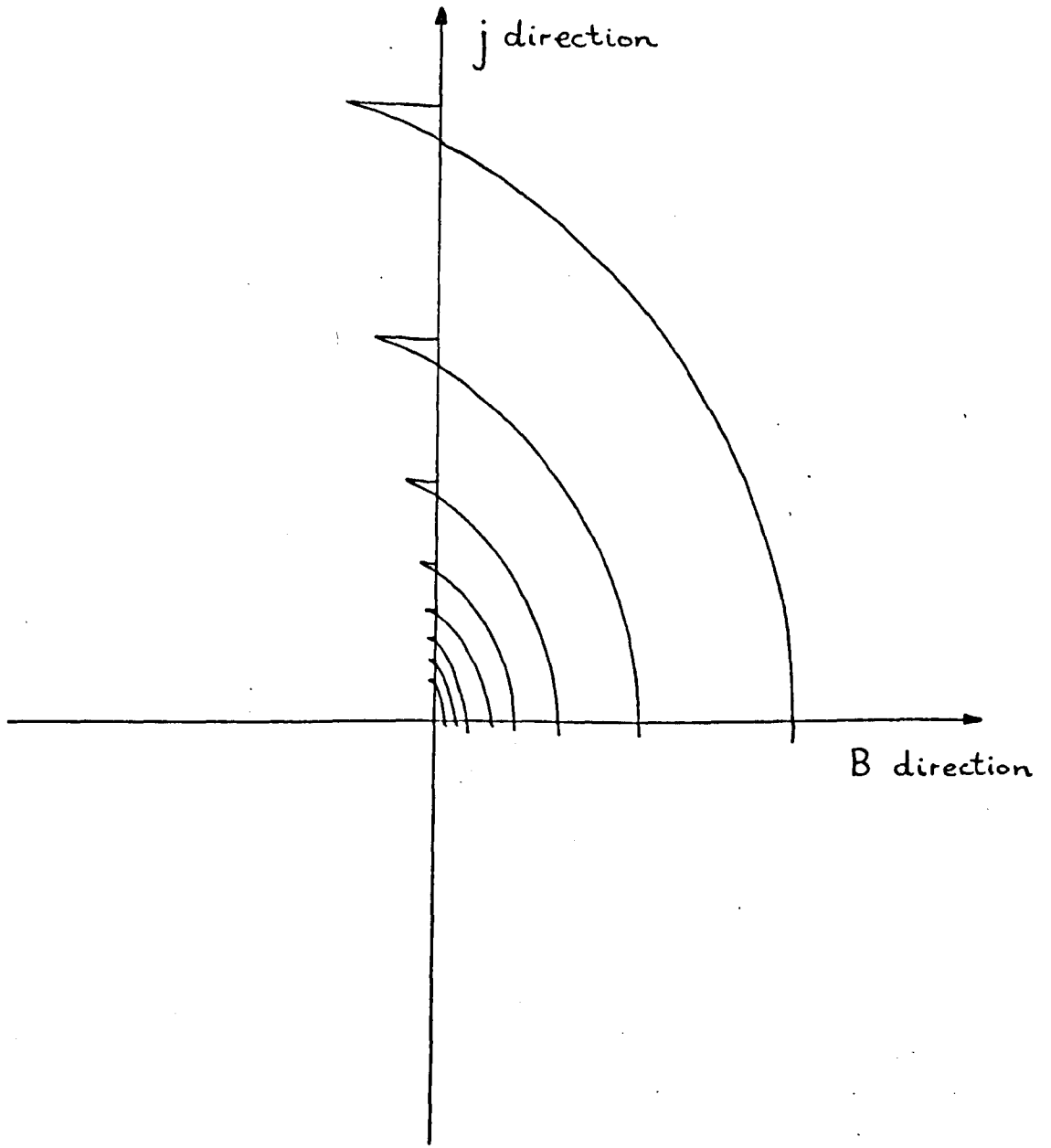


FIG. 3.10. WAVE PATTERN AFTER INITIAL DISTURBANCE - IGNORING SURFACE TENSION.

methods of Whitham, opens up a much more convenient way of directly plotting lines of constant phase.

At its simplest, Hunter points out that given the dispersion relation :-  $\omega = \omega(k_i, x_i)$  with  $k_i = \frac{\partial \phi}{\partial x_i}$   $\omega = - \frac{\partial \phi}{\partial t}$

then from the rules of partial differentiation it follows that along a characteristic, i.e. a group velocity ray in wave parlance :-

$$dt = \frac{dx_i}{\frac{\partial \omega}{\partial k_i}} = \frac{-dk_i}{\frac{\partial \omega}{\partial x_i}} = \frac{d\omega}{0} = \frac{d\phi}{-\omega + \sum_{j=1}^2 k_j \frac{\partial \omega}{\partial k_j}} \quad \dots 3.9$$

The first four terms are effectively stating what was expressed in 3.1.2, defining the locus of group velocity rays, the variations of  $\underline{k}$  along them, and the constancy of  $\omega$  along them. It is the final term in  $d\phi$  which makes it possible to include  $\phi$  directly in equations from which the loci for constant  $\phi$  at a given time may be obtained.

Now assuming the medium is homogeneous, i.e.  $\frac{\partial \omega}{\partial x_i} = 0$  then  $\underline{k}$  as well as  $\omega$  is constant along the group lines.

Thus eq. (3.9) can be integrated directly and

$$t = \frac{x_i}{\frac{\partial \omega}{\partial k_i}} = \frac{\phi}{-\omega + \sum_{j=1}^2 k_j \frac{\partial \omega}{\partial k_j}} \quad \dots 3.10$$

with the starting condition that all  $\phi$  are found at  $x_i = 0$  when  $t = 0$

$$\text{Now } \omega = \sqrt{\left[ (\rho_2 - \rho_1) g k + j B \frac{k_x^2}{k} + \alpha k^3 \right] / (\rho_1 + \rho_2)} \quad \dots 3.11$$

where we assume  $\underline{j}$  and  $\underline{B}$  mutually perpendicular and horizontal,  $k_x$  in the  $\underline{B}$  direction and  $\underline{j}$  positive resulting in  $\underline{j} \times \underline{B}$  acting downwards.

After differentiation, and subsequent substitution of

$$\tan \theta = \frac{k_y}{k_x}, \text{ eqs. (3.10) and (3.11) give :-}$$

$$\frac{t}{2\omega} = \frac{x(\rho_1 + \rho_2)}{(\rho_2 - \rho_1)g \cos \theta + 2jB \cos \theta - jB \cos^3 \theta + 3\alpha k^2 \cos \theta} \dots 3.12$$

$$= \frac{y(\rho_1 + \rho_2)}{(\rho_2 - \rho_1)g \sin \theta - jB \cos^2 \theta \sin \theta + 3\alpha k^2 \sin \theta} \dots 3.13$$

$$= \frac{\phi(\rho_1 + \rho_2)}{-2\omega^2(\rho_1 + \rho_2) + (\rho_2 - \rho_1)gk + jBk \cos^2 \theta + 3\alpha k^3} \dots 3.14$$

Substituting for  $\omega$ , and rearranging, eq. (3.14) becomes a polynomial in  $k$ .

$$\sum_{n=0}^5 k^n a_n = 0$$

where  $a_5 = \frac{t^2 \alpha^2}{\rho_1 + \rho_2}$

$$a_4 = 0$$

$$a_3 = -2t^2 \alpha [(\rho_2 - \rho_1)g + jB \cos^2 \theta] / (\rho_1 + \rho_2)$$

$$a_2 = -4\phi^2 \alpha$$

$$a_1 = t^2 [(\rho_2 - \rho_1)g + jB \cos^2 \theta]^2 / (\rho_1 + \rho_2)$$

$$a_0 = -4\phi^2 [(\rho_2 - \rho_1)g + jB \cos^2 \theta]$$

Thus at a given time  $t$ , for a given line of constant phase  $\phi$ ,  $k$  may be obtained for various  $\theta$ , and from  $k$  and  $\theta$ ,  $\omega$  is obtained. Then substituting the values of  $k$ ,  $\theta$  and  $\omega$  in eqs. (3.12) and (3.13) at time  $t$  the location  $(x, y)$  is obtained of the point on the line of constant phase  $\phi$  having a wave number in the  $\theta$  direction.

In this way, varying  $\theta$  between 0 and  $\frac{\pi}{2}$ , and reflecting the results in the axes, all possible values of  $k$  are covered, with no ambiguity in areas where  $k$  is double or treble valued, and by varying  $\phi$  in steps of  $\pi$  from  $\pi$  upwards, a true picture of the shape of troughs and crests (or more strictly of the lines of zero displacement) is obtained from an economic number of computer calculations. Another distinct advantage over the integration of  $k$  method is that the lines can be plotted directly, from the  $(x,y)$  values, instead of contour plotting in a  $\phi$  field defined only at discrete points.

The computer was programmed to follow the above procedure, (see Appendix) the only difficulty being to check what the five different roots of the polynomial were. Complex and negative roots were discarded as being of no physical significance, but if more than <sup>one</sup> purely real, positive root was found, it meant that there must be more than one closed loop in the locus of constant phase. This is conceivably possible with the introduction of surface tension.

### 3.3.2. Computational results

A programme was run on the computer (see Appendix) to obtain lines of constant phase due to a point impulse to a mercury surface, with surface tension =  $0.5\text{N/m}$ ,  $j = 5 \times 10^5 \text{ A/m}^2$  and  $B = 0.2 \text{ Wb/m}^2$ ,  $\underline{j} \times \underline{B}$  acting upwards. Patterns were obtained for time  $t = 1, 2, 3, 4$  secs. after the initial impulse, for ten phase values,  $\phi = \pi, 2\pi, \dots, 10\pi$  and these are shown in fig. (3.11), drawn full scale with 1/100 scale inset. In fact, since three real positive roots to the polynomial occurred in most cases, it was found difficult to plot the results directly by computer, and figs. (3.11) and (3.12) were drawn by hand from the computed values of rectangular co-ordinates  $x$  and  $y$ . It will be seen that there is a low frequency, large

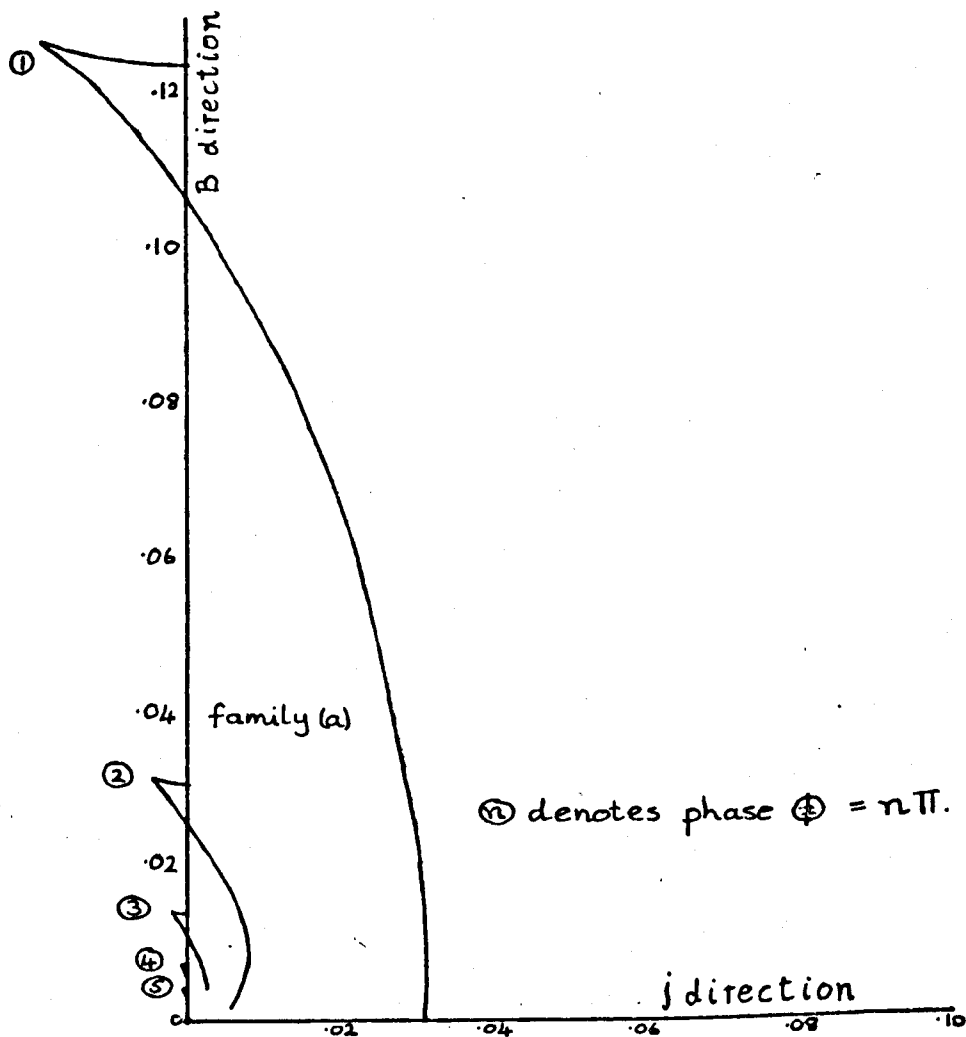


FIG. 3.11. CONSTANT PHASE LINES AFTER INITIAL IMPULSE.

a)  $t = 1 \text{ sec.}$

FIG. 3.11(b),  $t = 2$  secs.

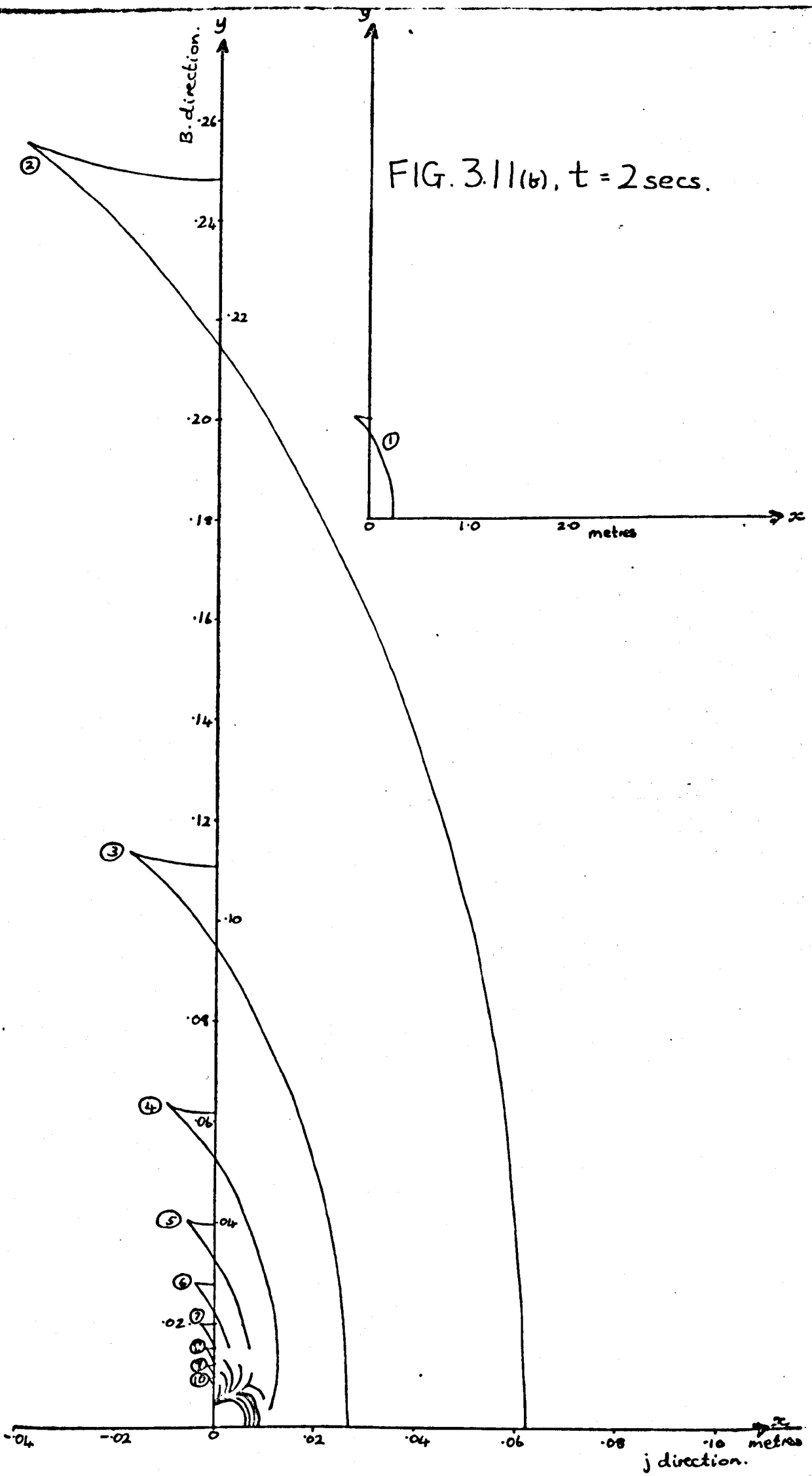


FIG. 3.11(a),  $t = 3$  secs.

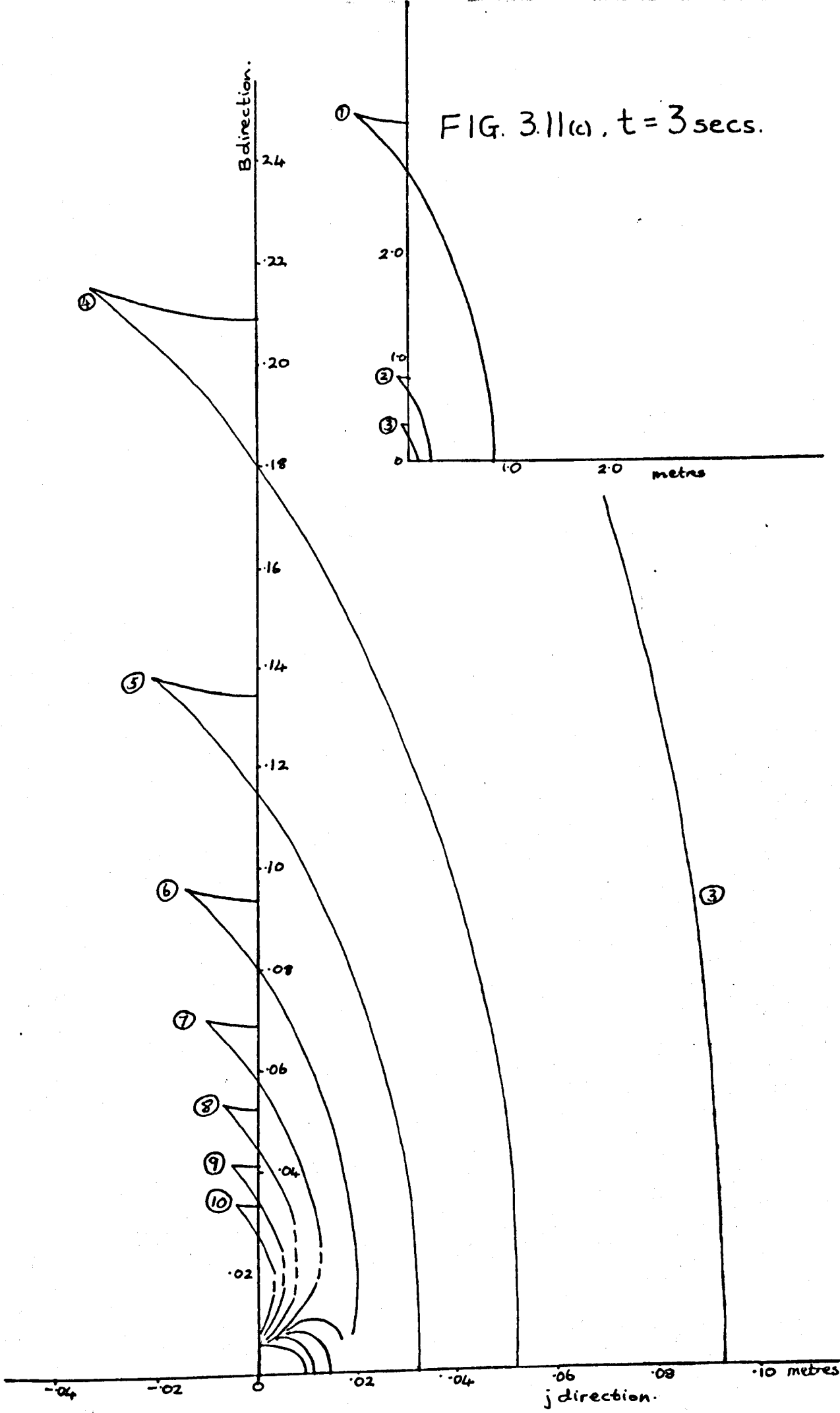
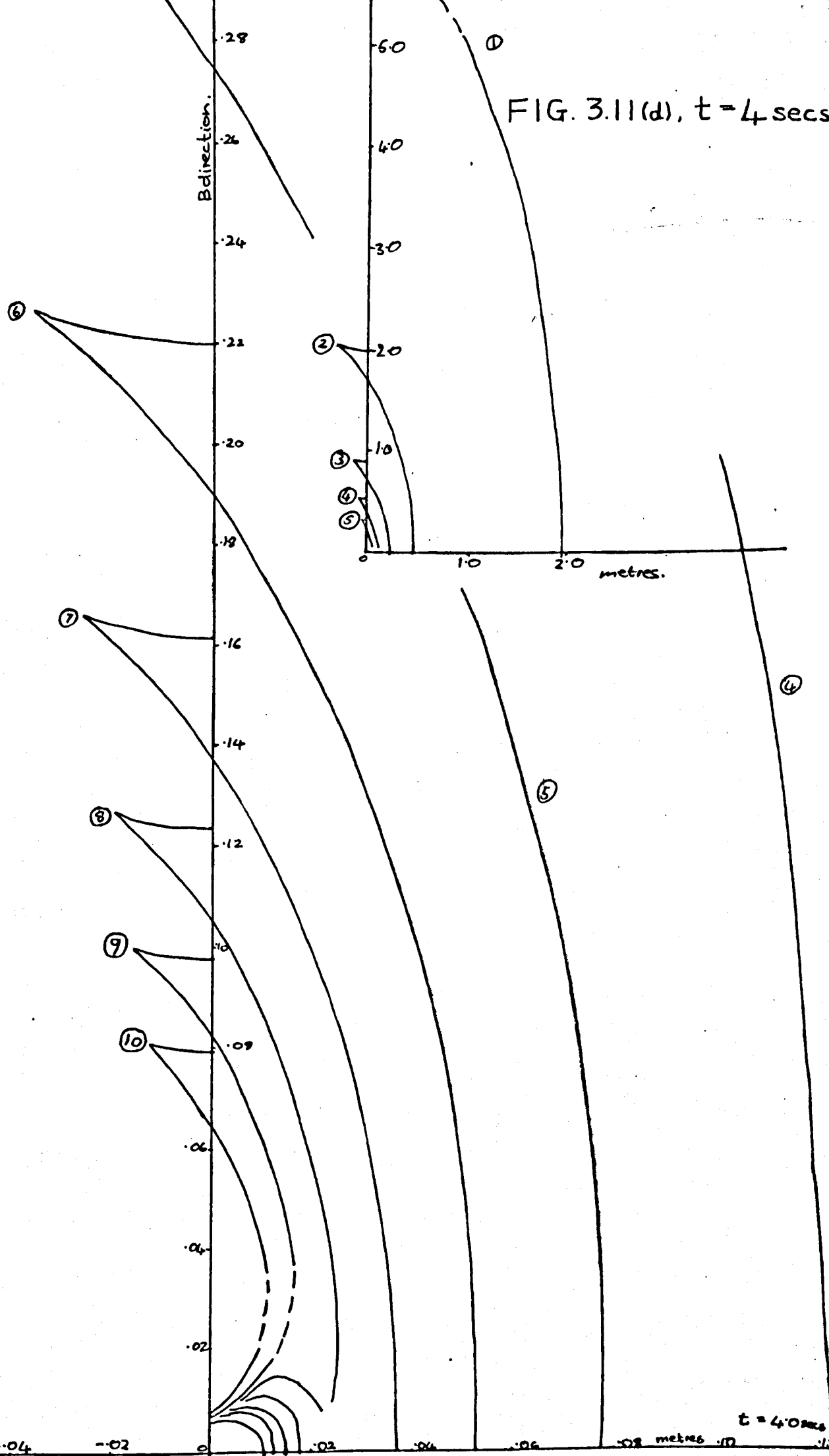


FIG. 3.11(d),  $t = 4$  secs.

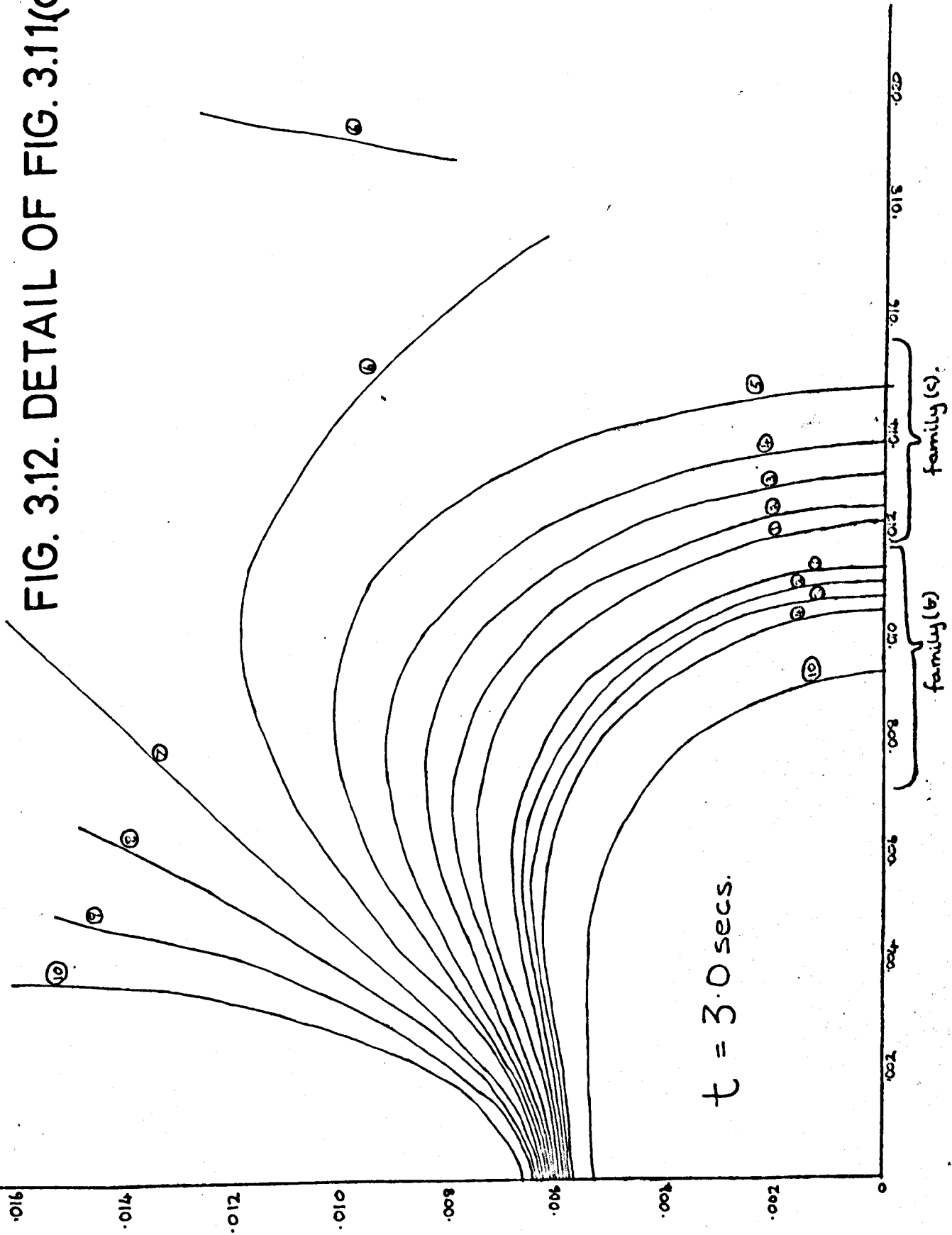


wavelength family (a) of curves, which are virtually unaffected by surface tension, and propagate rapidly away from the source, the lowest phases being the fastest, with lowest frequency. Then there are two families of higher frequency curves, which propagate much more slowly away from the source. These are shown, for  $t = 3$ , in more detail in fig. 3.12. Family (b) has the higher phases moving more slowly, and the frequency increases with phase number. Family (c) has  $\phi = \pi$  just outside  $\phi = \pi$  of family (b), but the higher phases travel faster, and frequency decreases with increasing phase number.

Now for  $t = 1$  and 2 secs., family (b) is present for phases  $\pi \rightarrow 10\pi$  and presumably embraces all phases. Families (a) and (c), however, do not contain higher values of  $\phi$ , and at certain other values of  $\phi$  the constant phase curve does not exist for the full range of  $\theta$  values. From the plots, it appears to be highly probable that for these cases, family (a) and (c) coincide into one line, as shown by the dashes. Presumably at any time, there is a maximum  $\phi$  above which only family (b) is present.

These results suggest that an experimental investigation would be fruitful, since for family (a) of constant phase lines the surface tension does not appear to have much effect on the anisotropy. Unfortunately, attempts to run the programme with typical two-fluid data were unsuccessful, the "roots" subroutine failing to find all of the roots of the polynomial. Presumably this was due to badly formed coefficients, and further investigation of the problem should overcome this difficulty. It may simply have been that the time  $t$  for which results were required was too small, and separation into discrete phase lines had not occurred.

FIG. 3.12. DETAIL OF FIG. 3.11(c).



### 3.4. The Refraction of Anisotropic Surface Waves

#### 3.4.1. The problem stated

When a train of waves travels in a medium where the dispersion relation varies with the space co-ordinates, then in general the wave train changes its direction and speed, and consequently lines of constant phase are bent. The simplest physical example of this phenomenon known as refraction is the bending of light waves at the interface between two media - in this case the spatial variation is a discontinuity. An example of a continuously varying medium producing refraction of light is the mirage effect.

In the realm of hydrodynamic surface waves, the refraction effect can be found in the case of long waves in shallow water of varying depth i.e. the sloping beach problem at its simplest, ignoring the added problem which occurs when the depth is so small that the linear approximation no longer holds and the waves form peaks and finally break. In the linear case, the dispersion is  $\omega^2 = gkh^2$ , and the wave pattern can easily be discovered by the method following. A review of various methods of dealing with this problem may be found in Stoker (1957) pp.133 - 137.

Clearly, our M.H.D. anisotropic surface waves present an opportunity for varying the dispersion relation with the spatial co-ordinates, and what makes this worth investigating, when the apparently similar sloping beach problem is already well documented, is the fact that these waves are dispersive with respect to both direction and wave number, so that the group velocity rays are bent in a different way from the phase velocity, by contrast to simple hydrodynamic long waves where phase and group velocity are always equal.

Now to satisfy the basic assumptions made in the theory of anisotropic surface waves and to have no motion in the absence of waves, it is necessary that the undisturbed  $\underline{j} \times \underline{B}$  force be everywhere conservative. It can easily be shown (see chapter 5) that for this to be satisfied, the only possible way of varying the dispersion relation by altering electromagnetic variables is to vary the current density such that  $(\underline{B} \cdot \underline{\text{grad}}) \underline{j} = 0$ .

We shall only consider the case where  $\underline{j}$  and  $\underline{B}$  are imposed perpendicular and horizontal so that the only possible case is where the tank floor slopes in the vertical plane containing  $\underline{j}$  and is level in the vertical plane containing  $\underline{B}$ . see fig.(3.13). Chapter 5 contains further discussion of the geometries possible when  $\underline{j} \cdot \underline{B} \neq 0$  and, though dealing with instabilities, is of course relevant to the case of the waves too. Thus if we take  $\underline{B}$  in the (2) direction and  $\underline{j}$  in the (1) direction, in the notation of fig. (3.14),  $\underline{j} = f(x_1 \text{ only})$

The problem is, then, given  $\underline{j} = f(x_1)$  with sufficient information about the frequency and direction of wave energy entering a given region, to determine the group velocity rays and the lines of constant phase within the region.

#### 3.4.2. The analytical solution

This is a problem where the methods of wave crest kinematics are a very convenient way of finding a solution.

If the simpler dispersion relation is used, ignoring surface tension effects.  $\omega^2 = gk(1 - \gamma \cos^2 \theta)$   
 where  $\gamma = \frac{jB}{\rho g}$  and  $\underline{j} = f(x_1)$ , then in the notation of fig.(3.14)  

$$\omega^2 = g \sqrt{k_1^2 + k_2^2} \left( 1 - \frac{\gamma(x_1) k_2^2}{k_1^2 + k_2^2} \right) \quad \dots 3.15$$

In two-dimensional space, eqs. (3.7) and (3.8) which define the

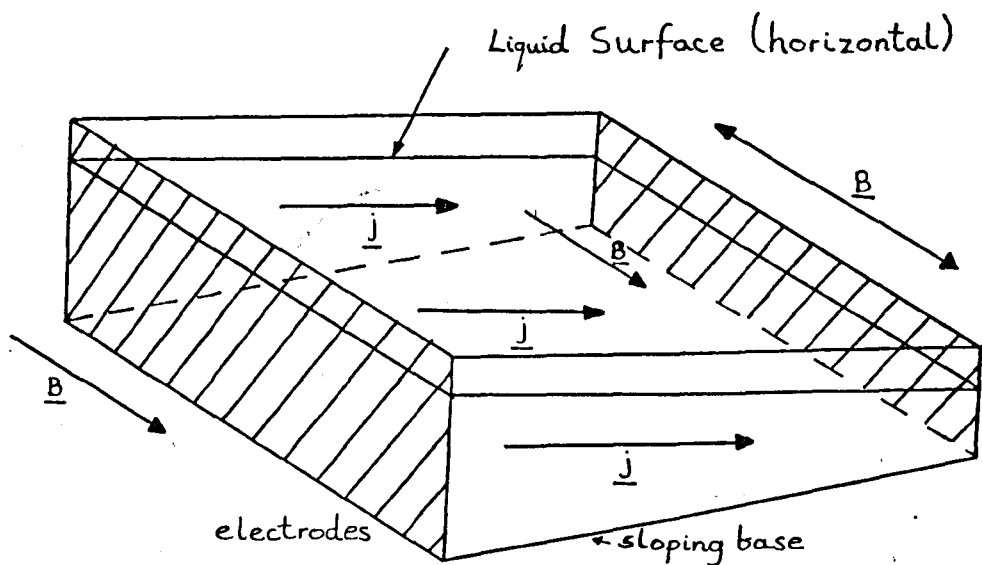


FIG.3.13. LAYOUT OF A TYPICAL SITUATION WHERE REFRACTION COULD OCCUR.

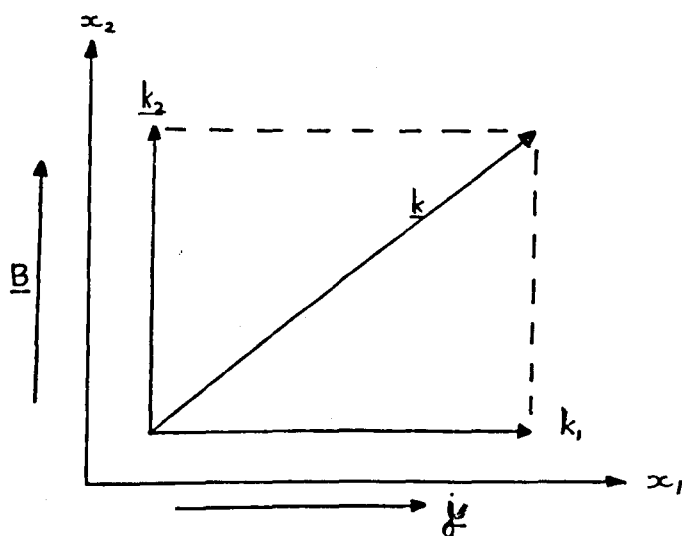


FIG.3.14. NOTATION FOR REFRACTION PROBLEM

variation of  $\underline{k}$  along a group velocity ray, become :-

$$\frac{dx_1}{dt} = \frac{\partial \omega}{\partial k_1}, \quad \frac{dx_2}{dt} = \frac{\partial \omega}{\partial k_2} \quad \text{define the group velocity ray...3.16}$$

$$\text{and along it :- } \frac{dk_1}{dt} = -\frac{\partial \omega}{\partial x_1}, \quad \frac{dk_2}{dt} = -\frac{\partial \omega}{\partial x_2} \quad \dots 3.17$$

$$\text{Now } \frac{\partial \omega}{\partial k_1} = \frac{g}{2\omega k} \left\{ k_1 + \frac{k_2^2 k_1 \gamma}{k^2} \right\} \quad \dots 3.18$$

$$\frac{\partial \omega}{\partial k_2} = \frac{g}{2\omega k} \left\{ k_2 - \frac{(2k_2 k^2 - k_2^3) \gamma}{k^2} \right\} \quad \dots 3.19$$

Time does not appear explicitly in the dispersion relation, so that a group velocity ray, defined from a given point in a given direction, will always be the same for a given frequency, so time may usefully be eliminated from equations (3.16) to obtain the equation for the group velocity rays in  $(x_1, x_2)$  space i.e.

$$\frac{dx_1}{dx_2} = \frac{\frac{\partial \omega}{\partial k_1}}{\frac{\partial \omega}{\partial k_2}} = \frac{k_1 k^2 + \gamma k_2^2 k_1}{k_2 k^2 + \gamma(k_2^3 - 2k_2 k^2)} \quad \dots 3.20$$

Similarly, if there is a steady state situation, where waves are produced continuously by an energy source of constant frequency, time may be eliminated from eqs. (3.17), using (3.16), to define  $\underline{k}$  in  $(x_1, x_2)$  space.

$$\text{i.e. } \frac{dk_1}{dx_1} = \frac{\frac{dk_1}{dt}}{\frac{dx_1}{dt}} = -\frac{\frac{\partial \omega}{\partial x_1}}{\frac{\partial \omega}{\partial k_1}}$$

$$\text{Similarly } \frac{dk_1}{dx_2} = -\frac{\frac{\partial \omega}{\partial x_1}}{\frac{\partial \omega}{\partial k_2}}, \quad \frac{dk_2}{dx_1} = -\frac{\frac{\partial \omega}{\partial x_2}}{\frac{\partial \omega}{\partial k_1}}$$

$$\text{and } \frac{dk_2}{dx_2} = -\frac{\frac{\partial \omega}{\partial x_2}}{\frac{\partial \omega}{\partial k_2}}$$

$$\text{Now } \frac{\partial \omega}{\partial x_1} = \frac{-g k^2 \frac{\partial \gamma}{\partial x_1}}{2\omega k} \quad \text{and } \frac{\partial \omega}{\partial x_2} = 0 \quad \text{since } \frac{\partial \gamma}{\partial x_2} = 0$$

Hence  $k_2$  is constant along a group velocity ray, and  $k_1$  is

governed by 
$$\frac{dk_1}{dx_1} = \frac{k_2^2 k^2}{k_1 k^2 + \gamma k_2^2 k_1} \frac{\partial \gamma}{\partial x_1} \quad \dots 3.21$$

$$\frac{dk_1}{dx_2} = \frac{k_2^2 k^2}{k_2 k^2 + \gamma (k_2^3 - 2k_2 k^2)} \frac{\partial \gamma}{\partial x_1} \quad \dots 3.22$$

Equations 3.20, 3.21, 3.22 can be solved numerically on the computer for the group velocity rays and wave number, given the frequency and initial direction of the wave energy, and the nature of  $\gamma(x_1)$ . In the next section, two cases will be solved, the typical plane wave case where the energy source is a line oscillation, and the point source case where energy is assumed to radiate equally in all directions.

If the energy were propagated with a spectrum of frequencies, as in the initial value problem, the solution would be more difficult. Eqs. (3.20), (3.21), (3.22) are independent of  $\omega$ , but in fact  $\omega$  governs the value of  $k$  at the source i.e. the starting point for the numerical integration. Hence the most straightforward, if laborious, method of solving for  $\underline{k}$  throughout the area would be to consider discrete values of  $\omega$  across the spectrum, solving to find the pattern of group velocity rays appropriate to each and then to obtain the location and wave numbers of energy at a given  $\omega$ . eq. (3.17) would be used to integrate along the appropriate group ray.

It should usually be possible to draw the lines of constant phase from a knowledge of wave number direction and magnitude at discrete points, integrating by eye. To plot lines of constant

phase directly, a method based on Hunter's results as in §3.3, would need to be adopted.

### 3.4.3 The numerical solution

The actual programmes will be found in the Appendix. The numerical methods used are described below.

#### A. Line source producing initially plane wave front

The area is conceived as a mesh of  $i \times j$  points, with  $i$  group velocity rays, each starting from the source line, evenly spaced, and each ray being defined in space, along with values for  $k_1$  and  $k_2$ , at  $j$  points along its length.

Each ray is traced in turn in the following way :-

Having established the location  $(x_{1,i,1}, x_{2,i,1})$  of the starting point  $p_{i,1}$  of ray  $i$  (see fig. (3.15)) the magnitude of the wave number at  $p_{i,1}$  can be obtained directly from  $\omega^2 = gk(1 - \gamma(x_{1,i,1}) \cos^2 \theta)$

where  $\theta$  is the angle between  $\underline{k}$  (initially normal to the source line) and the  $\underline{B}$  direction, and this is in fact the slope  $\tan^{-1} a$  of the source line  $x_2 = a x_1 + b$ .

Hence  $k_{1,i,1}$  and  $k_{2,i,1}$  may be found. Hence from (3.20) the

direction of the group velocity ray at  $p_{i,1}$  may be found.

If  $\left| \frac{dx_1}{dx_2} \right| < 1$  an increment  $p$  in  $x_2$  is chosen.

Hence, taking this condition,  $x_{2,i,2} = x_{2,i,1} + p$

and  $x_{1,i,2} \approx x_{1,i,1} + p \frac{dx_1}{dx_2} + \frac{p^2}{2} \frac{d^2 x_1}{dx_2^2}$

$\frac{d^3 x_1}{dx_2^3}$  and  $\frac{d^2 x_2}{dx_1^2}$  are easily obtained from

(3.20), (3.21) and (3.22) with  $k_2 = \text{constant}$ .

Then  $k_{1,i,2} = k_{1,i,1} + p \frac{dk_1}{dx_2}$

If  $\left| \frac{dx_1}{dx_2} \right| > 1$  an increment  $p$  in  $x_1$  is chosen, and the

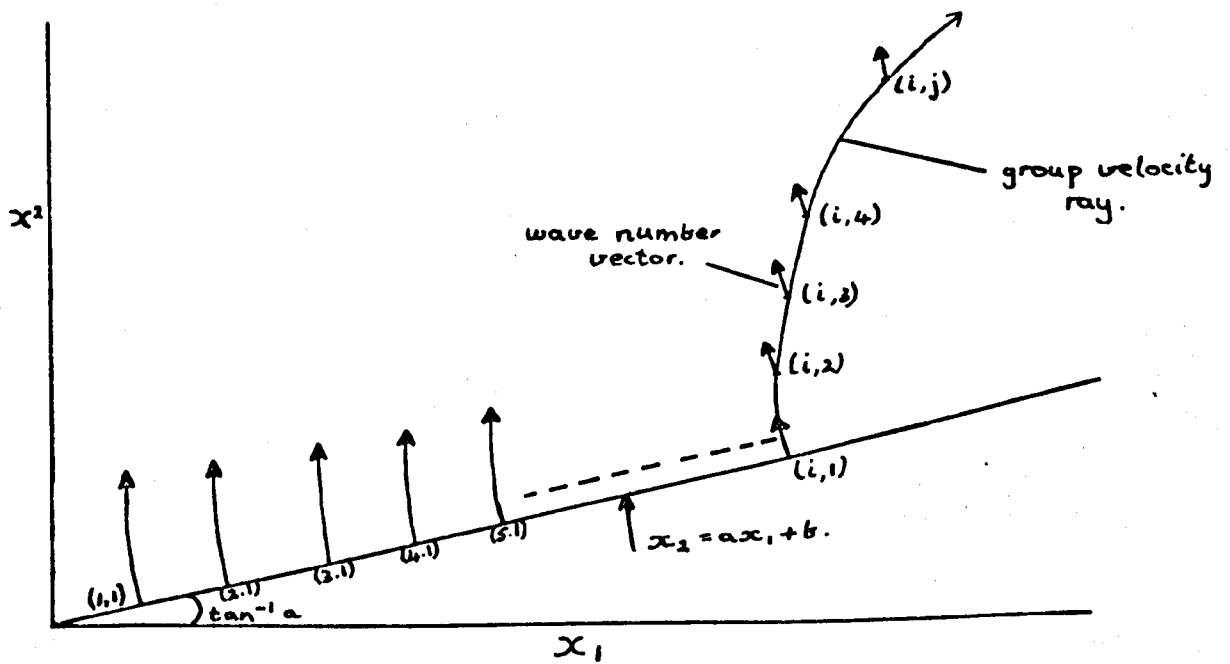


FIG. 3.15. NOTATION FOR NUMERICAL SOLUTION-LINE SOURCE.

derivatives adjusted accordingly. As a check before repeating the whole process to obtain  $p_{i,3}$ ,  $\left(\frac{dx_1}{dx_2}\right)_{i,2}$  which is obtained from the parameters at  $p_{i,2}$  is compared with that predicted

$$\text{by } \left(\frac{dx_1}{dx_2}\right)_{i,1} + p \left(\frac{d^2x_1}{dx_2^2}\right)_{i,1}$$

and if the error is above a stated limit  $\left[ 1\% \text{ of } \left(\frac{dx_1}{dx_2}\right)_{i,1} \right]$

the step is re-calculated with an increment of  $\frac{p}{2}$ , and this increment is successively halved until a tolerable error is reached. In this case, further steps are made with starting increments of  $\frac{p}{2}$ , but not recorded for plotting and printout until the total co-ordinate distance from the previously recorded point is at least  $p$ , and only then is the point  $p_{i,2}$  established and the process continued to find  $p_{i,3}$ . The final result is a series of points spaced approximately  $p$  apart along the ray.

By this method, it is hoped to keep the plotting of the rays within a possible maximum error of slope of 1% of  $45^\circ$ , i.e.  $\frac{1}{2}^\circ$  approximately. This is essential, since as the differential equations which form the basis of the numerical solution are defined along the rays, there is no chance of cross checking between rays, except by visual observation of obvious 'stray' rays appearing in the plot-out.

Special provision is made in the programme for the case where the wave number at a point is parallel to the  $x_2$  axis, since with  $k_1 = 0$ , (3.21) becomes infinite, although it is not needed in the solution for this particular point.

Figs. (3.16) and (3.17) are typical plot-outs, for linear and quadratic functions of  $\gamma(x_1)$ . The results are

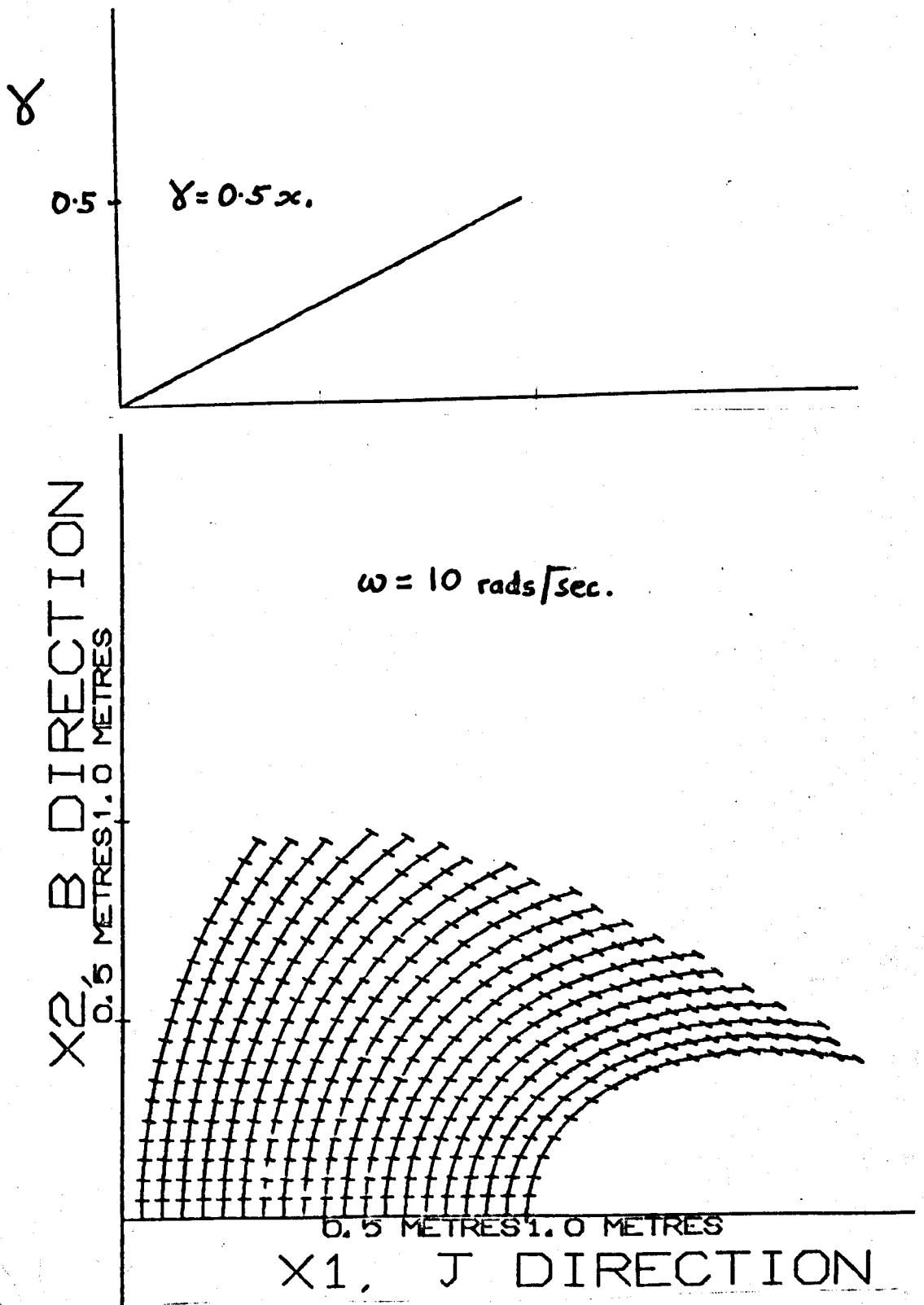


FIG. 3.16(a). COMPUTED PLOTS OF GROUP RAYS, LINE SOURCE LINEAR VARIATION OF  $\gamma$ . (short lines are normal to phase velocity at each point).

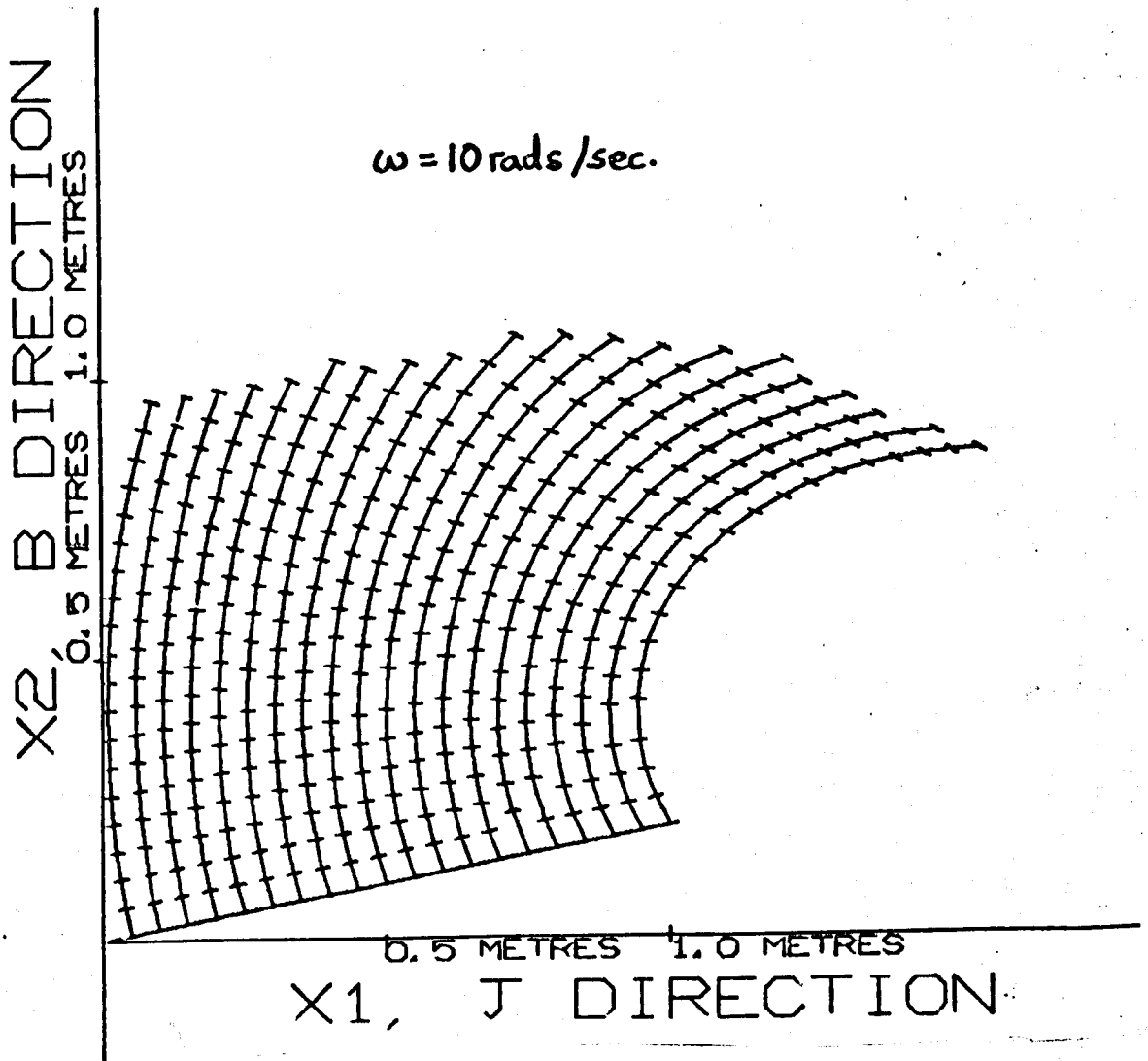
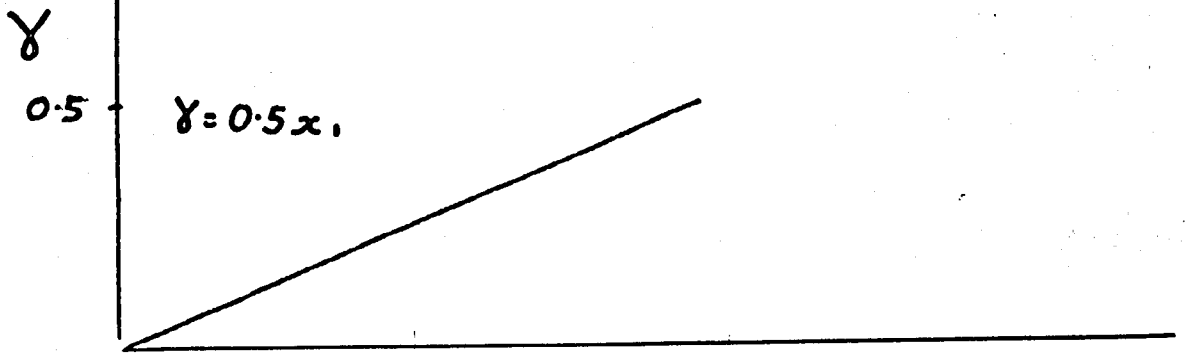


FIG. 3.16(b) COMPUTED PLOTS OF GROUP RAYS - LINE SOURCE LINEAR VARIATION OF  $\gamma$ .

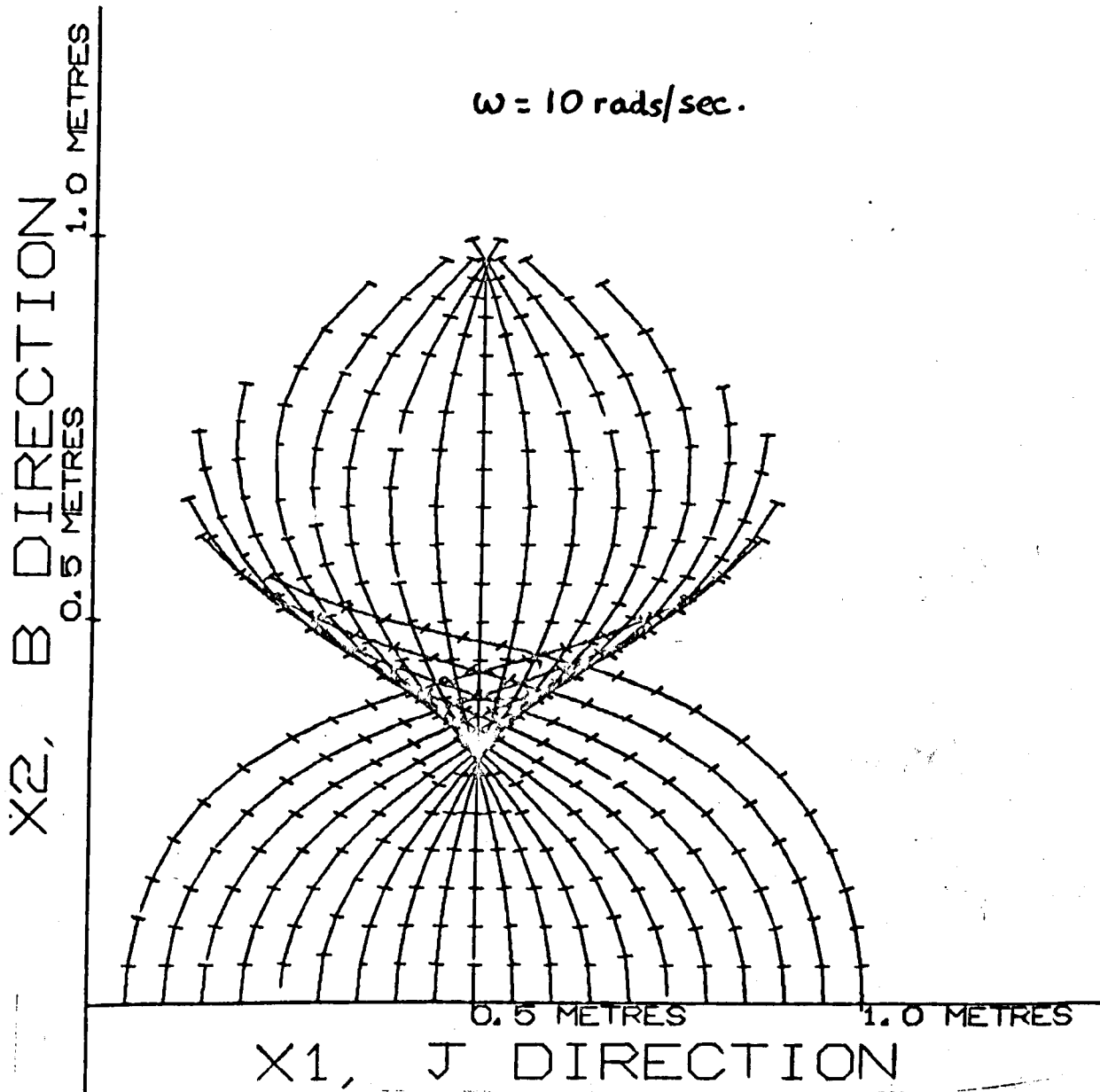
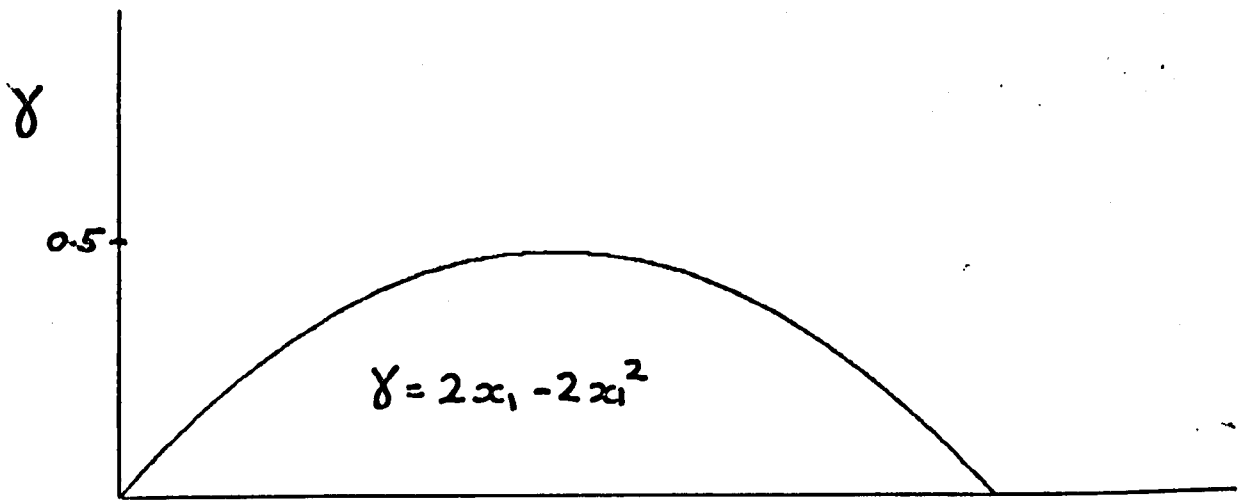


FIG. 3.17(a). COMPUTED PLOTS OF GROUP RAYS-LINE SOURCE QUADRATIC VARIATION OF  $\gamma$ .

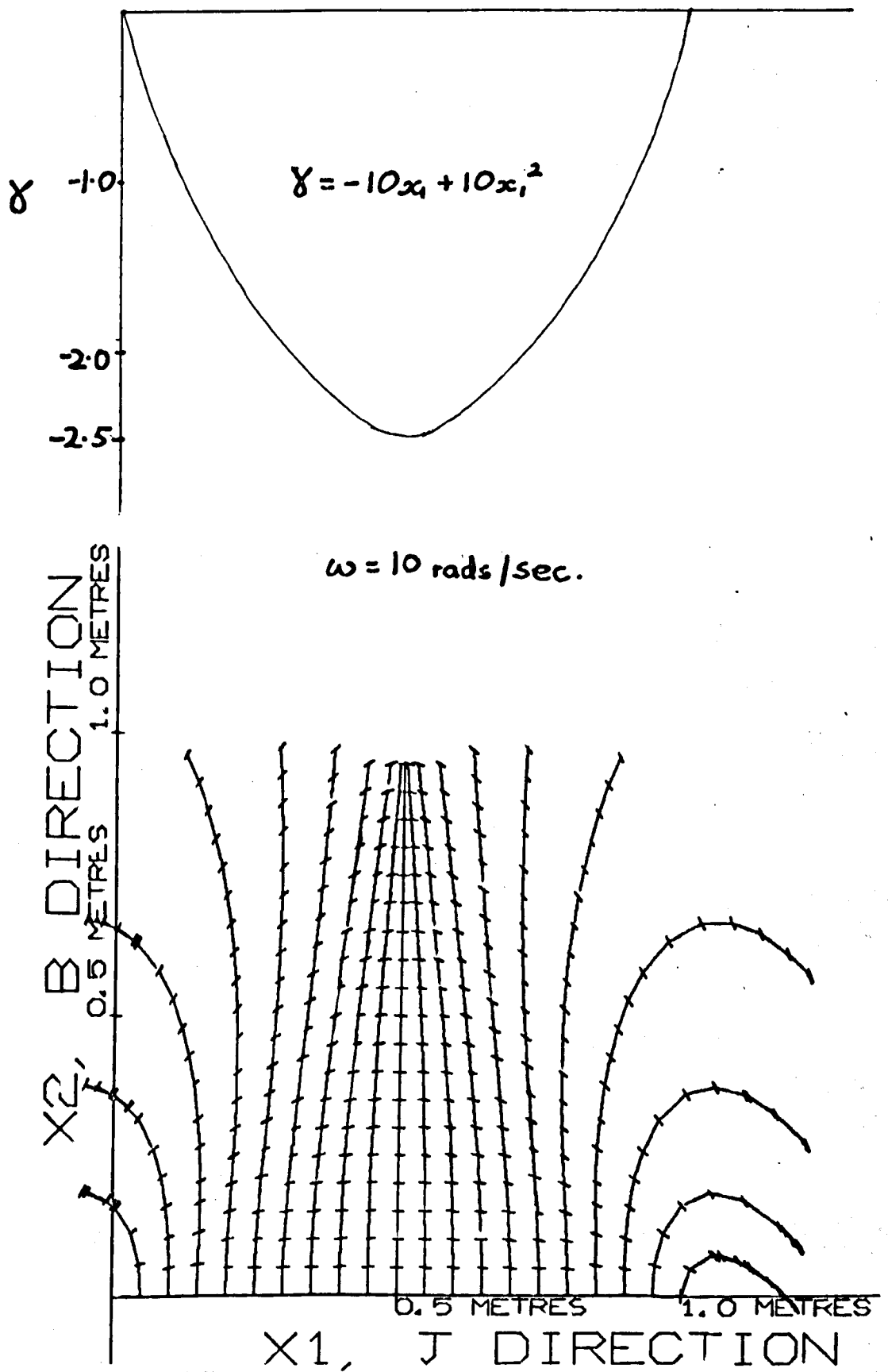


FIG. 17(b). COMPUTED PLOTS OF  
 GROUP RAYS LINE SOURCE,  
 QUADRATIC VARIATION OF  $\gamma$ .

presented as group velocity rays, plotted with a short line in a direction normal to the wave number vector at each  $p_{i,j}$ .

In all except 3.16 (b), the source line is the  $x_1$  axis.

#### B. Point source

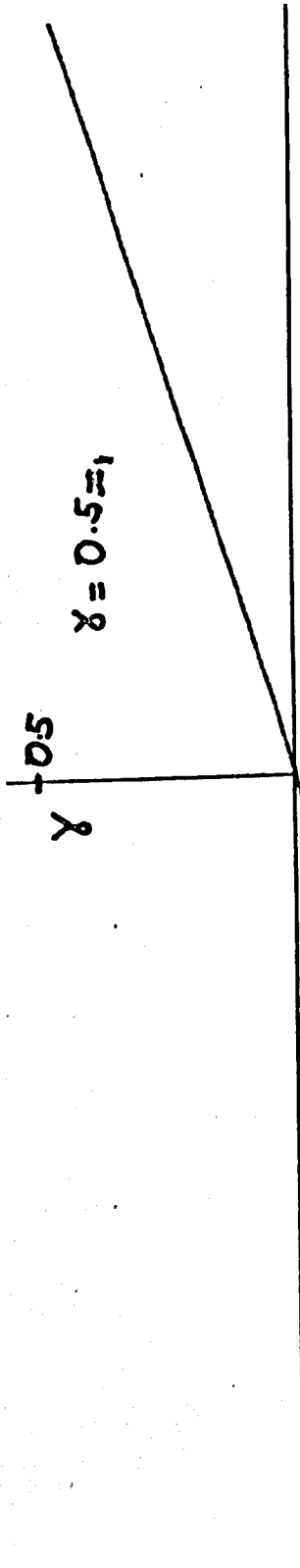
A slightly different approach must be used here, since the rays are not all predominantly in the same direction, at least to start with, and also there is no defined wave number vector direction to start with by which  $k_1$  and  $k_2$  and hence the derivatives may be defined.

Thus a nominally radial increment base is used, with  $i$  group velocity rays radiating from the origin.  $p_{i,j}$  is the same point for all  $i$ , i.e. the point source, but  $k_{1,i}$  and  $k_{2,i}$  are dependent upon the direction in which the group velocity ray leaves  $p_{i,j}$ . Assuming that energy is radiated equally in all directions, the rays are chosen to radiate uniformly, and this is achieved numerically in the sub-routine "Rays" by setting the wave number vector in the direction required for the group velocity, calculating the group velocity direction and using the deviation from its required direction to correct the wave number direction. This is repeated until the group velocity ray is correct to within  $0.1^\circ$ .

The procedure along the rays is similar to that used in the line source above, only instead of using an increment  $p$  in the  $x_1$  or  $x_2$  direction, the increment is made along the ray direction, and the component of  $p$  in the  $x_1$  or  $x_2$  direction is used in the incremental equation, in the  $x_1$  direction when

$$\left| \frac{dx_1}{dx_2} \right| > \left| \frac{dx_2}{dx_1} \right|$$

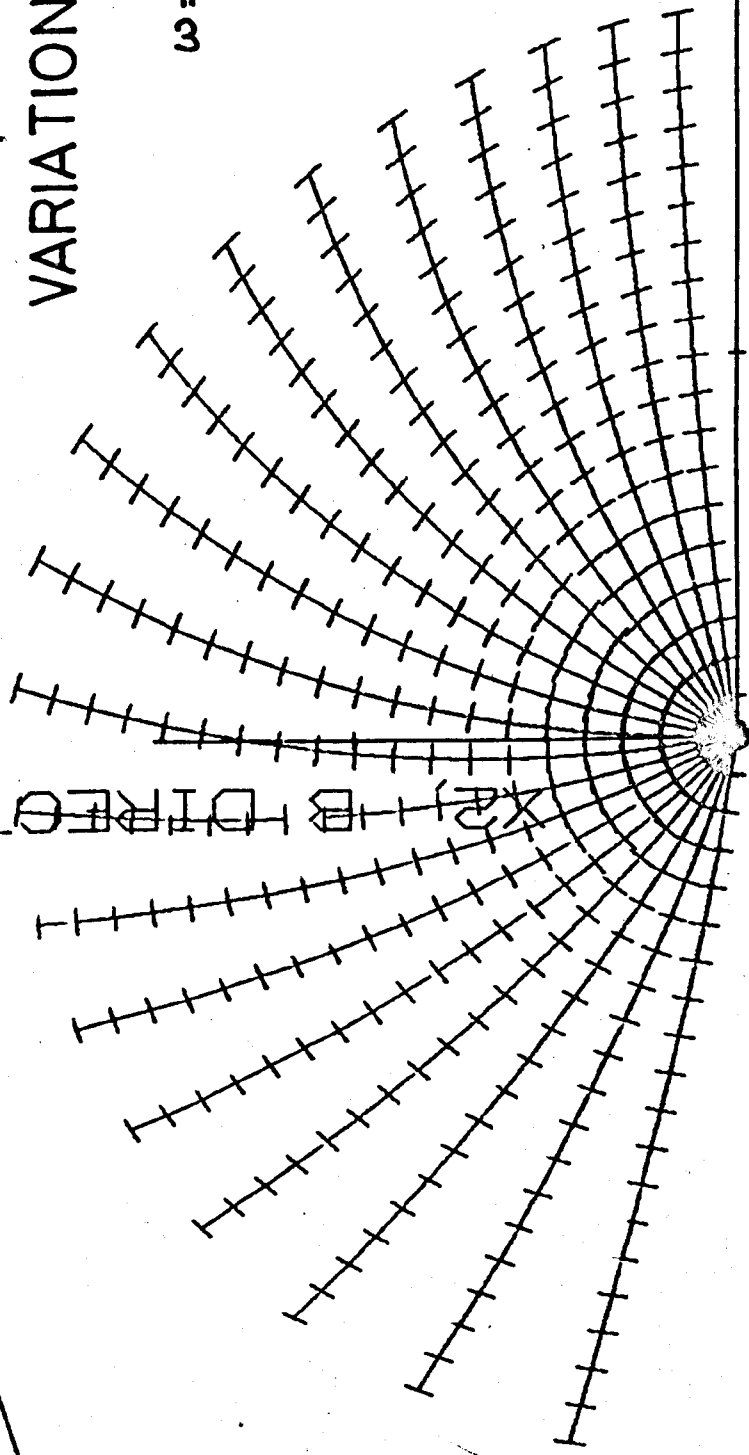
and vice versa. Typical results are shown in fig. 3.18.



NO. 10  
DIRECTION

FIG. 3.18. COMPUTED PLOT OF GROUP VELOCITY, POINT SOURCE, LINEAR VARIATION OF  $\delta$ .

$\omega = 10 \text{ rads / sec.}$



1.0 METRES

X1, J DIRECTION

### 3.5. The Kelvin Ship Wave Problem

#### 3.5.1. The problem stated

The effect of a local disturbance of pressure, travelling with constant velocity across a surface, the so called 'ship wave problem', is a well documented phenomenon in fluid mechanics e.g. Stoker (1957, section 8.1). It turns out that at any given time, the wave number vector has a fixed direction along a line drawn from the disturbance, at a given angle to the direction of travel of the disturbance. This is independent of time, and of the speed of the ship, providing it is uniform speed in a straight line. Hence a pattern of waves follows the disturbance, as shown in fig. (3.19), and this pattern is the same whatever the scale of the phenomenon, whether ocean liner or an obstruction in a flowing stream, provided that capillarity may be ignored, and also that the area is considered sufficiently large for the waves immediately local to the disturbance to be ignored, where the principle of stationary phase is not applicable, and the shape and size of the disturbance can no longer justifiably be approximated to a point. With those conditions, the pattern is purely a function of the dispersion relation of the wave system, and it is this which makes it an interesting phenomenon to investigate when applied to our M.H.D. anisotropic waves, since there will be a different pattern for each dispersion relation, governed by the anisotropy parameter  $\gamma$ . Because of the anisotropy, the pattern will also depend upon the direction of travel of the disturbance relative to the imposed electromagnetic parameters.

We take again the simplest case where  $\underline{j}$  and  $\underline{B}$  are orthogonal, and capillarity is ignored. The method of solution is expressed in two ways, following respectively the methods of Kelvin and Ursell.

We shall be principally concerned only with the kinematic problem of determining the pattern of waves and not with amplitudes.

### 3.5.2. Kelvin's method

Kelvin's approach is to be found set out in Lamb (1932, section 256) and is based on the principle of stationary phase. The ordinary problem is very much simplified by the fact that the group velocity is in the same direction as the phase velocity, and of half its magnitude, which permits a deceptively simple solution by geometrical construction to obtain the equations for lines of constant phase. The argument applied to the anisotropic case goes as follows; referring to fig. (3.20).

Let the disturbance  $O$  be moving with speed  $U$  in a direction at an angle  $\alpha$  to the direction of imposed magnetic field.

Consider the waves at point  $P$ . These will be the result of superposition of the effect of an impulse at each point along  $O$ 's path up to the present time so that one method of approach would be to solve the initial value problem for each point along  $O$ 's path, and knowing the time and direction from each point to  $P$ , the total effect at  $P$  could be integrated. But having in that step implicitly used the principle of stationary phase to solve the initial value problem, the principle is invoked again, to establish that only the waves due to the impulse being at points such as  $Q$  contribute significantly to the overall wave pattern at  $P$ , the effect of the impulse at the other points being to interfere destructively.

The first condition, then, given that the waves at  $P$  are due to the impulse at  $Q$  is that the group velocity of the waves at  $P$  must be  $\frac{\overline{QP}}{t}$  where  $t$  is the time  $\frac{\overline{OQ}}{U}$  since the disturbance passed through  $Q$ .

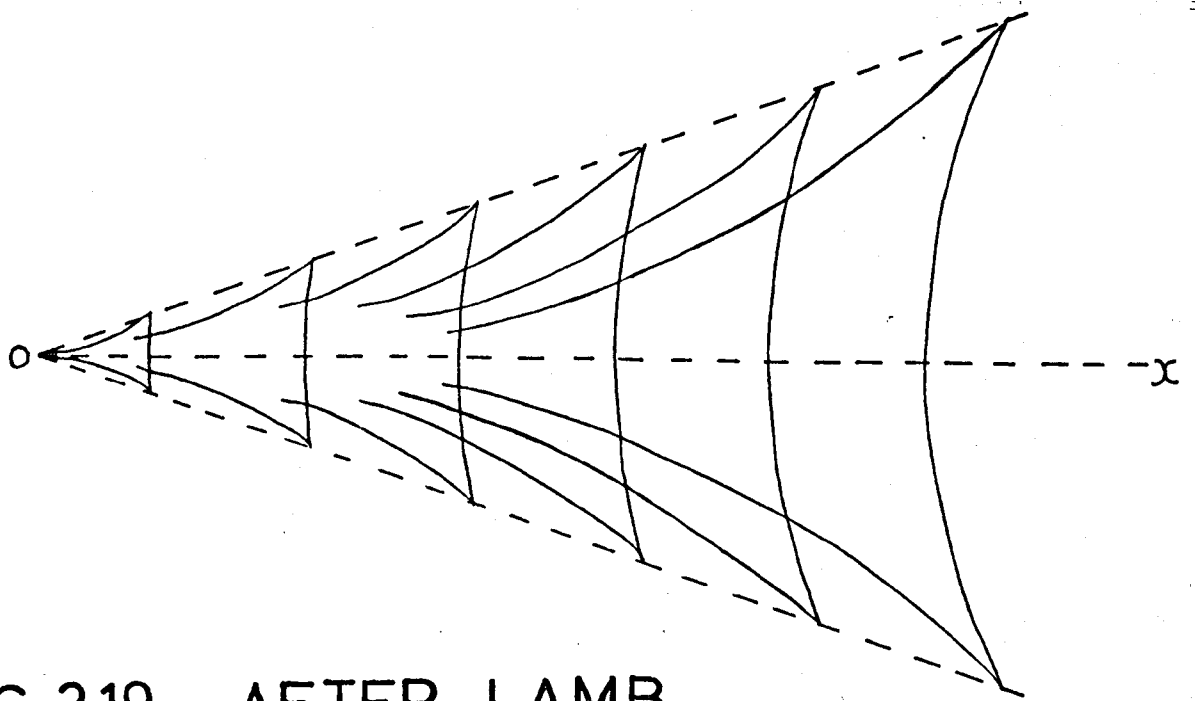


FIG. 3.19. AFTER LAMB.

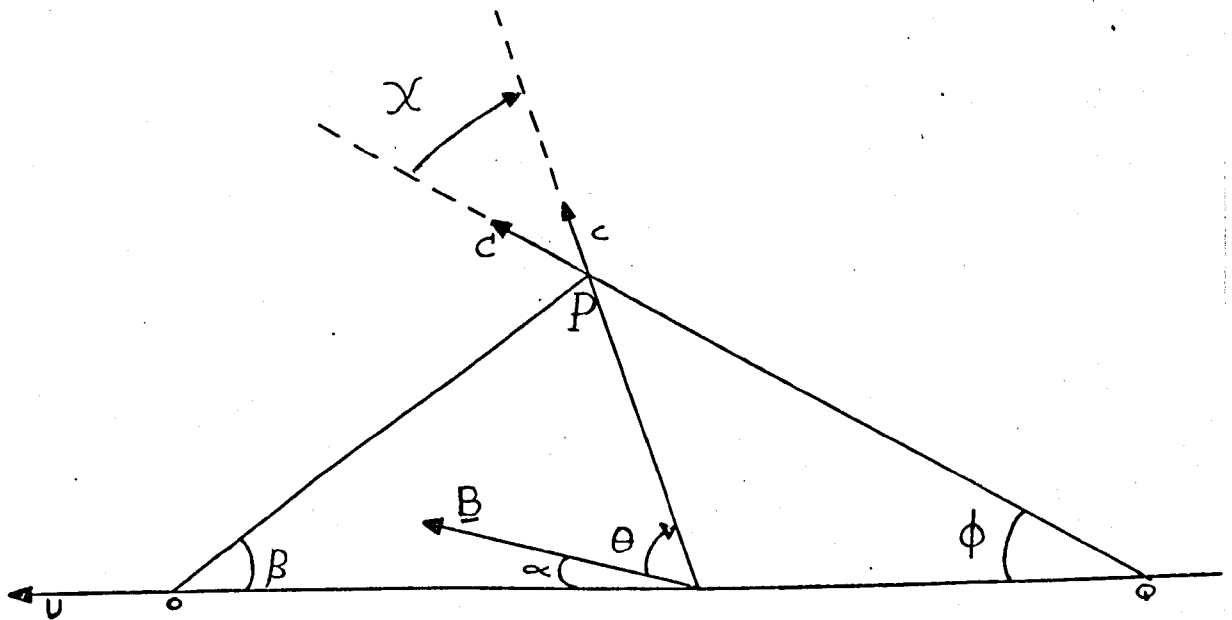


FIG. 3.20. NOTATION FOR LAMB'S METHOD.

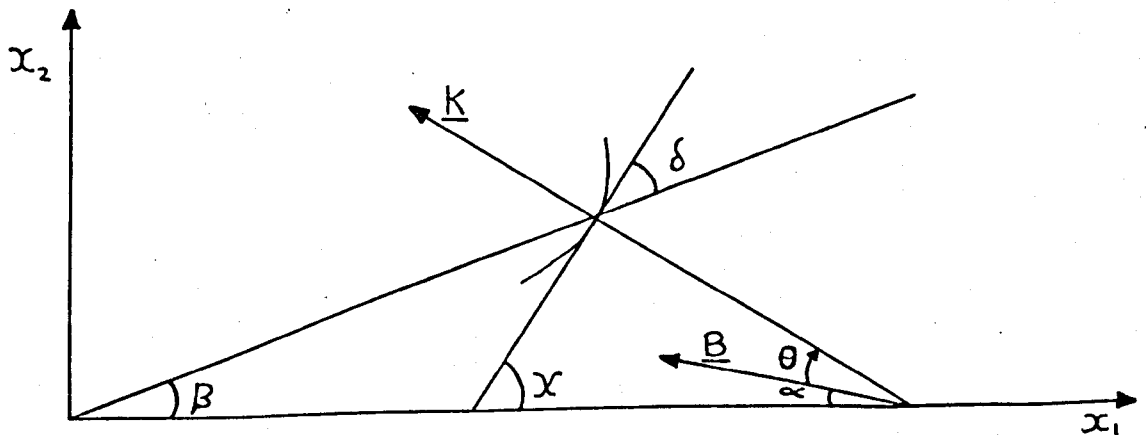


FIG. 3.21. NOTATION FOR URSELL'S METHOD.

Secondly the condition that the waves at P are due to Q and no other point along the disturbance path is that the component of the velocity of the disturbance in the direction of the wave number vector at P will be equal to the phase velocity at P.

Now if the dispersion relation be  $\omega^2 = gk(1 - \gamma \cos^2 \theta)$  the phase velocity for wave number vectors at angle  $\theta$  to B is :-

$c = \frac{g}{\omega_p} (1 - \gamma \cos^2 \theta)$ ,  $\omega_p$  being the frequency of the predominant wave number at P.

The group velocity for such waves is :-

$$C_k = \frac{g}{2\omega_p} (1 - \gamma \cos^2 \theta) \quad \text{in the } \underline{k} \text{ direction}$$

and  $C_\theta = \frac{g}{2\omega_p} \gamma \sin 2\theta$  in the direction of  $+\theta$  normal to k.

$$\therefore \chi = - \tan^{-1} \frac{C_\theta}{C_k} = - \tan^{-1} \left\{ \frac{\gamma \sin 2\theta}{1 - \gamma \cos^2 \theta} \right\}$$

$$\text{and } C = \frac{g}{2\omega_p} \sqrt{(1 - \gamma \cos^2 \theta)^2 + \gamma^2 \sin^2 2\theta}$$

$$\therefore \overline{QP} = Ct = C \frac{\overline{OQ}}{U} = \frac{g}{2\omega_p} \sqrt{(1 - \gamma \cos^2 \theta)^2 + \gamma^2 \sin^2 2\theta} \frac{\overline{OQ}}{U} \dots 3.23$$

$$\text{and } U \cos(\theta + \alpha) = c = \frac{g}{\omega_p} (1 - \gamma \cos^2 \theta) \dots 3.24$$

Hence U and  $\omega_p$  may be eliminated from (3.23) and (3.24), to reduce the problem to one of geometry alone, i.e.

$$\frac{\overline{QP}}{\overline{OQ}} = \frac{\cos(\theta + \alpha)}{2(1 - \gamma \cos^2 \theta)} \sqrt{(1 - \gamma \cos^2 \theta)^2 + \gamma^2 \sin^2 2\theta} = f \dots 3.25$$

$$\text{now } \overline{OP}^2 = \overline{OQ}^2 + \overline{PQ}^2 - 2 \overline{OQ} \overline{PQ} \cos \phi = \overline{OQ}^2 (1 + f^2 - 2f \cos \phi)$$

$$\text{and } \frac{\sin \beta}{\overline{PQ}} = \frac{\sin \beta}{f \overline{OQ}} = \frac{\sin \phi}{\overline{OP}}$$

$$\therefore \sin \beta = \frac{f \sin \phi}{\sqrt{1 + f^2 - 2f \cos \phi}} \dots 3.26$$

$$\text{where } \phi = \theta + \alpha - \chi = \theta + \alpha + \tan^{-1} \left( \frac{\gamma \sin 2\theta}{1 - \gamma \cos^2 \theta} \right) \quad \dots 3.27$$

(3.26), after substitution of (3.25) and (3.27), is the required equation relating  $\beta$  and  $\theta$ , which gives the direction of waves to be found along lines at angle  $(180 - \beta)$  to the direction of travel drawn from the position of the disturbance at any time.

### 3.5.3. Ursell's method

Ursell (1960) solved the problem of wave patterns on a non uniform steadily flowing stream where the more intuitive method of Kelvin is not easily applied. A summary of the method is to be found in Whitham (1961). It is based directly on the methods of wave crest kinematics.

We are concerned to find the pattern of waves relative to the moving object so first the transformation between the stationary and the moving frame is established, for frequency, phase and group velocity.

$$\text{i.e. } \underline{c} = (\underline{u} \cdot \hat{k}) \hat{k} + \underline{c}_0 \quad \dots 3.28$$

$$\omega = \underline{c} \cdot \underline{k} = (\underline{u} + \underline{c}_0) \cdot \underline{k} = \underline{u} \cdot \underline{k} + \omega_0 \quad \dots 3.29$$

$$\underline{c} = \underline{u} + \underline{c}_0 \quad \dots 3.30$$

Where the suffix  $_0$  refers to the stationary frame with moving disturbance and the unsuffixed parameters refer to the frame moving with velocity  $\underline{u}$  past a fixed object.

These transformations are necessary, since the dispersion relation  $\omega_0 = f(\underline{k})$  is in terms of the stationary frame, but in our moving frame the flow is steady and  $\omega = 0$ .

$$\therefore \text{ from (3.29) } (\underline{u} + \underline{c}_0) \cdot \underline{k} = 0 \quad \dots 3.31$$

From kinematic wave theory,  $\text{curl } \underline{k} = 0$

$$\therefore \frac{\partial k_1}{\partial x_2} = \frac{\partial k_2}{\partial x_1} \quad \dots 3.32$$

From (3.32), given that  $k_1$  and  $k_2$  are functionally related

in (3.31) it can be shown that 
$$\frac{\partial k_1}{\partial x_2} + \left(-\frac{dk_2}{dk_1}\right) \frac{dk_1}{dx_1} = 0$$

and similarly for  $k_2$  so that if 
$$\frac{dx_1}{dx_2} = -\frac{dk_2}{dk_1}, k_1 \text{ and } k_2$$

are constant. Consequently  $\frac{dx_1}{dx_2} = -\frac{dk_2}{dk_1}$  are straight, characteristic lines.

Let  $\underline{u} = (u, 0)$ ,  $\underline{k} = (-k \sin \chi, k \cos \chi)$ , 
$$\frac{dx_2}{dx_1} = \tan \beta$$

see fig. (3.21)

From the dispersion relation  $\omega_o = \sqrt{gk(1-\gamma \cos^2 \theta)}$

$$c_o = \sqrt{\frac{g}{|k|} (1-\gamma \cos^2 \theta)} \hat{k}$$

$\therefore (3.31) \rightarrow ([u, 0] + [-\sin \chi \sqrt{\frac{g}{|k|} (1-\gamma \cos^2 \theta)}, \cos \chi \sqrt{\frac{g}{|k|} (1-\gamma \cos^2 \theta)}]) \cdot [k \sin \chi, k \cos \chi] = 0$

$\therefore -uk \sin \chi + \sqrt{\frac{g}{k} (1-\gamma \cos^2 \theta)} k (\cos^2 \chi + \sin^2 \chi) = 0$

$\therefore u \sin \chi = \sqrt{\frac{g}{k} (1-\gamma \cos^2 \theta)}$  ... 3.33

On the characteristic lines  $\frac{dx_2}{dx_1} = \tan \beta = -\frac{dk_1}{dk_2} = \frac{d(k \sin \chi)}{d(k \cos \chi)}$   
 $= \frac{\tan \chi + k \frac{d\chi}{dk}}{1 - k \frac{d\chi}{dk} \tan \chi} = \tan(\chi - \delta)$  where  $\tan \delta = -k \frac{d\chi}{dk}$  ... 3.34

$\therefore \beta = \chi - \delta$ , and  $\delta$  is the angle between the characteristic and the wave crest - see fig. 3.21

$\frac{d\chi}{dk}$  may be obtained from differentiating (3.33) with  $\theta = 90 - (\chi + \alpha)$  and  $u$  and  $k$  cancel out, so that:-

$$\tan \delta = \frac{1}{2} \left\{ \frac{\sin \chi (1 - \gamma \sin^2(\chi + \alpha))}{\cos \chi (1 - \gamma \sin^2(\chi + \alpha)) + \frac{1}{2} \gamma \sin \chi \sin 2(\chi + \alpha)} \right\}$$

From this  $\delta$  can be computed for varying  $\chi$  and after bringing the results into a form compatible with those of 3.5.2 the two methods

can be shown to be in complete agreement.

### 3.5.4. Theoretical M.H.D. ship wave patterns

In the computer calculation of the results, using the first method,  $\beta$  is obtained for a range of  $(\theta + \alpha)$  from  $-\frac{\pi}{2}$  to  $+\frac{\pi}{2}$ , for various values of  $\gamma$  and  $\alpha$ .

See Appendix.

The trough and crest pattern, corresponding to those drawn by Lamb, is plotted from these values. It is not strictly a line of constant phase since there is a  $180^\circ$  phase change at the cusps.

The locus of the pattern is drawn from an arbitrary point  $(x_0, 0)$  see fig. (3.22), since for  $(\theta + \alpha) = \frac{\pi}{2}$ ,  $\beta$  is always 0.  $x_n, y_n$  are located at the intersection of the lines  $y_n = x_n \tan \beta$ , and a line<sup>is</sup> drawn from  $(x_{n-1}, y_{n-1})$  with slope

$$\frac{\pi}{2} - \frac{(\theta + \alpha)_n + (\theta + \alpha)_{n-1}}{2}.$$

The accuracy depends on the number of increments taken between  $(\theta + \alpha) = \frac{\pi}{2}$  and  $-\frac{\pi}{2}$  but with 36 increments there seemed to be sufficient accuracy to give a good indication of the salient features of the pattern. Typical patterns are shown in fig. (3.23). In this case  $\bar{x}$  ve  $\gamma$  represents an upward force, + ve a downward force.

For  $\alpha = 0$  or  $\frac{\pi}{2}$ , the pattern is symmetrical, though squashed or elongated relative to the O.H.D. case with  $\beta_{\max}$  increased or decreased. The polar plot of phase velocity has been sketched in some cases to show the relative orientation of the anisotropy relative to its effect on the ship wave pattern. It is interesting to note that where the crest might become excessively bent, in fact another pair of cusps form, so that for a certain range of  $\beta$ ,  $k$  is quadruple valued.

When the 'ship' direction is at an angle between 0 and

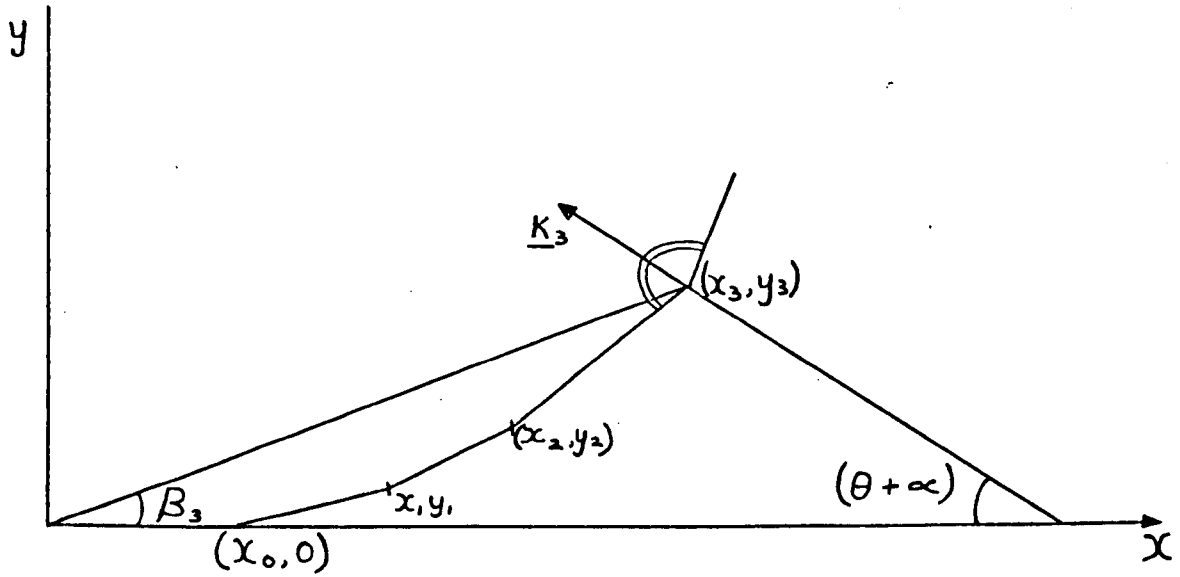


FIG. 3.22. TO ILLUSTRATE METHOD OF PLOTTING LINES OF CONSTANT PHASE.

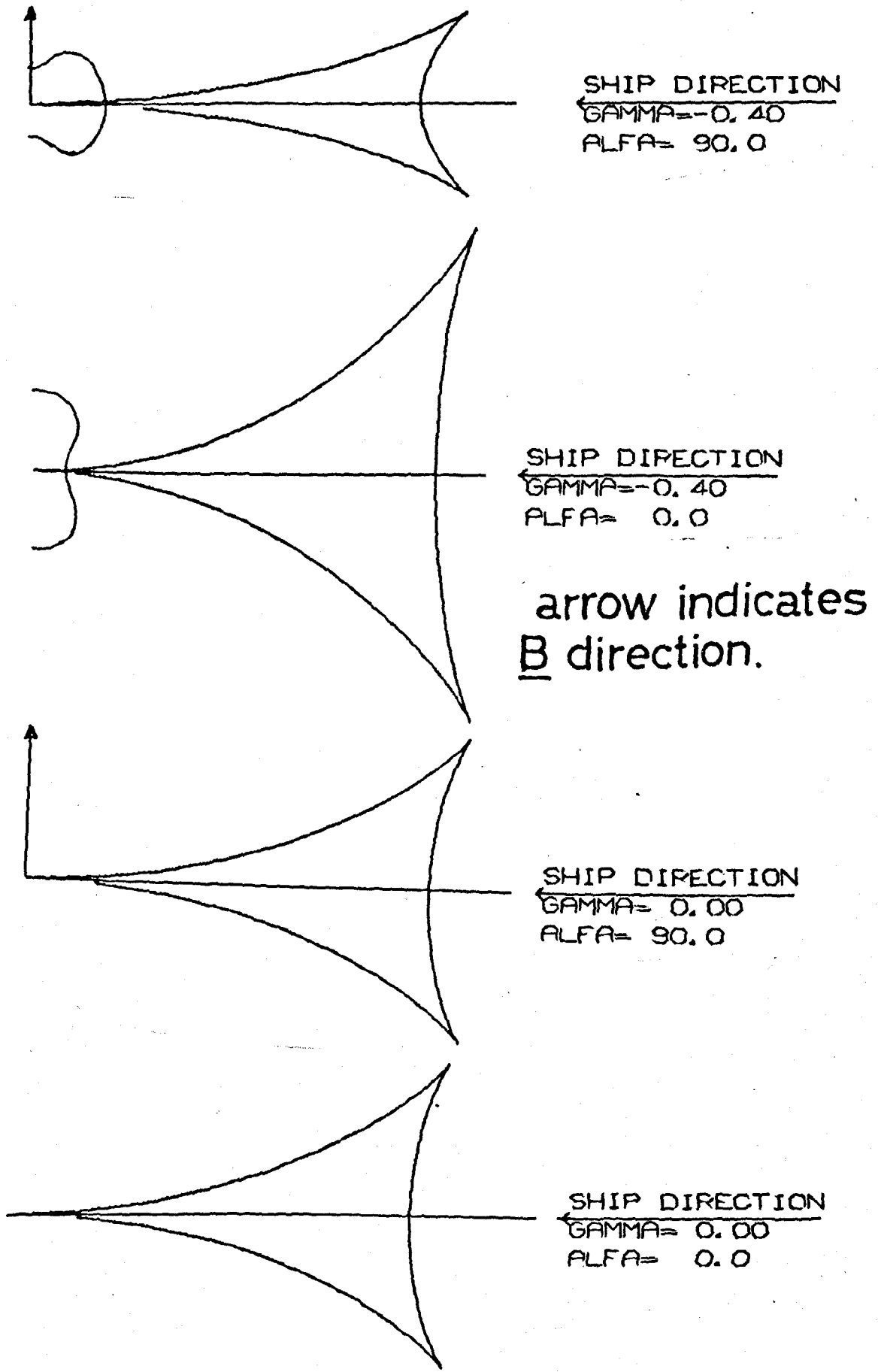


FIG. 3.23(a). COMPUTED SHIP WAVE PATTERNS  $\alpha = 0, 90^\circ$ .

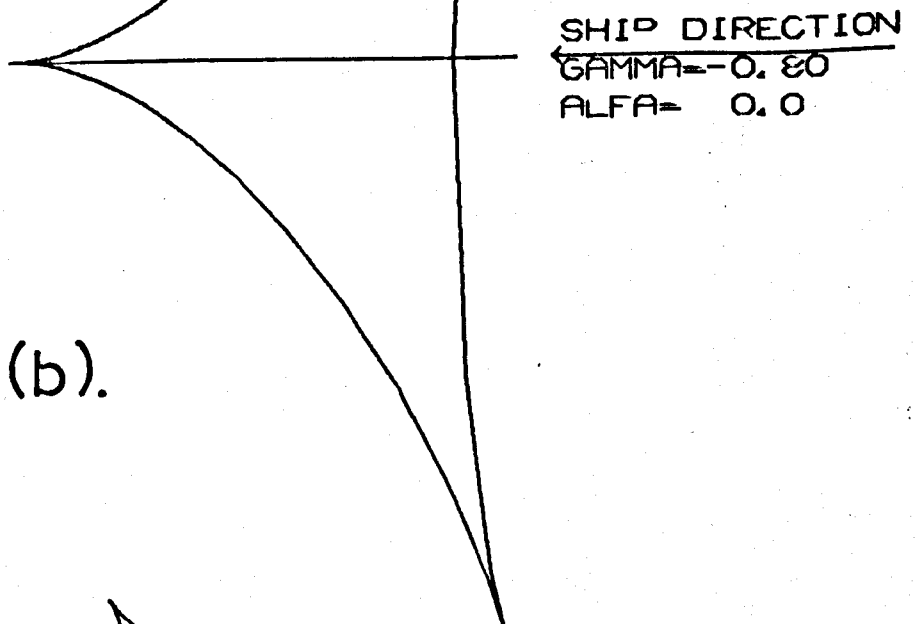
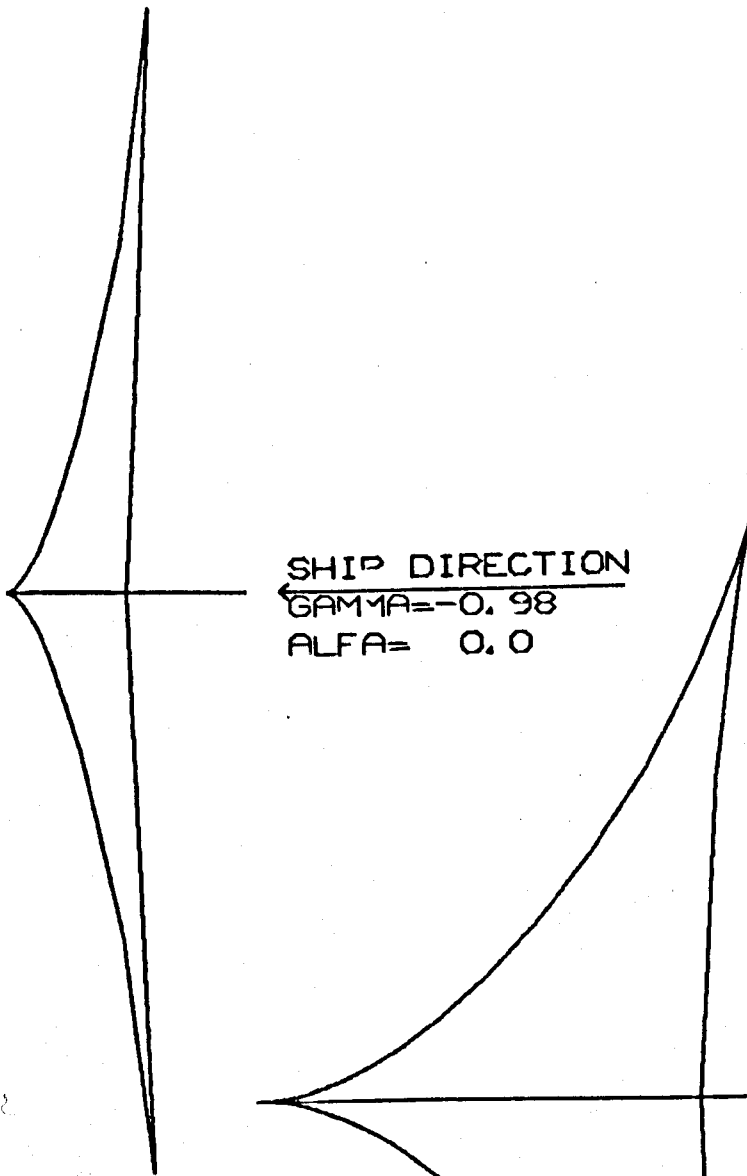
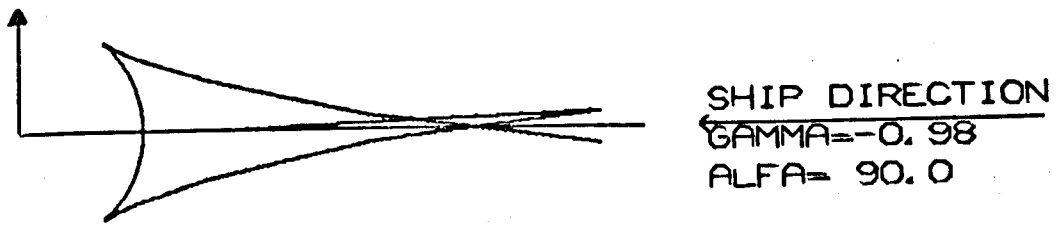
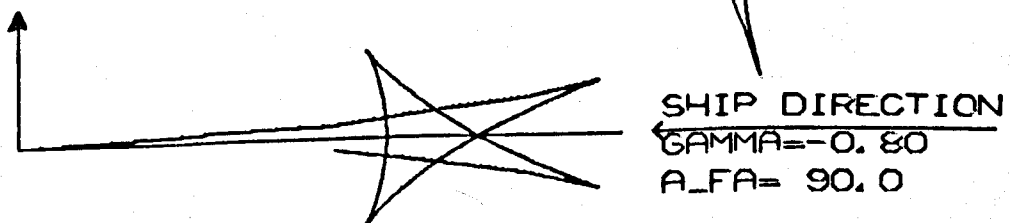


FIG. 3.23 (b).



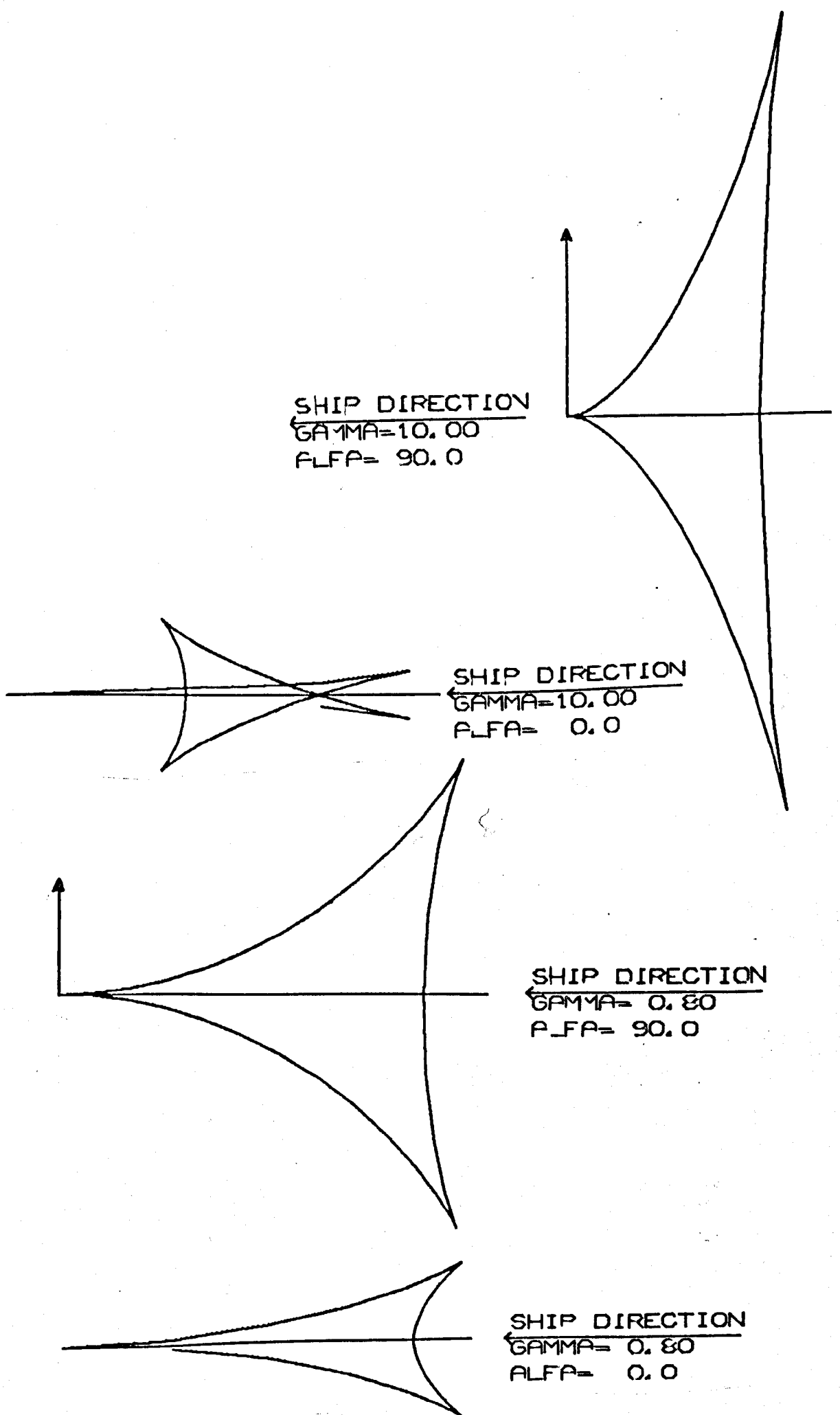


FIG. 3.23(c).

$\pm \frac{\pi}{2}$  to the orientation of the anisotropy, the pattern becomes unsymmetrical. and in certain cases violently so, as may be seen in fig. (3.24).

A typical example of the total wave pattern formed by a moving disturbance is shown in fig. (3.25), repeatedly drawing a particular pattern and increasing its size successively.

### 3.5.5. With surface tension included - the 'fish line' problem

The above results demonstrate clearly the effect of the anisotropy of M.H.D. surface waves in the ship wave problem. On approaching the problem from an experimental viewpoint, however, it is obvious that the scale involved in the ship wave problem is usually at least several metres, if surface tension is to be ignored, and so it is practically out of the question to demonstrate them, due to the spatial extent of the magnetic and electric fields required. The corresponding problem with surface tension included in the analysis is referred to by Lamb as the 'fish line' problem, originally solved by Rayleigh. In this case, ripples dominated by capillary action travel ahead of the disturbance and in the notation of fig. (3.21)  $\beta$  is double valued for each  $(\alpha + \theta)$ . It has been seen in fig. (2.10) how the M.H.D. anisotropy, and the use of two fluids, alters the  $c = f(k)$  relationship which dictates the relative size of wavelengths fore and aft of the disturbance for a given velocity, and the minimum velocity below which no wave pattern is formed. Thus it is of interest in itself to solve the problem for the M.H.D. case at a two fluid interface, to see how the minimum velocity to cause a disturbance is affected, as well as to provide theoretical predictions against which to test possible experimental results. Lamb's analysis (Lamb 1932 §272) for the O.H.D case cannot be extended this time, but Ursell's method lends itself to easy adaptation to include surface tension.

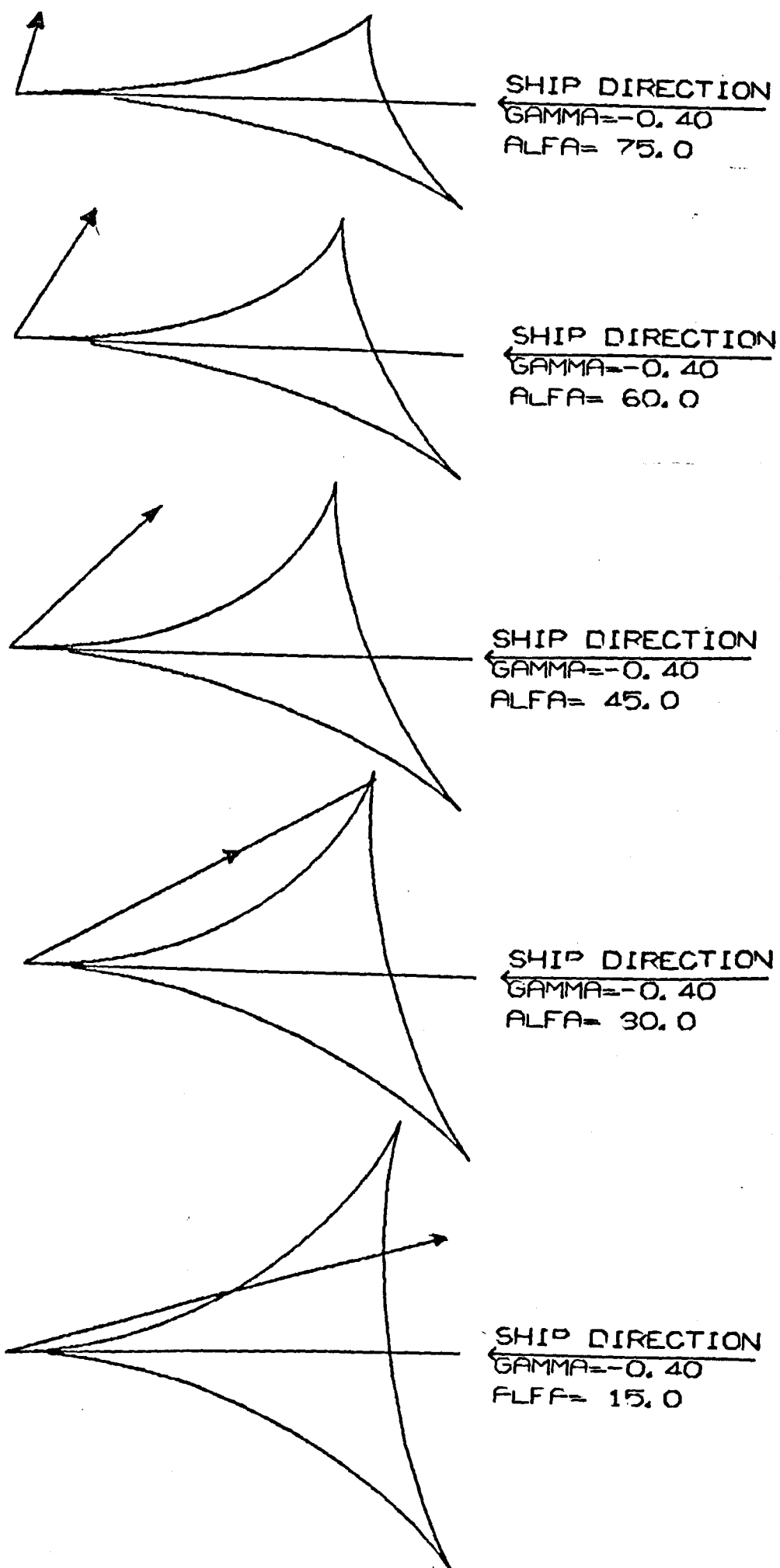


FIG.3.24(a). COMPUTED SHIP WAVE PATTERNS  $\alpha = -15, 15, 30, 45, 60, 75^\circ$ .

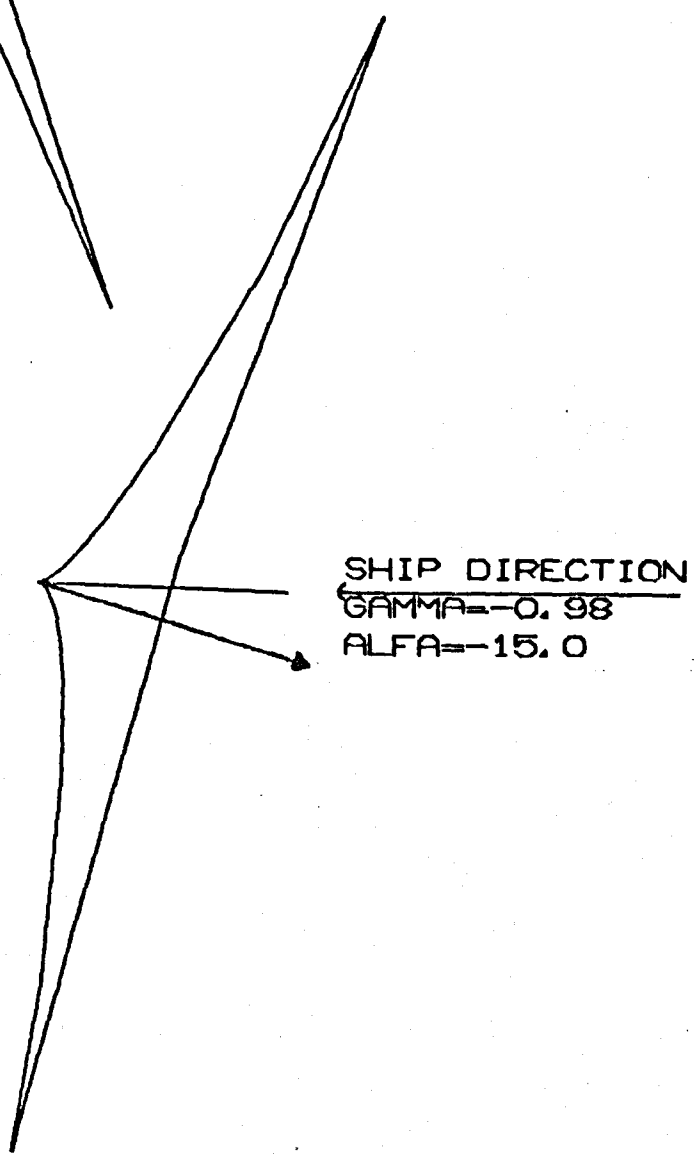
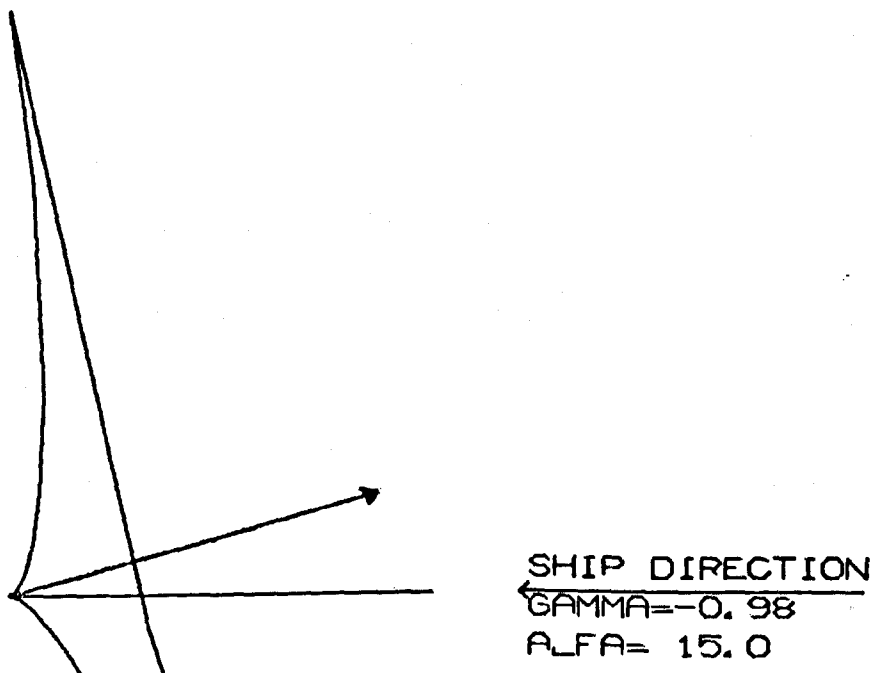


FIG. 3.24(b).

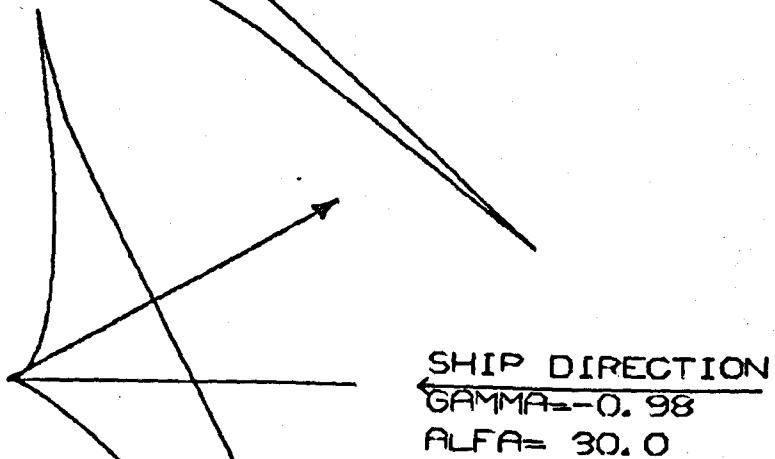
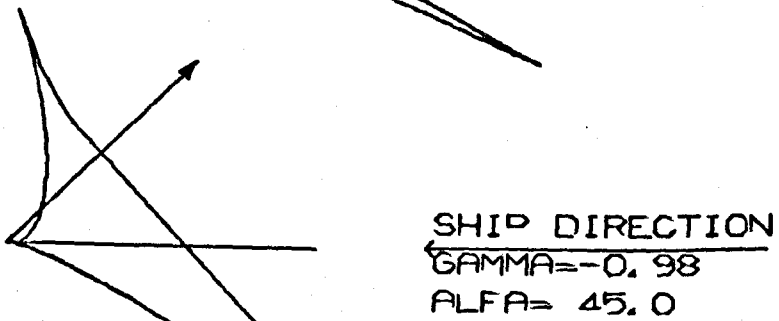
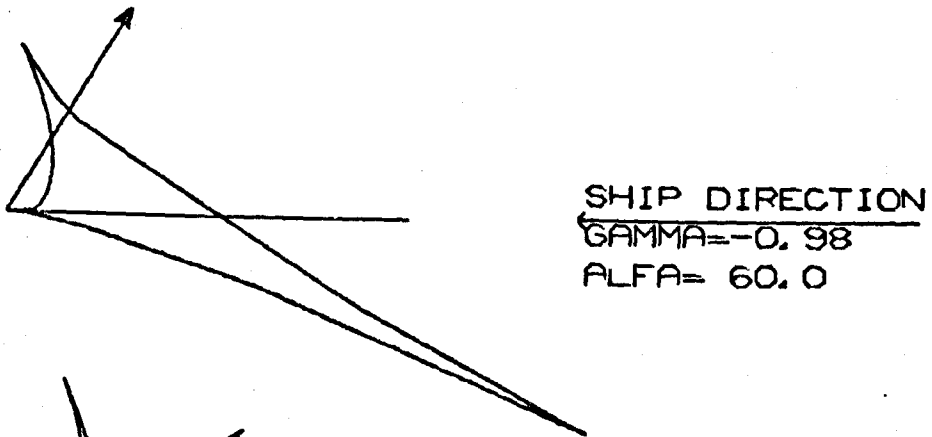
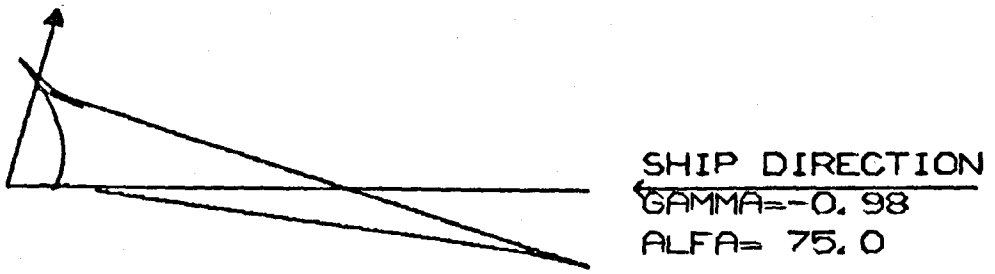


FIG. 3.24(c).

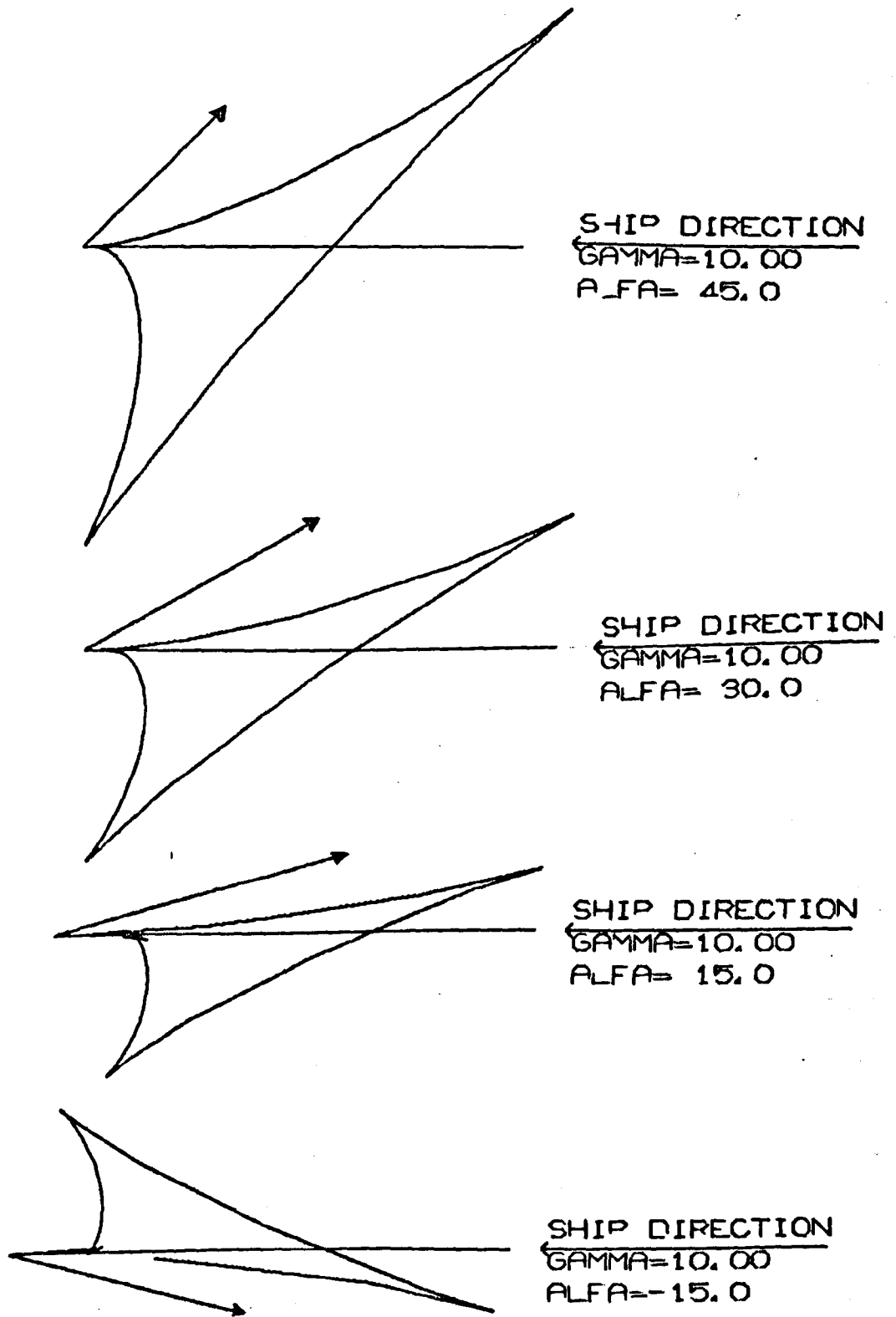


FIG. 3.24 (d).

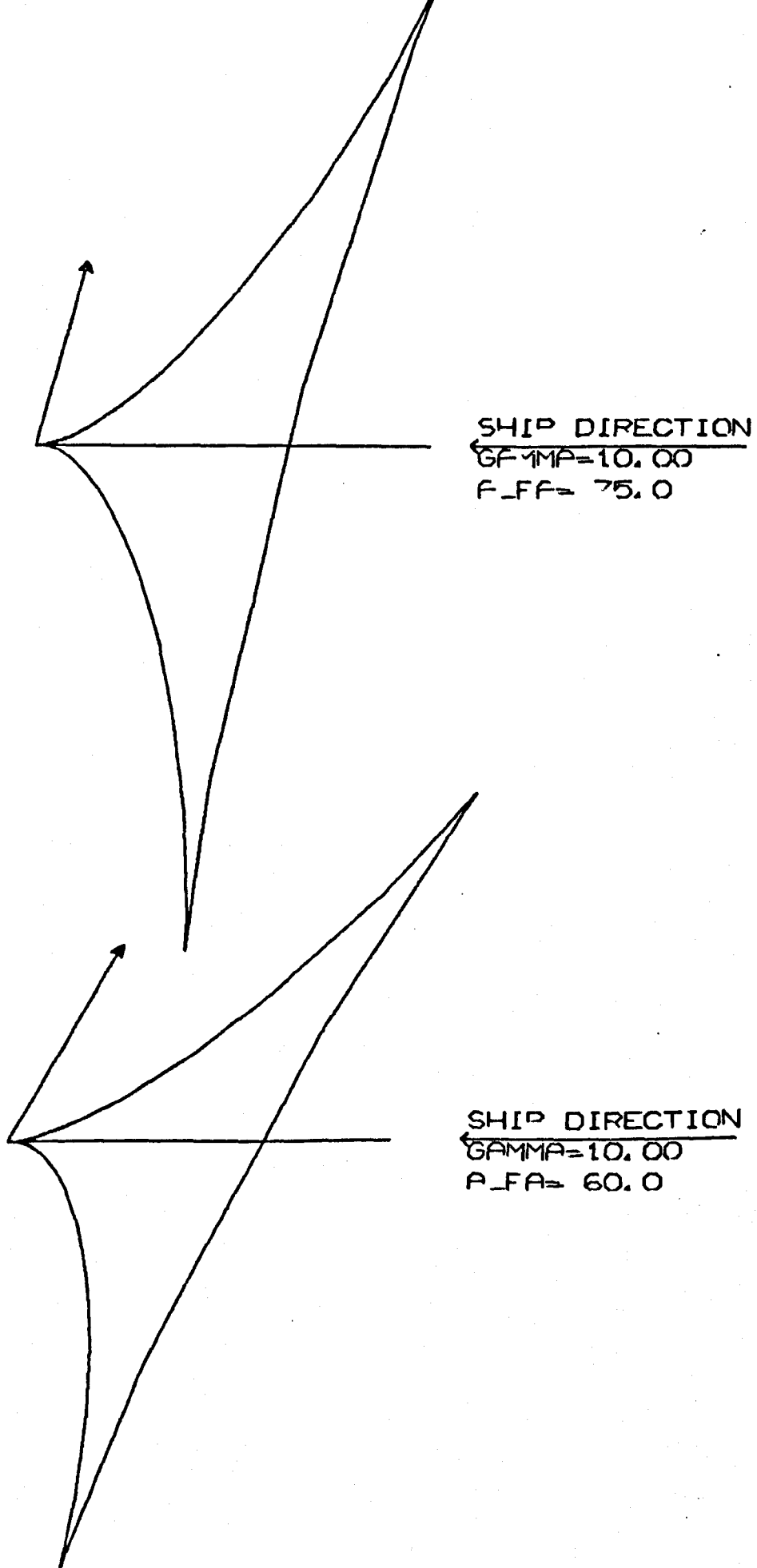


FIG. 3.24 (e)

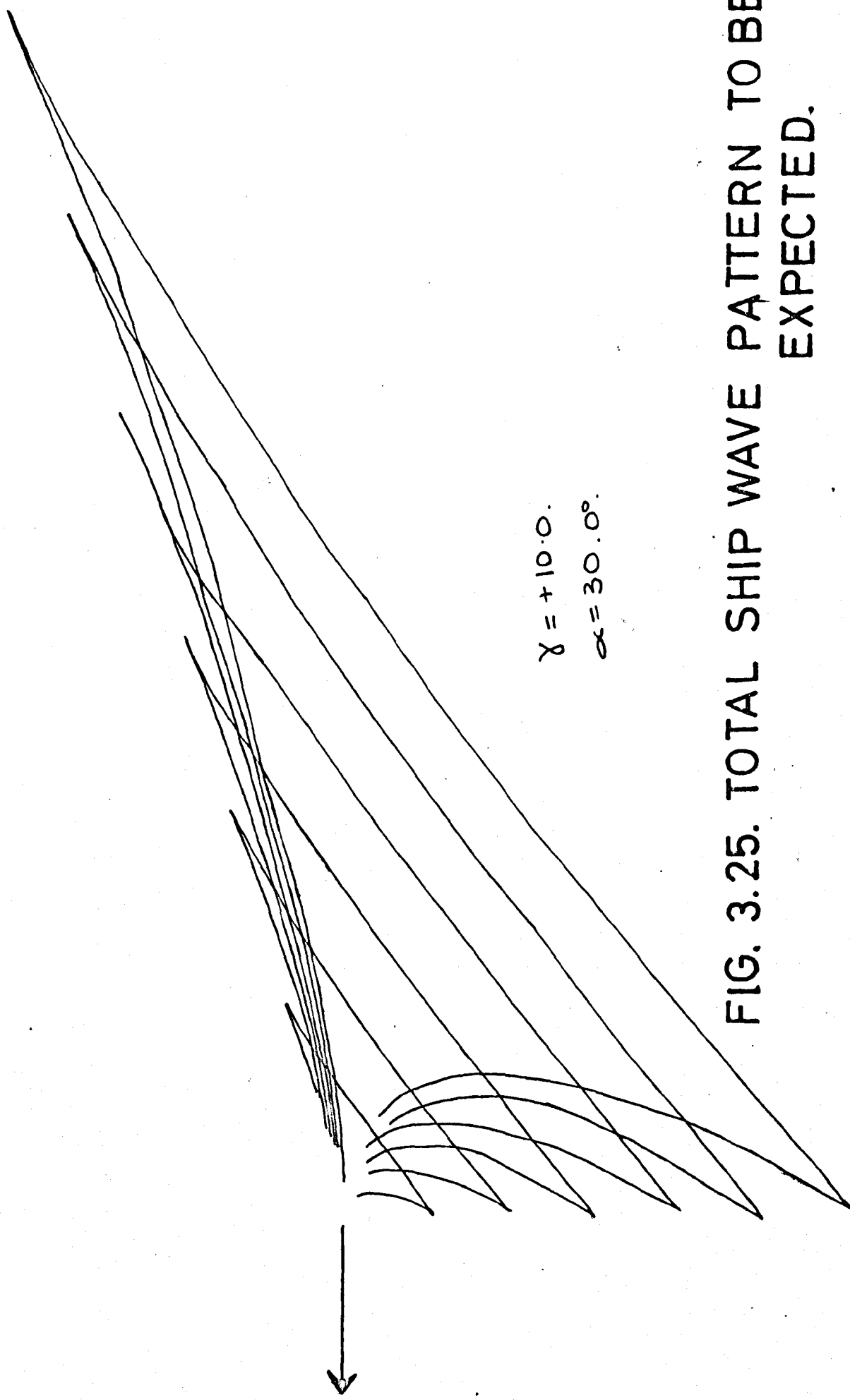


FIG. 3.25. TOTAL SHIP WAVE PATTERN TO BE EXPECTED.

In this case, the dispersion relation is taken as :-

$$\omega^2 = [(\rho_2 - \rho_1)g + jB \cos^2 \theta + \alpha k^2] \frac{k}{\rho_1 + \rho_2}$$

The analysis follows that of section 3.5.3. up to where  $\omega_0$  is included. From there (3.33) becomes,

$$u \sin X = \left[ \frac{(\rho_2 - \rho_1)g}{k} + \frac{jB \cos^2 \theta}{k} + \alpha k \right]^{\frac{1}{2}} / (\rho_2 + \rho_1)^{\frac{1}{2}} \quad \dots 3.35$$

3.34 is the same, since the characteristic lines are still straight,

$$\text{and now } \tan \delta = \frac{(\rho_2 - \rho_1)g + jB \sin^2(\alpha + X) - k^2 \alpha}{2 \omega (\rho_1 + \rho_2) u \cos X - jB \sin 2(\alpha + X)} \quad \dots 3.36$$

Double values of  $k$  are obtained by solving (3.35) for  $k$ , given

$X$  and hence  $\theta$ , and the values substituted in (3.36). It should be noted that unlike the ship wave problem,  $u$  does not cancel out and so affects the shape of the patterns.

The computer was used to solve these equations, with

$X$  varied in 36 steps from  $0 \rightarrow \pi$ , and  $\beta$  obtained from  $\beta = X - \delta$ .

In certain cases the quadratic equation for  $k$  had no real solution, and this corresponded to a wave crest direction which was not a part of the solution for a disturbance at that particular speed. Below a certain speed, depending on the parameters, this was the case for all  $X$ , i.e. an object travelling at that given speed would not produce any waves at all. Whereas in the O.H.D. case, the possible

$X$  would lie in the range  $\left(\frac{\pi}{2} - X_L\right) < X < \left(\frac{\pi}{2} + X_L\right)$

for the M.H.D. case the range would be  $X_{L_1} < X < X_{L_2}$

where  $X_{L_1} + X_{L_2} \neq \pi$  in general.

To plot the two separate curves, corresponding to the wave crest patterns for each value of  $k$ , the following method was adopted. As  $X$  was increased step by step, at  $X_{L_1}$  when the first real values of  $k$  were obtained, the  $x$  co-ordinate for each line was set at 1.0.

The  $y$  co-ordinate was then obtained from  $y = x \tan \beta$ , ( $\beta = X - \delta$ )

For the next and subsequent values of  $\chi$ , until  $\chi_{L_2}$  was reached, the x co-ordinates were obtained from :-

$$x_i = \frac{y_{i-1} - x_{i-1} \tan\left(\frac{\chi_i + \chi_{i-1}}{2}\right)}{\tan \beta_i - \tan\left(\frac{\chi_i + \chi_{i-1}}{2}\right)}, \text{ and } y_1 = x_1 \tan \beta_1$$

for the two respective curves. Finally, each curve was scaled separately to fit the page size and plotted on the same diagram.

Fig. 3.26 is typical of the sort of results produced for different orientations of ship direction to the electromagnetic parameters. The cusped curve represents the wave pattern behind the 'ship' ( or downstream of the stationary disturbance in a steadily moving stream) whilst the other curve represents the upstream ripples. The tick mark on the axis shows the position of the 'ship', and the total pattern to be observed could be generated by drawing radii from the mark, each radius always intersecting successive wave crests at the same angle. The upstream pattern has larger wave numbers than the downstream pattern, increasingly so as the speed of the 'ship' is increased. In the case of fig. <sup>3.26</sup>2.6 (a) at 0.5 m/s, the ratio of wave numbers for  $\chi = \pi$  is of the order of  $10^5$  whereas for <sup>3.26</sup>2.6 (b) at 0.1 m/s, it is of the order of  $10^3$ . As  $\chi \rightarrow \chi_{L_1}$  or  $\chi_{L_2}$  the wave numbers for the fore and aft families tend to equality.

The anisotropy of the patterns is most marked in the downstream pattern. In practice, what would probably show up clearest in a laboratory experiment would be that part of the downstream curves which crosses the line of travel, and the direction of these troughs and crests should show up the anisotropic effect. Also, the outer cusps will form lines, which will vary in direction with the anisotropy, outside of which the surface should be undisturbed.

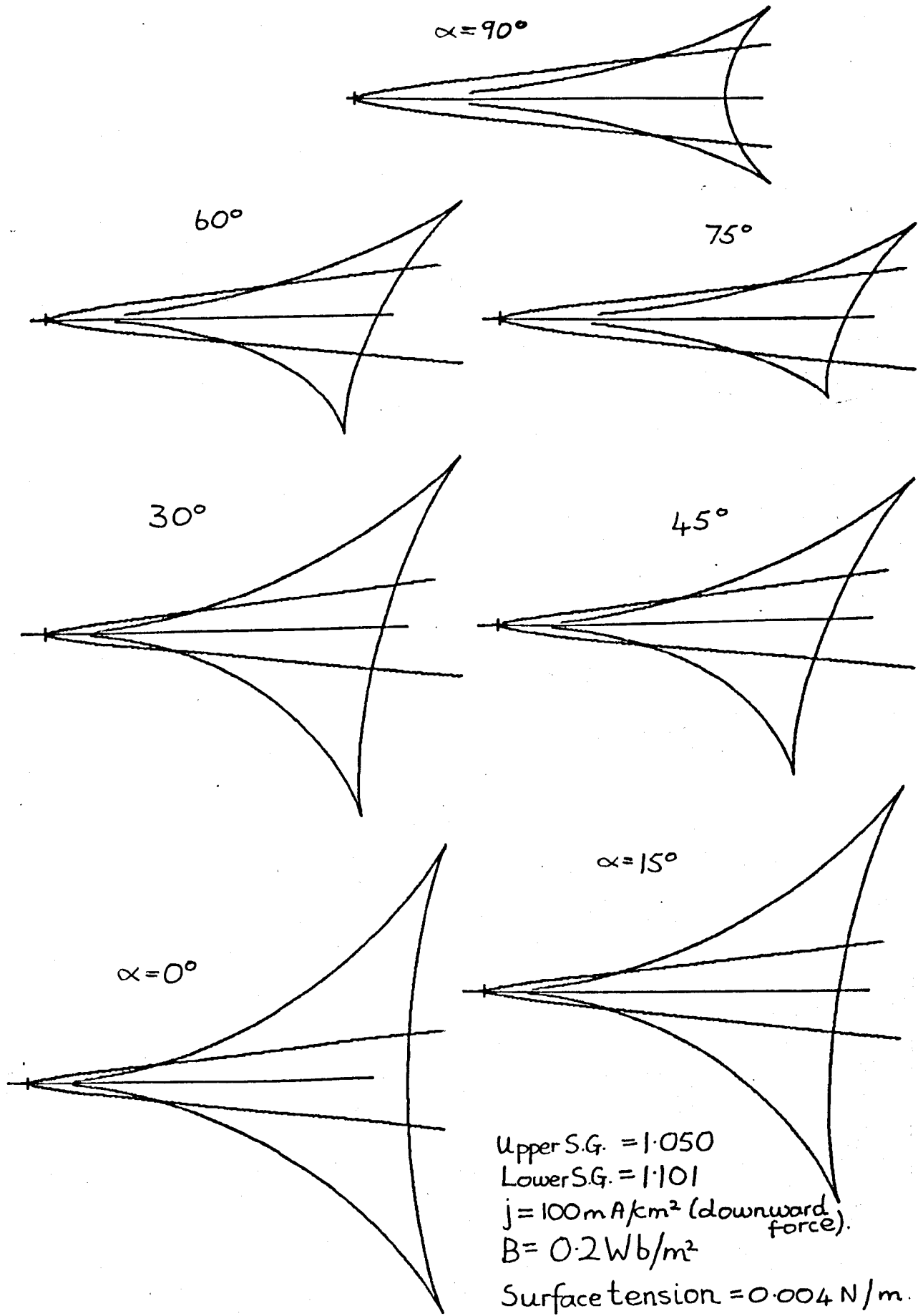


FIG. 3.26. "FISH-LINE" WAVE PATTERNS.  
 a) Velocity = 0.5 m/sec.

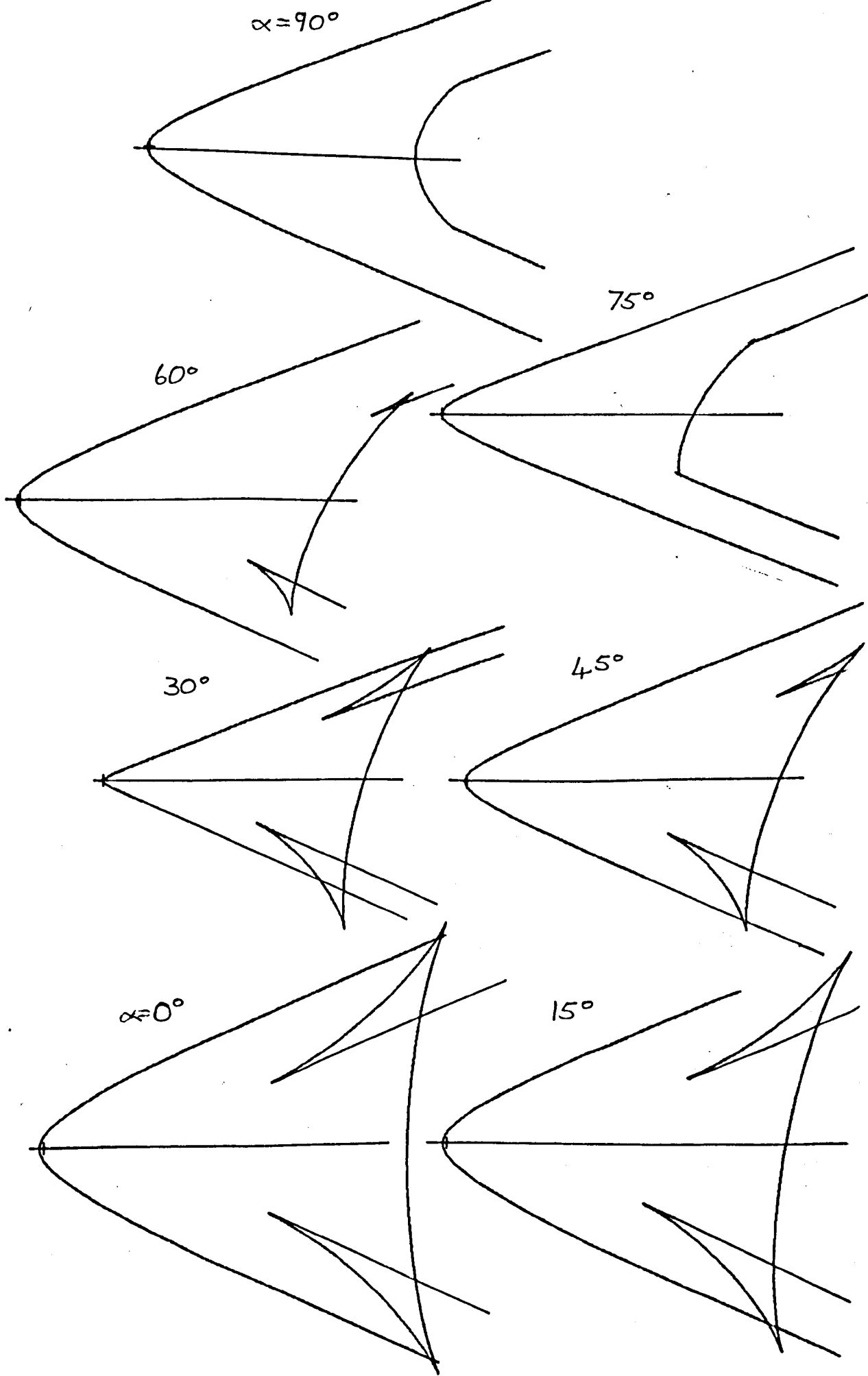


FIG. 3.26 (b) As for (a) except velocity = 0.1 m/s.

4. EXPERIMENTAL PRODUCTION OF ANISOTROPIC SURFACE WAVES

4.1 The Basic Problem

4.1.1. The nature and scope of the problem

This chapter describes the efforts to demonstrate in practice some of the phenomena whose existence is theoretically derived in chapters 2 and 3. The basic problem was to build suitable apparatus where the anisotropic surface waves would be both created and observed, and if possible, measured to give some comparison with theoretical predictions. The whole exercise illustrates well a fact which is both the strength and weakness of experimental M.H.D., viz that there are two sets of parameters, both electrical and fluid mechanical, which can be varied, and suitable values of which have to be satisfied by the materials used. Thus in a case like the one under investigation which basically just uses the electromagnetic forces to modify a fluid mechanical phenomenon without any true M.H.D. coupling effects, flexibility is gained by having the  $\mathbf{j} \times \mathbf{B}$  force as a type of gravity force, since it is possible to readily vary  $\mathbf{j}$  and  $\mathbf{B}$  whereas in the O.H.D. case it is not possible to alter  $g$  at all. However this is at the cost of limitations on the scale (since there is a limit to the spatial dimensions over which  $\mathbf{j}$  and  $\mathbf{B}$  can operate within a limited budget) and on the materials used, since the fluids chosen must have not only suitable fluid mechanical properties but also suitable electrical properties, and the containing vessels, probes etc., must also be chosen bearing in mind that electrical boundary conditions must be met.

At the outset it was decided that visual observation of the waves was to be used, since part of the aim of the project was to make it possible to observe visually an anisotropic wave system.

Visual observation gives a good indication of the wave patterns though it is not easy without the most sophisticated techniques to determine amplitudes by visual means. On the other hand amplitudes and frequencies can be recorded accurately by the use of surface-height sensing probes, but even with an array of probes it is not possible to plot the spatial distribution of troughs and crests very easily. Since the problem was posed in the theoretical chapters chiefly as a kinematic problem, concerned with wave patterns rather than amplitudes and in most cases at a fixed frequency throughout, visual observation was obviously the most suited to the particular needs of the problem:

Having established the use of visual observation it is worthwhile to show the extent of the experimental problem by listing all the parameters which to a greater or lesser degree were relevant to the success of the project, and therefore influenced the choice of fluids and equipment design.

Choice of working fluid

Density

Viscosity

Surface or interfacial tension

Miscibility with any other working fluids being used.

Electrical conductivity (including by-products of conduction  
if electrolytic)

Volatility

Toxicity

Corrosive nature

Flash point

Reflectivity of surface to light or transparency and refractive index

Availability and cost

External Parameters

- Magnetic field - magnitude  
spatial extent  
uniformity
- Electric current - magnitude  
- required voltage depending on conductivity
- Boundary conditions conductivity of containing vessel  
conductivity of probes, wave-makers etc.  
transparency to light to enable observation

4.1.2 The basic alternative systems

The central aim was to be able to produce a  $\underline{j} \times \underline{B}$  force of the same order as the gravity forces, and it was this which narrowed the choice of liquid down to three possible systems.

A magnetic field of  $0.2 \text{ Wb/m}^2$  was selected as being typical of a field which could be produced without too much difficulty by water cooled magnets. Moreover, currents induced by wave motion in such a field should be negligible compared with the applied current. At such field strengths, ohmic damping (see Shercliff 1969) should be negligible for the poorer conducting electrolytes. For the better conducting liquid metals, care would need to be taken that the magnetic field was kept low enough for ohmic damping to be no greater than viscous damping. It is convenient to take  $g$  as  $10 \text{ m/s}^2$ .

Given this the three basic alternatives were :-

a) Electrolyte as working fluid, covered by non-conducting liquid to reduce gravity effects.

After some tests, it was discovered that typically, an electrolyte could cope with a current of  $100 \text{ mA/sq.cm}$  ( $1000 \text{ A/sq.m.}$ ) for periods of a few minutes without overheating or producing very

much gaseous by-product at the electrodes. Here  $jB = 200$ . Thus for  $\rho g$  to be the same,  $\rho$  must be 20, and this is only achievable by superposing one liquid on another, so that

$\rho_2 - \rho_1 = 20$ . With electrolytes having  $\rho$  of order 1000 this means matching densities to within 2% of each other.

b) Mercury as working fluid

In mercury with copper electrodes  $j$  could easily be  $5 \times 10^5 \text{ A/m}^2$  so that  $jB = 10^5$ . Thus since  $\rho \approx 13 \times 10^4$ ,  $jB$  can be of the same order as  $\rho g$ . A superposed non-conducting liquid is unnecessary and would be of little benefit since any suitable transparent liquid would be of density an order of magnitude less.

c) A light liquid metal, such as liquid sodium or a sodium-potassium eutectic mixture. This also is capable of carrying  $5 \times 10^5 \text{ A/m}^2$  comfortably, so that  $jB = 10^5$  could be achieved. This would be ample to compare with  $\rho g = 10^4$ , and in fact the liquid metal would need to be covered from the atmosphere by an oil or other organic liquid so that  $(\rho_2 - \rho_1)g = 10^3$ . This system was first pioneered by Northrup (1907).

Alternative (c) was the best from the point of view of it being easy to provide a  $jB$  up to two orders of magnitude greater than required, so that any other practical constraints reducing  $j$  and  $B$  would not be likely to jeopardise the success of the experiment, whereas in cases (a) and (b),  $jB$  would have to be pushed to its maximum practical limit to achieve a situation where anisotropy should be significant.

However the danger of using extremely reactive liquid metals, the consequent expense and complication of necessary heating, handling and safety ancillary equipment, and the lack of expertise within the laboratory for dealing with liquid sodium and potassium,

made alternative (c) an impossibility, although in a laboratory equipped for such materials it provides the most suitable range of experimental parameters - notably because of the low density and good conductivity of liquid sodium and potassium.

Thus the alternatives (a) and (b) were the ones used.

#### 4.2 Preliminary Experiments Using Mercury

##### 4.2.1 Introduction

Attempts were initially made to produce anisotropic surface waves using a small mercury rig, making use of equipment immediately to hand. The main aim of this attempt was to discover whether the practical problem was trivial, and if not, what the major experimental difficulties would be. Although not very successful, their description is included here since some progress was made and understanding gained which would be useful to incorporate into any new mercury experiments. The basic shortcoming of this rig was the small size (6.3 cms x 15 cms) of the plan area of the trough, necessary principally to fit the magnet used, but also necessary so that the total electric current required would not be too great to be supplied by available generators, and also so that the pertinent area of the liquid surface would be small enough for waves to be observed easily by reflective methods.

##### 4.2.2. The experimental equipment

a) The magnetic field: This was supplied by a large water cooled Lintott electromagnet, the one used by Hunt (196<sup>7</sup>~~8~~) who has described it in detail. It has a magnet gap 3" wide, 66" long by 9" deep, and will produce a field up to  $1.2 \text{ Wb/m}^2$  accurate to within 0.5% over the centre volume of 60" x 3" x 3". This was fed by a 1000 A 60V DC motor generator.

b) The tank containing mercury. This was made of perspex, 1" thick floor and ends with  $\frac{1}{4}$ " thick side walls, see fig. 4.1. After an incident when with an upward  $j \times B$  force the mercury surface went unstable due to the M.H.D. Rayleigh-Taylor phenomenon, resulting in mercury being thrown a height of 8ft or more to the ceiling of the special mercury laboratory, a lid was fitted.  $\frac{1}{4}$ " copper bars were bent to fit into the ends of the tank to act as electrodes, and the return path was carried immediately underneath the tank to eliminate induced magnetic field as far as possible.

c) Current supply: This was supplied by another motor generator capable of supplying 1000 A at 60V, via the bus bars fitted inside the mercury laboratory. Since a large current was required at a voltage drop of much less than 1 volt across the mercury, a large stabilizing resistor was placed in series with the tank, so that 1000 A was drawn from the generator at 30V, effectively ensuring constant loading of the generator. With a typical depth of 2.5 cms, to attain a density of  $5 \times 10^5 \text{ A/m}^2$ , 750A needed to be supplied. Thus if this density was to be maintained, given the current supplies available, the cross sectional area of mercury could be increased very little more, whether by widening the tank and using a wider magnet gap or increasing the depth of mercury. This, in fact, was the biggest obstacle to increasing the size of the mercury experiments.

d) Wave production. The aim was to produce the wave pattern due to a point source oscillating at constant frequency, and from this observe the anisotropy. It would have been fruitless to use plane waves and measure wavelengths in different directions since the size of the tank would result in interference by reflection and there would not be sufficient room for a wave train to develop.

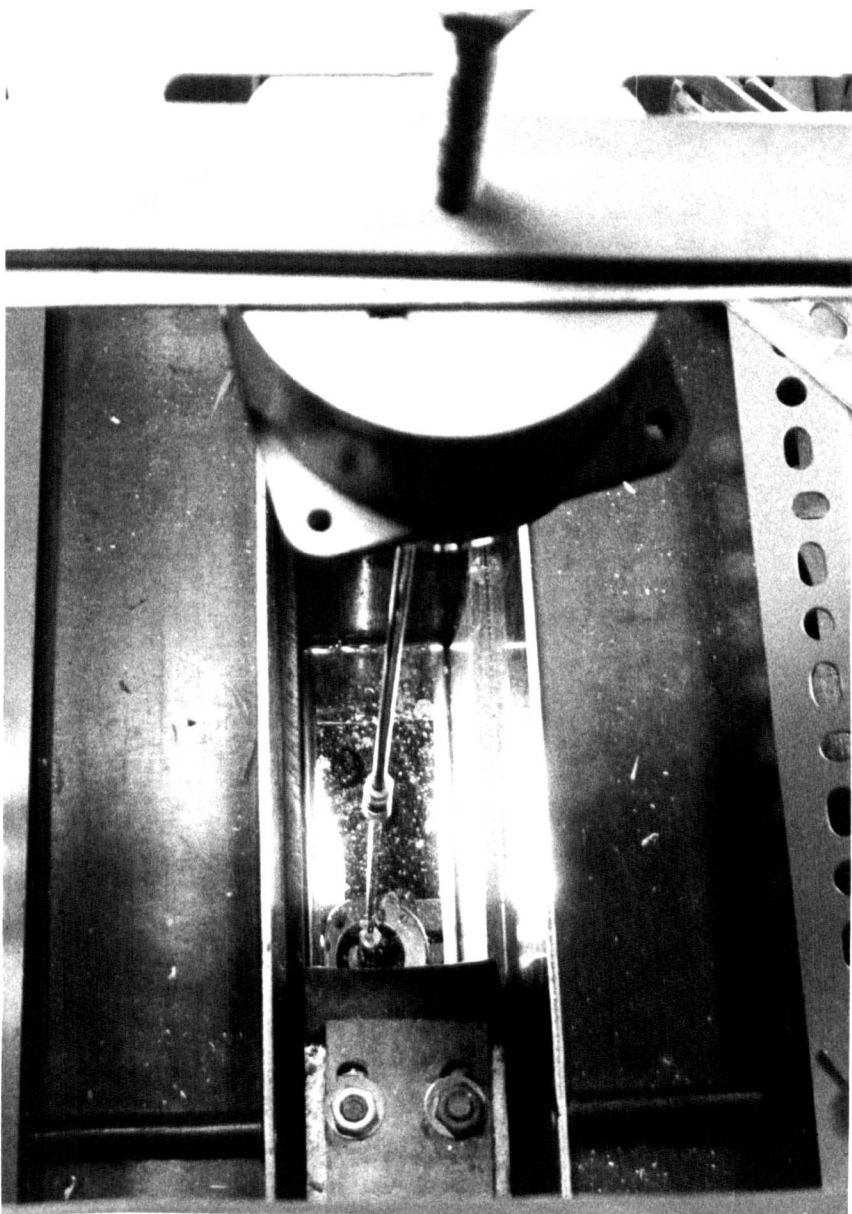


FIG. 4.1. TANK FOR MERCURY  
EXPERIMENTS.

The only other alternative to demonstrate anisotropy in the confined space would have been resonance experiments with the standing wave modes, but these were rejected since they would not show up the anisotropy explicitly, nor were they expected to be very conclusive because of the dominant and varying meniscus edge effects in the mercury.

Wave production was effected by means of a Derritron VP2 vibrator coupled to a suitable sine wave signal generator and amplifier. This was capable of producing frequencies down to 4 c/s without distortion. This was suspended on a Dexion framework above the magnet gap, and the vibration transmitted to the mercury surface through a brass push rod having a conical shaped probe tip 1 cm in diameter,  $45^\circ$  semi-vertical angle, which protruded a few millimetres into the surface. Initially a perspex tip was used, it being necessary to prevent the probe earthing the surface at that point by an earth path through the vibrator. However with the current and field switched on it was found that the distortion of current round the probe caused considerable motion resulting from the consequent rotational  $\mathbf{j} \times \mathbf{B}$  forces. A copper cap was then placed over the perspex, still insulating it from the push rod, but being a better conductor than mercury this still had the effect of distorting the current, and the motion was more violent. The spurious motion was reduced to a minimum, though not completely eliminated, by using a probe tip made of Nicontin 75 - a copper/nickel alloy, having a conductivity almost equal to that of mercury, and by letting it protrude as little into the surface as was necessary to transmit sufficient energy to the waves to make observation possible.

e) Observation. Various methods of observing the waves were considered, notably visual methods and direct probes.

A surface-height measuring probe was developed, using 2mm pencil 'lead', held in a brass clamp, the end of the lead dipping into the mercury. With an electrical circuit to measure the resistance of the lead not immersed, using a fairly soft 'B' grade lead (which gives the optimum resistance), and given a clean mercury surface, such a probe was found to be able to record the surface height accurately, though dirt brought contact resistance and meniscus problems. Even with these drawbacks the probe would give a good indication of a wave train passing the probe station, but the use of the probe was discontinued for the more general reasons outlined in 4.1.1. and optical observation methods pursued.

The obvious optical method that was chosen was the reflection of light from the mercury surface. With the surface illuminated by parallel light normal to the undisturbed surface, viewing from above will reveal a uniformly illuminated surface, but with a disturbed surface, only those parts of the surface that are horizontal will appear illuminated. Thus a wave train would show up light where the troughs and crests are, and dark elsewhere. A general view of the system adopted is shown in fig. 4.2 and the optical path diagrammatically in fig. 4.3. A 10" condenser lens was used with the point light source at its focus, and the horizontal parallel beam was directed on to the surface by a mirror at  $45^\circ$  with a hole in its centre to let the vibrator probe through to the mercury surface. Viewing was facilitated using a semi-surface-silvered mirror in the path of the horizontal beam. The system was lined up with the help of

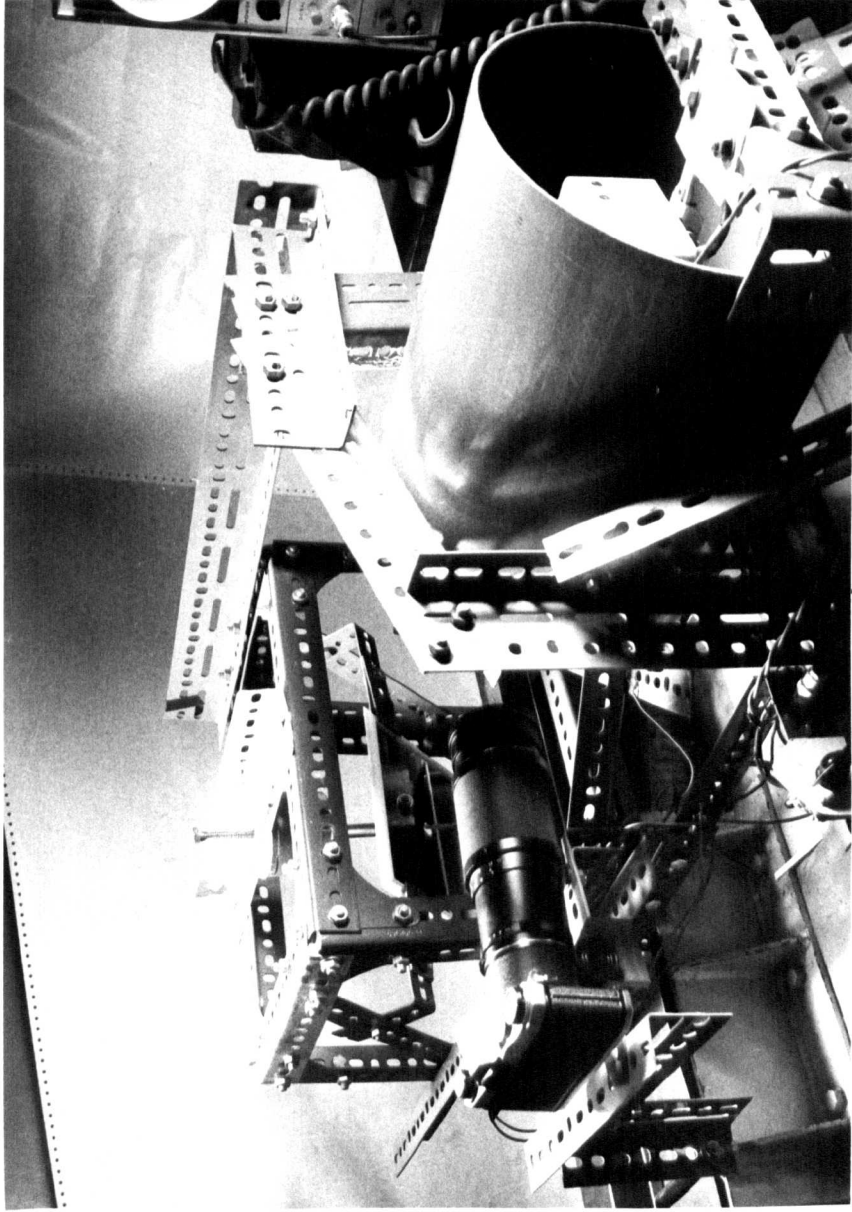


FIG. 4.2. GENERAL VIEW OF MERCURY  
EXPERIMENTS EQUIPMENT.

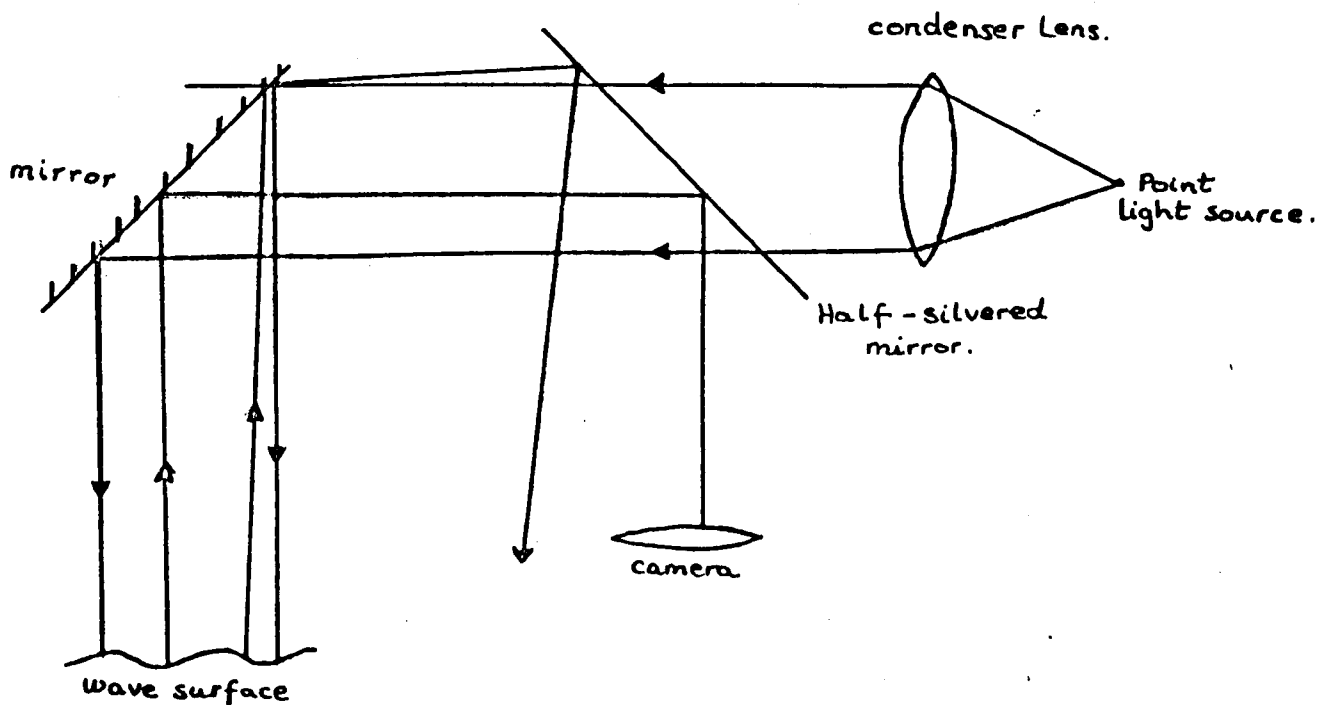


FIG. 4.3. OPTICAL PATH FOR MERCURY WAVE EXPERIMENT.

the vertical probe, using this to ensure that the viewing line was normal to the surface and then moving the source until uniform bright illumination was gained. To get a close up view of the surface a Pentax S.1.a camera was used with a 200mm telephoto zoom lens and a No.2 extension tube.

The final problem was that of 'freezing' the motion, at a suitable time after the initiation of vibration, long enough for the starting transients to have disappeared and the steady wave system to be established, but before the energy front had propagated to the sides of the tank and produced reflected waves and consequent interference. The observation system adopted was to open the camera shutter with the rig in darkness, start the vibrator with a switch that also started an electronic timer which, after a fixed time of the order of a few tenths of a second, operated a relay to make the circuit of the electronic flashlight which was being used as the light source. By varying the interval of the timer, the optimum wave pattern was obtained on the photograph.

#### 4.2.3. Observations and Conclusions

Using the equipment and method described in 4.2.2., attempts were made to obtain photographs showing oval wave crests and troughs proceeding from the point source. Different frequencies were tried, between 4 c/s and 30 c/s. It was found that at the lower end of this frequency range the surface slopes produced were insufficient to be observable using the given optical system, probably because of the long wavelengths involved and the fact that less energy was transferred to the waves (it being dissipated in moving the meniscus up and down). At the higher end of the frequency scale, wavelengths were so short (2 or 3 mm) that surface tension effects dominated and the

ripple pattern was circular. At intermediate frequencies, around 10 c/s, there was a definite difference between photographic records with the current off, when the waves were circular, and with the current on, when photographs such as fig. 4.4. were obtained. Clearly there is some suggestion of anisotropy in these photographs. They are, nonetheless, not conclusive for a number of reasons.

(a) Although care was taken to eliminate spurious fluid motions, and none was readily apparent, it is quite possible that fluid motions could be causing some advection of the wave crests, resulting in the observed pattern. (for fuller explanation of this see later in section 4.4).

(b) It is not clear whether what is observed, so soon after switch-on, is a phenomenon at the imposed frequency or a result of starting transients.

(c) Although it appears that the wave front has not yet been reflected at the side walls, the observed pattern could be the result of the interference of reflected waves.

(d) Working in such a small area, any variation in surface tension from place to place will not appear as an isolated kink in the wave crest pattern, but as a major part of the whole pattern. The symmetry of the observed results suggest that this is not causing the observed pattern, but nonetheless it is a problem to be considered.

All these objections to the validity of the observations could be overcome to some extent by using a larger tank. Unfortunately, the use of a larger tank is made virtually impossible by the requirements of providing a sufficiently large total current supply, and of observing a larger area by

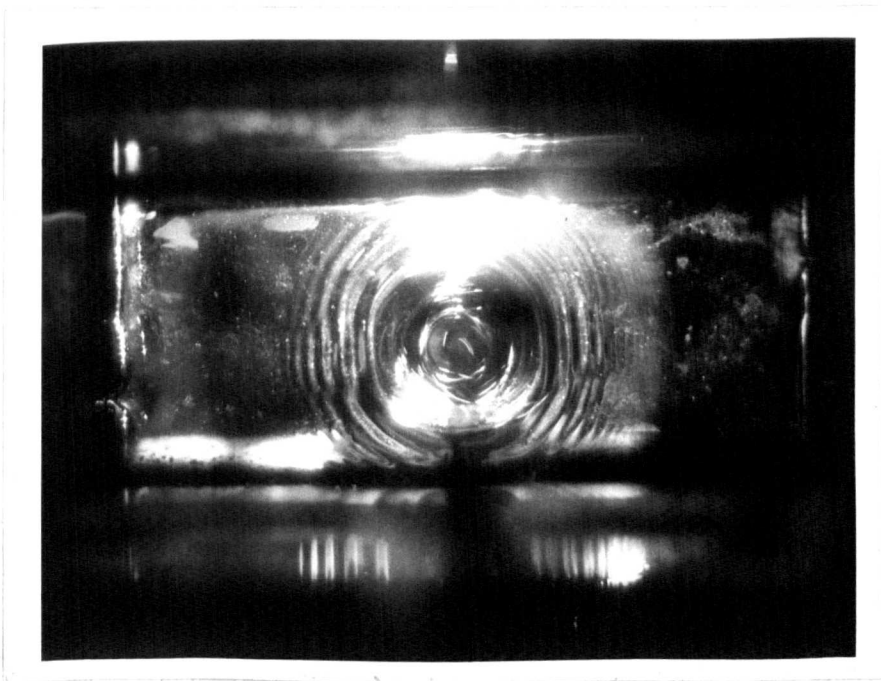


FIG. 4.4 TYPICAL PHOTOGRAPHIC  
RECORD OF MERCURY EXPERIMENT.

a reflection technique. For these reasons, it was felt that the mercury experiments had been developed as far as was reasonably practical, and attention was turned to using an electrolyte as the conducting fluid, yet with the encouragement that what had been observed probably, if not conclusively, was anisotropic wave propagation.

#### 4.3 Experimental Rig for use with Electrolyte

(Figures (4.5) and (4.18) show overall views of the experimental rig)

##### 4.3.1. The fluids used

a) The most obvious and suitable choice of electrolyte was copper sulphate ( $\text{CuSO}_4 \cdot 5\text{H}_2\text{O}$ ) solution, in conjunction with copper electrodes. Whilst not being quite as good a conductor as dilute hydrochloric acid solution, this had the advantage of being less corrosive whilst not producing gaseous by-products of electrolysis, and a solution having a concentration with specific gravity of about 1.10 was found to be able to carry a current density of 100 mA/sq.cm, under an electric field of about 3 volts/cm. It had the further advantages of being cheap, easily obtainable, and safe to handle, non inflammable, transparent to visible light, and being distinguishable by its colour from any liquid used to cover it. Being an aqueous solution its viscosity and surface tension were taken to be similar to that of water.

The choice of an upper non-conducting fluid of specific gravity around 1.1 was more difficult. An organic solvent or oil seemed the most promising type of fluid to search for, since most of these are not miscible with water. A silicon oil would have been ideal for its low volatility, non corrosive, non toxic and non flammable nature, but the molecular structure is such that the higher density oils have greater viscosity, and those with specific

gravity greater than 1.0 have viscosities at least two or more orders of magnitude greater than water, which from § 2.3.3. is unacceptable. The remaining alternative seemed to be to use a heavy chlorinated hydrocarbon solvent mixed with a light oil or organic solvent to achieve the required density. Trichloroethylene was ruled out since it readily attacks perspex, but carbon tetrachloride ( $\text{CCl}_4$ ) (sp.gr.1.595) was used in small instability experiments (see chapter 6). However in the wave tank with a large surface area the solvents evaporated, causing the density of the upper fluid to vary, and creating a health hazard from the toxic tetrachloride vapour. No less volatile solvent could be found, and the only way to avoid evaporation was by using a lid and taking care in the handling of the fluids, but to minimise the serious health risk, 1,1,1 trichloroethane (methyl chloroform,  $\text{CH}_3\text{CCl}_3$ ) was used, which has a much lower toxicity rating (see Sax - 1963) and should not produce any permanent damage to health although it is fairly anaesthetic. It was cheap and easily available under the proprietary name of "Genklene" produced by I.C.I. as a safe alternative to  $\text{CCl}_4$  and trichloroethylene. It has the same non-flammable properties, is an electrical insulator, only very slightly soluble in water, transparent to light, has a viscosity of around 1.2 cp (cf water at 1.0 cp) and specific gravity about 1.32.

It was mixed with white spirit (turpentine substitute, specific gravity = 0.85), which was chosen for its relatively low flammability, cheapness and availability. Olive oil was also used to mix with the Genklene but the viscosity of the mixture was up to two orders of magnitude greater than water, and waves would not propagate more than a couple of centimetres, justifying the assumption made above that the silicone oils would not be suitable either.

b) Handling the fluids

The copper sulphate solution in distilled water and the Genklene/white spirit mixture were made up in separate 5 gallon polythene containers, the specific gravity being tested with a sensitive hydrometer which measured specific gravity to the nearest 0.0005. One of the storage containers can be seen in fig. (4.5) in place for filling the wave tank. This was done slowly, filling from the bottom of the tank, copper sulphate first, and then letting the organic solvent bubble slowly through the copper sulphate to form a layer on the top. It was done this way to keep the solvent out of contact with the corners of the tank as much as possible to prevent it from attacking the perspex cement. Some trouble was experienced initially with the Genklene and white spirit dissolving some white p.v.c. insulation on the wiring to the electrodes and depositing it as an opaque screen on the lid, but thereafter anything likely to contaminate the liquids was excluded from the tank. In use, the liquids gradually became contaminated with copper particles and a green powder produced at the electrodes - probably a basic sulphate of copper ( $4 \text{Cu}^{++} \text{SO}_4^{--} 4\text{OH}^-$ ) due to the presence of small amounts of hydroxyl ions released by electrolysis with the water. When the liquids were drained to clean the tank, attempts were made to separate the two liquids, in a tall glass cylinder, and although it was found possible to do this, the liquids were sufficiently dirty by this time to make them unusable again, and so had to be thrown away after a few runs. They were not allowed to remain in the wavetank for more than a couple of days at a time for fear of corrosion to the perspex.

To reduce the interfacial tension, a proprietary surface tension reducing agent, Teepol, was added to the copper sulphate

solution in its container before use - a concentration of 5 cc to 10 litres was found to reduce the surface tension by an order of magnitude, without causing any noticeable blurring by mixing of the sharply defined interface between the two liquids. It was not found possible to measure accurately the interfacial tension, since it varied with time and place due to contamination of the fluids, but experiments with a length of glass capillary tube in a measuring cylinder containing both liquids showed that without Teepol the interfacial tension was around  $0.04 \text{ N/m}$ , and with Teepol added it could be reduced to around  $0.004 \text{ N/m}$ . It was also noted that when Teepol was used, a fine skin of impurities, or possibly the products of a reaction between the Teepol and the organic fluids, formed at the interface when the fluids were warmed by the passing of heavy electric currents after a prolonged run of a few minutes. This further necessitated the throwing away of the liquids after a few short runs or one protracted run.

For safety, rubber gloves were always used when handling the liquids, and cleaning out the tank. The lid of the tank reduced most of the vapour hazard, but an extractor fan was used to keep the working area clear of Genklene vapour. Being heavier than air this was easy to remove at ground level whilst breathing fresh air at head level.

#### 4.3.2 The scale of the experiments

Given the choice of working fluids, the next thing to be determined was the size of tank required, the spatial extent of magnetic field to be provided and the total current and potential differences to be supplied to the electrodes, so that these could be designed accordingly. The scale of the experiment was dependent upon the size of wavelength it was intended to observe. It has already been noted in 2.4.2 that the larger the wavelength the less

the surface tension dominates and the more anisotropic is the wave dispersion. Given specific gravities for the two liquids of about 1.080 for the upper and 1.100 for the lower, assuming  $B = 0.2 \text{ wb/m}^2$  and  $j = 100 \text{ m A/sq cm}$  and taking interfacial tension as somewhere between 0.004 and 0.04 N/m, the curves of figs. 2.8 and 2.9 apply, which relate maximum and minimum wavelengths and anisotropy ratio to frequency. From these it can be seen that to provide an anisotropy ratio of about 0.9, the largest that is likely to show up convincingly in experiment, a frequency less than 1.0 to 1.5 c/s is required corresponding to wavelengths of 2.5 - 10 cms or more. To have longer wavelengths and still maintain the surface wave approximation  $kh \gg 1$  would require a depth of the order of 10 cms or more, requiring an unacceptably high total current, and so 10 cms was considered to be the maximum practicable wave length. To enable such waves to develop and to be observed in the middle of a train away from the immediate influence of walls or wave maker, the tank would need to be of dimensions of at least 50 cms. square and consequently a magnetic field uniform over a volume 50 cms x 50 cms x 20 cms was required.

It was appropriate at this stage, having decided on the approximate scale of wavelengths, to make sure that the frequency /wave number relation for such wavelengths was not such that viscous effects would control the dispersion relation.

Table 4.1 shows the relative magnitude of the different terms in equation 2.34, given the above experimental parameters, for the highest and lowest wave numbers at the maximum frequency for reasonable anisotropy at the given surface tension.

If  $\sigma$  is assumed to be the same order as  $\omega$ ,  $m \approx \sqrt{\frac{\sigma}{2}}$ , and hence the term involving  $m$  may be evaluated.

Table 4.1 ; Relative magnitude of terms in the dispersion equation (2.34)  
involving viscosity (all in s.i.units)

$\rho_1$	1.080			
$\rho_2$	1.100			
B	0.2			
J	1000			
$\mu_2$	$1.0 \times 10^{-3}$			
$\mu_1$	$1.3 \times 10^{-3}$			
$\nu_2$	$0.9 \times 10^{-6}$			
$\nu_1$	$1.2 \times 10^{-6}$			
$\alpha$	0.004		0.04	
$\omega$ rads/sec	<del><math>1.0 \times 2\pi</math></del> $1.5 \times 2\pi$	<del><math>2\pi</math></del> $1.5 \times 2\pi$	<del><math>1.0 \times 2\pi</math></del> $4.0 \times 2\pi$	<del><math>2\pi</math></del> $1.5 \times 2\pi$
k rads/sec	$4.3 \times 2\pi$	$58 \times 2\pi$	$16 \times 2\pi$	$21 \times 2\pi$
$(M + \nu_M) 2k^2 \sigma$	$2.4 \sigma$	$4.25 \sigma$	$0.32 \sigma$	$0.56 \sigma$ (a)
$\sigma^2$	$\sigma^2$	$\sigma^2$	$\sigma^2$	$\sigma^2$ (b)
$4k^4 M \nu_M$	0.33	1.07	$6.33 \times 10^{-3}$	$19.6 \times 10^{-3}$ (c)
$\omega^2$	90	90	40	40 (d)
$4k^3 M (\mu_2 m_2 + \mu_1 m_1)$	$1.25 \sigma$	$3.1 \sigma$	$0.063 \sigma$	$0.15 \sigma$ (e)
$(\rho_1 + \rho_2)$				

Now if viscosity is to have little effect, the  $\sigma^2$  and  $\omega^2$  terms should be an order of magnitude greater than the others. If the value of  $\omega$  is substituted for  $\sigma$ , this is found to be adequately satisfied for the  $\alpha = 0.04$  case, and tolerably so for the larger wave number in the  $\alpha = 0.004$  case, but for the shorter wavelength, term (a) is about  $1/4$  and (e) is  $1/3$  of (d). This suggests we are working at the limits of our inviscid assumption, and that further efforts to match the densities more closely would be counter-productive.

All the wave experiments were intended to represent surface waves on a deep fluid. It was not found possible in the limited space to work with long waves in shallow fluid, since the small depth required for such waves could not be maintained in the two fluid case without the surface tension gathering the lower fluid up into isolated 'islands'. Moreover it would probably be extremely difficult to observe long waves whose amplitude was small enough to satisfy the linearity condition  $\frac{\delta h}{h} \ll 1$

#### 4.3.3. The Magnet

##### (a) Basic design

From the above considerations it was decided that a field of strength  $0.2 \text{ wb/m}^2$ , with a uniformity of  $\pm 5\%$  was required over a volume of  $50 \text{ cms} \times 50 \text{ cms} \times 20 \text{ cms}$  high (the field being in the direction of one of the  $50 \text{ cm}$  sides) with considerably better uniformity over the central  $30 \text{ cms} \times 30 \text{ cms}$  of working space. Since there was no available magnet, one had to be designed, and for this sort of volume it soon became apparent that an iron cored electro-magnet could not provide the uniformity required without large expensive pole pieces much greater in face area than the working section, whilst the large air gap would

destroy the advantage of using iron for an efficient magnetic circuit. Thus a Helmholtz coil pair, with the magnetic return path through air, turned out to be the cheapest design for these specific requirements. Based on a mean diameter of one metre, the centres 50 cms apart, the two coils were designed to produce a field slightly in excess of  $0.22 \text{ Wb/m}^2$  to within 5% over a central volume of 50 cms x 50 cms x 50 cms, and had the advantage both of providing a considerably greater volume of less uniform magnetic field which may prove useful for further M.H.D. experiments, and also of enabling visual observation of experiments within the magnetic field from all six sides of the cubic working volume. The magnet was to be designed to operate with a motor generator set rated at 60V, 1000 A, D.C. maximum, and so each coil would be made up of as many turns as were required to produce the required field, each turn carrying 1000 amps. To stop the bulk of the metal from encroaching on the working volume, and to keep the cost down, the best design was to use water cooled conductors, so that less metal need be used, and the design limit was then on the maximum total resistance to enable 60V to produce 1000 amps, rather than on the energy dissipation, which could be coped with by suitable design of water cooling circuits. The other major design choice was to use aluminium as the conductor. Having only  $\frac{2}{3}$  the conductivity of copper,  $1\frac{1}{2}$  times as much metal would be required, but being only  $\frac{1}{3}$  as heavy as copper, and about  $\frac{1}{10}$  the cost per unit weight at that time, aluminium was obviously the cheaper by a large margin.

#### (b) Construction and Installation

A general view of the magnet is given in fig. (4.6).

The detailed design and construction was carried out by the

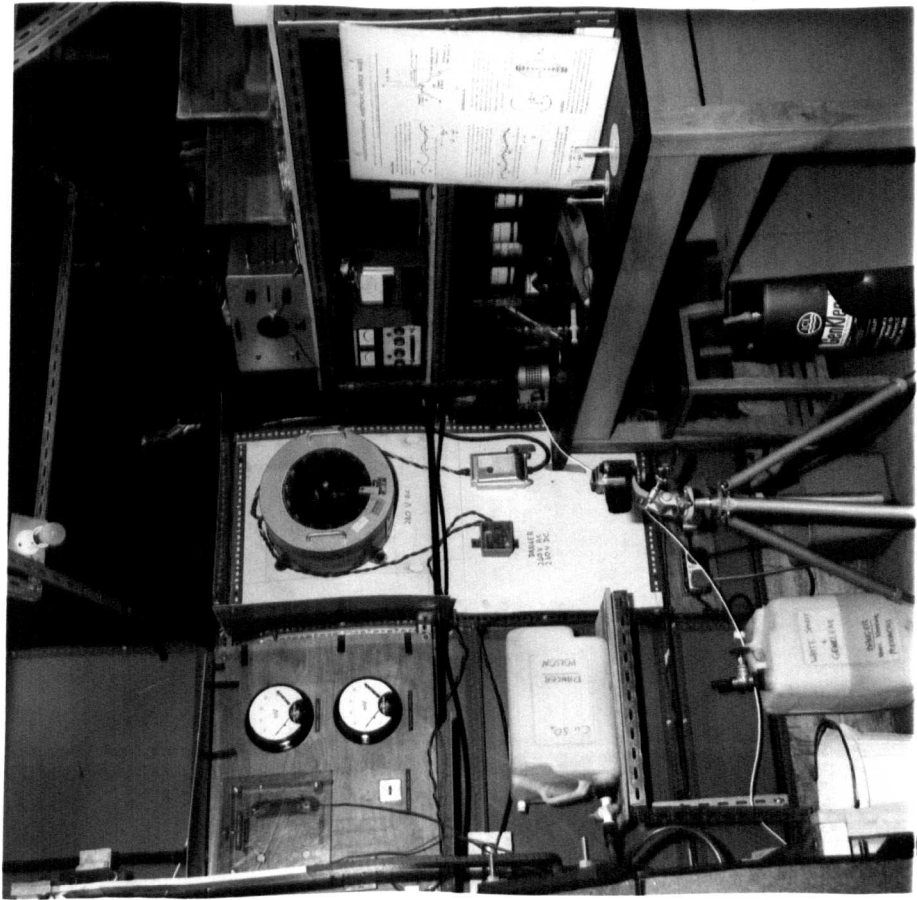


FIG. 4.5. VIEW OF ANCILLARY APPARATUS.

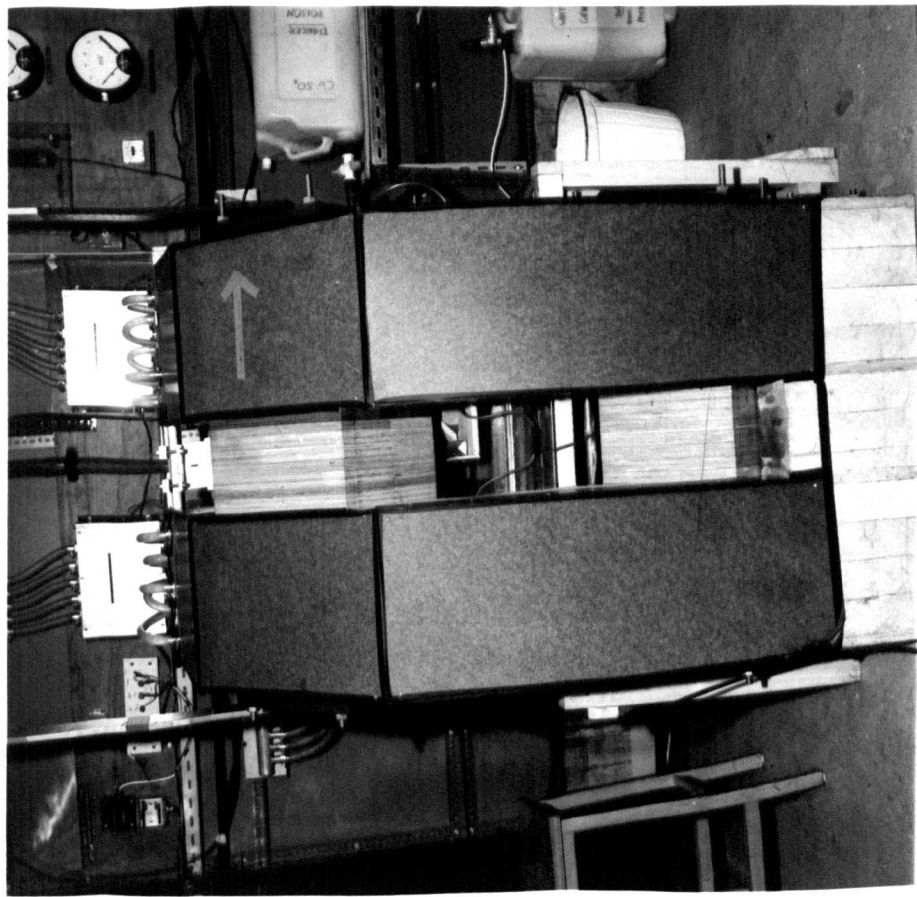


FIG. 4.6. VIEW OF HELMHOLTZ COIL MAGNET.

workshop of U.K.A.E.A. (Culham). Each coil consists of 5 pancake coils, each of 25 turns of aluminium hollow conductor with the section shown in fig. (4.7). The coils were wound with epoxy resin impregnated tape between the windings which was baked solid after completion of each pancake. The pancakes were held together by stainless steel tie rods between plywood end plates, separated from each other by polythene sheets, and the two main coils were kept apart by four solid blocks of hardwood. The coils were wired electrically in series, whilst the cooling water circuits were in parallel. The most difficult problem to overcome was that of obtaining the aluminium conductor section which had to be specially extruded, and this delayed the delivery of the magnet by nearly a year. When the magnet arrived, it was mounted on a solid softwood base, formed to take the coils over the bottom 90° of arc of their circumference. The tie bars were initially eased off to allow the coils to settle home before the final plumbing and electrical connections were made. Connection to the motor generator set was by way of 1/2" x 3" aluminium bus bars, and joints were made by clamping clean faces together with 'Electrolube' grease between the faces. The cooling water was led from a 2" aluminium manifold pipe through 3/4" nylon reinforced plastic tube to the inlet, and led out in a similar way through the flow monitoring devices. Each pancake was designed to take one gall/minute flow at 80 psi inlet pressure, and this was provided at first by the laboratory mains. It is planned to instal a distilled water closed loop cooling circuit with heat exchanger, to prevent corrosion of the aluminium, and what is more at risk, to prevent scaling up of the comparatively narrow cooling water passages by the mains water.

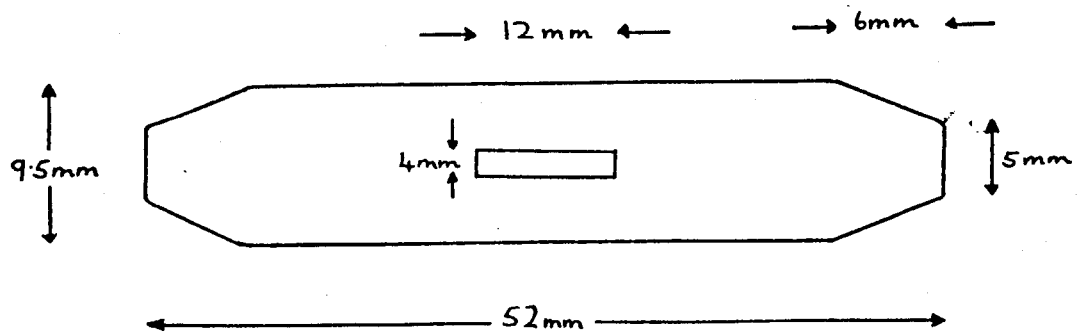


FIG. 4.7. MAGNET HOLLOW CONDUCTOR SECTION. (2 x full scale).

(c) Magnet protection devices

The electrical inlet and outlet of the magnet were connected by a 1" x  $\frac{1}{2}$ " aluminium bus bar through two heavy duty diodes, so that under normal running the magnet was not shorted out, but should the external supply circuit be suddenly broken (e.g. by a bus bar connection being cut) the energy stored in the magnetic field would be able to dissipate ohmically by currents circulating through this short circuit link.

The magnet was protected from overheating by cooling water flow monitors linked automatically with the motor generator. Fig. (4.8) shows one of the flow monitors, and fig. (4.9) the associated electrical circuits. When the flow is sufficiently high i.e. about 0.9 galls/minute, the aluminium float is raised up inside the glass tube, rather like a rotameter flow measurer, except that being cylindrical rather than conical there is a go/no go state rather than a gradual movement as the flow is increased or decreased. When all the floats are up, signifying that sufficient cooling water is flowing through all the coils, a light beam operates a light switch, making a low voltage circuit which activates a relay closing a switch in a mains voltage magnetic holding circuit for the main contacts of the motor generator. Thus unless the water is flowing the motor generator will not run without being held in manually. The device is fail-safe, except that to allow the motor generator to be used for other purposes when the magnet was disconnected, a switch was installed to bypass the relay.

(d) Calibration, uniformity etc.

Fig. (4.10) shows a plot of magnetic field along the axis of the coils, at the centre of the magnet, against the current through the coils. Using the traversing gear described in a later

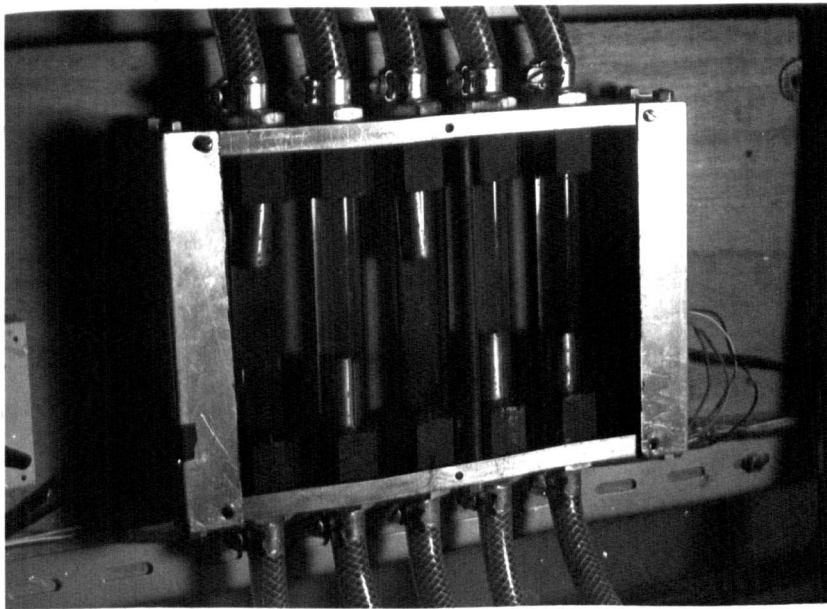


FIG. 4.8. FLOW MONITOR.  
(front removed).

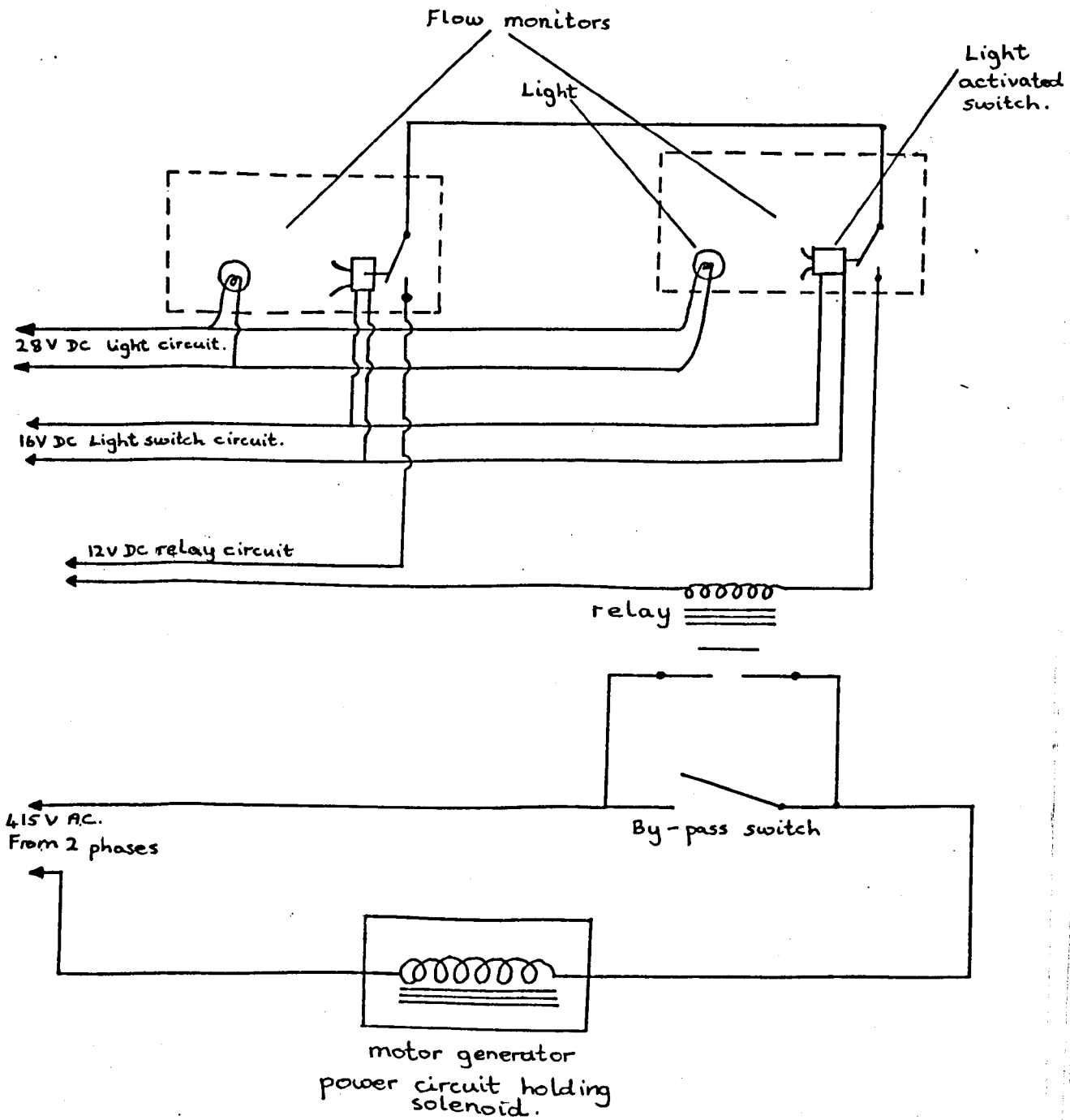


FIG. 4.9. MAGNET PROTECTION ELECTRICAL CIRCUITS.

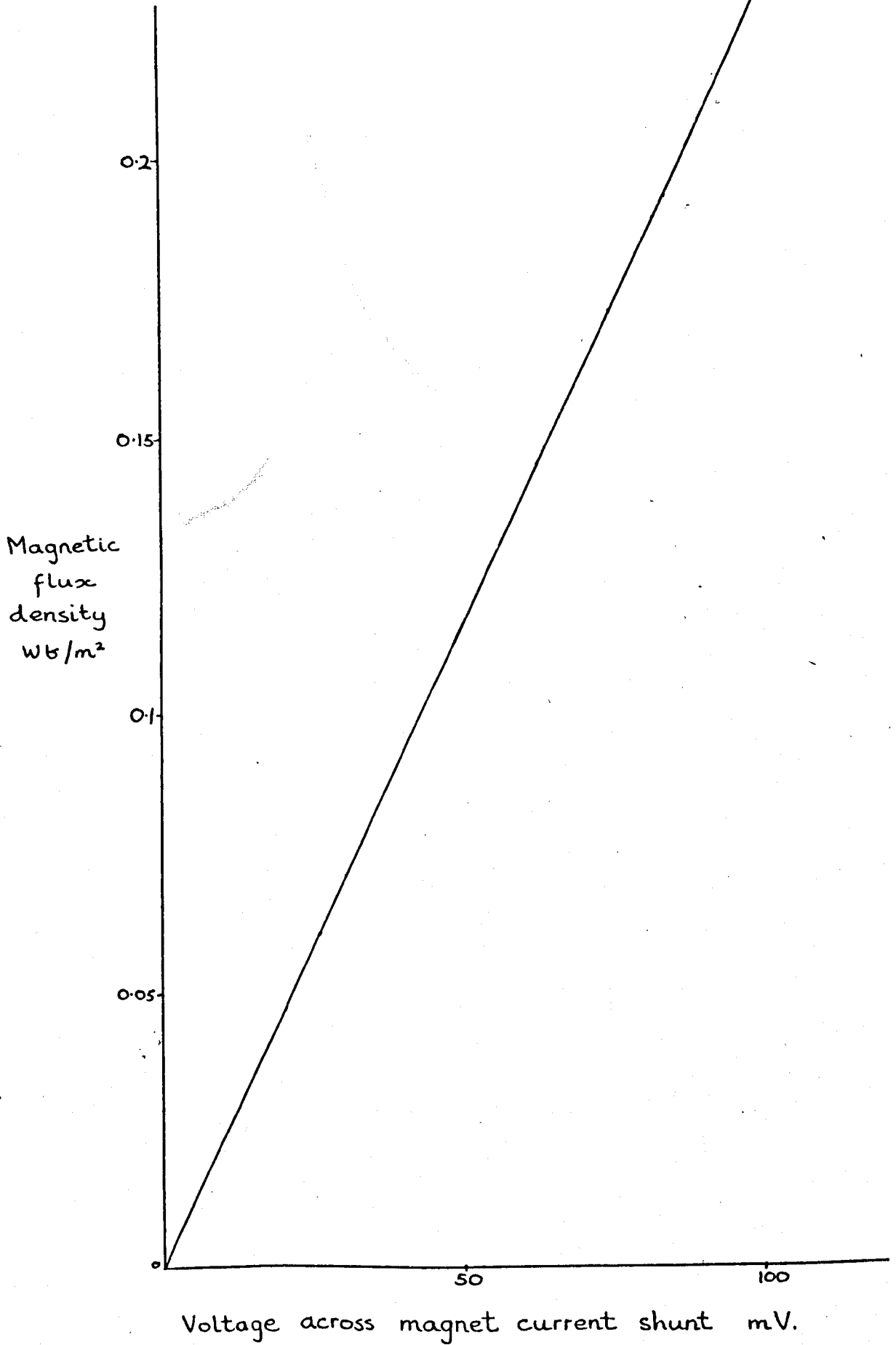


FIG. 4.10. MAGNET CALIBRATION CURVE.  
(axial field at centre of magnet)

section, a Hall probe magnetometer was traversed across the working volume, to measure the axial field, and the horizontal field normal to the axis, for the plane at which the fluid interface was planned to be. Sample values were taken at different planes a few cms above and below this, to cover the volume covered by the tank, but no difference in field could be detected. From fig. (4.11) it can be seen that the field is uniform to within 5% over the centre 50 cms x 50 cms area, and within 1% over the central 20cms x 20 cms. The field normal to the axis is plotted in fig. (4.12). A constant has been added to the measured field to make the value <sup>zero</sup> at the centre, since whilst the probe was at the same orientation throughout, it may have been slightly rotated from the desired direction and so measured a small component of the axial field, which would be the same throughout. Over the central 20cms x 20cms the transverse field is effectively zero, within the limits of the measuring instruments, and over the 50 cms x 50 cms area rises to just over 5% of axial field in the corners.

#### (e) Stray field

With a large magnet having an air return flux path, it was envisaged that trouble could be caused by stray field. The field outside the magnet is plotted in fig. (4.13). Whilst not spreading beyond the experimental area in a strength likely to affect other work in the laboratory the stray field did pose a hazard in the area immediately around the magnet. The coils themselves were boxed in with hardboard to protect against shorting and damage by ferrous metal objects attracted to the magnet by mistake. Reed relays in the light switches of the flow monitoring devices as well as other magnetic sensitive electronics and transformers had to be located well out of the way,

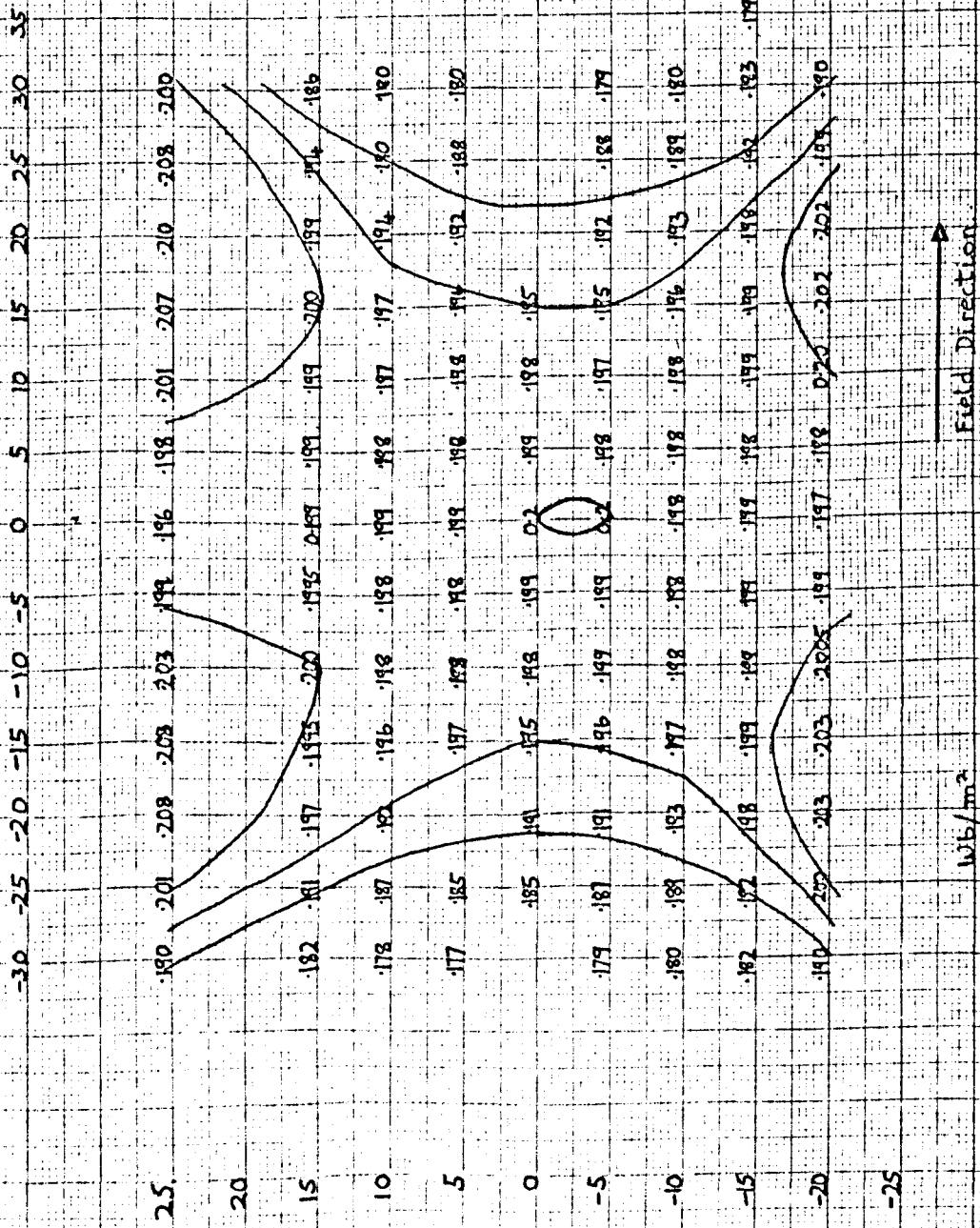


FIG. 4.11. AXIAL FIELD PLOT (Horizontal plane through centre).



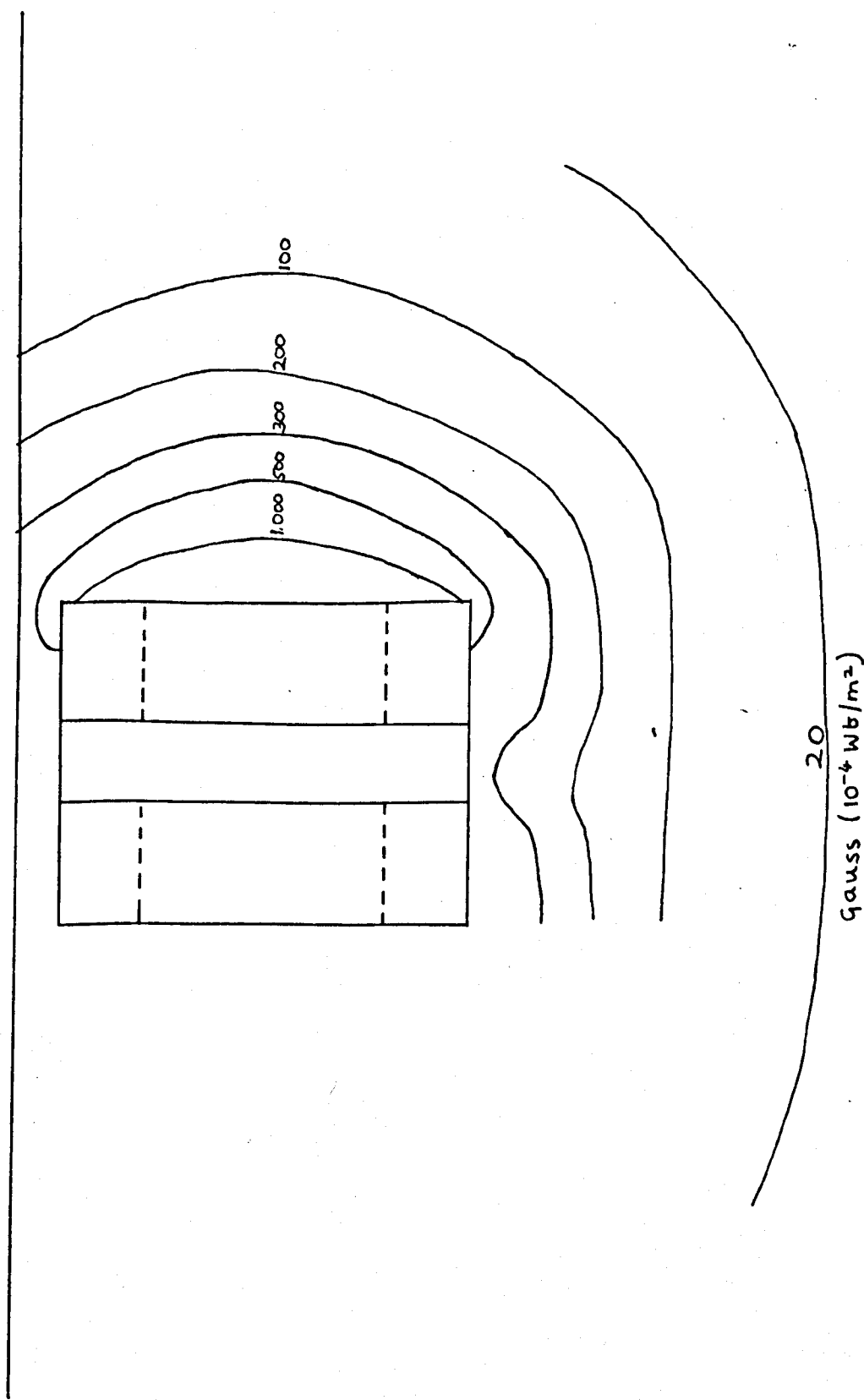


FIG. 4.13. STRAY FIELD ROUND MAGNET AT LEVEL OF MAGNET CENTRE

and mechanical equipment having ferrous parts such as camera shutters and the drive to the wave maker were found to be affected by the stray field. Whereas with iron cored magnets, electrical equipment and small motors etc will operate comfortably just outside the working section, in this case the strong stray field was an important factor in the design of much of the ancillary equipment.

#### 4.3.4 The electric current supply

The current was supplied to the working fluid through copper mesh electrodes, mesh size 28 per inch. This was used in preference to solid copper since it was found to be less prone to silting up over areas wide enough to cause distortion to the current density pattern, and its overall contact resistance seemed to be lower than solid copper. Also, it was easier and cheaper to replace than solid copper sheet. The DC supply required to produce 100 mA/sq cm over a cross section of 70 cms x 2.5 cms and a length of 70 cms between electrodes, was found to be up to 20 A at up to 200V. After some trial attempts with the laboratory DC supply, regulated wastefully through a variable resistor bank in series, an AC supply was used, voltage controlled through a 20A Variac Auto transformer, and then full wave rectified through a diode bridge. No attempt was made to smooth the ripple as the 100 c/s frequency would not be 'felt' by the fluid (as discussed later in 5.5). Fig. (4.5) shows the Variac in place, and the DC connections to the left of it, along with voltmeter and ammeter for the DC supply and the magnet supply current ammeter. The P.V.C. sheet surrounding the electrical connections was placed there to reduce the risk of accident should a hose come off the cooling water high pressure manifold.

#### 4.3.5 The wave tanks

The main wave tank designed for use to demonstrate the existence of anisotropic surface waves, is shown in fig. (4.14). It was 70 cms x 70 cms, built of perspex, since this was easily worked, strong enough for the job in hand, transparent to light, and although a little difficulty was experienced with Genklene attacking the joints, in general it was easily bonded and formed a fluid-tight seal using perspex cement. The only alternative would have been to use a glass bottom and metal frame and walls, but the problem of a fluid seal, and of insulating the metal from shorting out the electrolyte far outweighed the problem of Genklene corroding the perspex. This tank was designed for use with  $\underline{j}$  always normal to  $\underline{B}$ , and advantage was taken of the fact that  $\underline{j}$  varying in a plane normal to  $\underline{B}$  will not cause rotational  $\underline{j} \times \underline{B}$  forces, by shaping the tank floor down at the electrode edges to form a deeper trough into which the electrode fitted. This enabled current densities at the electrode/electrolyte interface to be considerably less than in the main bulk of the fluid, reducing contact resistance. At all four of the edges 10° sloping beaches were incorporated at the level at which the interface was expected to be, to help prevent reflection of waves interfering with observation. These 'beach' sections were removable to assist cleaning, and to enable the electrodes to be cleaned and replaced. Fig. (4.15) shows the detail of the design at the side walls.

A filling and draining hole was provided on one end wall, at the bottom of the trough section on one side, with a tap on the outside. A lid was built of 10 mm perspex with a rim around it, fitting inside the tank with 5 mm clearance all around so that it

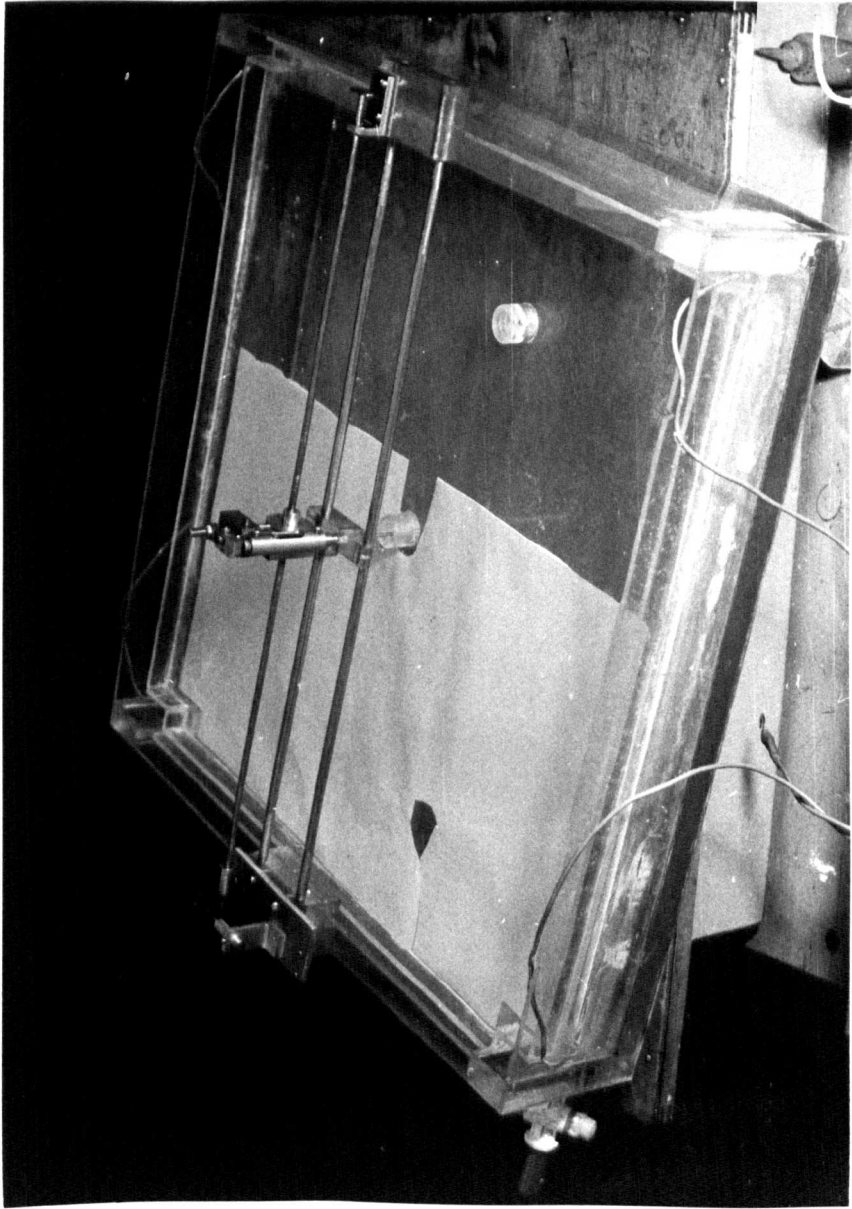


FIG. 4.14. MAIN WAVE TANK.

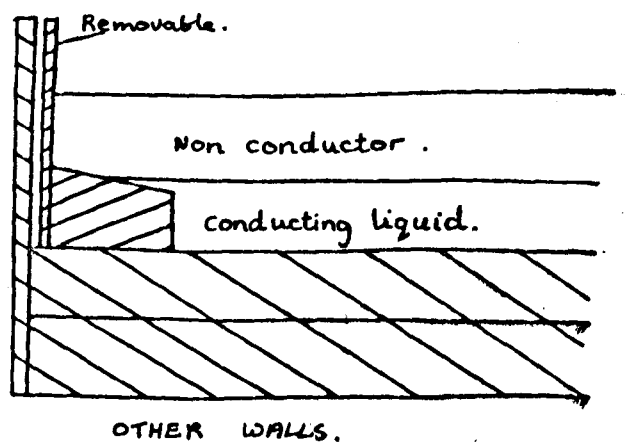
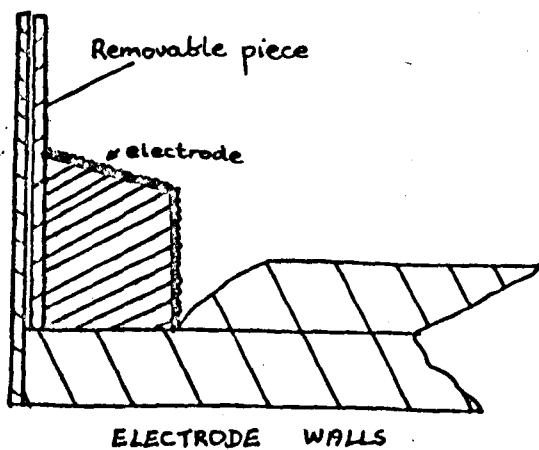


FIG. 4.15. SKETCH OF DETAILS OF LARGE TANK.

floated on top of the upper liquid and not only prevented evaporation but provided a solid top surface for the upper liquid, thus preventing further waves on the top surface. Holes (protected from leakage by circular rims) were provided where necessary for probes and other ancillaries, described later.

The tank itself was supported on a wooden trestle frame, straddling through the centre of the magnet, bringing the level of the beaches of the tank into line with the centre of the magnet. It is seen in position in fig. (4.16).

After experience with this large tank, a second tank was built, shown in fig. (4.17). It was designed particularly so that it could be used in the instability experiments of 6.6., i.e. to be able to swivel inside the magnet so that the current could be directed at any orientation to the magnetic field. For this purpose it was smaller (40 cms x 40 cms), though 20 cms deep to cope with deeper fluids, and was fabricated from perspex, a 24 mm thick base with 8 mm walls. Because it was to be used at any orientation the base was perfectly flat, and no beaches were used. The electrodes were again copper mesh, covering the whole of two opposite walls supported by silver soldering onto a brass frame, held in place by P.V.C. sheet bent over the edges of the tank, which also provided protective insulation against accidental touching. A perspex lid with a rim was also made to fit inside and float on the upper liquid. The whole tank was supported inside a framework made of brass angle, with rollers at the four corners running on a circular rail of bent brass sheet on a plywood base. The plywood base rested on the wooden trestle in the magnet, and when in the centre of the magnet, the tank could be freely swivelled through  $360^\circ$ .

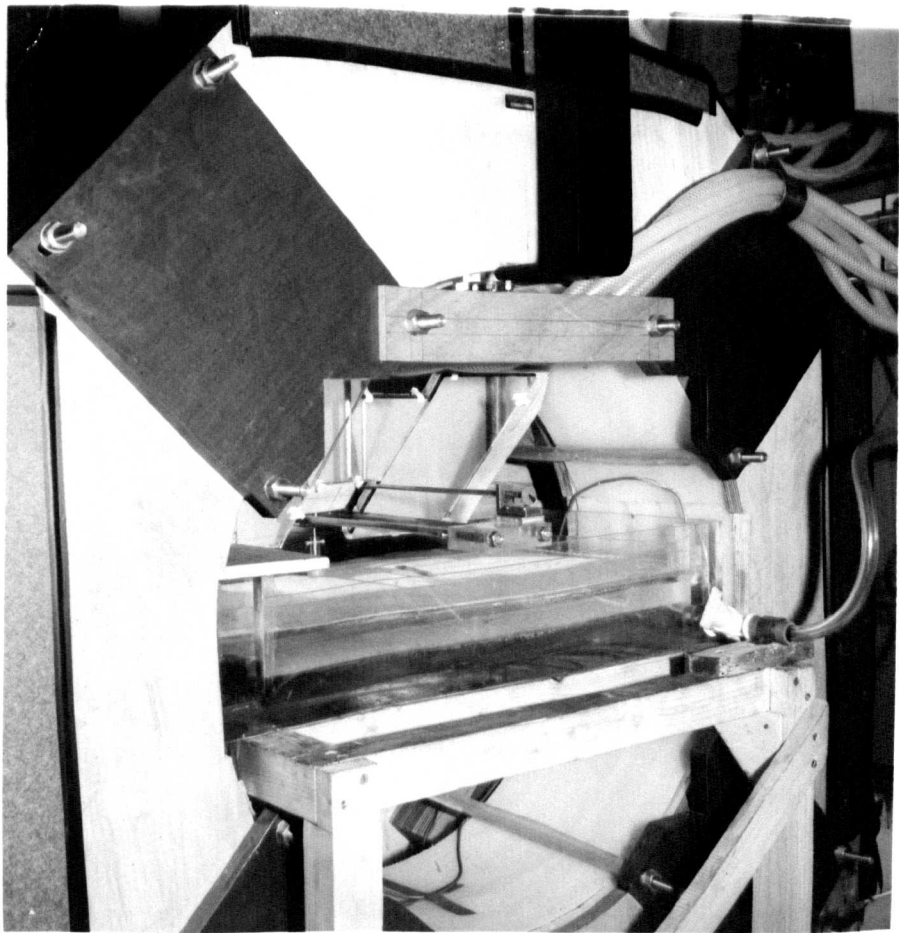


FIG. 4.16. LARGE TANK IN POSITION

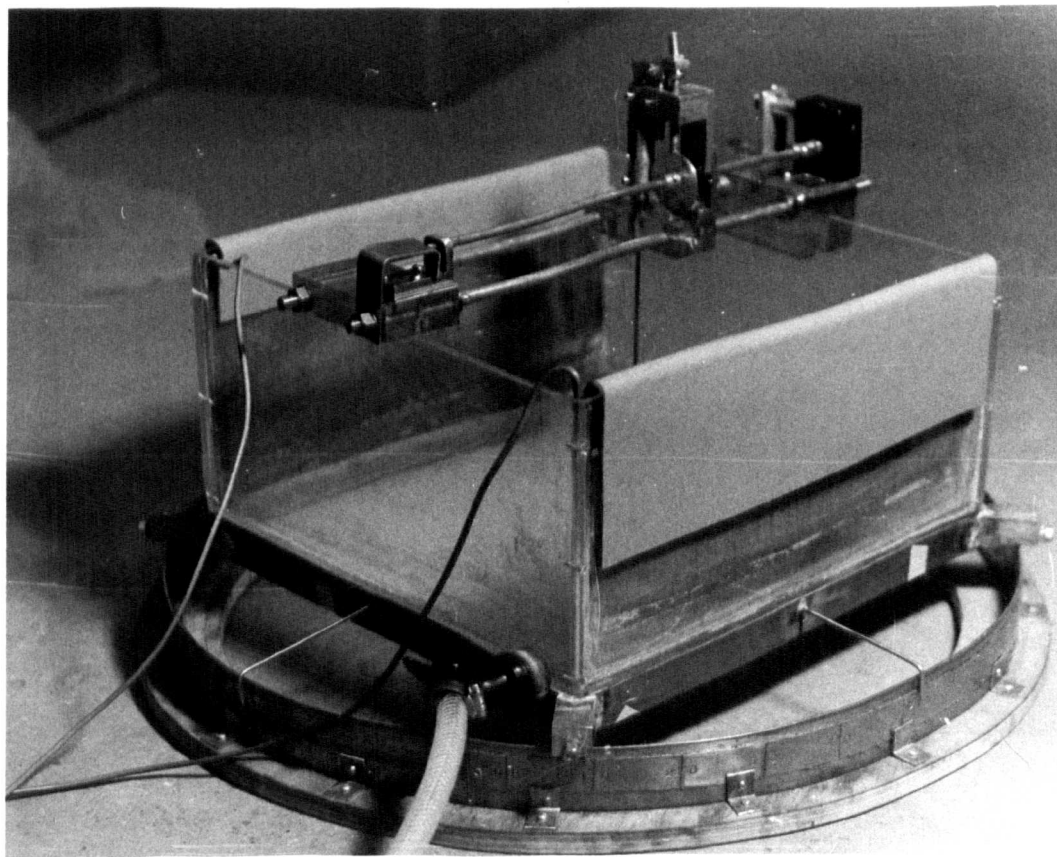


FIG. 4.17. SMALLER TANK.

Whereas the large tank could not be removed easily once in place, for fear of stresses cracking the walls away from the base, this one could be slipped in and out without harm in its brass frame. Being smaller it was easier to obtain greater current densities at lower voltages and since it had been discovered that the large tank was more than big enough for the size of wavelengths which showed up well enough to photograph, this smaller tank proved to be the best for the wave experiments.

#### 4.3.6 Wave generation equipment

From 4.3.2. it will be seen that the frequency of waves to be generated lies in the region of  $\frac{1}{2}$  to  $1\frac{1}{2}$  cycles/sec. This was too slow to be generated by simple electromechanical vibrators, since fairly pure sine wave forms were required to eliminate harmonic frequencies etc., and so a mechanical method had to be used. Such a seemingly simple problem was made much more complicated by the presence of the magnetic field, since no small electric motor could be used either in the working section, or anywhere near the magnet. Also it was designed to obstruct the view of the surface as little as possible, and also to make provision for the location of the wave maker to be moved to any part of the surface.

The actual probes used to transfer the vibrations to the fluids will be described in the relevant sections later in the chapter, but the mechanism used to create the vibrational motion is shown clearly in fig. (4.14). It consists of a push rod and spring, rocker arm and cam, the cam being circular with a slightly offset centre, producing a good approximation to a sine wave oscillation in the push rod with a peak to peak amplitude of 2 mm. This assembly was mounted on two brass rods running the length of the tank above the lid, supported on the tank walls, and the cam

was rotated by a third brass rod, running parallel to the support rods, itself fed through a 100:1 step down gearbox which was driven through an 8ft long flexible drive by a 1/4 hp AC electric motor well away from the field. The motor had to be powerful enough to overcome energy losses in the flexible drive, and to cope with loss of power at slow speeds since it was voltage controlled through a variac, whilst still being able to run at constant speed once set. At these speeds, frequency was measured by timing a given number of cycles with a stop watch.

The probe gear could also be adapted to fit the smaller tank, whilst the brass rod supports and perspex slides provided a support for the Hall probe to enable traversing to any part of the tank area.

#### 4.3.7. Wave observation

Waves were observed by direct visual means. After some trial and error, a light source was used consisting of a 60 watt halogen car headlamp bulb, with filament vertical, since this provided a very concentrated, almost point, light source. This was placed near the floor, between the two coils, so that it illuminated the tank from the bottom. A piece of tracing paper was spread across the tank lid, and this acted as a screen. Following the normal ripple tank principle (see Llowarch (1961) ), waves at the interface created light and dark patterns on the surface, and since there was a distance of only about 5 cms between the interface plane and the plane of the paper, c.f. 50 cms to the light source, the dark and light patterns directly represented the presence of troughs and crests. For this purpose, the difference in refractive index between the two working fluids was found to produce fairly well defined patterns for small amplitude waves, though the larger the wavelengths the fainter it became.

To provide a visual record, and to enable measurements to be made, it was decided to photograph the pattern. At first, the patterns on the paper were observed through the top opening of the magnet, using a 28 mm wide angle lens on a Pentax S1a camera, but probably due to the stray field there, the camera shutter malfunctioned. Therefore a mirror was installed inside the magnet at 45 degrees to the vertical, to enable viewing from one end (see in fig. 4.16). In this case an ordinary 55 mm lens was used, and the camera could be set up on a tripod. A double orange filter was used, since the green/blue colour of copper sulphate is the worst for good definition on a panchromatic film, and a 400 ASA Kodak tri-X film was used, the exposure being 1/125sec at f.2, and force developed for 15 mins. at 68° in full strength Kodak D76 developer to bring out the contrast. The negatives obtained were sufficiently good to enable the contrast of light and dark bands to be brought out strongly in the printing, and typical examples will be seen later in this chapter.

To help strengthen the contrast of patterns on the screen, stray light was reduced by enclosing the whole working area and equipment within a black polythene 'tent', framed with aluminium 'dexion', which also served both to keep the equipment dust free, and to encourage a draught of fresh air through the area, driven by the extract fan.

The viewing arrangement with the smaller tank, standing higher in the magnet, was reversed. The light source was placed above the tank, the screen fastened on the underside of the tank base, and the 45° mirror positioned below the tank, which gave a clearer view of the surface, although the shadow cast by the wave making gear was just as much an obstruction to view as the gear itself was in the original viewing arrangement.

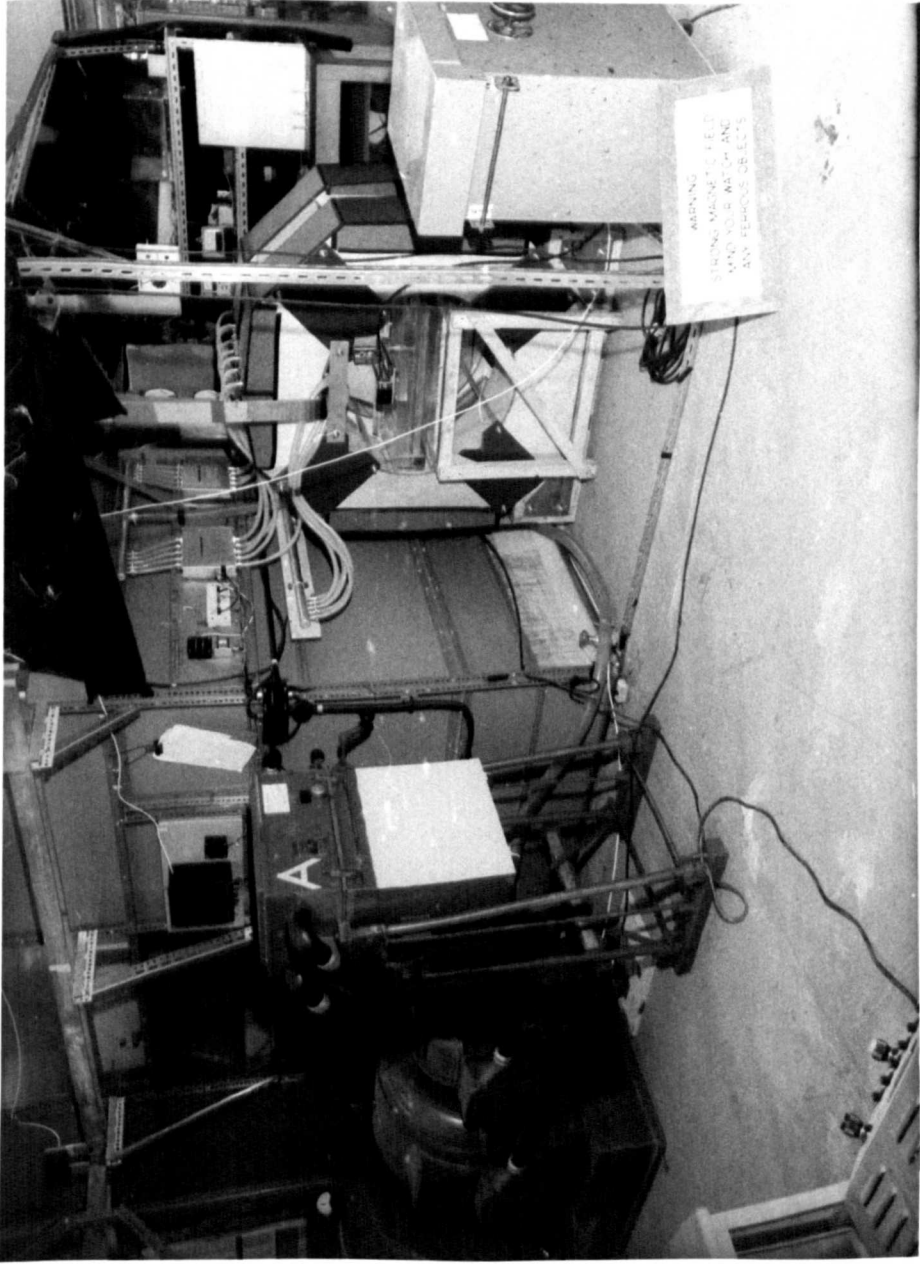


FIG. 4.18. OVERALL VIEW OF EQUIPMENT.

#### 4.4. Point Source Experiments

The first experiments to be attempted to demonstrate the existence of anisotropic surface waves, were those using a point oscillating source, with the intention of obtaining lines of constant phase corresponding to the theoretical values predicted in fig.(2.6).

The wave maker was set up opposite a hole in the centre of the lid of the large tank, and a plunger attached to the oscillating brass rod. This was made of  $\frac{1}{2}$ " perspex rod, with a hole drilled down the centre to take the brass rod, and a disc of  $\frac{1}{16}$ " perspex sheet glued to the base. Initially, a 1" diameter disc was used (the smallest one seen in fig. 4.19), with the disc situated just at the interface of the two fluids. However, it was found that the waves generated by this probe showed up on the observing screen for only a couple of centimetres from the probe, and then were lost, because the amplitude of waves from a point source decreases inversely as the square root of the radius from the point, due to energy radiation considerations alone, even without considering damping effects. Thus this point probe proved unsuccessful. As a compromise approximation to a point source, 2" and 4" circular discs were used, so that more energy could be fed into the system to enable the waves to persist at a visually observable amplitude for a greater distance, although the ovality of the pattern to be expected would be less in this case than for a true point source.

A new problem then appeared. Anisotropy was observed but it was orientated at  $90^\circ$  to what was expected, and in fact it persisted a few seconds after the current was switched off.

After the motion of small particles of impurity was noticed, it was realised that this anisotropy was a spurious effect, due to convection of waves by flow in the fluid. The origin of this flow

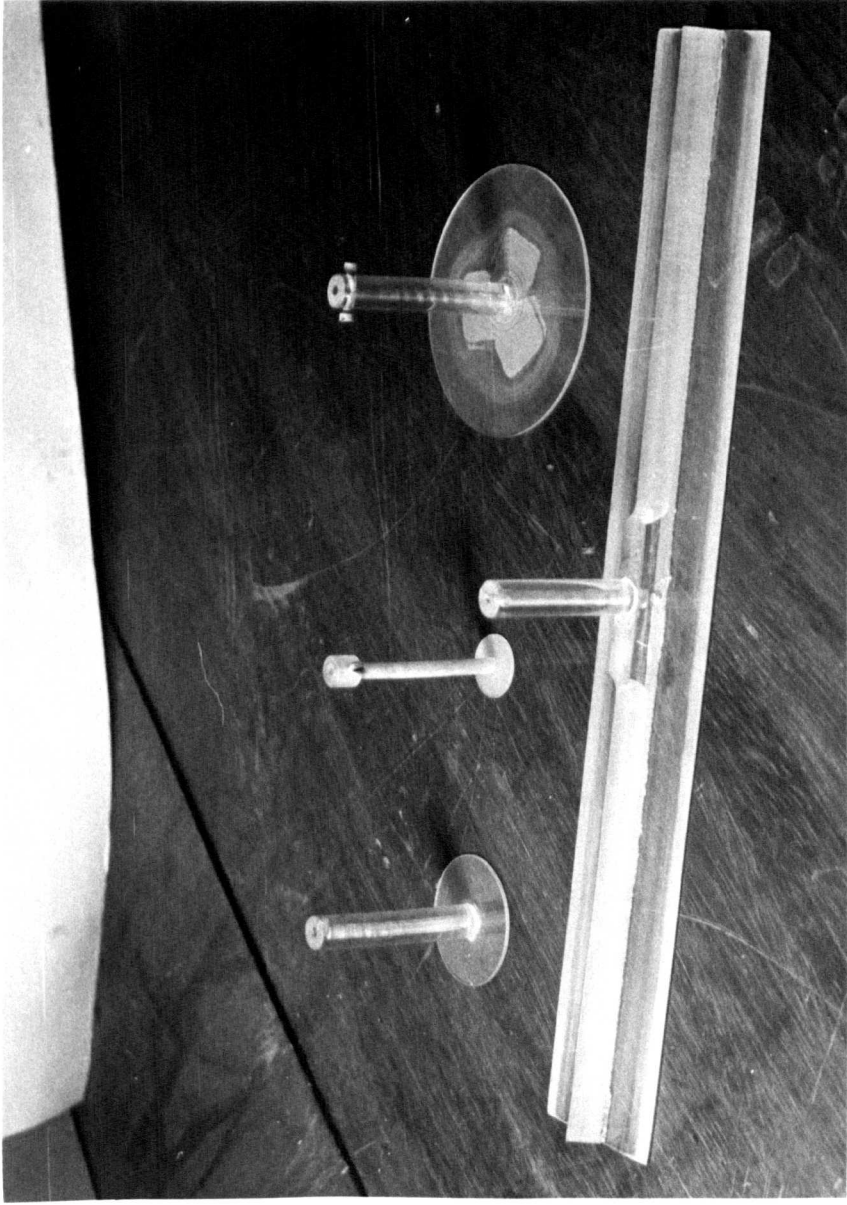
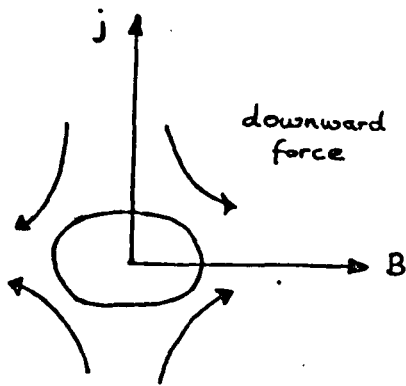


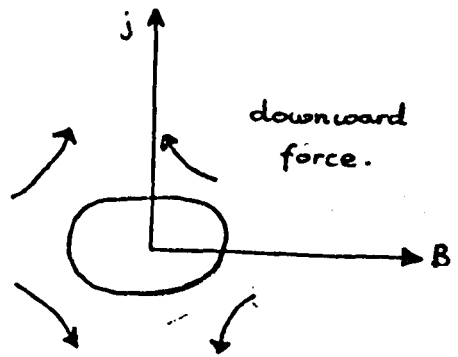
FIG. 4.19. PLUNGERS USED TO PRODUCE WAVES.

was traced back to the fact that the probe was positioned so that its mean position was slightly below the interface level, and consequently, averaged over time, there was a net disturbance to the current flow such as to produce rotational  $\underline{j} \times \underline{B}$  forces inducing flow. Fig. (4.20) shows the sort of flow pattern expected from the  $\underline{j} \times \underline{B}$  forces, predicted for the cases of the net surface disturbance upwards or downwards, for upward or downward  $\underline{j} \times \underline{B}$ . It will be noted that for the surface distorted upwards, (possible because surface tension holds the interface attached to the probe), the spurious currents would produce an effect on the waves not unlike the one being sought, and this must be guarded against. It was decided that subsequently all wave motions should be induced by the plunger wholly in the upper fluid, not making contact with the interface. This was found to be successful in eliminating spurious currents, but markedly reduced the amplitude of the wave motion at the interface. It shows that in fact the two fluid system is virtually essential to show up M.H.D. anisotropic surface waves unambiguously without these spurious motions which were also experienced in the preliminary mercury experiments. Using the large tank, and taking the above precautions, although a definite change in the wave pattern could be seen on switching the electric current on, it was not possible to produce anisotropy in the wave pattern which would show up consistently and undisputedly in photographs, even when operating at the maximum voltage available.

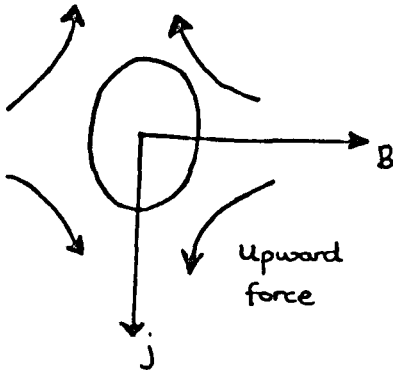
It was not until the smaller tank was used, with the possibility of higher current densities, and after experience of handling the fluid to reduce surface tension, that any observable ovality of the waves was obtained. This is shown in fig.(4.21) along with details of the  $\underline{j} \times \underline{B}$  forces involved. Even here, using a 2" plunger, decreasing amplitude was a problem, and the



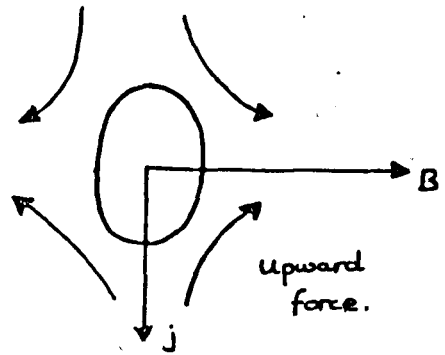
Surface disturbed upwards



Surface disturbed downwards.



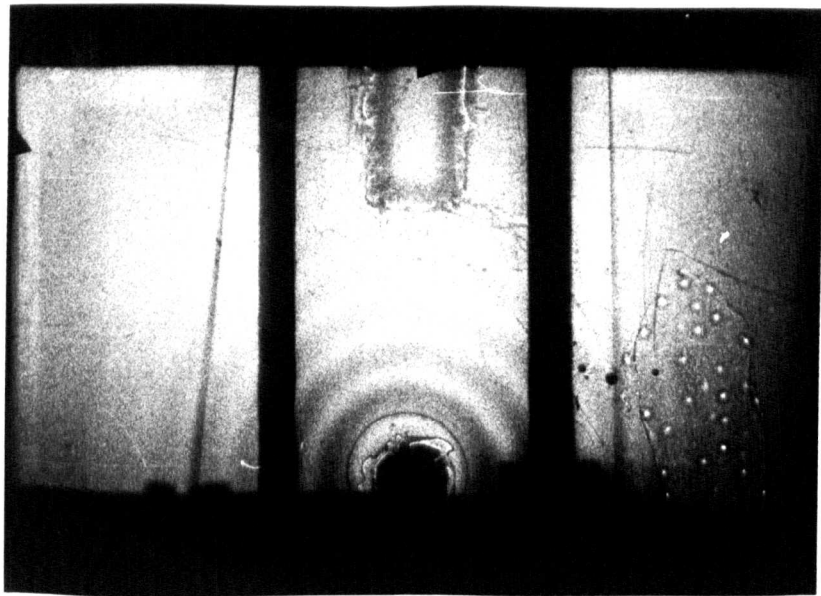
Surface disturbed upwards.



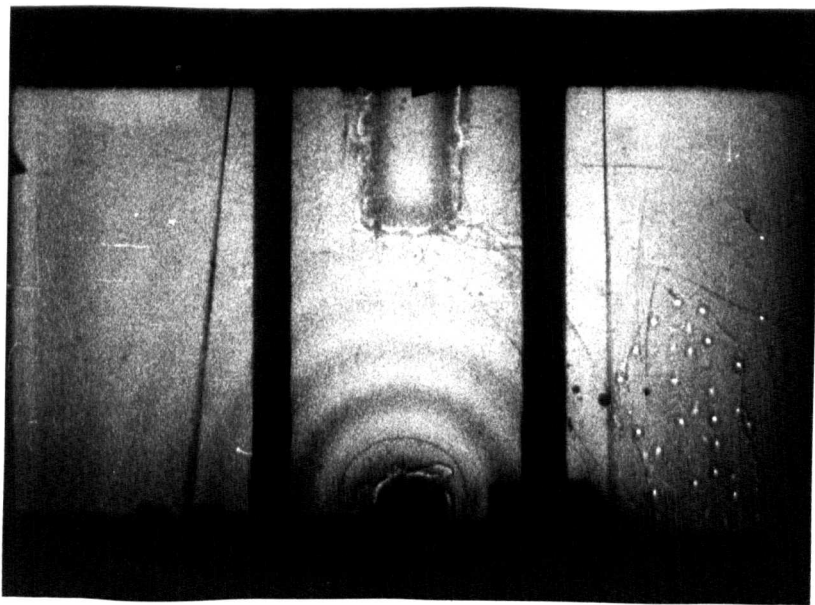
surface disturbed downwards.

## FIG. 4.20 EXPECTED FLOW PRODUCED BY DISTURBED SURFACE.

(the ovals represent the wave pattern predicted by the theory, if the mean surface level were not disturbed.)

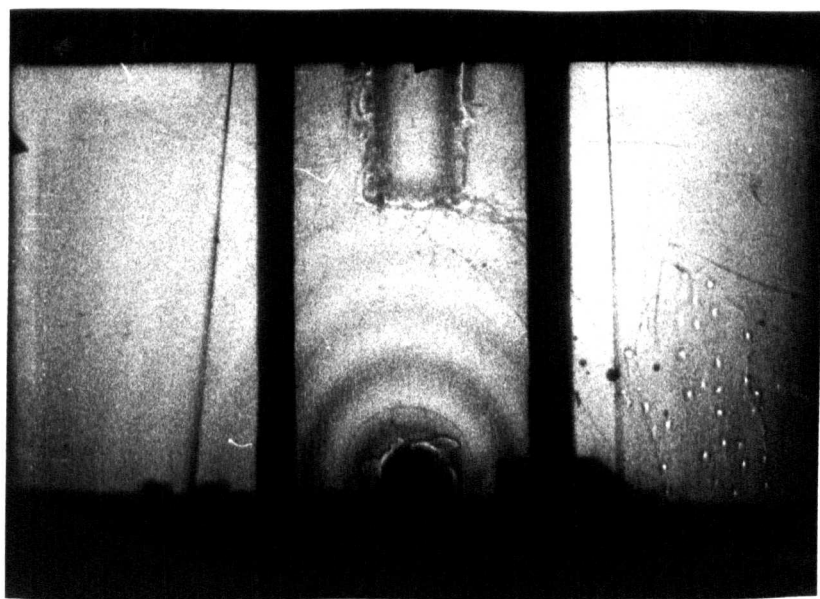


(a)  $\omega = 1.37 \text{ c/s}$  ,  $j = 0$

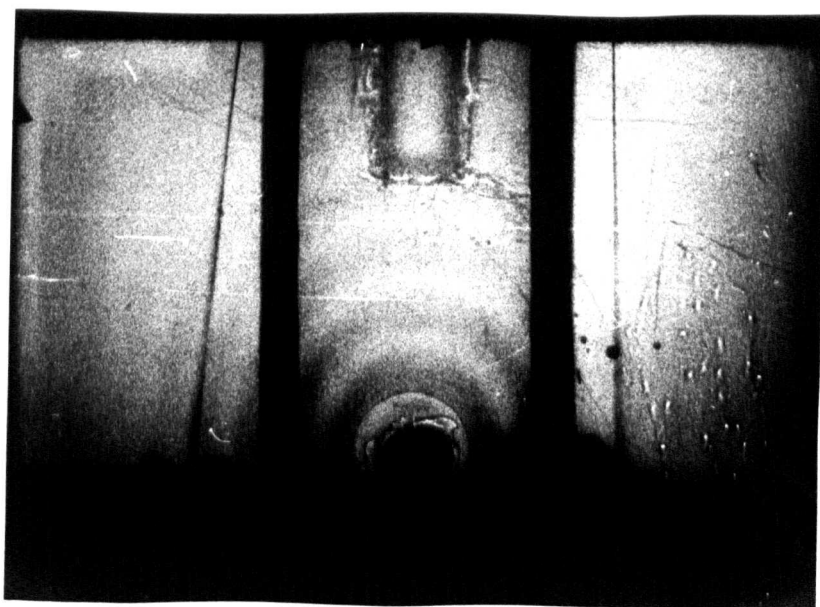


(b)  $\omega = 1.37 \text{ c/s}$  ,  $j = 33 \text{ mA/cm}^2$ , downward force

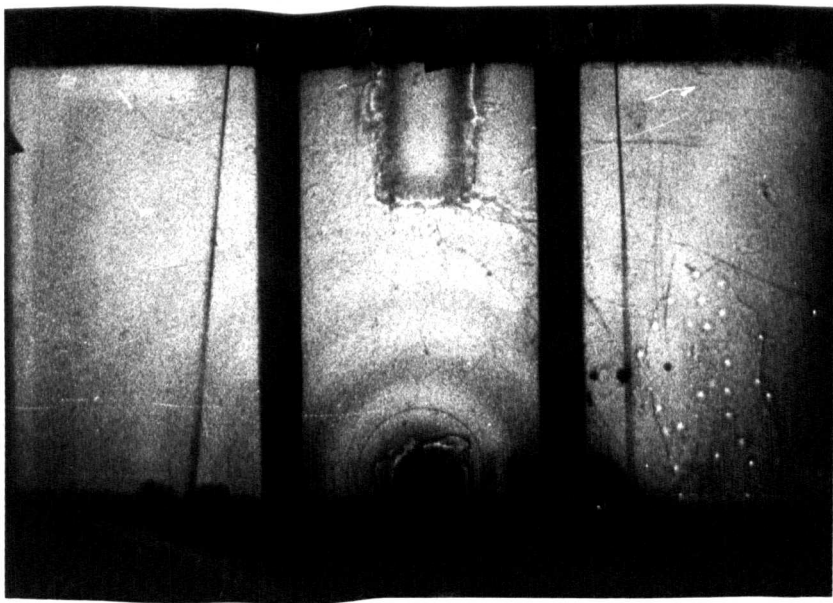
FIG. 4.21. ANISOTROPIC WAVES FROM  
 A POINT SOURCE.  $\rho_{\text{UPPER}} = 1.074$  ,  $\rho_{\text{LOWER}} = 1.098$   
 Depth of copper sulphate = 2.5 cms , Magnetic field = 0.21 Wb/m<sup>2</sup>



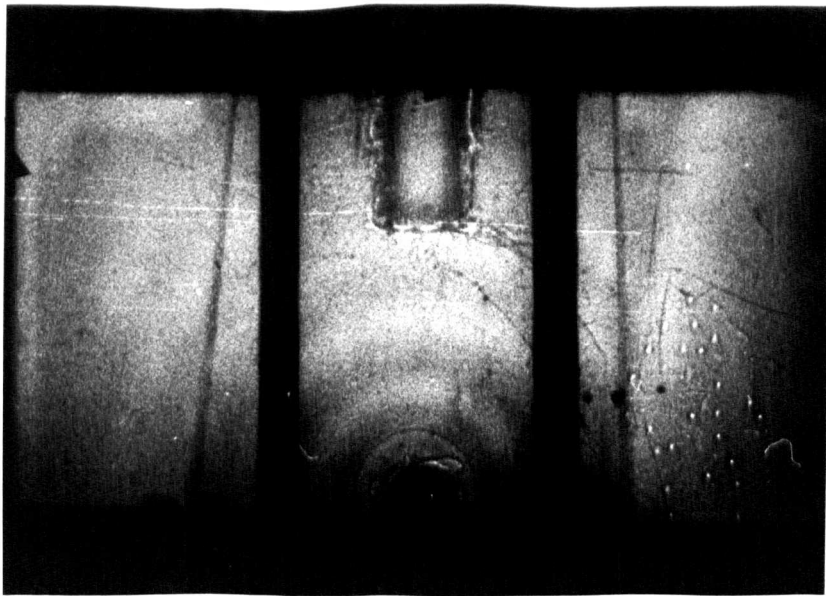
(c)  $\omega = 1.37 \text{ c/s}$ ,  $j = 66 \text{ mA/cm}^2$  downward force



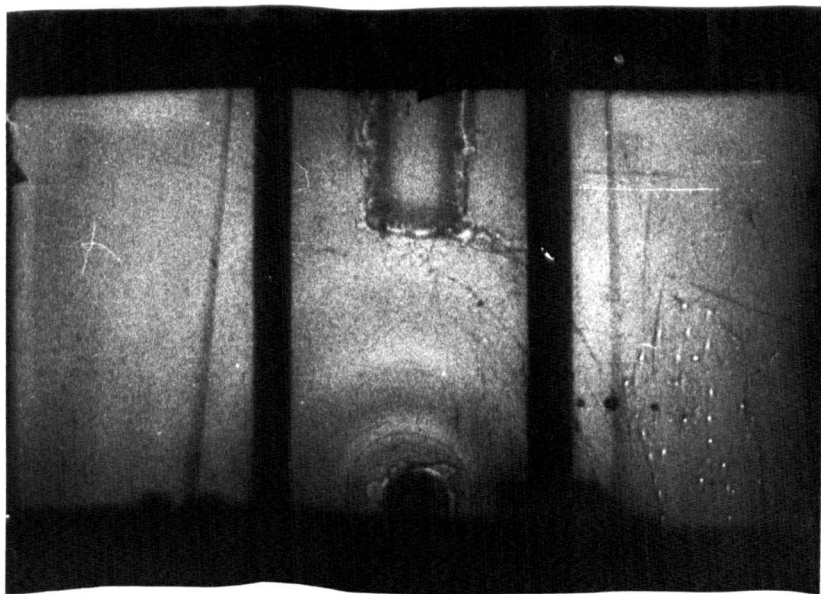
(d)  $\omega = 1.37 \text{ c/s}$ ,  $j = 100 \text{ mA/cm}^2$  downward force



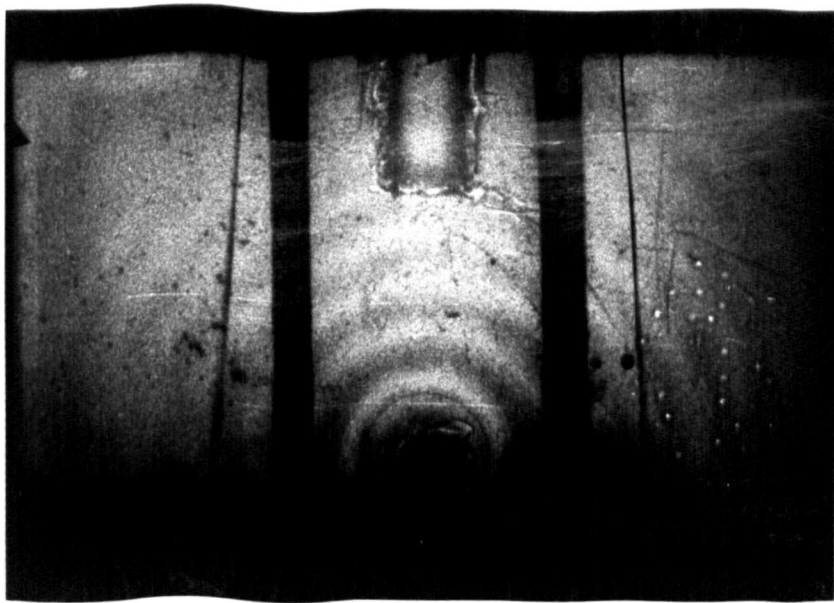
(a)  $\omega = 1.18 \text{ c/s}$       $j = 0$



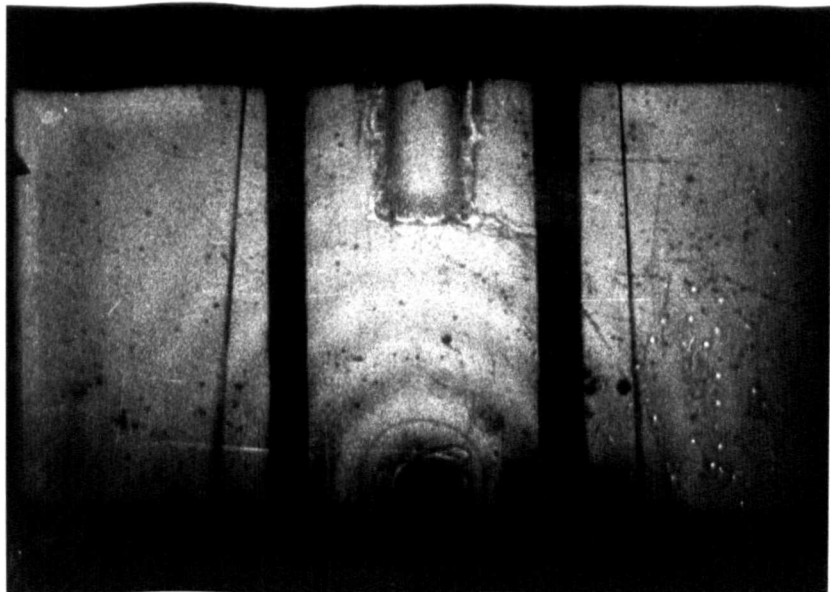
(b)  $\omega = 1.18 \text{ c/s}$ ,  $j = 66 \text{ mA/cm}^2$ , downward force



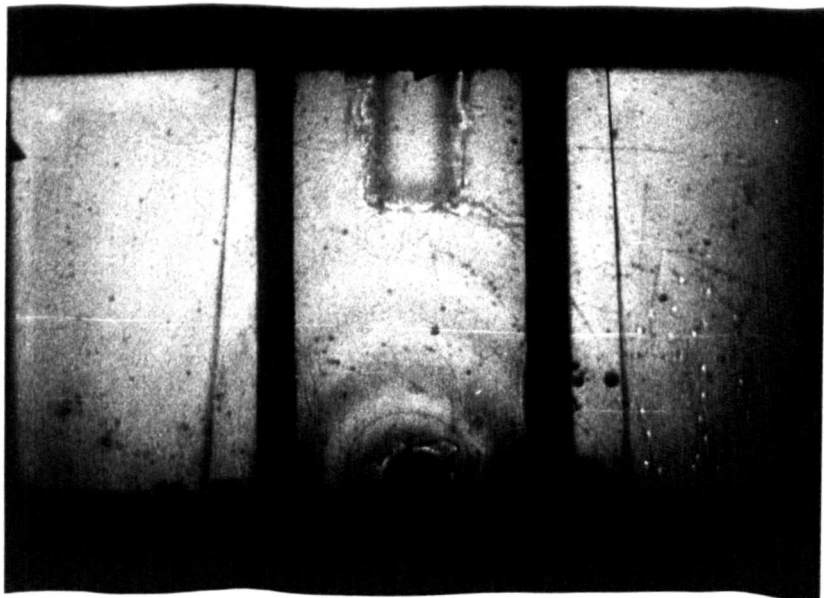
(c)  $\omega = 1.18 \text{ c/s}$  ,  $j = 100 \text{ mA/cm}^2$  , downward force



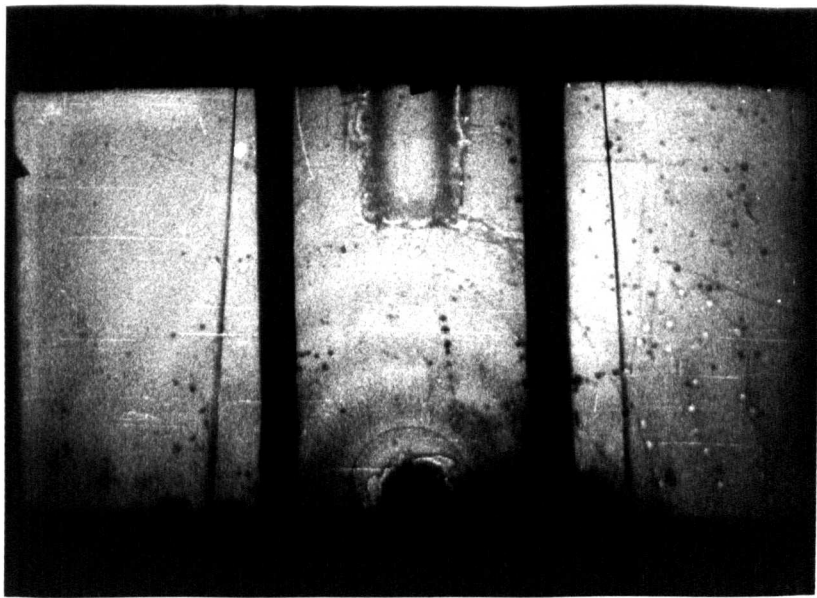
(h)  $\omega = 1.61 \text{ c/s}$   $j = 0$



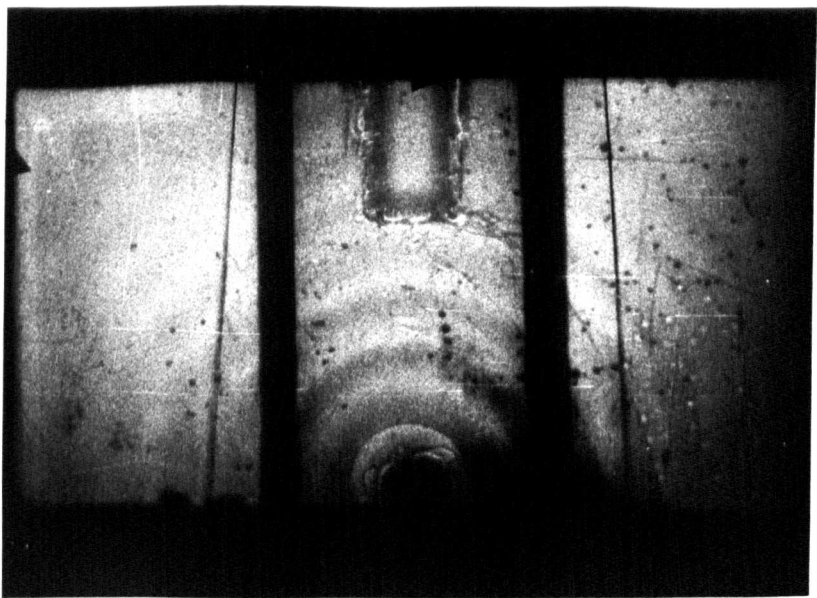
(i)  $\omega = 1.61 \text{ c/s}$   $j = 66 \text{ mA/cm}^2$  downward force



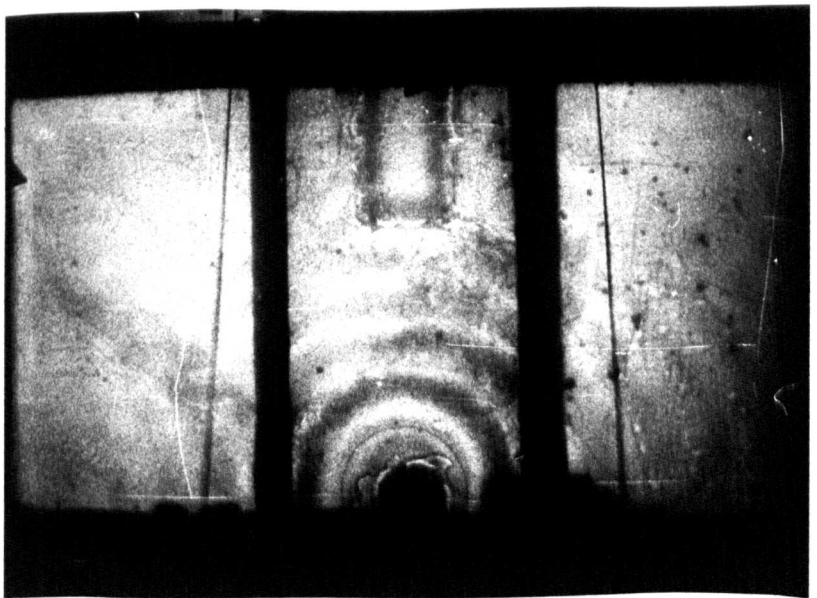
(j)  $\omega = 1.61 \text{ c/s}$   $j = 125 \text{ mA/cm}^2$  downward force



(k)  $\omega = 1.41$  c/s  $j = 0$



(l)  $\omega = 1.41$  c/s  $j = 33$  mA/cm<sup>2</sup> upward force



(m)  $\omega = 1.41$  c/s  $j = 66$  mA/cm<sup>2</sup> upward force

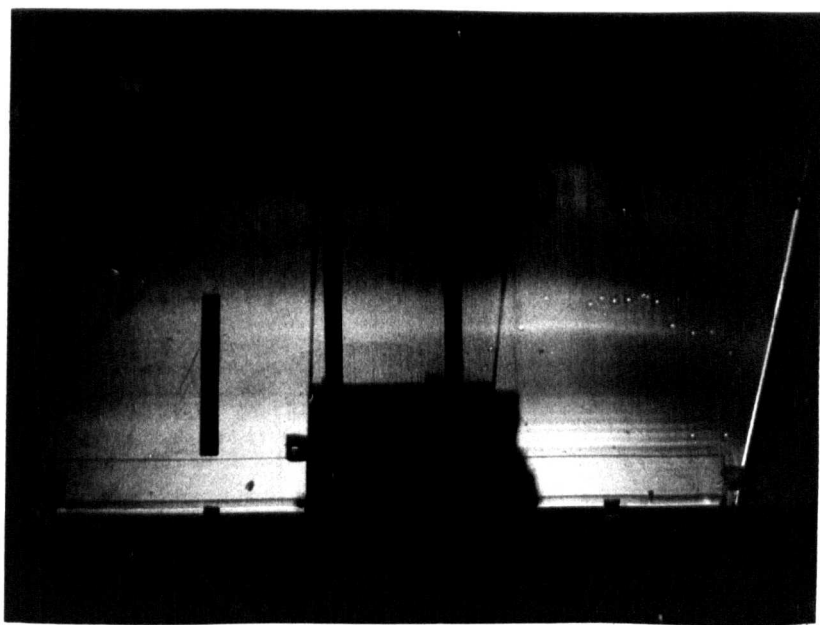
shadow of the wave making gear a hindrance to clear observation. However by the time these photographs were obtained, the existence of anisotropic surface waves had already been proved by the following method.

#### 4.5 Line Source Experiments

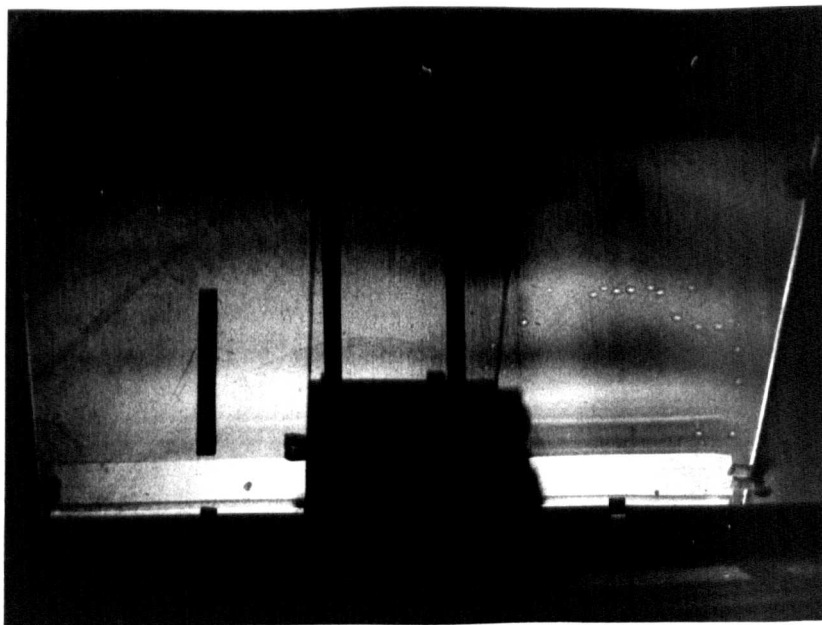
To overcome the problem of the previous section, decrease of amplitude due to radial energy flow, it was decided to mount a series of experiments using a line source. The line plunger shown in fig. (4.19) was used, being 4 cms x 40 cms, 1/16" thick perspex, with a bar of shaped  $\frac{1}{2}$ " perspex along the top centre to hold it rigid. Using this, even when keeping it wholly in the upper fluid, it was found that waves showed up much better, and could be observed on the screen for 20 cms or more away from the probe. Also, larger wavelengths up to 10 cms, could be shown up with the greater amplitude, whereas in the point source experiments 5 cms was the maximum wavelength that could be observed.

A series of photographs was taken, with the magnetic field on and the wave maker set at a particular frequency, for waves in the B direction at different values of current. A piece of P.V.C. cut exactly 10 cms long was placed on the screen to act as a calibration for the photograph. The wavelengths could be measured to within about 5% accuracy on the photographs, judging by eye the position of subsequent crests or troughs and where possible measuring over two or three wavelengths. However, by comparing different photographs and measuring systematically, an accuracy of 2½% in the actual ratio of wavelengths between photographs was probably obtained. Typical photographs are shown in fig. (4.22), whilst fig. (4.23) shows a plot of the ratio of (wavelength/wavelength without current), against ( $j \times \underline{B}$  / gravity force) ratio.

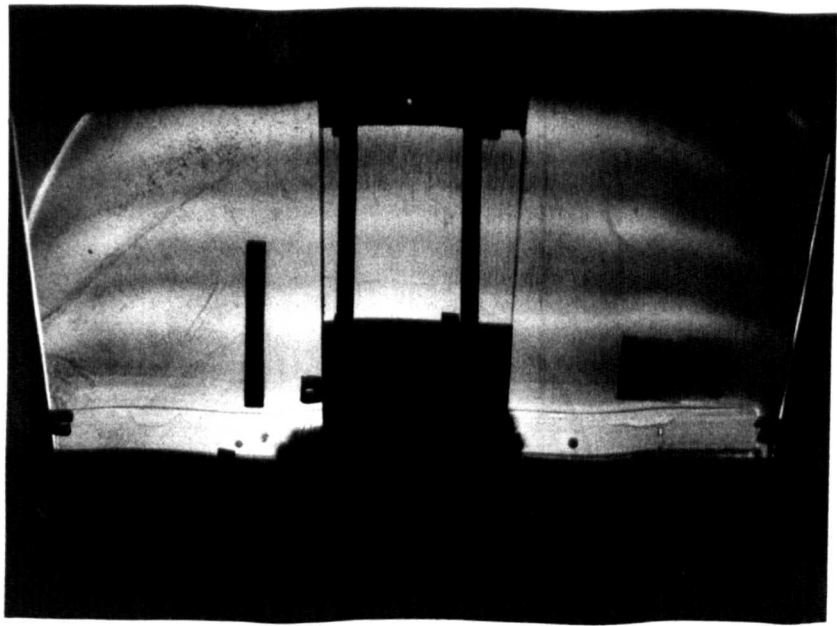




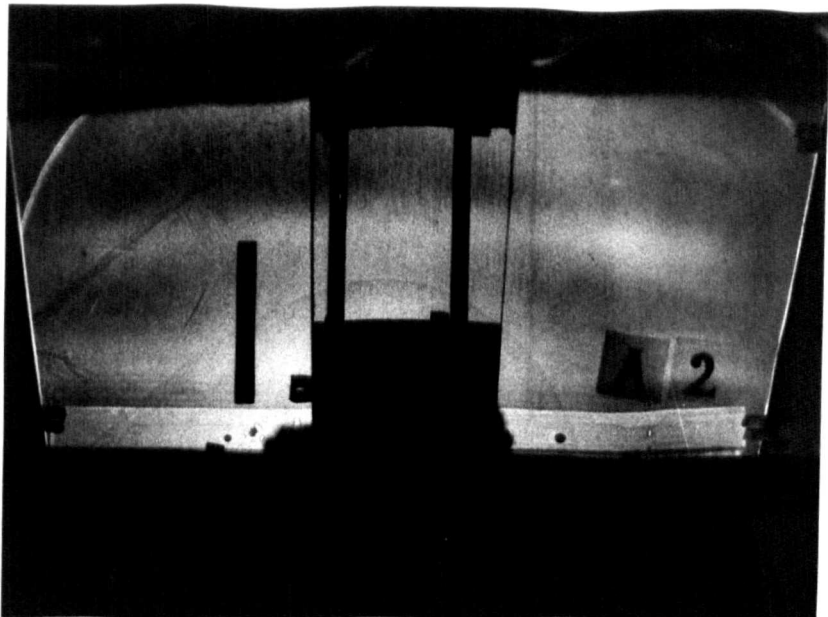
c)  $j = 42 \text{ mA/sq cm}$ .  $\omega = 0.55 \text{ c/s}$ .  
Upward force.



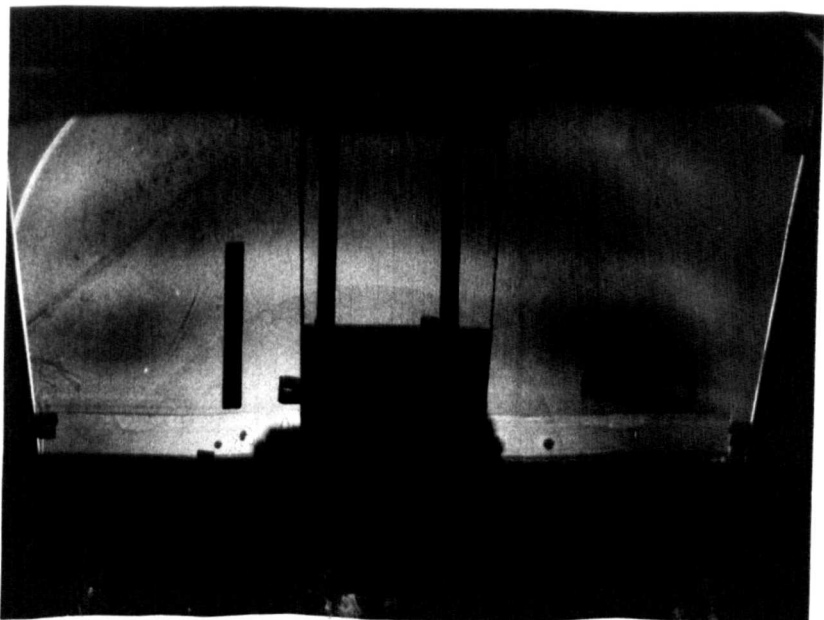
d)  $j = 100 \text{ mA/sq cm}$ .  $\omega = 0.55 \text{ c/s}$ .  
Upward force.



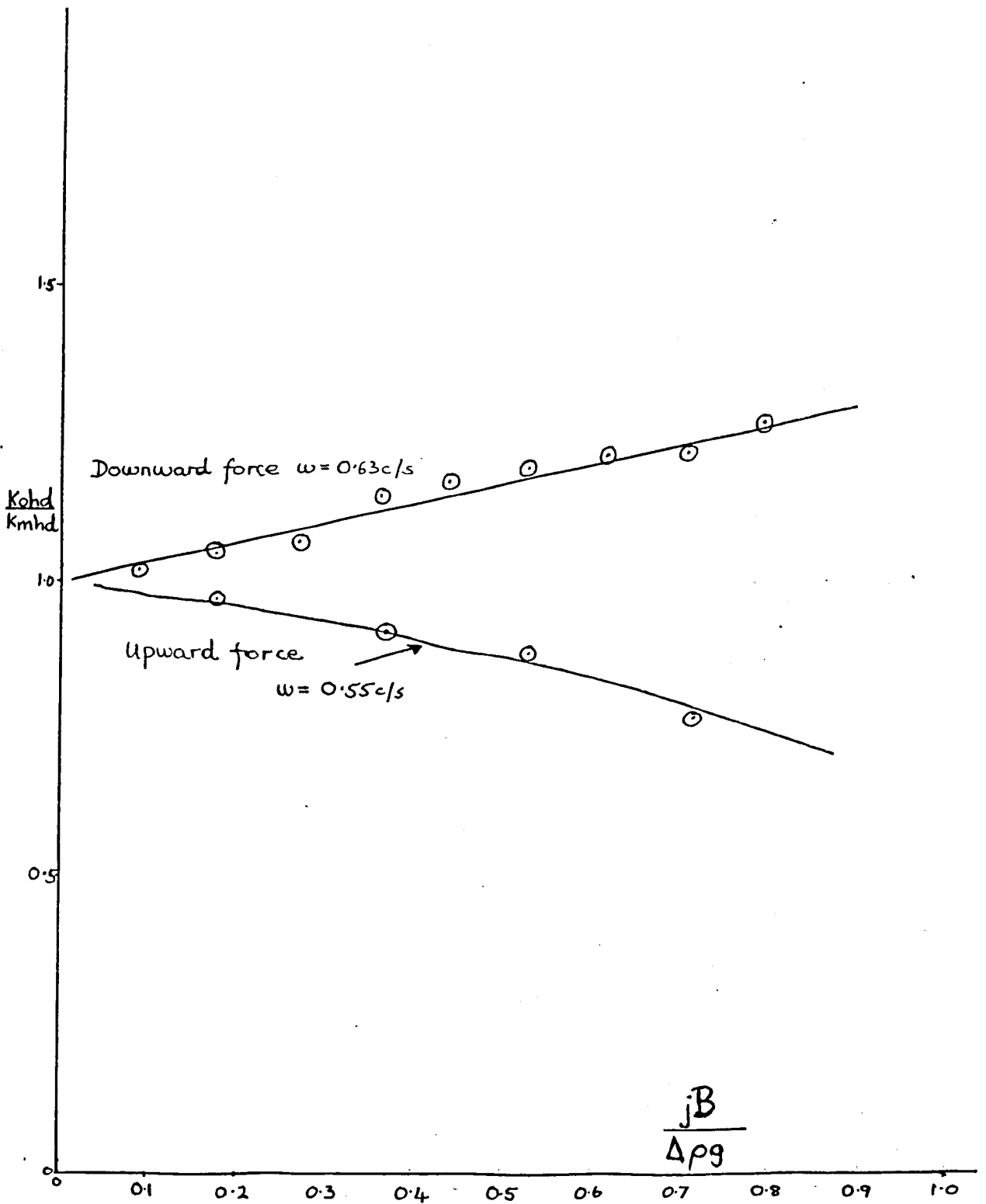
e)  $w = 0.63 \text{ c/s}$   $j = 0$  downward force



f)  $w = 0.63 \text{ c/s}$   $j = 92 \text{ mA/sqcm}$  downward force



g)  $w = 0.63 \text{ c/s}$   $j = 83 \text{ mA/sqcm}$  downward force



$$B = 0.192 \text{ wt/m}^2$$

$$\rho_{upper} = 1.071$$

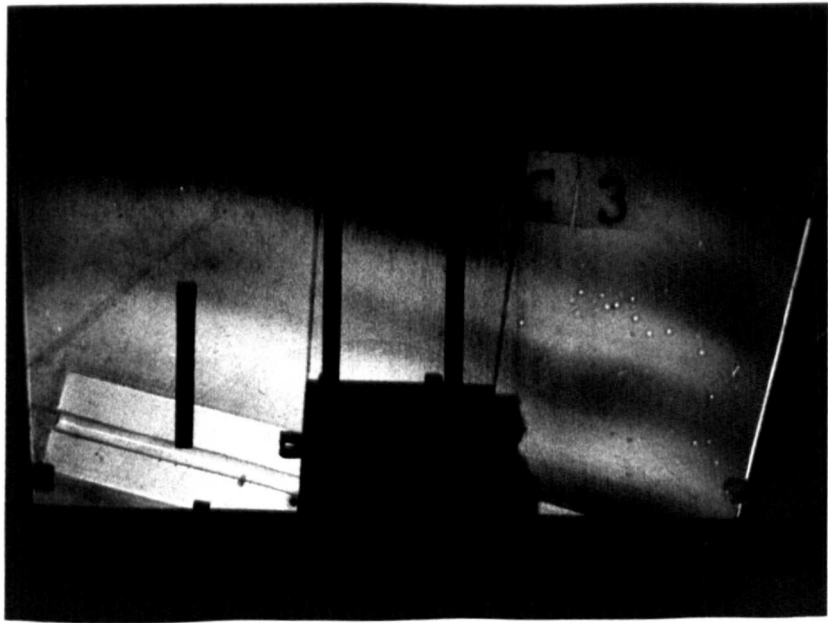
$$\rho_{2 \text{ lower}} = 1.094$$

FIG. 4.23. ANISOTROPY RATIO AGAINST THE PARAMETER  $\frac{jB}{\Delta \rho g}$ , ( $\underline{k}$  in  $\underline{B}$  DIRECTION)

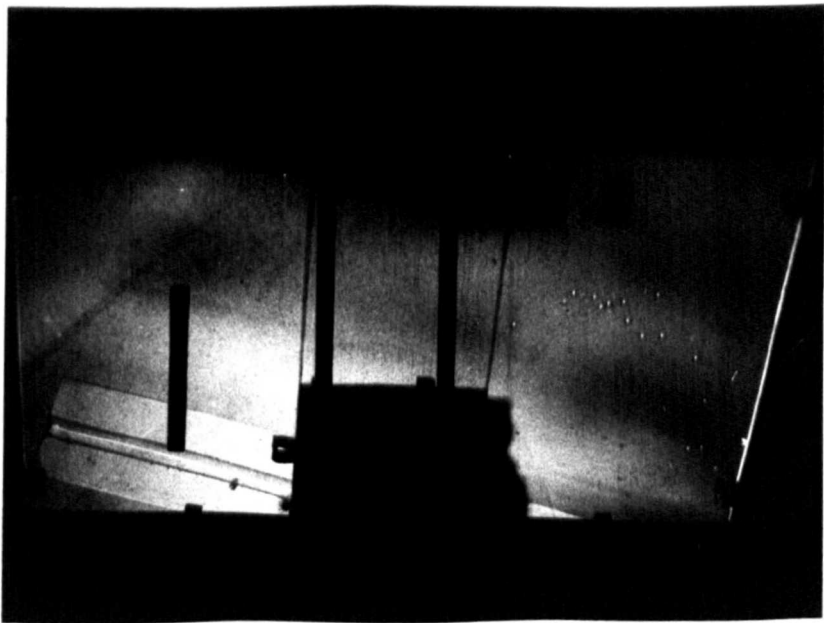
The bent waves in the photograph were due to warping of the plunger after some time in the warmed Genklene. Measurements were taken from the centre section.

A further series of experiments was then run to obtain the same ratio of (wavelength/wavelength without current on) for different wave directions, taking two photographs for each direction, one with and one without the current on, to enable direct comparison between the two, thereby avoiding any error due to a slight change in frequency or surface tension or density during the run. The 10 cm marker was always placed in a direction along the wave normal, to eliminate any error due to the mirror not being at  $45^\circ$  and hence distorting the photographic record. Typical photograph pairs are shown in fig. (4.24). This was repeated for various frequencies and the measured ratio results are shown in fig. (4.25). These show a good general agreement with their equivalent (phase velocity) theoretical plots of fig. (2.6). Only downward  $j \times B$  forces were used in this series since greater forces could be obtained without the fluid going unstable anywhere.

Although it is not possible to make a direct quantitative comparison with theoretical results because of the difficulty of accurate measurement of surface tension, and the variation of specific gravity as the fluids heat up due to ohmic dissipation, the results thus obtained are considered to be adequate experimental evidence to support the general theory of the existence of M.H.D. anisotropic surface waves. The primary goal of this work has therefore been achieved.

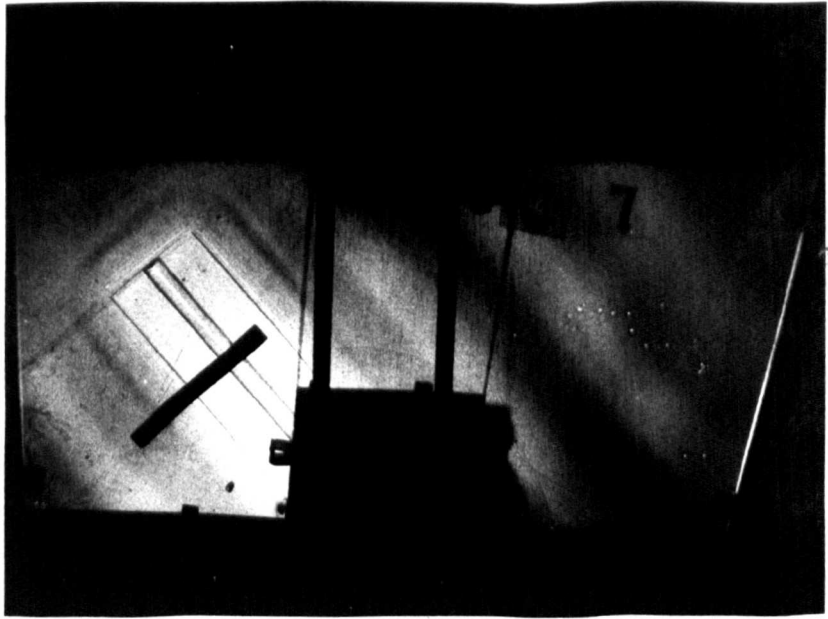


a)  $j = 0$ .  $\omega = 7.1 \text{ c/s}$ .

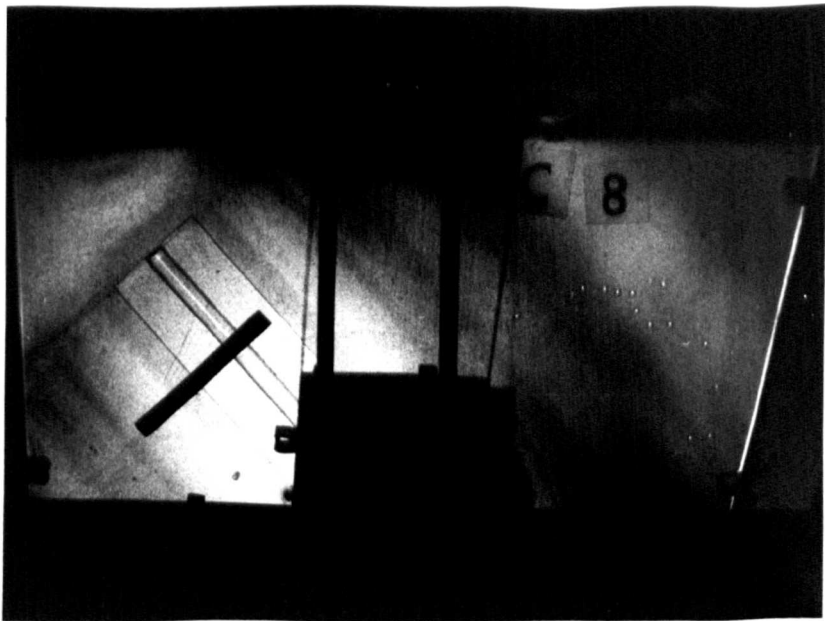


b)  $j = 83 \text{ mA/cm}^2$ .  $\omega = 7.1 \text{ c/s}$ .  
downward force.

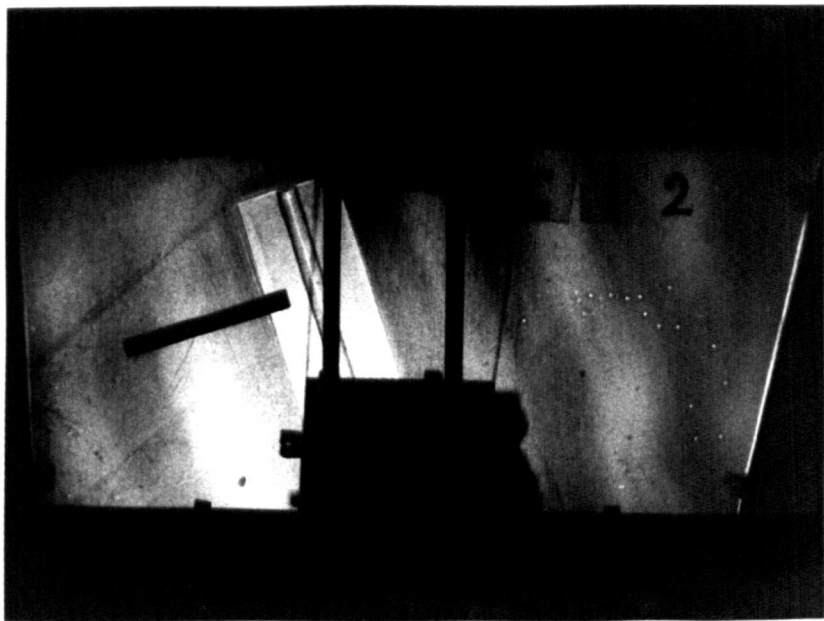
FIG. 4.24. WAVES FROM A LINE SOURCE  
DIFFERENT ORIENTATIONS.  
(densities and mag. field as in fig 4.22)



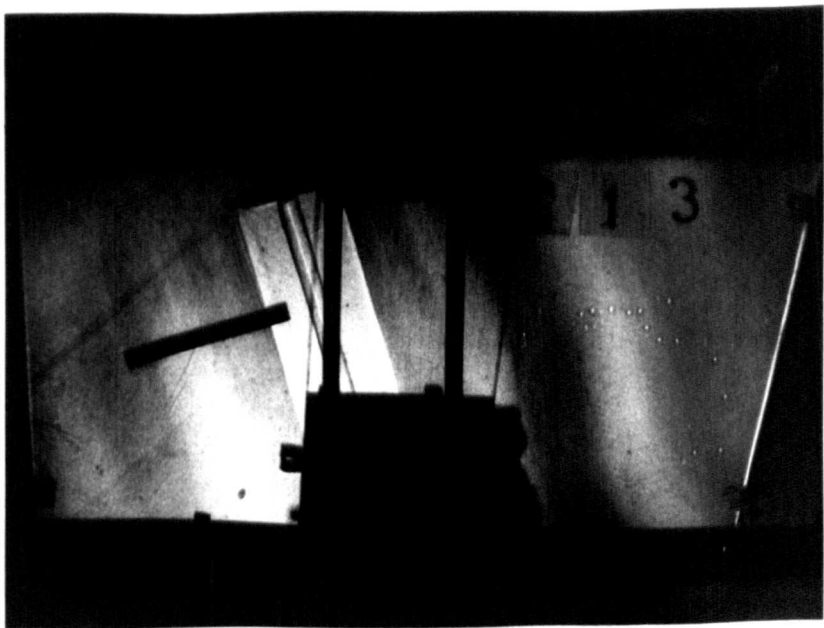
c)  $j = 0$        $\omega = 6.5 \text{ c/s}$



d)  $j = 83 \text{ mA/cm}^2$ .       $\omega = 6.5 \text{ c/s}$   
downward force.



e)  $j = 0$        $\omega = 6.0 \text{ c/s}$



f)  $j = 83 \text{ mA/sq cm}$        $\omega = 6.0 \text{ c/s}$   
downward force.

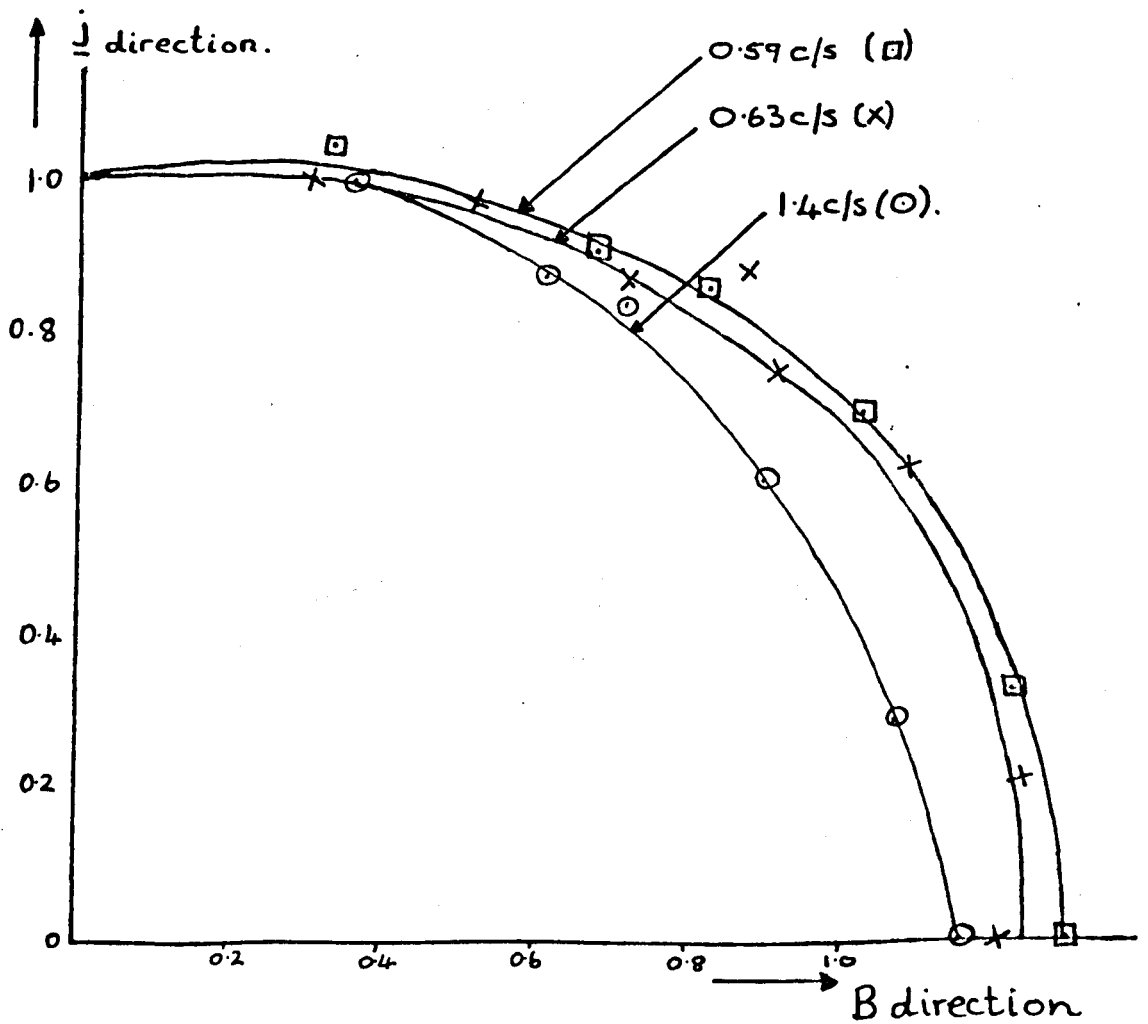


FIG. 4.25. ANISOTROPY RATIO AGAINST WAVENUMBER DIRECTION. (Polar Plot).

Downward force :  $jB \approx 0.72$ .

$B = 0.192 \text{ wb/m}^2$   $\Delta p g$

$\rho_{\text{upper}} = 1.071$

$\rho_{\text{lower}} = 1.094$

#### 4.6. Experiments to Show up other Anisotropic Surface Wave Phenomena

##### 4.6.1. Introduction

Following the theoretical work described in chapter 3, it was hoped to demonstrate the existence of some of the phenomena predicted there. It soon became apparent that as well as the inaccuracies of measurement, other inaccuracies of general wave motion would make it impossible to set up experiments which could hope to do anything more than show that a difference existed between the O.H.D. and M.H.D. cases of such phenomena as refraction, reflection and the ship wave or fish line problem. This was because to study these effects properly, a much larger area is required so that study can be made in the centre of a large wave train rather than using a narrow wave train. Clear demonstrations were also difficult because the comparatively low energy content of the wave train for the frequency/wave number characteristics for the two fluid interface rendered it susceptible to being distorted by comparatively small spurious effects, such as a slight fluid convection motion, or variations of surface tension from place to place due to impurities.

##### 4.6.2 Refraction experiments

To demonstrate the refraction phenomena described in 3.4 the simplest case was chosen, of a line source producing waves in the O.H.D. case with normals in the B direction, and a ridge shaped floor, (drawn in fig. 4.26) so that the current density would increase hyperbolically from the outside to the centre.

The false floor was constructed of 1/16" perspex on 1/4" ridge ends with a 1/4" perspex support in the centre, and open so that copper sulphate would fill the underneath too, and so prevent a prismatic wedge of air, or perspex (had it been solid) from bending the light and producing spurious results. The design was such that it was expected that all the current would flow over the

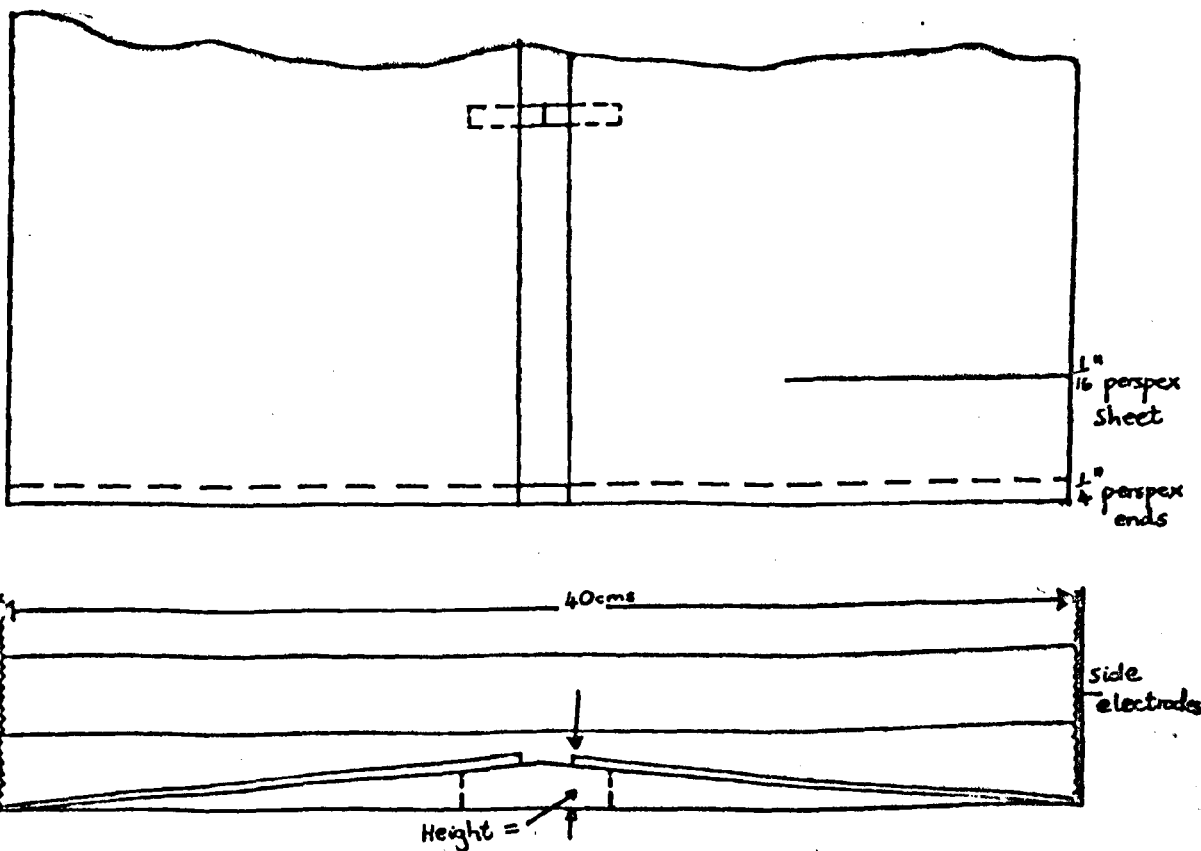


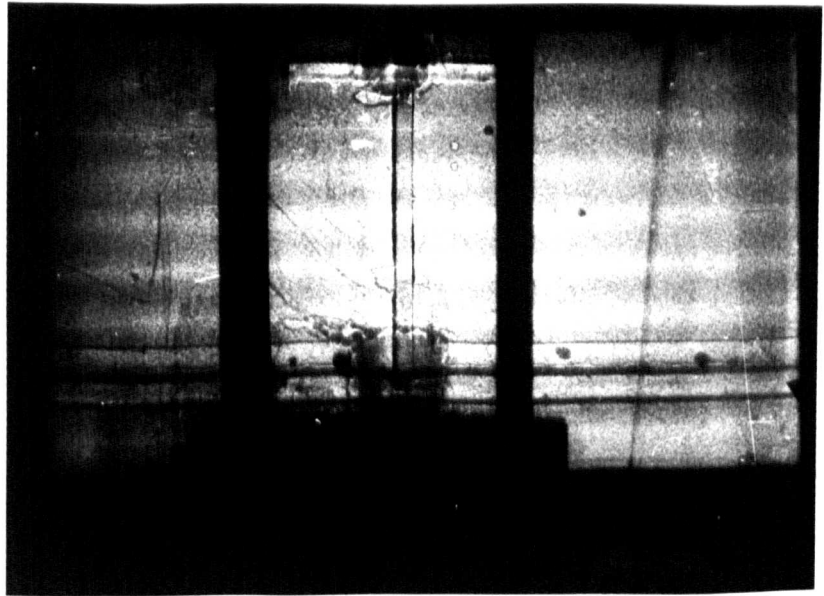
FIG. 4.26. SKETCH OF FALSE FLOOR FOR WAVE REFRACTION EXPERIMENT.

top of the false floor, and the absence of any rotational  $\underline{j} \times \underline{B}$  motions bore this out when the current was switched on. The copper sulphate was let in to a depth of 2.8 cms at the sides, 1.3 cms at the top, and so wavelengths were restricted to 5 cms maximum for the effect of depth not to influence the O.H.D. case. The smaller tank was used, and the line source was a cut down version of that used in the previous section. For a range of frequencies photographs were taken with the total current at various values from 0 to 18 amps, and  $\underline{j} \times \underline{B}$  upward and downward. The results are the general shape predicted by the theory, particularly for the downward force, and are shown in fig. (4.27). The upward force produced a less well defined effect, probably because of the onset of the sort of instability described in chapter 6.

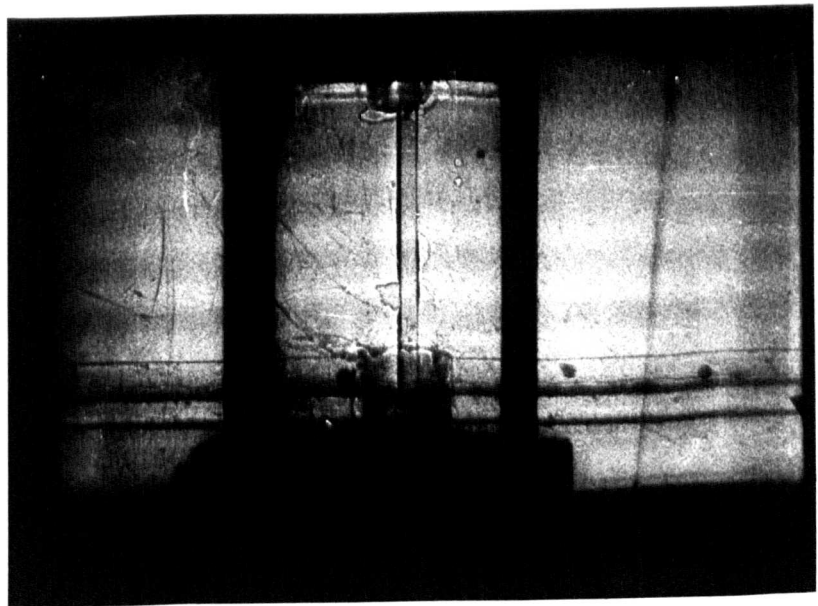
#### 4.6.3 Reflection experiments

It was hoped to be able to verify fairly definitely the reflection characteristics described in 3.2, using the line wave maker. First, using the large tank, attempts were made to reflect the waves at a 'mirror' consisting of a half barrier, in the upper fluid only so that the current should not be distorted. The tank walls could not be used since they would be parallel or normal to the axes of anisotropy, and consequently would not show up any unusual reflection behaviour. However it was found that what little reflection did occur did not show up sufficiently to be photographed, and it was suspect as to whether this was true reflection since the incident and reflected angles did not appear to be equal even in the O.H.D. case.

Therefore, it was planned to use the smaller tank and make use of the theory of 2.5.2., that the orientation of anisotropy would rotate at half the angle of rotation of  $\underline{j}$  from the usual ( $\underline{j} \cdot \underline{B} = 0$ ) position. In this way, the walls of the tank would



(a) current = 0



(b) Total current = 5 amps

## FIG 4.27 WAVE REFRACTION

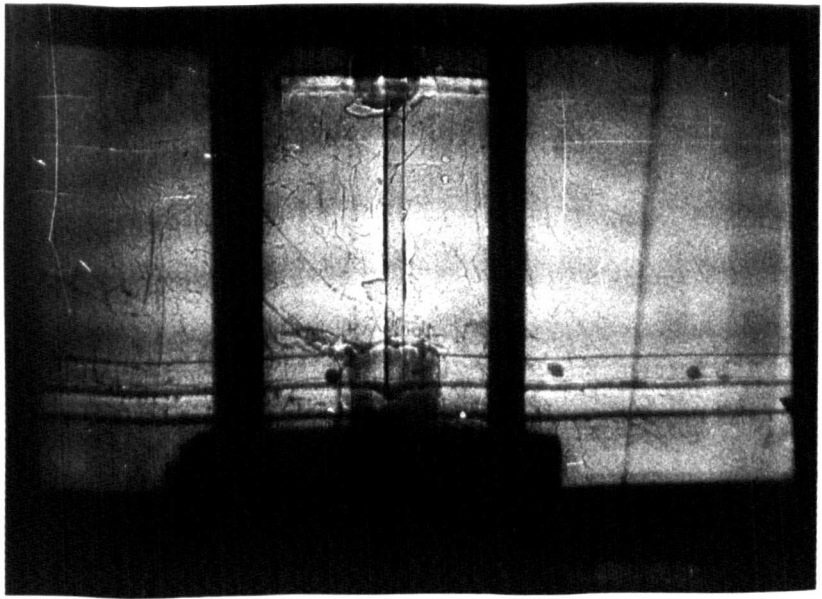
Depth of upper fluid = 3.0 cm

Depth of lower fluid = 1.3 → 2.8 cm

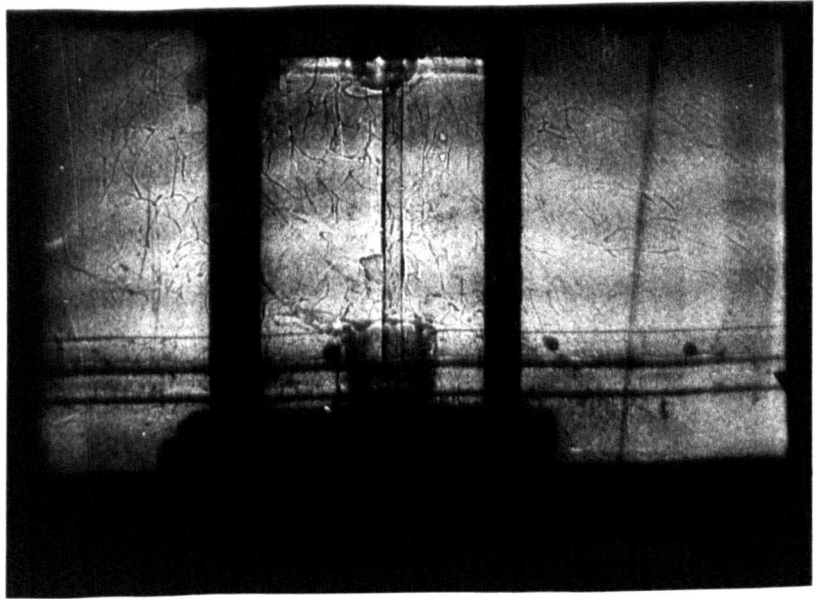
$\omega = 1.43 \text{ c/s}$

$\rho_{\text{upper}} = 1.081$        $\rho_{\text{lower}} = 1.100$

Magnetic field = 0.20 Wb/m<sup>2</sup>



(c) Total current = 10 amps



(d) Total current = 15 amps.

no longer be normal or parallel to the major and minor axes of the anisotropy, and should make ideal 'mirrors'. However, having set up such a situation, it was found impossible to obtain reflection of the waves, even in the O.H.D. case, as the photograph of fig. (4.28) makes clear. Presumably, the relatively low energy content of the wave train enables the slightest meniscus effect at the tank walls, and viscous effects near the wall, to absorb most of the wave energy so that any that is reflected is not visible.

Since this set-up had been thought to be the most likely to assist reflection, the attempt to demonstrate reflection characteristics was stopped here. However it must be pointed out that there should be much less of a problem in this respect with liquid metal experiments, since in that case the waves would be faster and contain more energy, with weaker viscous effects.



FIG 4.28. ATTEMPTED  
WAVE REFLECTION

## 5. VARIATIONS OF THE M.H.D. RAYLEIGH-TAYLOR INSTABILITY

### 5.1.1. Introduction

The Rayleigh-Taylor instability is the instability of an interface between two fluids, when one of them is accelerated towards the other. In hydrodynamics the normal circumstances under which it occurs are when a heavy fluid is supported above a less dense one, and gravity provides the accelerating force. However, in the realm of M.H.D., it is quite possible to use the  $\underline{j} \times \underline{B}$  force to accelerate a conducting fluid towards a non-conducting fluid, if the imposed magnetic field and electric current produce a force with component normal to the interface. For simplification, in this investigation, consideration will be mainly restricted to the case where  $\underline{j}$  and  $\underline{B}$  are imposed mutually perpendicular, parallel to the undisturbed interfacial plane. For this to be truly classified as a Rayleigh-Taylor type of stability problem, the  $\underline{j} \times \underline{B}$  force must be conservative in the undisturbed state, so that the initial condition for the problem is a state of equilibrium. whether stable or not, with the fluids at rest, the gravity and Lorentz forces being balanced by the internal pressure gradients within the fluids. Although gravity forces will be considered in the theoretical analyses, since they must always be of comparable order with  $\underline{j} \times \underline{B}$  forces in the laboratory experiments performed, it will be assumed that they are always stabilizing - i.e. with the current switched off, the lighter fluid lies above the heavier.

Thus the general arrangement is as shown in fig (5.1). What is already known about the M.H.D. Rayleigh-Taylor instability is its anisotropy. It turns out that modes in the x,z plane

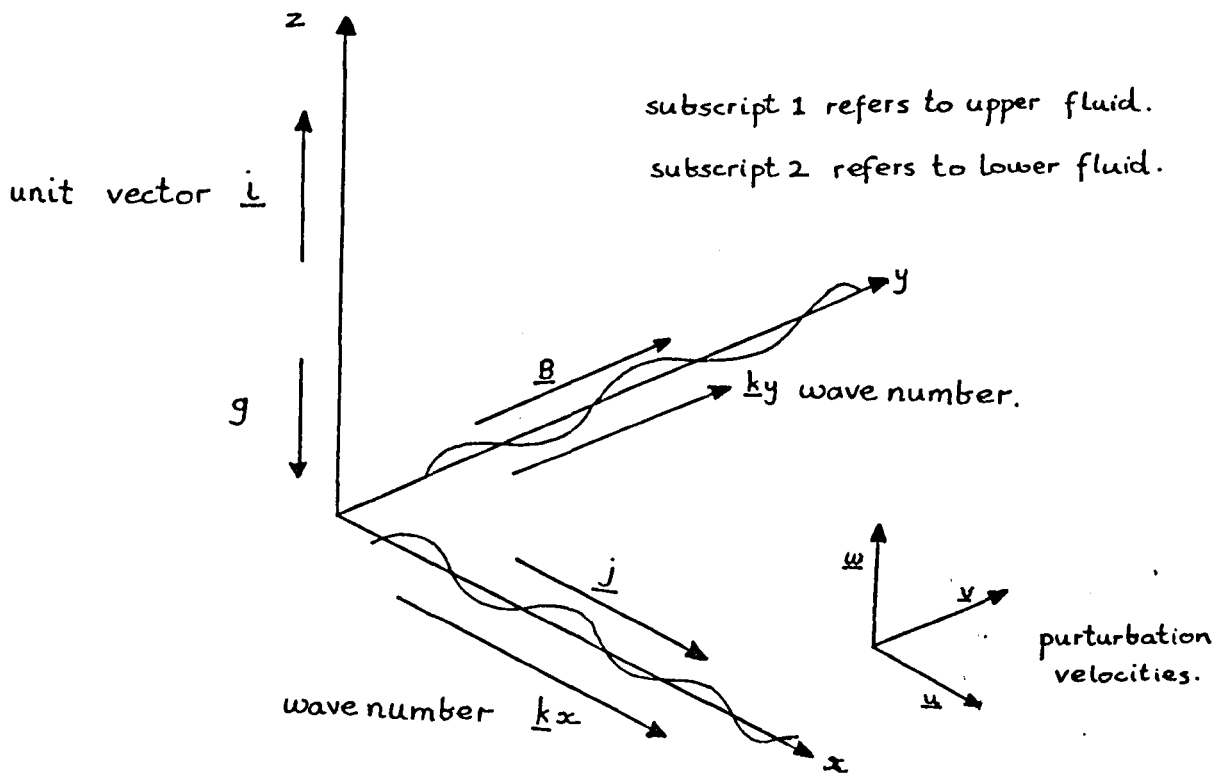


FIG. 5.1. GENERAL NOTATION FOR M.H.D. RALEIGH-TAYLOR PROBLEM.

(i.e. of wave number  $k_x$ ) are stable, whereas those in the  $z, y$  plane are not, an effect due to the same causes as those causing surface waves to be anisotropic (see 2.5.1). Now since the instability is produced by externally imposed electromagnetic fields, acting on the conducting liquid differently to the non-conductor so that the interface becomes unstable, it is possible that  $\underline{j}$  and  $\underline{B}$  can be varied in certain ways, still maintaining the conditions set out above, so that the instability can be influenced and its modes altered. Purely from academic interest, it was thought worthwhile to investigate such possibilities, since any new mode of instability thus predicted should be quite easy to observe experimentally. Also, study is made more generally of the effect of  $\underline{j} \times \underline{B}$  forces on the stationary equilibrium shape of a fluid interface, worthwhile both to complete the understanding of an uninvestigated area of M.H.D., and also since it stimulates a deeper understanding of what is normally looked on as a trivial O.H.D. phenomenon - the shape of free or interfacial surfaces.

#### 5.1.2. Other work on the M.H.D. Rayleigh-Taylor Instability

There is a considerable literature on the effect of imposed magnetic fields upon the ordinary Rayleigh-Taylor instability, where induced eddy currents in a conducting fluid modify the motion and usually tend to stabilize the situation in a way similar to viscosity. Such action is strongly anisotropic, depending upon the orientation of the magnetic field (Chandrasekhar 1961, Murty 1961).

However much less has been written about the situation here considered, where current also is imposed, induced currents are ignored, and the  $\underline{j} \times \underline{B}$  force is the actual destabilizing force. Lemaire (1963) has analysed the simple case ignoring surface tension and gravity, whilst Duc (1968) and Baker (1965) report experiments measuring the growth rates of the instability.

The original motivation behind these researches was the application to striated M.H.D. generators, where bands of alternately poor and good conducting gases pass through the generator, and mixing of the bands occurs due to the Rayleigh-Taylor instability at their interface (Devime et al. 1966). These all treat only the simple instability, and there is apparently no attempt in the literature to consider in more detail what effects the  $\mathbf{j} \times \mathbf{B}$  force can have on a surface, nor to explore some of the interesting variations which the flexibility of M.H.D. makes possible.

### 5.1.3. The irrotationality condition

The condition for the  $\mathbf{j} \times \mathbf{B}$  force to be conservative initially, before the instability gets under way, is that  $\text{curl } \mathbf{j} \times \mathbf{B} = 0$ . Also  $\text{div } \mathbf{B} = 0$ , and it will be assumed that  $\text{div } \mathbf{j} = 0$  too, so that

$$(\mathbf{B} \cdot \nabla) \mathbf{j} - (\mathbf{j} \cdot \nabla) \mathbf{B} = 0 \quad ; \dots 5.1$$

In the notation of fig. 5.1, assuming that  $\mathbf{B}$  is always  $(0, B_y, 0)$  and that  $\mathbf{j}$  is always imposed in the x direction only, for any cases where  $B_y$  varies, 5.1 becomes :-

$$B_y \frac{\partial j_x}{\partial y} - j_x \frac{\partial B_y}{\partial x} = 0$$

This condition allows the practical possibility of varying  $\mathbf{j}$  in both x and z directions, and  $\mathbf{B}$  in the z direction, without causing rotational forces in the unperturbed state, but making possible new modes of instability. The effect of  $\frac{\partial B}{\partial z} \neq 0$  has been mentioned by Lemaire and Baker, but no attempt of observing it is recorded, nor is the anisotropic nature of the  $\frac{\partial B}{\partial z}$  term considered. Thus these cases will be analysed in } 5.3.

## 5.2. The $\mathbf{j} \times \mathbf{B}$ Force and the Shape of a Fluid Surface

### 5.2.1. The need to consider the problem

In ordinary hydrodynamics it is taken for granted that, except for the influence of surface tension, a liquid surface will be flat and horizontal if the fluid is stationary, and any contours in the surface must be associated with motion. However when  $\mathbf{j} \times \mathbf{B}$  forces are imposed on a liquid with a free surface, it is not so obvious what shape of surface or interface can be maintained, when the  $\mathbf{j} \times \mathbf{B}$  force is either conservative or rotational, and it is also pertinent to enquire what the effect of a surface disturbance will be to the electric current path and resulting  $\mathbf{j} \times \mathbf{B}$  field.

It is necessary to consider the possible exceptions to the obvious expectation that the surface must still remain flat, so that when experiments are performed to observe instabilities, the movement of the surface may be confidently held to be due to the instability itself and not one of the possibilities to be looked into now.

### 5.2.2. The effect of conservative $\mathbf{j} \times \mathbf{B}$ upon surface shape

Ignoring the influence of surface tension, the interface must lie normal to the resultant of body forces acting on the fluids on either side of the interface. This may be shown as follows:-

In the absence of surface tension the boundary condition on pressure at the interface is:  $\Delta p = 0$  (where  $\Delta$  represents the difference in the parameter across the interface). Denoting the upper fluid by 1 and the lower fluid by 2, with  $s$  a direction in the plane of the interface and  $n$  normal to it, then  $(\frac{\partial p}{\partial s})_1 = (\frac{\partial p}{\partial s})_2$

In the case where  $\mathbf{j}$  is imposed horizontally, and  $\mathbf{B}$  at angle  $\theta$  to the horizontal (see fig 5.2), let the surface lie at  $\phi$  to the horizontal, then  $\frac{\partial p_1}{\partial z} = -\rho g$  ,  $\frac{\partial p_1}{\partial y} = 0$

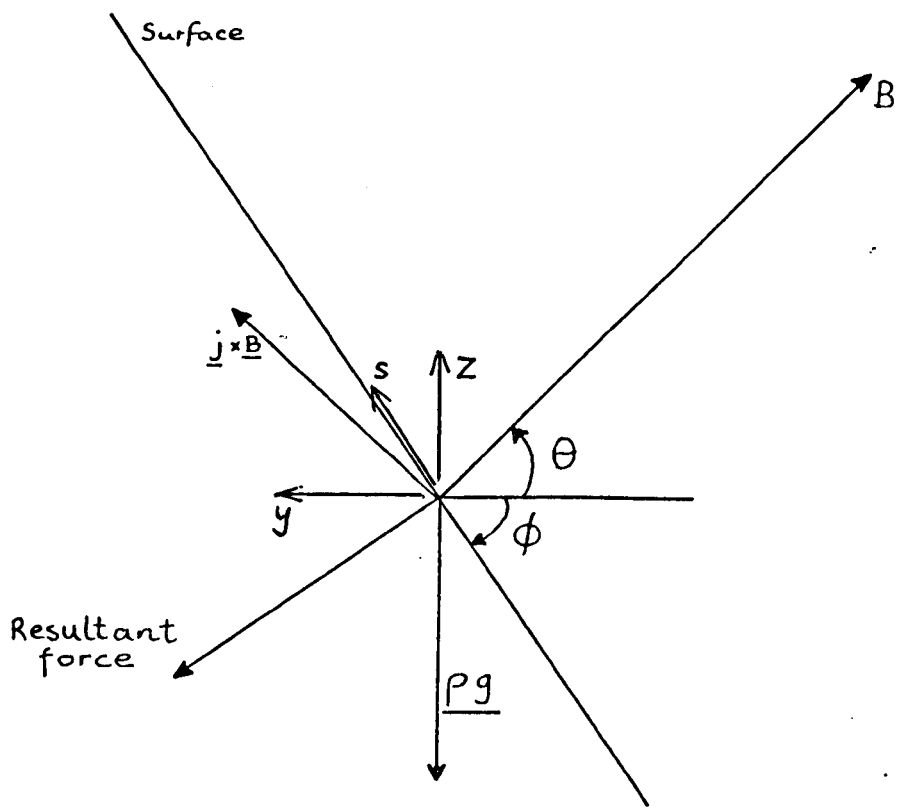


FIG. 5.2. THE EFFECT OF INCLINED B UPON SURFACE INCLINATION.

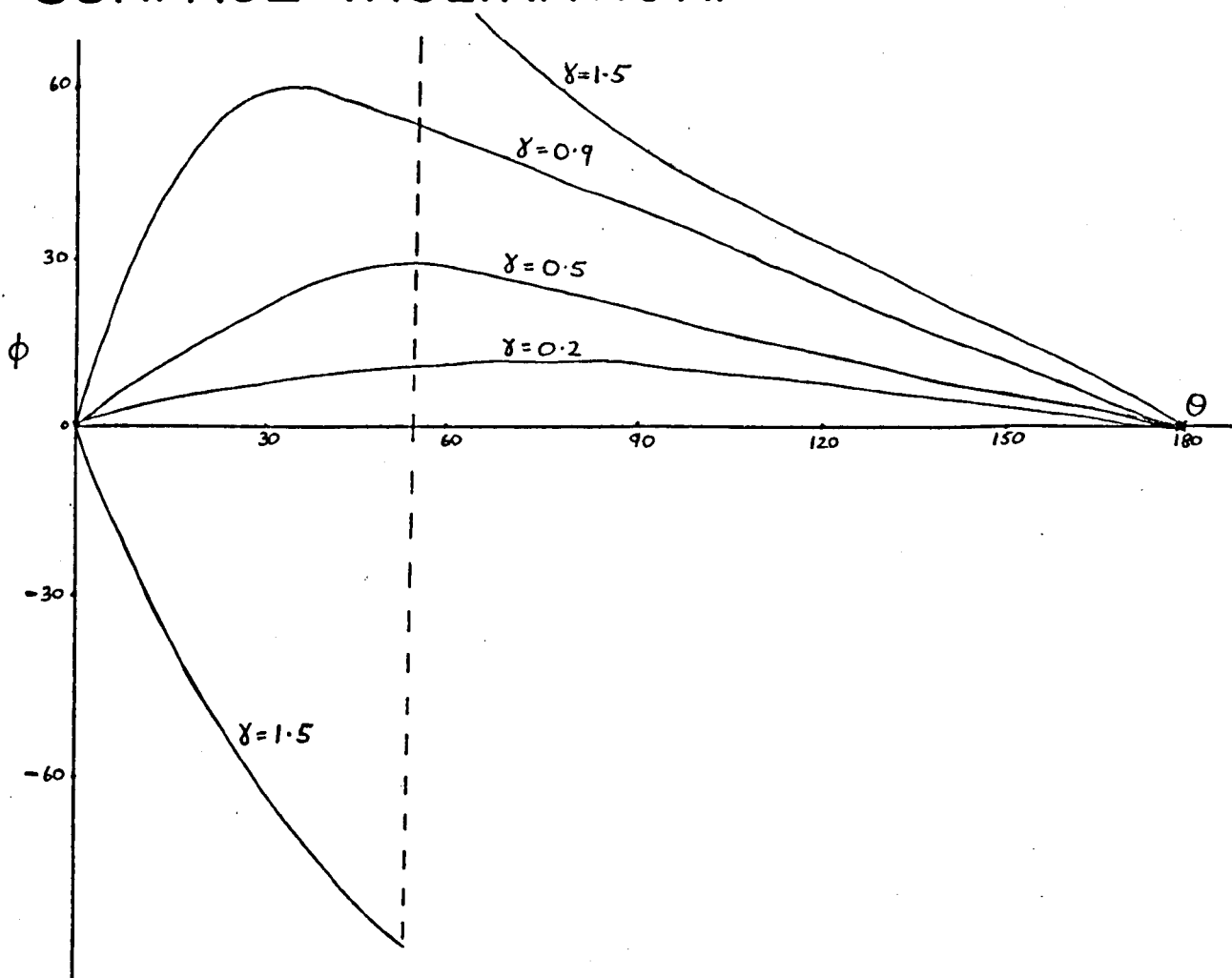


FIG. 5.3. VARIATION OF SURFACE INCLINATION WITH MAGNETIC FIELD INCLINATION.

$$\frac{\partial p_2}{\partial z} = -\rho_2 g + jB \cos \theta, \quad \frac{\partial p_2}{\partial y} = +jB \sin \theta$$

now 
$$\frac{\partial p}{\partial s} = \frac{\partial p}{\partial z} \sin \phi + \frac{\partial p}{\partial y} \cos \phi$$

hence 
$$\tan \phi = \frac{-jB \sin \theta}{(\rho_1 - \rho_2)g + jB \cos \theta} = \frac{-\gamma \sin \theta}{\gamma \cos \theta - 1} \quad \text{if } \gamma = \frac{jB}{(\rho_2 - \rho_1)g}$$

The dependence of  $\phi$  on  $\theta$  for various  $\gamma$  is shown in (fig.5.3).

It can be seen that the interface can be supported at any inclination to the horizontal, provided  $\gamma > 1$ . However, if  $\phi$  is greater than  $90^\circ$ , there is a situation where heavier liquid is above lighter liquid, and though the interface is stable to oscillations in the plane in which the interface is inclined (i.e. the vertical plane containing  $\underline{B}$ ) it will clearly be unstable to oscillations in the normal plane (see fig.5.4). Here, then, is a means of supporting liquid surfaces at an inclination to the horizontal without there being any fluid motion. Indeed the surface could be held curved in a variety of shapes (providing  $\phi < 90^\circ$ ) in the plane containing  $\underline{B}$ , by imposing a suitably curved magnetic field (subject of course to  $\text{curl } \underline{B} = \text{div } \underline{B} = 0$ ). Conversely, this could possibly form the basis of a visual method of testing for the uniformity of a fairly strong field. If a tank of mercury were placed in the field, and a strong enough current passed through, any bending of the field could be immediately detected optically from distortions of the surface, assuming that the surface area was large enough not to be dominated by surface tension.

The next question is to ask whether, given a horizontal magnetic field, a liquid surface can be supported non-horizontal

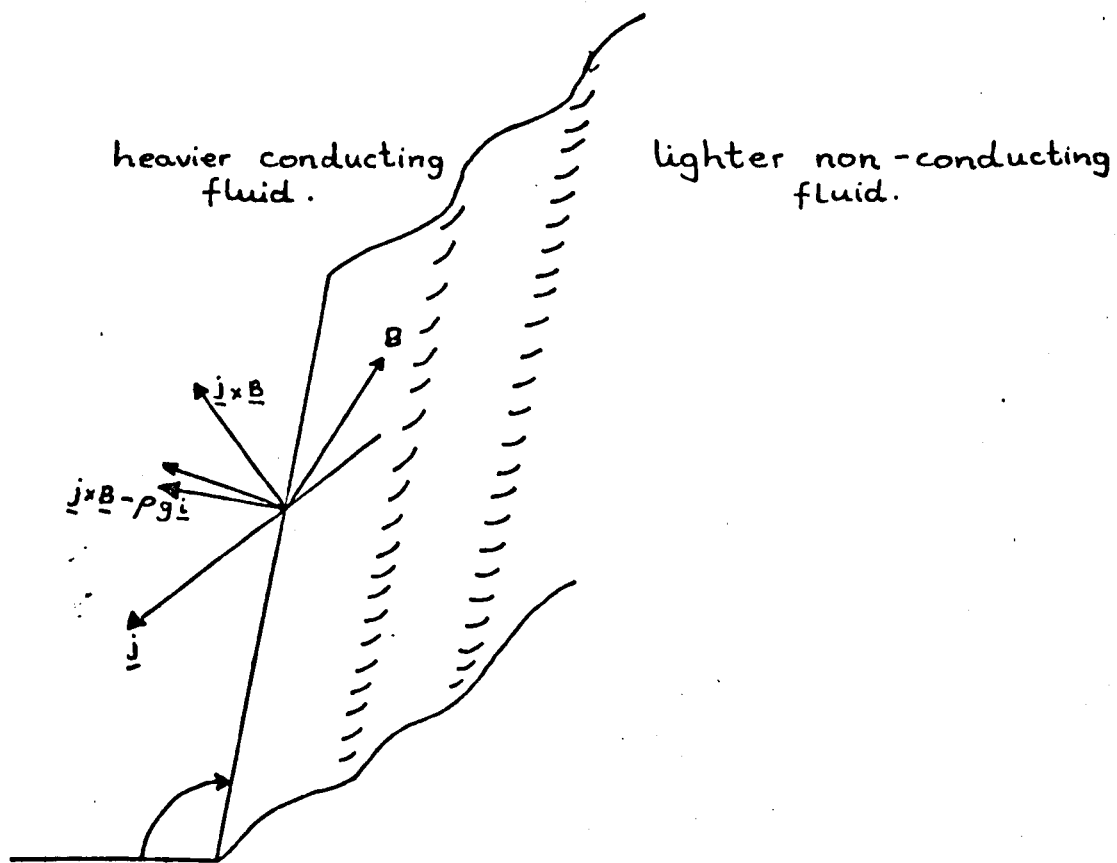


FIG. 5.4. PLANE OF INSTABILITY WHEN HEAVIER FLUID IS LIFTED ABOVE LIGHTER FLUID BY  $\underline{j} \times \underline{B}$  FORCE.

by the electric current. The answer in fact must be negative, since the current at the interface, (which is the relevant current) must always be parallel to the surface. Even if both liquids were of different but finite conductivities, the current parameter pertinent to the discussion would be  $\Delta \underline{j}$ , which is  $\underline{j}_{1s} - \underline{j}_{2s}$  (since  $\underline{j}_{1n} = \underline{j}_{2n}$  because  $\text{div } \underline{j} = 0$ ). Now by a similar argument to that above, but with  $\theta$  representing the inclination of current direction to the horizontal, again  $\tan \phi = \frac{-\gamma \sin \theta}{\gamma \cos \theta - 1}$ , and with the boundary condition on current requiring  $\theta = \phi$ , then  $\theta = \phi = 0$  is the only possibility. Thus, in the later discussion of intermediate positions of interface stability, with a non-level interface, it can be confidently asserted that a conservative  $\underline{j} \times \underline{B}$  field cannot hold the interface non-level unless  $\underline{B}$  itself is not horizontal.

It could be an interesting exercise to consider the fluid motion resulting from rotating the magnetic field, slowly enough to ignore inductive effects, or to trace the fluid motion to its new position of stability subsequent to switching on an inclined field.

### 5.2.3. The effect of rotational $\underline{j} \times \underline{B}$ forces

The question again is whether it is possible, without corresponding fluid motion, to maintain a non-level surface to the liquid using rotational  $\underline{j} \times \underline{B}$  forces, of any configuration. In general, such forces would generate motion in the fluid, which would then cause the surface to be distorted, so that for no motion to occur, the disturbed surface would have to cause equal and opposite rotational forces to balance  $\underline{j} \times \underline{B}$ . But from O.H.D. theory of waves and surface instabilities, if  $\underline{F}$  is the restoring or destabilising force field,  $\text{curl } \underline{F}$  is everywhere zero except along the surface itself, since it is possible (in the inviscid theory at least) to solve using a velocity potential.

Thus for the fluids to remain at rest, with a distorted surface, the rotational  $\underline{j} \times \underline{B}$  would have to act at the surface only, i.e. provided by a current sheet.

The simplest case to envisage would be a horizontal magnetic field, with a current sheet at the interface, the current always being horizontal and perpendicular to  $\underline{B}$ , but varying in the  $\underline{B}$  direction, i.e.  $(\underline{B} \cdot \text{grad})\underline{j} \neq 0$ .

However in the considerations of the M.H.D. Rayleigh-Taylor instability,  $\underline{j}$  is by no means confined, indeed cannot conceivably be restricted to a current sheet at the interface, except when dealing hypothetically with perfect conductors and so it is concluded that it is not possible to maintain a distorted surface by a rotational  $\underline{j} \times \underline{B}$  force without fluid motion.

#### 5.2.4. The effect of a disturbed surface on the $\underline{j} \times \underline{B}$ configuration

In order to understand the problems to be investigated later, it is necessary now to change the point of view somewhat, and to consider the converse of the above sections, viz given a distorted surface, supported by surface tension or by a particular fluid motion, what is the effect on what was for the undisturbed state a conservative  $\underline{j} \times \underline{B}$  force field. The  $\sigma (\underline{v} \times \underline{B})$  induced currents will be ignored here, since it would be possible using small imposed  $\underline{B}$  and large  $\underline{j}$  for them to be negligible. Also, just the simplest case will be considered where, in the undisturbed state,  $\underline{j}$  and  $\underline{B}$  are mutually perpendicular and horizontal.

Particularly, it is useful to know what surface shapes will cause a rotational  $\underline{j} \times \underline{B}$  to occur, with its consequent production of motion, which in its turn will further modify the surface shape.

The condition for rotationality (5.1) is

$$(\underline{B} \text{ grad})\underline{j} - (\underline{j} \text{ grad})\underline{B} \neq 0$$

Now  $\underline{j}$  is governed by the surface shape, since  $j_n$  is always zero.

$\underline{B}$  will not be affected by the surface shape, and if  $\underline{B} = (0, B_y, 0)$ ,

then for irrotationality  $\underline{j}$  must not vary in the  $y$  direction.

Thus if the surface height be  $h$  see fig. (5.1), then for

$$\frac{\partial j}{\partial y} = 0, h = f_1(x \text{ only}) \text{ or } h = f_2(y \text{ only})$$

But as soon as  $h = f(x, y)$ , the current will be distorted so that motion is induced by rotational forces.

Thus the usual modes of M.H.D. Rayleigh-Taylor instability as considered by Lemaire et al, do not give rise to rotational  $\underline{j} \times \underline{B}$  forces.

It is worth noting for the case where the instability with  $\frac{\partial B}{\partial z} \neq 0$  is considered, that in this case (5.1) requires that  $\underline{j}$  has no  $z$  component anywhere for irrotationality, so that  $h = f_1(x)$  is unacceptable, and  $h = f_2(y)$  is the only mode of surface disturbance not to cause rotational forces.

It should also be stated that although the small amplitude assumption, made in the chapters on wave motions, enabled us to ignore rotational forces caused by the surface disturbance, that assumption is not normally valid for instabilities.

#### 5.2.5 The effect of surface tension in the presence of $\underline{j} \times \underline{B}$ forces

It is usual when dealing with O.H.D. and M.H.D. problems of a free surface to include surface tension, if required, simply by adding a suitable term to the relevant equation - usually through the boundary condition on pressure. This is the procedure adopted in the next section of this chapter. However, surface tension can introduce further complications through magnetohydrostatics, i.e. in

the stationary state without wave or instability motion it can still interact with the electromagnetic parameters. In the way described in 5.2.4, through maintaining a surface distorted from the horizontal, it can cause rotational  $\underline{j} \times \underline{B}$  forces and hence indirectly cause spurious motions to occur. What is even more troublesome in experimental work is the fact that the equilibrium magnetohydrostatic surface shape changes as  $\underline{j} \times \underline{B}$  is varied, even when stability is maintained.

In two dimensions (adopted for simplicity) the interface between two stationary liquids in hydrodynamics has its height  $z_0$  governed by surface tension such that

$$\frac{(\rho_2 - \rho_1)}{\alpha} z_0 - \frac{\partial^2 z_0}{\partial x^2} / \left[ 1 + \left( \frac{\partial z_0}{\partial x} \right)^2 \right]^{\frac{3}{2}} = 0$$

with the boundary conditions of  $\frac{\partial z_0}{\partial x} = \tan$  (angle of contact) at the edge wall and  $\frac{\partial z_0}{\partial x} \rightarrow 0$  as  $x \rightarrow \infty$  in a semi-infinite fluid. (Batchelor 1967, p.66) This is the familiar meniscus effect which is taken for granted and allowed for in so many experimental situations.

With imposed  $\underline{j} \times \underline{B}$  ( $\underline{j}$  perpendicular to  $\underline{B}$  which is in the  $x$  direction), the equation becomes,

$$A \frac{z_0}{\alpha} - \frac{\partial^2 z_0}{\partial x^2} / \left[ 1 + \left( \frac{\partial z_0}{\partial x} \right)^2 \right]^{\frac{3}{2}} = 0 \quad \text{where } A = (\rho_2 - \rho_1)g - jB$$

( $\underline{j} \times \underline{B}$  assumed acting upwards)

Thus varying  $j$  or  $B$  will cause the surface to change its shape. In particular, there will be a noticeable movement of the surface to a new position when a  $\underline{j} \times \underline{B}$  force of the same order as the gravity force is suddenly switched on. Now when  $(\rho_2 - \rho_1) \ll \rho_2$  as is the case when the two fluids are closely matched in density the meniscus effect becomes very pronounced, even in the O.H.D. case, and so it can be a dominating feature of M.H.D. experiments,

if care is not taken to reduce the surface tension. Figs (5.5 and 6) show typical surface shapes for mercury/air and electrolyte/organic liquid interfaces for various values of  $\underline{j} \times \underline{B}$ .

These are plotted from

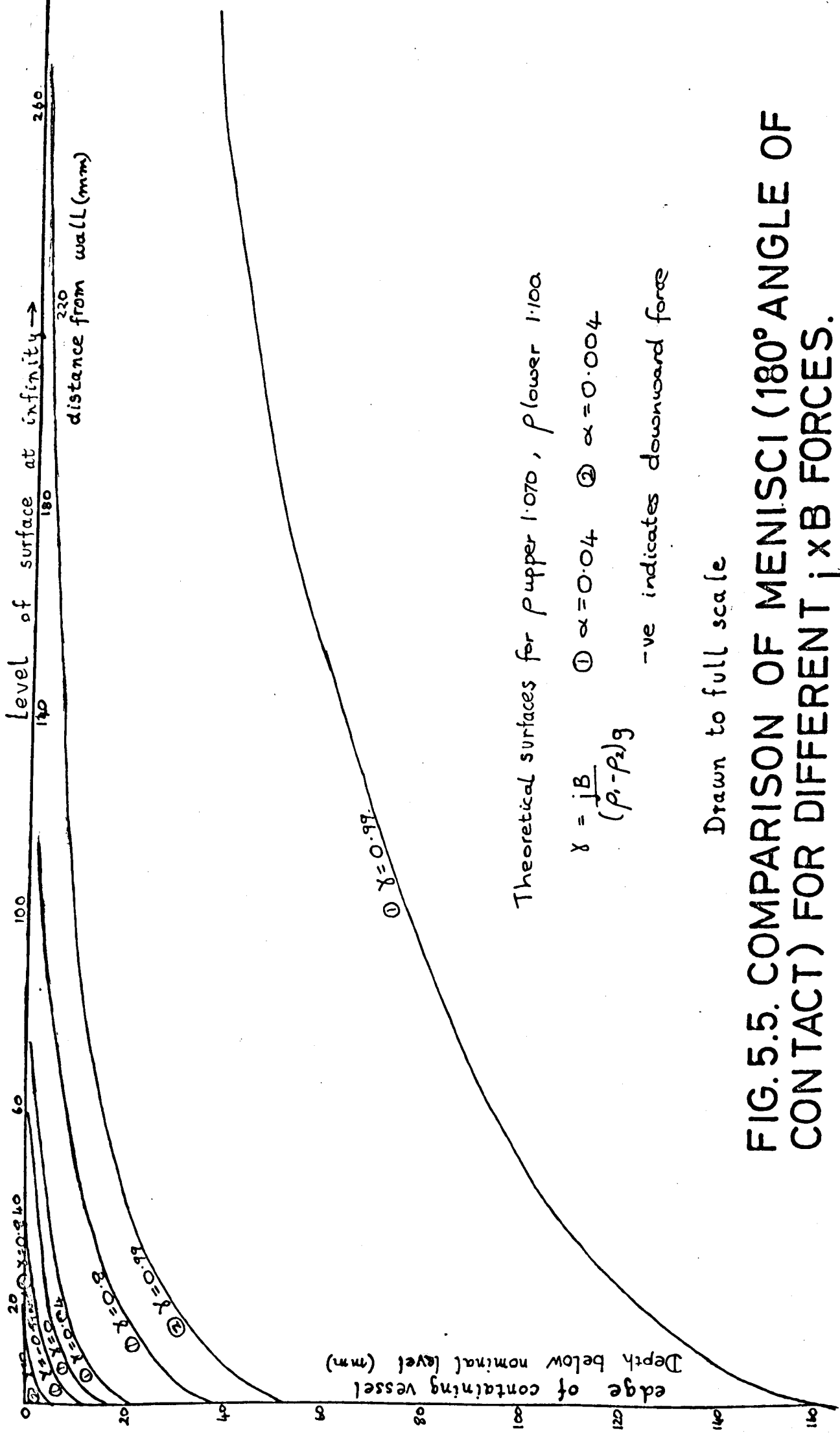
$$\frac{x}{d} = \cosh^{-1}\left(\frac{2d}{z_0}\right) - \cosh^{-1}\left(\frac{2d}{h}\right) + \left(4 - \frac{h^2}{d^2}\right)^{\frac{1}{2}} - \left(4 - \frac{z_0^2}{d^2}\right)^{\frac{1}{2}}$$

where  $d^2 = \frac{\alpha}{A}$  ,  $h^2 = (1 - \sin \theta) \frac{2\alpha}{A}$  ,  $h$  being the height of the meniscus above (or below) the surface level at  $x \rightarrow \infty$  , and  $\theta$  the angle of contact.

If the surface tension is such as to cause the meniscus effect to dominate in the given tank dimensions, then if growth rates of instabilities are being measured after a sudden switch-on of  $\underline{j} \times \underline{B}$ , the initial motion will be due not only to instability, but to the surface tending to move to its (unstable) equilibrium position. If alternatively, the instability is observed by a gradual increase of  $\underline{j} \times \underline{B}$  until the interface goes unstable, care must be taken whilst observing surface elevation that the surface movement to accommodate the changing meniscus shape is not mistaken for the true onset of instability.

It must be made clear that this effect is purely due to the meniscus, and is unrelated to the usual influence of surface tension tending to stabilise a surface, at least for the shorter wavelengths. This may be illustrated by noting that if the angle of contact in fact is  $90^\circ$ , no matter how great the surface tension is this meniscus phenomenon will disappear.

As well as being something to be avoided in instability experiments, it also gives rise to an interesting variant of the Rayleigh-Taylor instability to be described in chapter 6.



Theoretical surfaces for  $\rho_{upper} 1.070$ ,  $\rho_{lower} 1.100$

$\chi = \frac{jB}{(\rho - \rho_2)g}$   
 ①  $\alpha = 0.04$     ②  $\alpha = 0.004$

-ve indicates downward force

Drawn to full scale

FIG. 5.5. COMPARISON OF MENISCI (180° ANGLE OF CONTACT) FOR DIFFERENT  $j \times B$  FORCES.

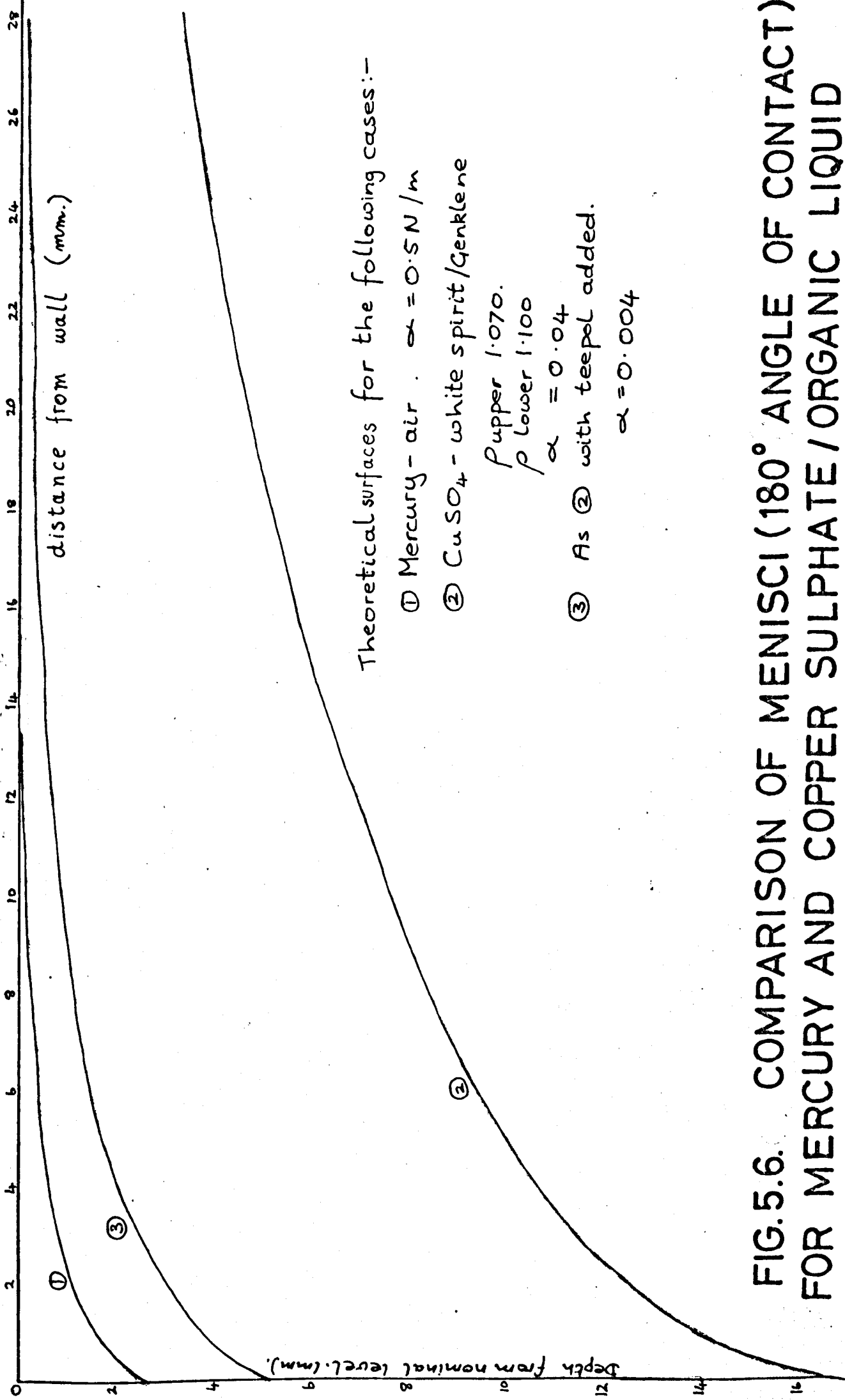


FIG. 5.6. COMPARISON OF MENISCI ( $180^\circ$  ANGLE OF CONTACT) FOR MERCURY AND COPPER SULPHATE / ORGANIC LIQUID

### 5.3. Variations of the M.H.D. Rayleigh-Taylor Instability

#### 5.3.1. Solving the basic configuration

Before looking at the various configurations suggested in 5.1.3., it is necessary to first consider the basic problem where  $\underline{j}$  and  $\underline{B}$  are imposed mutually at right angles, horizontal and uniform throughout. The stability ~~question~~<sup>equation</sup> is, of course, the same as the dispersion relation already obtained in 2.3.1. From there it will be seen that as  $jB$  is increased, the first mode to become unstable is that in the plane containing  $\underline{B}$  and the vertical i.e. the instability will grow with troughs and crests in the  $\underline{j}$  direction.

The stability problem has also been solved by Lemaire, separately considering modes in the  $\underline{j}$  direction and modes in the  $\underline{B}$  direction, starting from the perturbation equations governing a fluid with density and conductivity varying continuously, in a manner similar to that used by Chandrasekhar to solve the O.H.D. Rayleigh-Taylor problem. It is rather more cumbersome than the approach used by Shercliff to solve the surface wave problem, but it provides a useful starting place for the consideration of variations to the basic configuration, particularly  $\frac{\partial B}{\partial z} \neq 0$ . Therefore it is briefly included here, extended from Lemaire's solution, not only to include surface tension and gravity forces, but also to cope in one solution with waves in any direction.

The notation is explained in fig. (5.1). The variables  $V_x, V_y, V_z$ , represent perturbation velocity,  $\delta p$  the perturbation pressure,  $\delta E_x, \delta E_y, \delta E_z$  the perturbation electric field, whilst  $E_x$  is the imposed field. All these variables are assumed to vary as  $F(z)e^{nt + ik_x x + ik_y y}$  and the interface is assumed to be  $z = z_0$ , where  $z_0 = Z_0 e^{nt + ik_x x + ik_y y}$ . Given the fluids are

initially in stationary equilibrium, on applying a small perturbation to the interface, of the form stated above, the perturbation equations are :-

$$\text{div. } \underline{v} = 0 :- \quad \frac{\partial v_z}{\partial z} + ik_x v_x + ik_y v_y = 0 \quad \dots 5.1$$

$$\text{equation of motion, x direction :- } ik_x \delta p + \rho n v_x = -\sigma \delta E_z B_y \quad \dots 5.2$$

$$\text{y direction :- } ik_y \delta p + \rho n v_y = 0 \quad \dots 5.3$$

$$\text{z direction :- } \frac{\partial}{\partial z} (\delta p) + \rho n v_z = -g \delta \rho + \delta \sigma E_x B_y + \sigma \delta E_x B_y - \frac{k^2}{n} v_{z_0} \propto \delta [z-z_0] \quad 5.4$$

where  $\delta [z-z_0]$  represents Dirac's  $\delta$ -function about  $z_0$

$$\text{div } \underline{E} = 0 :- \quad \frac{\partial}{\partial z} (\delta E_z) + ik_x \delta E_x + ik_y \delta E_y = 0 \quad \dots 5.5 \quad *$$

$$\text{curl } \underline{E} = 0 :- \quad ik_x (\delta E_z) - \frac{\partial}{\partial z} (\delta E_x) = 0 \quad \dots 5.6$$

$$ik_x (\delta E_y) - ik_y (\delta E_x) = 0 \quad \dots 5.6$$

$$\frac{D\sigma}{Dt} = 0 :- \quad n \delta \sigma + v_z \frac{\partial \sigma}{\partial z} = 0 \quad \dots 5.7$$

$$\frac{D\rho}{Dt} = 0 :- \quad n \delta \rho + v_z \frac{\partial \rho}{\partial z} = 0 \quad \dots 5.8$$

After various eliminations (5.4) reduces to

$$ik_x B \delta E_z \frac{\partial \sigma}{\partial z} + k^2 \rho n v_z - \frac{\partial}{\partial z} (\rho n \frac{\partial v_z}{\partial z}) = \frac{g k^2}{n} v_z \frac{\partial \rho}{\partial z} - E_x B \frac{k^2 v_z}{n} \frac{\partial \sigma}{\partial z} - \frac{k^4}{n} \propto v_{z_0} \delta [z-z_0] \quad \dots 5.9$$

The boundary conditions are :-

$$\text{At the interface } z = z_0 :- v_{z_0} = \frac{\partial z_0}{\partial t} + v_x \frac{\partial v_z}{\partial x} \quad \text{which is}$$

$$\text{linearised to } \frac{\partial z_0}{\partial t} \quad \text{i.e. } v_{z_0} \approx n z_0$$

and the boundary conditions on current if the upper fluid is

$$\text{a non conductor is :- } \frac{\partial z_0}{\partial x} = \frac{\sigma_2 \delta E_{z_0}}{\sigma_2 (E_x + \delta E_{x_0})} \approx \frac{\delta E_{z_0}}{E_x}$$

$$\text{i.e. } (\delta E_z)_0 = E_x \frac{\partial z_0}{\partial x} = ik_x z_0 E_x \quad \text{within the lower fluid.}$$

\* The examiners have pointed out that it has not been shown why  $\text{div } \underline{E} = 0$ .

In the main bulk of each fluid (5.9) becomes :-

$$k^2 v_{z1} - \frac{\partial^2 v_{z1}}{\partial z^2} = 0, \quad z > 0$$

and  $k^2 v_{z2} - \frac{\partial^2 v_{z2}}{\partial z^2} = 0, \quad z < 0$

thence  $v_{z1} = n z_0 e^{-kz} \quad \therefore \left(\frac{\partial v_{z1}}{\partial z}\right)_0 = -k n z_0$

$$v_{z2} = n z_0 e^{kz} \quad \therefore \left(\frac{\partial v_{z2}}{\partial z}\right)_0 = +k n z_0$$

Integrating (5.9) across the interface, the terms with continuous variables vanish, and if  $\sigma_1 = 0$  :-

$$k_x^2 B E_x \sigma_2 + (\rho_1 + \rho_2) n^2 k = g k^2 (\rho_1 - \rho_2) + k^2 B E_x \sigma_2 - k^4 \alpha$$

$$\text{or, } -n^2 = \frac{(\rho_2 - \rho_1) g k + k^3 \alpha - \frac{k_y^2}{k} B E_x \sigma_2}{(\rho_1 + \rho_2)}$$

or, if  $k_x = k \sin \theta, k_y = k \cos \theta$

$$-n^2 = \frac{(\rho_2 - \rho_1) g k + k^3 \alpha - k \cos^2 \theta B E_x \sigma_2}{\rho_1 + \rho_2} \quad \dots 5.10$$

which is exactly the same result as for the deep fluid case of eq. (2.19).

Instability will occur when  $k_y^2 B E_x \sigma_2 > (\rho_2 - \rho_1) g k^2 + k^4 \alpha$

so that as  $E_x$  is increased from 0, instability will occur first

in the  $k_y$  mode, in which case  $B E_x \sigma_2 > (\rho_2 - \rho_1) g + k_y^2 \alpha$

is the instability condition. Thus the first mode to go unstable

would be for  $k_y \rightarrow 0$  if that were possible, but in effect this

means that on gradually increasing  $E_x$  instability will occur with

the largest wave length possible given the dimensions of the

containing vessel and the angle of contact of the interface at the

walls, i.e. there is a minimum possible wave number  $k_{y \text{ min}}$ .

On the other hand, if  $E_x$  is suddenly switched from zero to a value such that  $E_x B \sigma_2 > (\rho_2 - \rho_1) g k + k_{y \min}^2 \propto$

the mode of instability to appear will be that having the maximum growth rate, i.e.  $k_y^2 = \frac{B E_x \sigma_2 - (\rho_2 - \rho_1) g}{\alpha}$

### 5.3.2 Variation of current density in the current direction

As a possible variation of the basic configuration, we shall first consider the case where  $\frac{\partial j_x}{\partial x} \neq 0$

in the notation of fig. (5.1). In particular, it is fruitful to consider the sort of arrangement drawn in fig. (5.7) which satisfies these conditions, although other configurations could also be considered.

The interesting nature of this configuration is immediately apparent on considering the situation when  $\underline{E}$  and  $\underline{B}$  are imposed of such a strength that in the main bulk of the fluid,  $\underline{j}$  is such that  $\underline{j} \times \underline{B}$  does not overcome the gravity force, whereas over the hump in the floor of the tank,  $\underline{j}$  is increased so that  $\underline{j} \times \underline{B}$  there acts to destabilise the surface. The surface above the hump will tend to go unstable, and the mode of the instability will be, according to the normal M.H.D. Rayleigh-Taylor pattern, with  $\underline{k} = k_y$  i.e. troughs and crests running in the  $j$  direction. However, these troughs and crests will run into regions either side of the hump which are stable, and even where it is unstable, the growth rate will vary in the  $x$  direction, so that the troughs and crests might be expected to vary in amplitude from zero in the stable region to a maximum above the centre of the hump.

As the instability grows, considering the problem intuitively, there will be a tendency for fluid to flow from

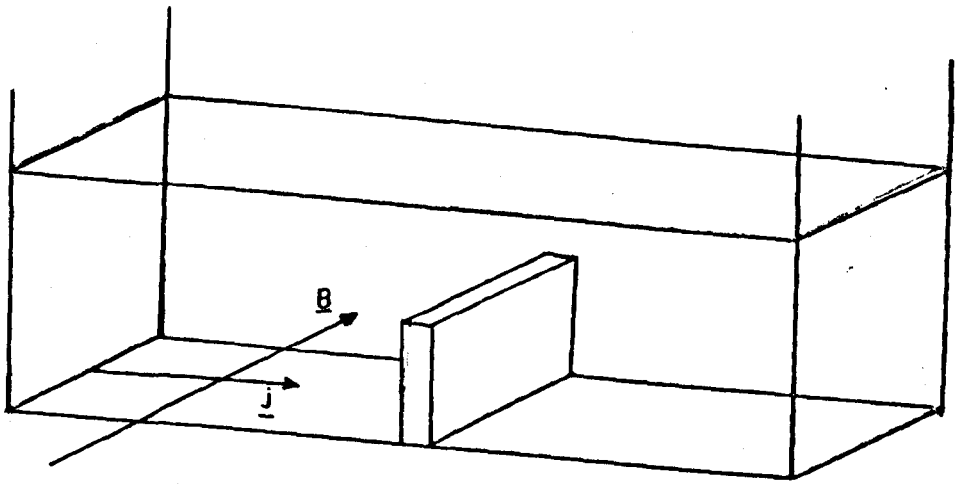


FIG. 5.7. TYPICAL TANK CONFIGURATION  
FOR  $\frac{\partial j}{\partial x} \neq 0$ .

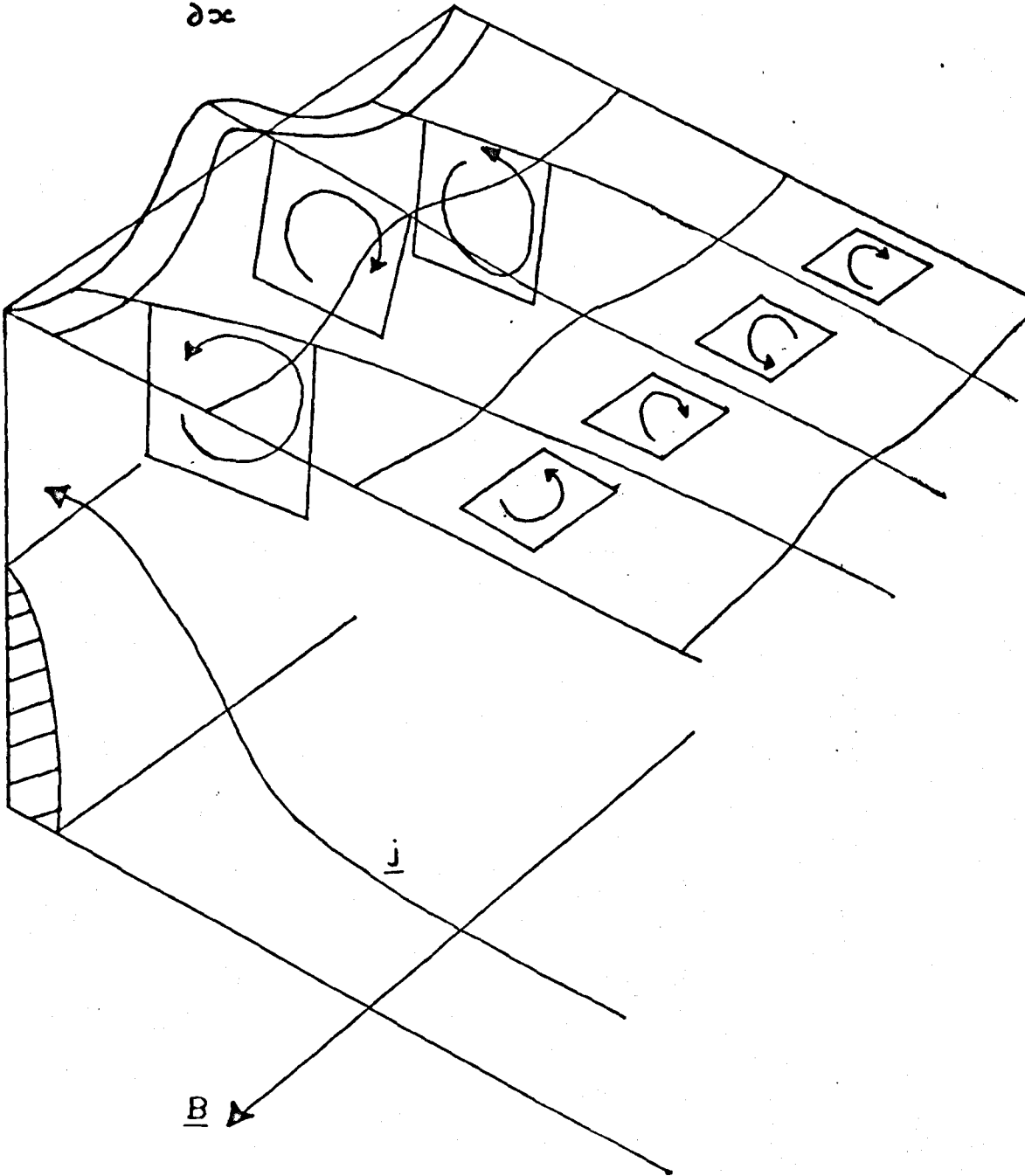


FIG. 5.8. PREDICTED SURFACE PROFILE.

the centre of the crests down to the stable region, and conversely from the stable region down the troughs to the centre. Is it possible that this flow could not only retard the growth of the instabilities, by eroding the peaks and filling up the troughs, but when the instability has grown to a certain level, exactly balance out the growth, producing a situation where there is a steady flow within the fluid but the interface is stationary in a state of intermediate stability humped in the sort of shape shown in fig. (5.8) ? If this is the case, it could be described from the instability point of view as a cellular type motion derived from the stationary situation as in the Bénard problem - yet without any variation of fluid properties within the fluid itself, whilst from an M.H.D. standpoint it would be classed as an electrically driven secondary flow where the primary flow is in fact static equilibrium. Viewed either way it would be a novel instability situation.

Various approaches have been made in an attempt to solve the problem analytically, but so far with no success:-

(a) Consider the two dimensional approach in the Oxz plane. This immediately fails, since of course in this plane on its own no instability is possible as shown above in 5.3.1.

The motion must essentially be 3-dimensional, since the mode will be basically of  $\sin \frac{u}{\lambda}$  type in the Oyz plane of varying amplitude and perhaps wavelength in the x direction. This is plainly seen if we take a section in the Oyz plane, and consider the isolated stability of that section. The maximum growth rate and corresponding wavelength will vary depending on where we take the section, i.e. will vary with x.

With the surface disturbed in both vertical planes, then, we have the situation explored in 5.2.4. where the surface shape itself gives rise to rotational  $\underline{j} \times \underline{B}$  forces, further complicating the problem, and since it is not clear what velocities are involved, it is not reasonable to ignore the  $(\underline{v} \times \underline{B})\sigma$  induced electric currents.

(b) It is possible to simplify by considering the initial growth rates of the <sup>in</sup>stability. Hence we can postulate that velocities are negligible, and surface distortions are insufficient to have produced any appreciable diversion of current. The way to proceed then would be as above in 5.3.1., considering the perturbation equations in three dimensions. But this proves very complicated since the most that can be assumed is an  $e^{ky}$  dependence and the whole approach becomes hopelessly complex.

(c) A third analytical approach is to consider a possible developed secondary flow in its steady state. But this involves the solution of the 3 dimensional electrically driven flow problem, where in the steady state the balance of forces is between the rotational  $\underline{j} \times \underline{B}$  and viscous dissipative forces. Under the present experimental conditions the Hartmann number is low, excluding the simplification of asymptotic solutions as in High Hartmann No. problems, and the analysis is beyond reasonably simple solution as far as can be seen.

Hence the intuitive prediction of a quasi-stable flow pattern with a disturbed surface has not been confirmed analytically, and must be confirmed or disproved by experiment. As a further rough check on the feasibility of such a motion the results of 5.2.4 can be used to indicate what effect a surface shape such as fig. (5.8) would have on the electromagnetic parameters, and whether their distortion encourages or discourages a quasi-stable state.

The arrows included in fig. (5.8) show the direction of curl ( $\underline{j} \times \underline{B}$ ) due to the distortion of  $\underline{j}$  by the surface shape, and it will be noted that it is such as to promote the motion already suggested, although only experiment can determine whether the motion is sufficient to halt the instability altogether, or whether it just slows it down.

### 5.3.3. Variation of current density in the vertical direction

This case of  $\frac{\partial \underline{j}_x}{\partial z} \neq 0$  is another possible variation from the normal M.H.D. Rayleigh-Taylor instability, still maintaining an irrotational force field in the undisturbed state. However, it is not as interesting as the previous case, because it can only be achieved in practice by having a fluid with conductivity varying in the z direction. Viewed purely from the angle of the Rayleigh-Taylor instability, which is essentially an instability of a surface or interface, it could be possible to stabilise an overwhelmingly unstable  $\underline{j} \times \underline{B}$  force in a conducting fluid by greatly reducing  $\underline{j}$  in the layer of conducting fluid adjacent to the surface, since the Rayleigh-Taylor instability is dependent only upon the forces in the fluid next to the surface, and not the sum of the forces in the whole fluid. However, to achieve this situation would require a variation in the conductivity of the fluid, and in practice this would give rise to an internal fluid instability akin to the instability of a density stratified fluid with an adverse density gradient. The study of waves and instabilities in conductivity stratified fluid with imposed  $\underline{j} \times \underline{B}$  forces is a whole area requiring further study, but is deviating from the present study and so will not be dealt with further.

5.3.4. Variation of magnetic field in the Z direction

The case where  $\frac{\partial B}{\partial z} \neq 0$  differs from the previous case in that  $\underline{B}$  is in no way linked with the fluid parameters, as  $\underline{j}$  is, and this configuration can easily be achieved in practice.

Lemaire's solution already mentioned in 5.3.1. included the possibility of  $\frac{\partial B}{\partial z} \neq 0$  but to discover the influence of  $\frac{\partial B}{\partial z}$  on modes in any direction, it is necessary to turn to the analysis of 5.3.1. Allowing for  $\frac{\partial B}{\partial z}$  being a non zero constant leads to a term in  $\frac{\partial B}{\partial z}$  on substituting for  $\delta p$  in (5.4), and (5.9) becomes:-

$$\begin{aligned} ik_x B \delta E_z \frac{\partial \sigma}{\partial z} + ik_x \sigma \delta E_z \frac{\partial B}{\partial z} + k^2 \rho n v_z - \frac{\partial}{\partial z} (\rho n \frac{\partial v_z}{\partial z}) \\ = \frac{g k^2}{n} v_z \frac{\partial \rho}{\partial z} - E_x B \frac{k^2 v_z}{n} \frac{\partial \sigma}{\partial z} - \frac{k^4}{n} \alpha v_{z_0} \delta [z-z_0] \end{aligned}$$

The boundary conditions are the same, but in the main bulk of the lower fluid

$$k^2 v_{z_2} - \frac{\partial^2 v_{z_2}}{\partial z^2} + \frac{1}{\rho_2 n} ik_x \delta E_z \sigma \frac{\partial B}{\partial z} = 0$$

Clearly  $\delta E_z = (\delta E_z)_0 e^{|k|z} \quad (z < 0)$   
 $= ik_x z_0 E_x e^{|k|z}$

$$\therefore v_{z_2} = \left( n z_0 - \frac{\sigma \frac{\partial B}{\partial z} k_x^2 z_0 E_x}{2 k \rho_2 n} z \right) e^{|k|z}$$

$$\therefore \left( \frac{\partial v_{z_2}}{\partial z} \right)_0 = k n z_0 - \frac{\sigma \frac{\partial B}{\partial z} k_x^2 z_0 E_x}{2 k \rho_2 n}$$

$$\therefore k_x^2 B E_x \sigma_2 + (\rho_1 + \rho_2) n^2 k - \frac{1}{2} \sigma_2 \frac{k_x^2}{k} E_x \frac{\partial B}{\partial z} = g k^2 (\rho_1 - \rho_2) + k^2 B E_x \sigma_2 - k^4 \alpha$$

$$\text{or } -n^2 = \frac{(\rho_2 - \rho_1) g k + \alpha k^3 - \frac{k_x^2}{k} B E_x \sigma_2 - \frac{k_x^2}{2 k^2} \sigma_2 E_x \frac{\partial B}{\partial z}}{(\rho_1 + \rho_2)}$$

in  $\theta$  notation:-

$$-n^2 = \frac{(\rho_2 - \rho_1) g k + \alpha k^3 - k (\cos^2 \theta) B E_x \sigma_2 - \frac{1}{2} (\sin^2 \theta) \sigma_2 E_x \frac{\partial B}{\partial z}}{\rho_1 + \rho_2}$$

This agrees with Lemaire's conclusions that  $\frac{\partial B}{\partial z}$  does not affect ( $k = k_y$  only) modes, but can produce instability in the ( $k = k_x$  only) modes, when  $E_x \frac{\partial B}{\partial z}$  is positive, and proves further that if instability does occur due to  $\frac{\partial B}{\partial z}$ , it will do so in the ( $k = k_x$  only) mode in preference to other ( $k = k_x, k_y$ ) modes. The condition for the instability to occur in the ( $k = k_x$  only) mode is that

$$\frac{1}{2} E_x \sigma \frac{\partial B}{\partial z} > (\rho_2 - \rho_1) g k + k^3 \alpha$$

It is worth noting that if  $\frac{\partial B}{\partial z}$  is negative, and  $E_x$  is negative (i.e.  $\underline{j} \times \underline{B}$  acts downwards) the instability should still occur and this invited experimental verification. According to this analysis, in an infinite fluid an extremely small positive  $E_x \frac{\partial B}{\partial z}$  is sufficient to produce an instability in the  $k \rightarrow 0$  mode (i.e. wavelength  $\rightarrow \infty$ ). In practice this will be limited, both by the maximum wavelength (i.e.  $k_{\min}$ ) possible in the containing vessel, and also by the depth of fluid, since the analysis makes the assumption of infinite depth, which for small amplitude sinusoidal modes means a depth greater than half a wavelength.

Thus there will be a minimum  $E_x \frac{\partial B}{\partial z} \left[ = (\rho_2 - \rho_1) g k_{\min} + \alpha k_{\min}^3 \right]$

below which instability will not occur.

It is also interesting to note that for  $E_x \frac{\partial B}{\partial z}$  above this minimum, the mode of maximum growth rate is not dependent upon  $E_x$  as it was dependent in 5.3.1. upon  $B E_x$  but will always be the  $k_{\min}$  mode.

### 5.3.5. Variations of $E_x$ with time

Whereas a time dependent magnetic field will in general induce eddy currents to flow in the conducting liquid, resulting most likely in rotational forces, variation of  $E_x$  with time (assuming that induced magnetic field is ignored) will not contravene the restriction laid down in 5.1.1. such that the phenomenon be truly classified as an M.H.D. Rayleigh-Taylor phenomenon.

With an eye to practical possibilities, it is of particular interest to investigate the effect on the stability of the interface, of an alternating current imposed in place of the direct current. Normally, in the class of M.H.D. problems where current and magnetic field are both imposed and induced field is ignored, the imposition of 50 cps A.C. is equivalent to no current at all, since the typical response time for fluid mechanical motion is much greater than the time for one cycle of A.C., and the constantly reversing  $\underline{j} \times \underline{B}$  forces are consequently not 'felt' by the fluid. However, it could be argued heuristically that in this case, for part of the cycle the  $\underline{j} \times \underline{B}$  force acts as a restoring force, tending to produce oscillatory motion, whilst for another part it acts as a destabilising force, tending to produce an exponentially increasing instability motion, and it is by no means obvious that these two different types of influence will balance each other out with time, e.g. it could be argued that the exponential increase of amplitude of an initial perturbation over say  $1/3$  cycle when the force is promoting instability, will not be recovered by the sinusoidal variation of the other  $2/3$  cycle when the force is restoring, and the effect over a period

of time will be in fact for instability to occur. Thus an analytical investigation was considered worthwhile.

Considering the simplest M.H.D. Rayleigh-Taylor instability situation, for instability modes in the  $k_y$  direction only,

eq.(5.10) becomes

$$-n^2 = \frac{gk(\rho_2 - \rho_1) + k^3 \alpha - \sigma k E_x B}{\rho_2 + \rho_1}$$

where the equation of motion of the interface is

$$\frac{\partial^2 z_0}{\partial t^2} = n^2 z_0$$

If  $E_x = E_0 \cos \omega t$ ,  $n^2 = \frac{B \sigma E_0 \cos \omega t}{\rho_1 + \rho_2} k - \frac{(\rho_2 - \rho_1)g + k^2 \alpha}{\rho_1 + \rho_2} k$

Thus there is a stabilising force when  $B \sigma E_0 \cos \omega t < (\rho_2 - \rho_1)g + k^2 \alpha$

In fact this is the motion described by Mathieu's equation,

and on substituting  $p = \frac{\omega t}{2}$ ,

$$a = \frac{4k}{\omega^2} \left\{ \frac{(\rho_2 - \rho_1)g + k^2 \alpha}{\rho_1 + \rho_2} \right\},$$

and  $q = \frac{2B E_0 \sigma k}{\omega^2 (\rho_1 + \rho_2)}$ ,

becomes

$$\frac{\partial^2 z_0}{\partial p^2} + (a - 2q \cos 2p) z_0 = 0$$

which is the

canonical form of the Mathieu equation. The stability properties of this equation are well known (McLachlin 1947) and for the values of  $a$  and  $q$  likely to be encountered in this work, the relevant portion of the stability plot of  $a$  against  $q$  is shown in fig.(5.9). Typical values for  $a$  and  $q$  for the practical cases already discussed are around  $40/\omega^2$  for the two fluid case, and  $2000/\omega^2$  for mercury experiments. Thus the practical possibility of  $\omega = 100$  rads/sec (mains frequency) will keep  $a$  and  $q$  well within the stable triangle between the origin and the first unstable region.

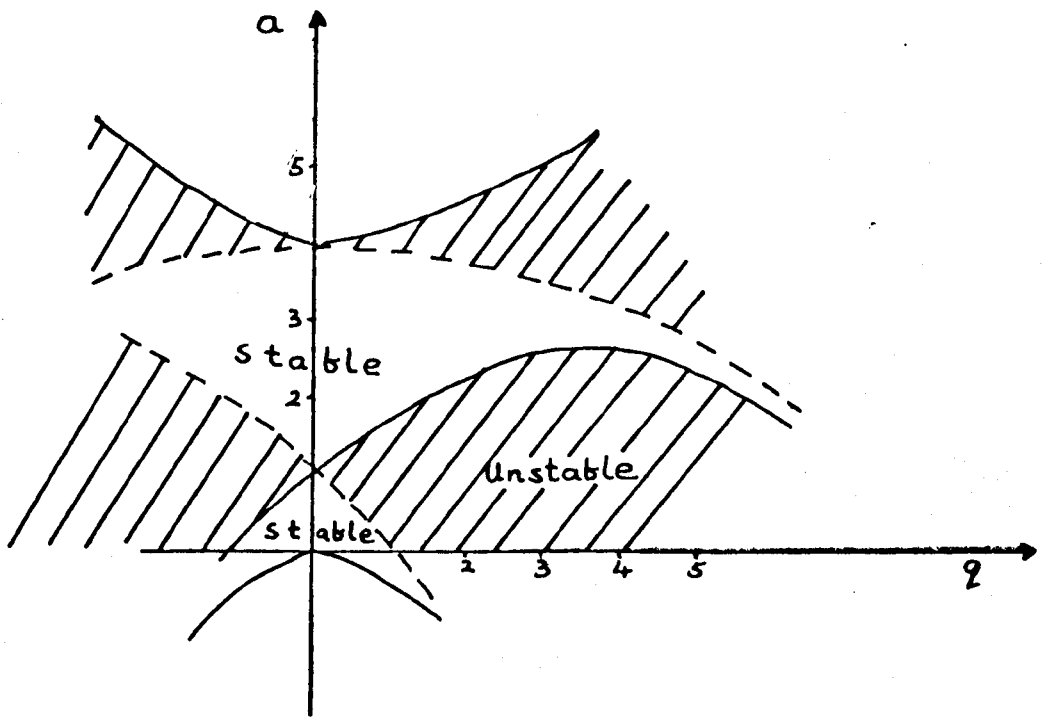


FIG.5.9. MATHIEU FUNCTION STABILITY DIAGRAM.

in the first quadrant. Thus the appeal to an analytical investigation of the effects of A.C. supports the assumption that even in this case, time variations of the electromagnetic parameters can be considered as integrated over a period equal to a typical response time of the fluid mechanical motion.

#### 5.4. The Effect of Varying the Orientations of $\underline{E}$ and $\underline{B}$

Just as, in the case of surface waves, the variation of the angle  $\beta$  between  $\underline{j}$  and  $\underline{B}$  caused the major and minor axes of anisotropy to rotate, so the orientation of the most unstable mode (which corresponds to the minor axis of anisotropy) will rotate as  $\beta$  is varied.

In the notation of fig. (2.11) and § 2.5.2., the most unstable mode is that for which  $j_s B_n$  is a minimum. Reference to eq. (2.36) shows that, for a given  $\beta$ ,  $j_s B_n$  will be a minimum when  $\sin(\beta - 2\theta) = -1$  i.e.  $\theta = \frac{\beta}{2} + \frac{\pi}{4}$

This result invites experimental verification, and will be pursued in 6.6.

If it is assumed that the dimensions of the containing tank limit  $k$  to be greater than  $k_{min}$ , then the condition for instability to occur in the most unstable mode is that :-

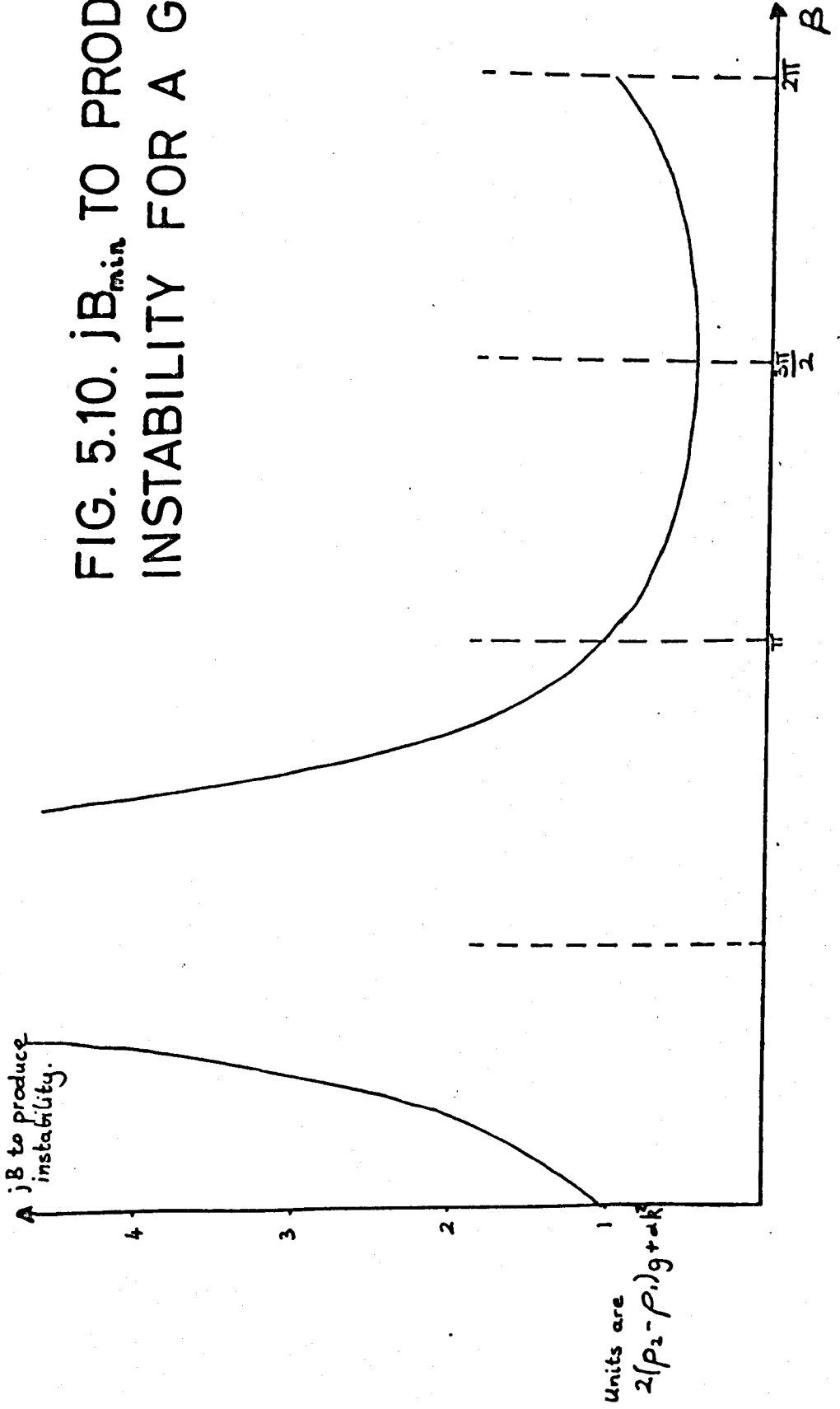
$$\frac{jB}{2} (1 - \sin \beta) > (\rho_2 - \rho_1)g + k_{min}^2 \alpha$$

Hence the minimum value of  $jB$  to cause instability is

$$\frac{2[(\rho_2 - \rho_1)g + k_{min}^2 \alpha]}{(1 - \sin \beta)}$$

which varies with  $\beta$  as shown in fig. (5.10). Where  $\beta = 0$  or  $\pi$ , there is agreement with Murty (1961).  $\beta = \frac{\pi}{2}$  is the standard instability configuration already considered in this chapter, and when  $\beta = \frac{3\pi}{2}$ , instability is impossible. However,

FIG. 5.10.  $jB_{\min}$  TO PRODUCE  
INSTABILITY FOR A GIVEN  $\beta$



$$\text{for } \beta = \frac{3\pi}{2} \pm \epsilon$$

(where  $\epsilon$  may be a small angle), instability is theoretically possible given a great enough value of  $|j B|$  .

6. EXPERIMENTAL WORK RELATING TO THE M.H.D. RAYLEIGH-TAYLOR  
INSTABILITY

6.1. Introduction

This chapter contains a description of experimental work on the stability of interfaces between two liquids, when one of them experiences a  $\underline{j} \times \underline{B}$  force acting in a direction towards the other, i.e. experiments relating to the M.H.D. Rayleigh-Taylor instability described theoretically in chapter 5. The basic configuration considered is that where a non conducting fluid rests in equilibrium above a conducting fluid of greater density. A mutually perpendicular and horizontal magnetic field and electric current are imposed on the conducting fluid such that the resultant  $\underline{j} \times \underline{B}$  force acts vertically upwards towards the non conducting fluid.

As was mentioned in chapter 1, the theory and practical work in this study went hand in hand. Initially, the aim was to discover, in as simple an apparatus as possible, what happened when various modifications were made to the basic M.H.D. Rayleigh-Taylor configuration, i.e.  $\underline{j}$  varying in the  $\underline{j}$  direction,  $\underline{B}$  varying in the vertical direction as explained in chapter 5. Thus a lot of the experimental work was purely exploratory, with no intention of making any accurate measurements but simply to observe visually. These experiments gave a greater grasp of the subject and enabled the theoretical work to be developed, and better understood. 6.4 and 6.5 describe these cases. However, in setting up the initial experiments, the problem of surface tension was discovered, affecting the stable equilibrium surface shape (described theoretically in 5.2.5), and this is investigated experimentally in 6.3. Also, as the experiments of 6.4 progressed, an interesting large amplitude instability motion was observed, and so an experiment was set up

to observe and record this phenomenon under the most suitable conditions. This is described and commented on in 6.4.2. Finally an experiment was undertaken to show the effect of the relative orientation and magnitude of  $\underline{j}$  and  $\underline{B}$  on the plane in which the instability occurred. Only this last experiment was designed to furnish quantitative results which could be used to verify theoretical analysis. All the other experiments were intended to be descriptive, since in general the theoretical work related to them was not able to support a complete analysis capable of furnishing quantitative predictions which could then be experimentally verified.

Usually, experimental work involving instabilities is concerned very much with measuring growth rates, and although this was considered, and some attempts were made to measure growth rates, a sufficiently accurate yet simple method could not be developed. As Duc, Lemaire, and to a lesser extent Baker have already made accurate observations of the Rayleigh Taylor instability growth rates, it was not considered worthwhile to develop the more sophisticated apparatus necessary to measure growth rates accurately, since the main aim of the practical work was to observe the general characteristics of the Rayleigh-Taylor instability, for which growth rates have not been predicted theoretically.

## 6.2 General Experimental Considerations

### 6.2.1 Choice of working fluid

The factors affecting the choice of working fluid are similar to those already discussed in the chapter describing the practical production of anisotropic surface waves. Initially, mercury was used, but eventually rejected, since

very high current densities were required (of the order  $5 \times 10^5$  A/sq.m +) so that 1000 A was required even in a small tank with cross sectional area of mercury of 15 sq.cms, if destabilising forces of the same order as the gravity forces involved were to be obtained. Moreover, with such high forces, and no liquid covering the mercury, a sealed perspex lid to the tank was essential, precluding all but visual means of observation, and subsequent choices of liquid were found to be much easier and safer to work with.

As in the wave experiments copper sulphate solution was used as the conductor, and to enable destabilising  $\underline{j} \times \underline{B}$  forces to compete with the stabilising gravity forces, this was covered by a non conducting fluid matched to within 1% or 2% of its specific gravity. For this a mixture of carbon tetrachloride or trichloroethane with either olive oil or white spirit was found most suitable. Initially carbon tetrachloride was acceptable as the heavy solvent, while using small quantities in a small tank, but when the larger quantities were used for a large tank, trichloroethane was used for its less toxic properties. Olive oil was used where increased viscosity was of positive help in slowing down instability motions, and otherwise white spirit was used and viscous effects ignored.

#### 6.2.2 Magnetic field

Three magnets were used in different experiments. Most of the initial work was done in the Lintott electromagnet with 3" gap referred to in 4.2., and described in Hunt (1967). This was used at fields up to  $0.6 \text{ Wb/m}^2$ .

Another conventional electromagnet was used for the experiments described in 6.4.2 where a wider gap was required. This was another Lintott electromagnet, with a gap of 6" and pole faces of area 12" x 6", over which the field was uniform to within 5%. Using the available motor generator producing 60V, the magnet drew about 375A and would produce a field of  $0.7 \text{ Wb/m}^2$ . A more detailed description of this magnet is to be found in Fussey (1969).

The third magnet used for the larger experiments was the Helmholtz coil pair described in chapter 4, producing a field up to  $0.2 \text{ Wb/m}^2$  over a volume at least 50 cms cubed, to within 5% uniformity.

### 6.2.3. Containing vessels and scale of experiments

All the vessels used were made of perspex, glued and in certain cases screwed. Electrodes were copper gauze, supported at opposite faces of the tanks. For experiments in the two narrower magnets the tank was 3" wide outside, about  $2\frac{3}{4}$ " by 10" long inside. To provide as large an electrode area as possible, and to help eliminate spurious instability and motion near the electrodes the bottom of the tank was sloped to form a deeper trough where the electrodes fitted, in the same way as the wave tank was designed, and described in 4.3.5.

A much larger tank, 40 cms x 40 cms x 20 cms, was used in the Helmholtz coil magnet, and is the same as the one used for certain of the wave experiments. Since it was designed to rotate inside the magnetic field, the floor could not be sloped near the electrodes, but had to be flat so that  $(\underline{B} \cdot \underline{\text{grad}})_{\underline{j}} = 0$  even when  $\underline{B} \cdot \underline{j} \neq 0$ . Further description will be found in 6.6. This tank was fitted with a lid floating in the upper liquid, since its use was for photographing the instability, whereas the smaller tanks were used without lids to enable depth probes to be inserted.

#### 6.2.4. Current supply

The principal advantage of using the narrow magnets with a 15 sq.cm cross sectional area of conducting liquid, was that a small Farnell D.C. stabilised current/voltage source could be used. It was capable of producing 2 amps at 30V, and could be used in either the constant current or constant voltage mode. This was found adequate for most experiments where 30 volts between electrodes was sufficient to produce the required current density of order 100m A/sq.cm at the point where the instability was occurring. Where a higher voltage was required to maintain 100m A/sq.cm, a second power supply was used in series.

These then provided the scope for fine control and stabilisation of current necessary in producing the quasi-stable motions described in 6.4, and in attempts to measure growth rates enabled a pre-set current to be instantaneously switched on which was impossible to do with the 1000 amps used for the original mercury experiments.

#### 6.2.5. Depth Probes

In an effort to measure some of the instability effects originally observed visually, various attempts were made to design probes for measuring the surface or interface height under different conditions.

Most measurements of Rayleigh-Taylor instability to be found in the literature have been made by optical photographic means e.g. Lewis (1950) measuring growth rates from a sequence of high speed photographs. However, the M.H.D. case does not lend itself to being photographed easily, since the containing vessel is usually located between magnetic poles, and though mirrors could be used to overcome this as described in 6.6., the most interesting plane to view is that in which the instability

occurs. This would require viewing in the current direction, an impossibility because of the electrodes obstructing the line of view. For this reason it was decided to investigate possible methods of direct measurement of surface height. Some of these were more successful than others, and those to measure growth rate were not fully developed since the experimental programme did not require it. However, the various attempts are all described since it is felt that they can contribute in general to research in this field.

The probes were all used in the narrow magnet and supported in the traversing mechanism to be seen in the general view of fig.(6.1). This enabled traversing in two longitudinal directions along brass guide rods, while the probes were held vertically in a vertically mounted micrometer screw traversing gear, enabling variation of probe height accurate to less than a thousandth of an inch. Four different types of probe were used :-

(a) Touch probe

This was the simplest, and most obvious type. Since the copper sulphate solution is electrically conducting, a wire just dipping into the surface can be made to complete a circuit via the tank electrodes, and so if the wire be lowered until the circuit is just made, the surface height can be registered. This is useful only for static surfaces, and its usefulness is further reduced because with a simple D.C. circuit, there is a tendency to disturb the current flow already in the fluid, and hence to affect the phenomenon being observed. It was also found to be surprisingly difficult to obtain repeatability of results with this type of probe, probably because of the meniscus effect, and surface tension preventing electrical contact of the probe tip until it was protruding a few thou into the fluid.

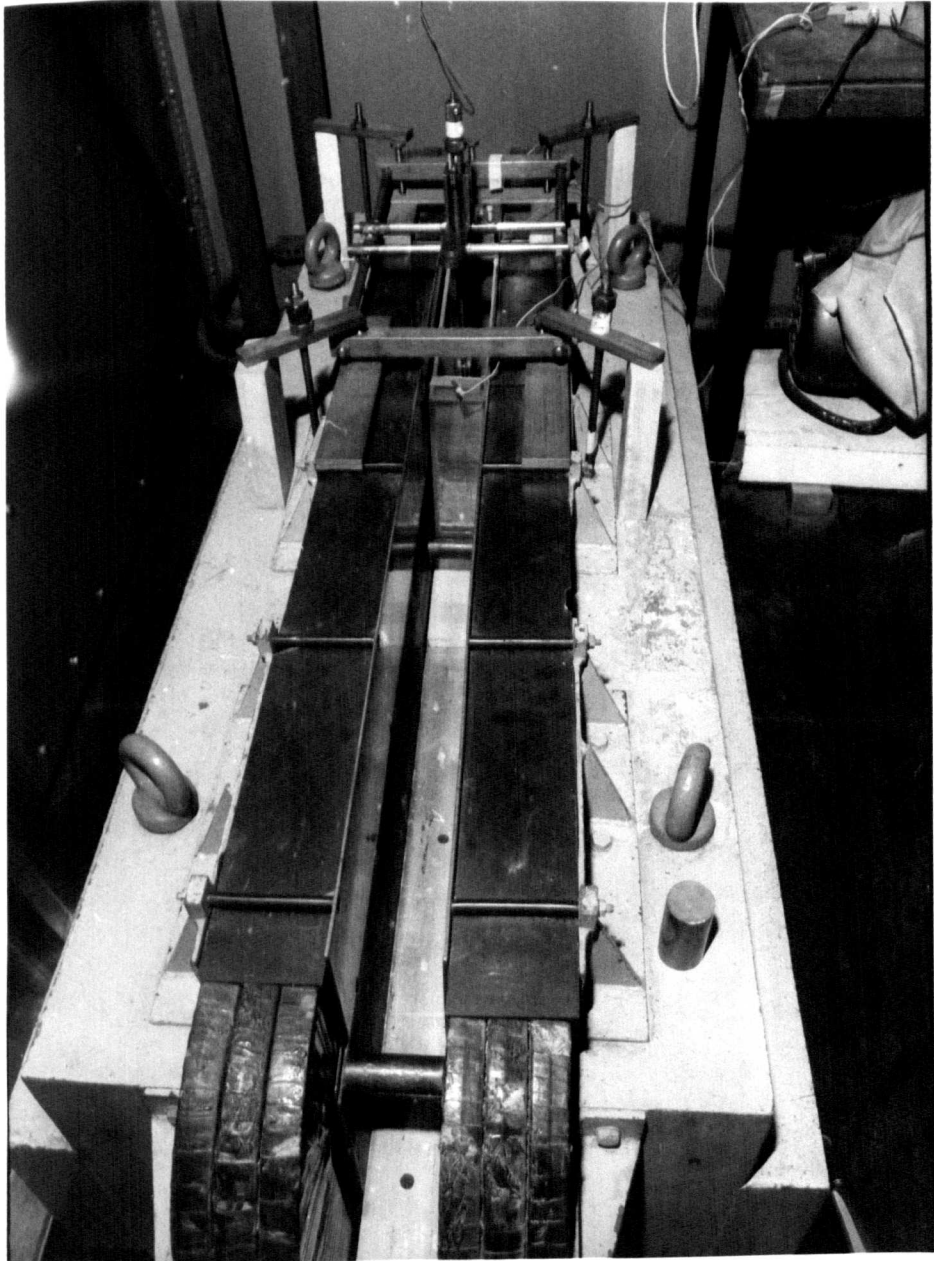


FIG. 6.1. GENERAL VIEW OF INSTABILITY  
MEASURING RIG.

(b) Capacitive probe

Following the work of Baker, a capacitive probe was tried in conjunction with a Wayne Kerr meter. Standard probes as used in mechanical vibration work were utilised and found to be repeatably accurate and sensitive. The most suitable one for our purpose was that designed to measure 0.1 inch full scale deflection on the Wayne Kerr meter. However, in use in the white spirit/carbon tetrachloride mixture, with the copper sulphate interface as the reference surface, the sensitivity was found to be half the stated value, and full scale deflection in the meter was 0.2" presumably because of the difference in dielectric properties between the organic liquid and air. Also the D.C. output from the Wayne Kerr meter was monitored on a U.V. recorder well beyond full scale deflection on the instrument dial, and a calibration of D.C. voltage output against height above the surface was plotted. fig. (6.2). This can be seen to be almost linear over the first 0.2 inches, but is still usable up to 0.8 inches if results are checked against the calibration curve. The one serious drawback which prevented the use of this probe, despite the considerable advantage of its never being in contact with the conducting surface, was that the diameter of the probe face was 0.75 inches. Since the surface movements being measured were of rippled surfaces with wavelengths of the order of 0.75 inches, the average height recorded by the capacitive probe was of little use, and no repeatable records of the growth rate of instabilities could be obtained, since the nature of the instability is not for the surface to rise en masse, but for ripples to increase in amplitude exponentially with time, part of the surface rising while part falling. Similarly the measurements of static surface height were not reliable when the surface was not flat.

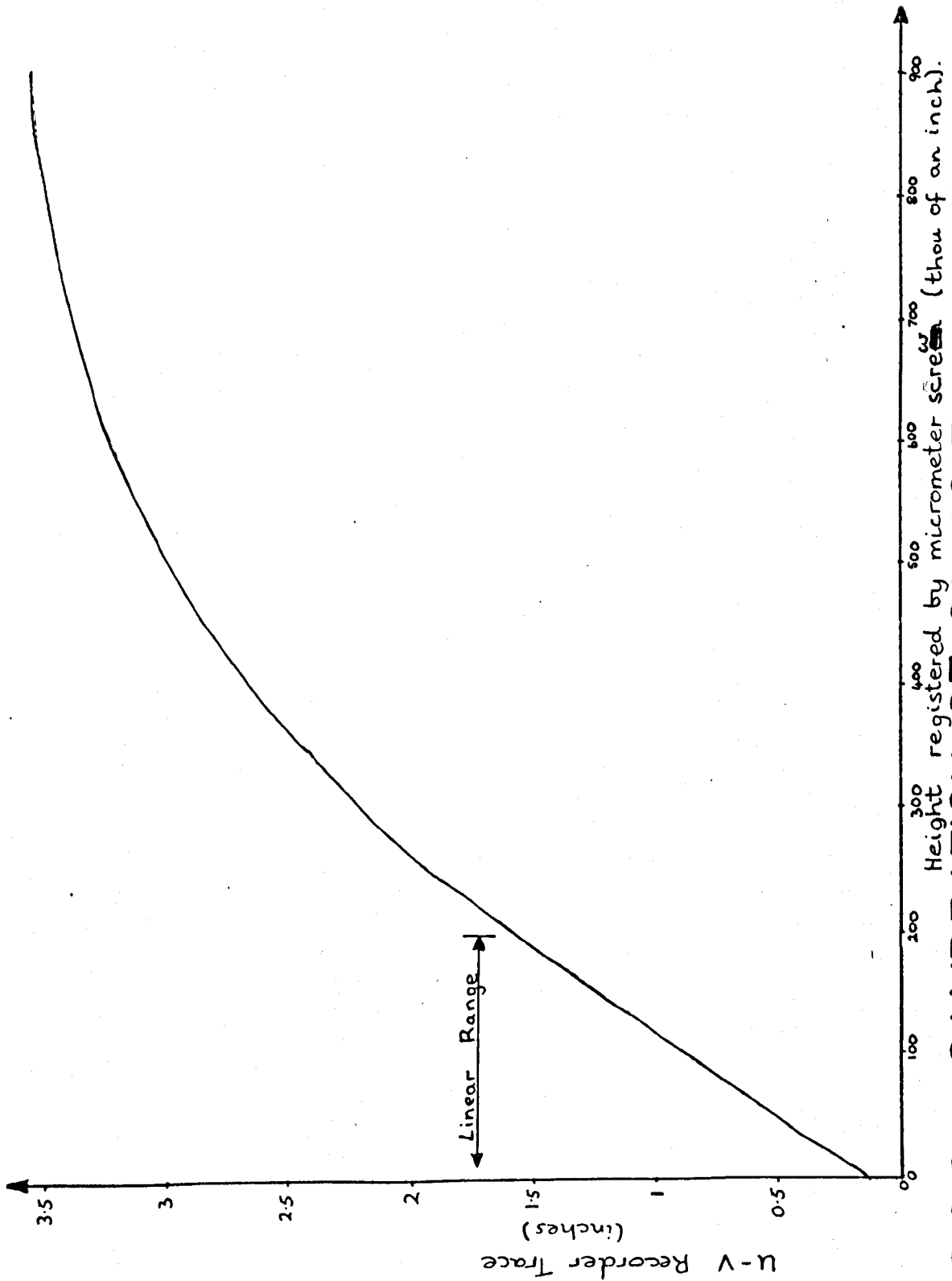


FIG.6.2. CALIBRATION OF CAPACITIVE PROBE.

(c) A - C resistive probe

This probe consisted essentially of two lengths of wire protruding vertically into the conducting fluid, the depth to which they were immersed being related to the electrical resistance of the current path through the fluid between the two wires. After some trial and error, the probe shown in fig. (6.3) was used. The wires of 0.56 mm gauge were made of palladium to reduce corrosion and by-products of electrolysis in the copper sulphate, held 2.5mm apart in holes drilled in a small cylinder of perspex, with 19mm protruding. The leads to each wire were carried inside a stainless steel tube and after soldering to the pieces of wire, the joints were insulated and the tube bonded to the perspex block with araldite. The electrical circuit is shown in fig. (6.4). Alternating current was used, to reduce contact resistance and electrolysis effects, and also so that the probe could be isolated by capacitors from disturbing the D.C. current flow imposed in the working fluid. A low output impedance frequency generator was used to provide a 4 volts 600 c/s signal, and the current passing through the probe was measured from the voltage across a low resistance in series with the probe. The output impedance and measuring resistor were low compared with the impedance of the probe, so that the voltage across the probe was almost constant, and the current measured would be inversely proportional to the resistance through the probe, itself approximately inversely proportional to the depth of the wire immersed. Since the device would not be truly linear, and would need a calibration curve anyway, it was not thought worthwhile to use more sophisticated electronics to provide a constant voltage signal. The voltage across the reference resistor was measured by a Hewlett Packard R.M.S. voltmeter, and the D.C. output from this monitored by the U.V; recorder.

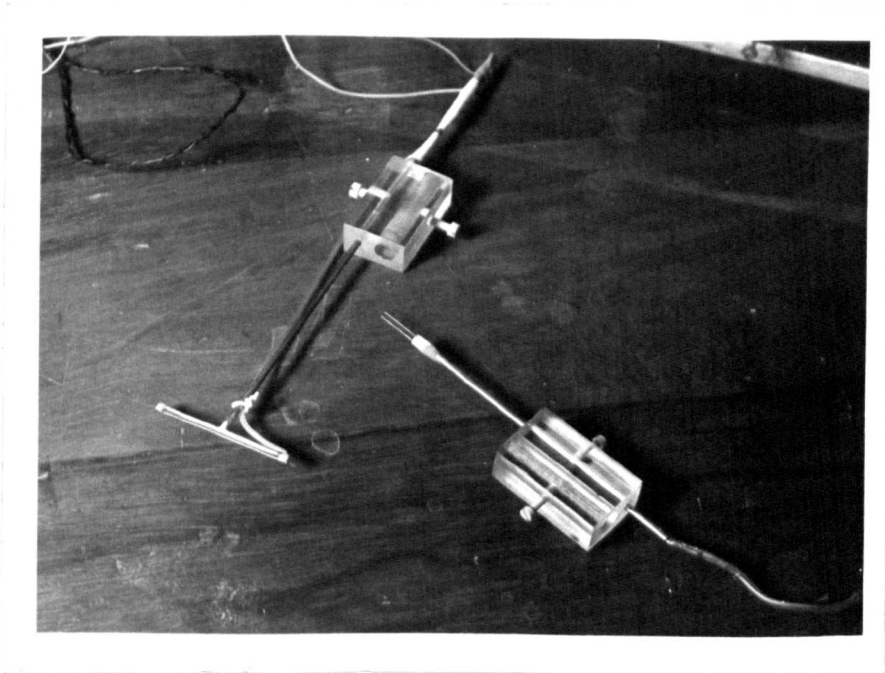


FIG. 6.3. DEPTH PROBES.

T-probe

resistive probe

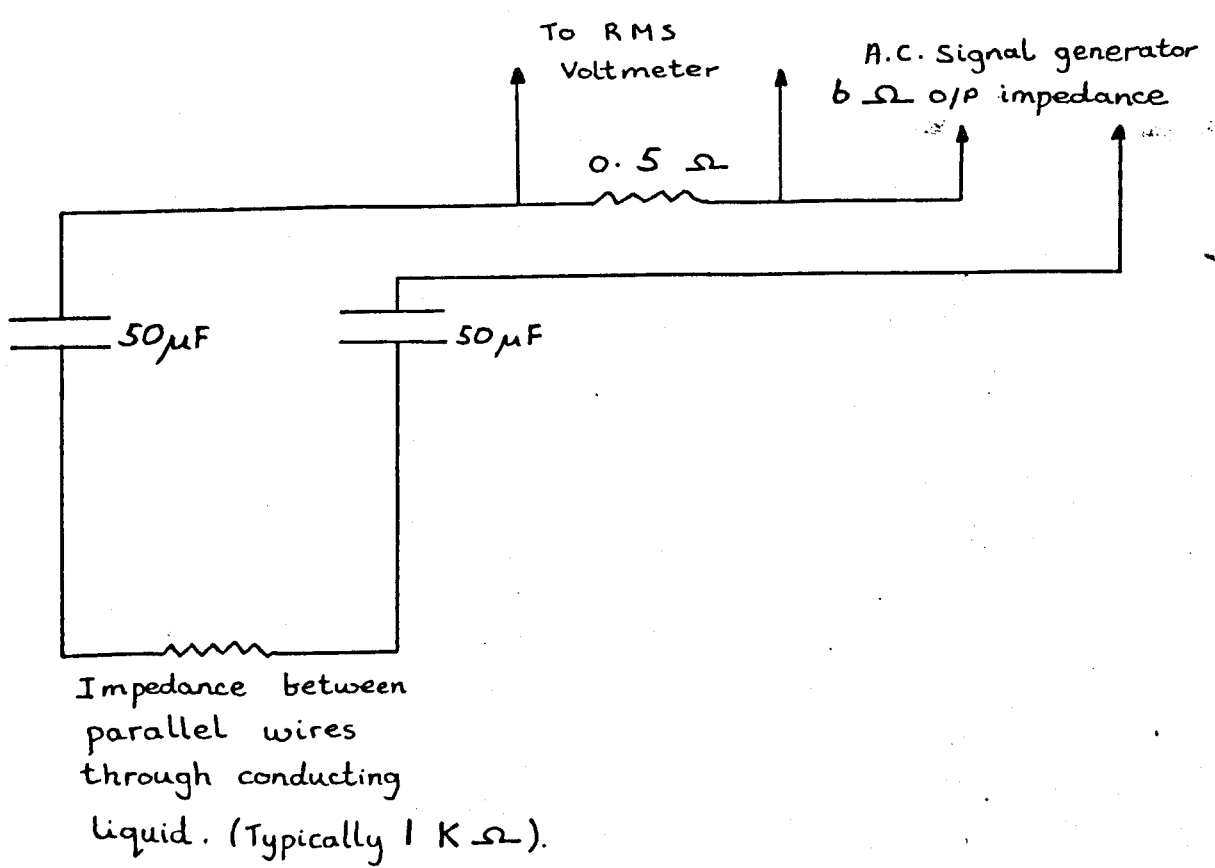


FIG. 6.4. CIRCUIT FOR RESISTANCE PROBE.

A typical calibration curve is shown in fig. (6.5), traversing both upwards and downwards. It will be seen that there is good consistency of results obtained, and a fairly linear dependence over the measured range, which was taken with the probe dipping into the surface 100 thou at its minimum. However, due to the small meniscus effect, a different, but repeatable curve was obtained when traversing in different directions, requiring that when actual measurements were made in a test run, the direction of travel of the probe relative to the surface had to be noted.

This probe was found to be suitable for measuring the height of a disturbed but stationary surface, as in 6.3 and 6.4 since it recorded height virtually at a point, provided the two wires were lined up in the  $j$  direction i.e. the direction of troughs and crests in which the height varies very little between the two wires.

However, it was not found to be possible to obtain repeatable curves of voltage against time on the U.V. recorder when instability growth rates were being measured. This was attributed to three possible causes

- a) The response time of the A.C. rms voltmeter was too slow.
- b) The meniscus and contact resistance effects, whilst consistent and therefore of no disadvantage in the static case, caused the measured height to lag behind the actual height in a less consistent manner.
- c) The instability mode was slightly different for different runs so that for one run there might be a crest at the probe and for the next run a trough or somewhere between trough and crest, making any consistency between results impossible. With better electronics

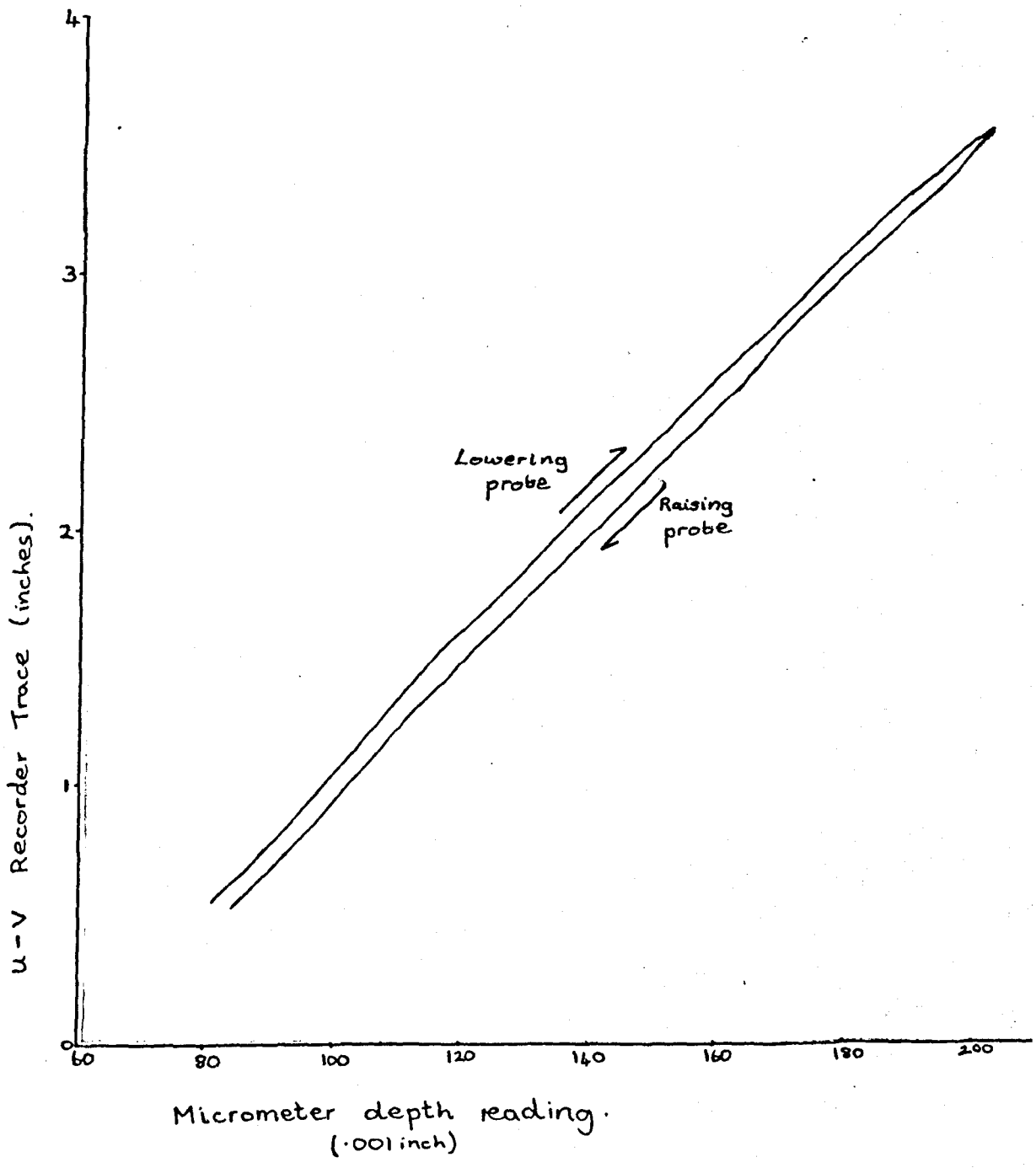


FIG. 6.5. TYPICAL CALIBRATION CURVE FOR RESISTANCE PROBE.

a) could have been eliminated and with careful cleaning, and consistent experimental technique (b) should be contained within tolerable limits but (c) springs from the nature of the instability itself, and it was this problem which prevented further use of this probe for measuring growth rates.

(d) Parallel wire T probe

For measuring growth rates of instabilities directly, the averaging of a wide area capacitance probe, and the single point measurements of the resistive probe are both unsuccessful. What is required is to measure the growth rate of amplitude at the peaks, or at the troughs of the instability. Whilst the approximate mode of the instability can be predicted, it cannot be known before it occurs exactly where the troughs and crests will lie. From these factors, the probe shown in the top of fig. (6.3) was designed.

At the cost of not being able to trace a continuous record of surface height at a point, it is able to measure the velocity of the surface at the crests, at a given height above the undisturbed surface.

It consists of a T-shaped stainless steel tube of 3mm diameter down rod and 2mm cross bar which lies with the bar across the trough in the B direction (normal to the direction of troughs and crests). Supported below the bar, and insulated from it, by Isopon resin glue, is a length of 0.38 mm gauge Palladium wire, parallel to the bar, and a fixed distance of about 1 mm from it.

The electrical connections of the wire and bar are shown in fig. (6.6.). The mode of operation is simply to switch on the tank current, which is monitored by the U.V. recorder, and as the instability grows the first peak touches the wire and varies its

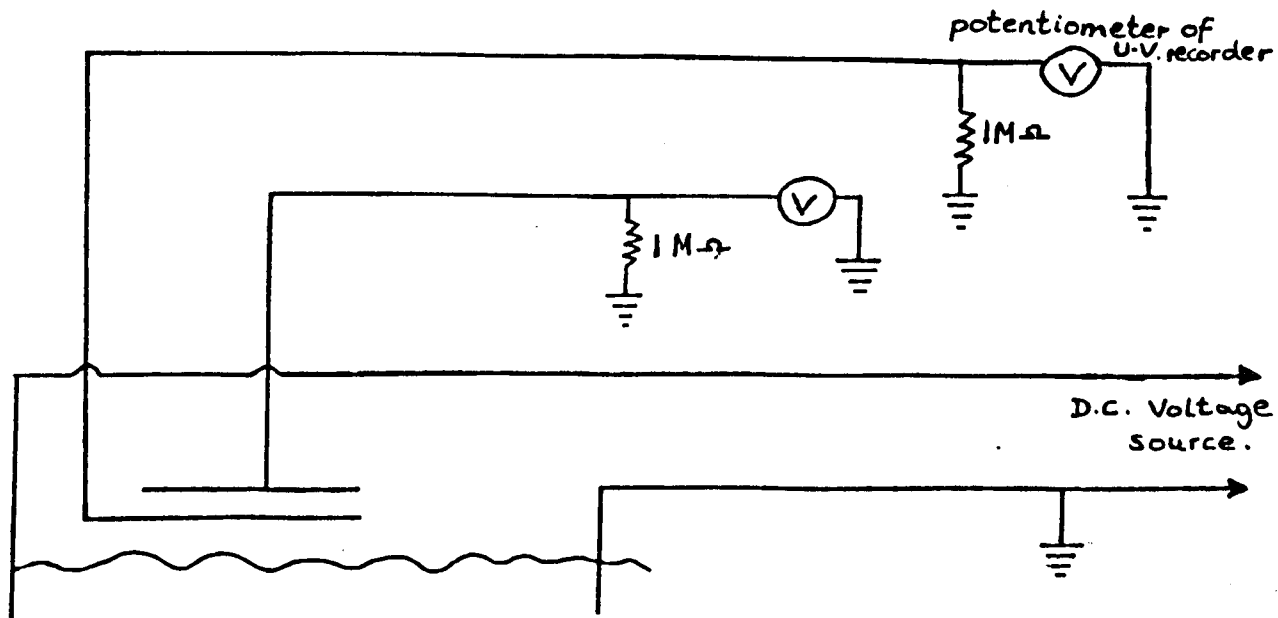


FIG. 6.6. CIRCUIT FOR T-PROBE.

potential which is recorded on the U.V. recorder, and then a short time later raises the potential of the bar. There is negligible current flow through the probe due to the high impedance of the recorder so that the instability is unaffected electrically by striking the probe. The  $1M\Omega$  resistor is used to restore the probes to ground potential after the surface has subsided to its rest position.

If the probe is held at a fixed height  $l$  above the surface, and the wire is a distance  $a$  below the bar, and if the time for the instability to travel from rest to the wire is measured from the U.V. recorder trace as  $t_1$ , and between the wire and bar as  $t_2$ , then if the instability is assumed to be governed by the equation

$$z_0 = C e^{nt} \quad \text{then} \quad l = C e^{nt_1}$$

and provided  $a$  is small c/f  $l$ , then since  $\frac{dz_0}{dt} = n C e^{nt}$ ,

$$\frac{a}{t_2} \approx n C e^{nt_1} \quad \text{and} \quad n = \frac{a}{l t_2}.$$

or if that approximation is not valid, since  $l + a = C e^{n(t_1+t_2)}$ ,

$$\frac{l+a}{l} = e^{n t_2} \quad \text{and} \quad n = \frac{1}{t_2} \log_e \left( \frac{l+a}{l} \right)$$

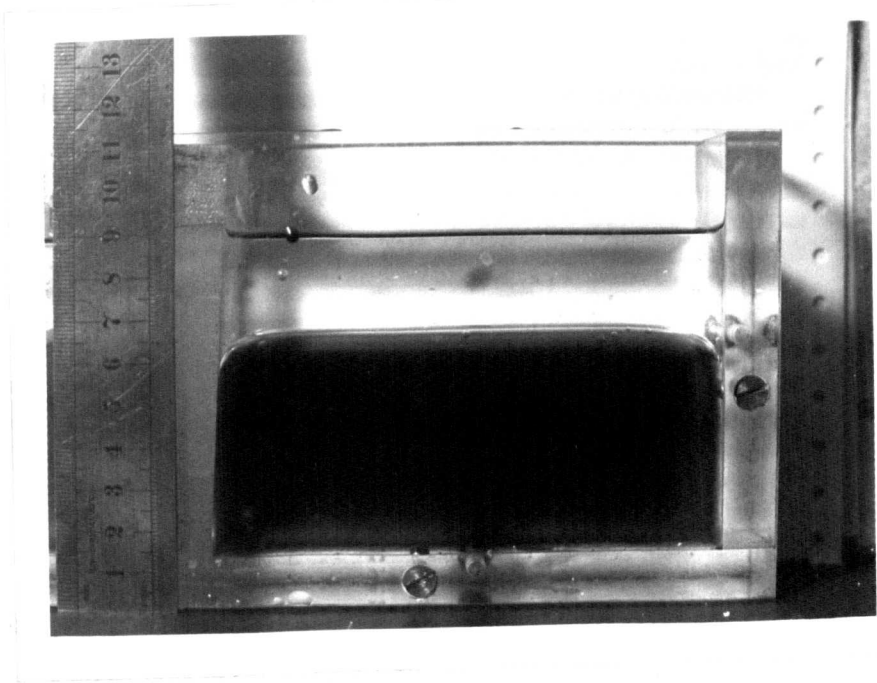
Although for the reasons stated in 6.1 no serious experiments to measure growth rates were made, this probe provided fairly consistent results in test runs of the basic M.H.D. Rayleigh Taylor instability, and is thought to be consistently better for measuring growth rates than any of the other depth probe methods. Possible inaccuracies lie in the need for the wires to be parallel to the bar, and the bar parallel to the surface and also in measuring the distance  $l$ . The technique used was to lower the probe until electrical contact was made between the wire and the copper sulphate, and then to raise it the fixed distance  $l$  on the micrometer screw. Another possible source of error could be in the

motion of the instability being hindered by the presence of the probe in the upper fluid. The size of the bar was necessary for rigidity but if accurate measurements of growth rates of the M.H.D Rayleigh-Taylor instability are required in the future, it is suggested that a development of this probe be built with supports at either side, and any number of separate wires held in tension between them each with its own electrical circuit and U.V. track, enabling the progress of the instability peak to be monitored with accuracy, the wires being thin enough not to impede the motion.

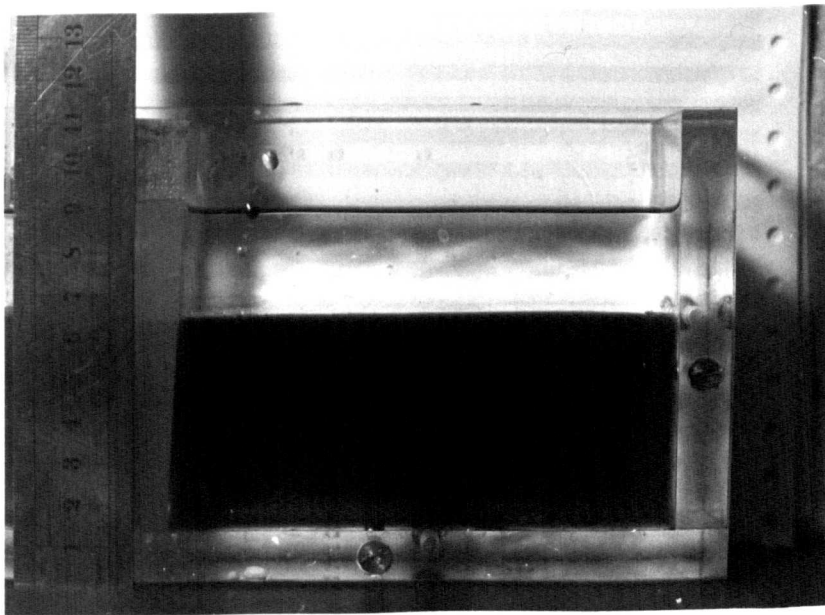
### 6.3 The Effect of Teepol on the Surface Tension

Since it plays such an important part in all the work of this thesis, it was thought worthwhile to demonstrate the effect which matching the fluid densities so closely has on the meniscus, and then to show the effect of introducing a detergent such as Teepol into the copper sulphate solution. The most graphic way to demonstrate these effects is by photographs, Fig. (6.7) shows a layer of trichloroethane/white spirit S.G. 1.056 on top of a layer, 3.5 cms deep, of copper sulphate solution, S.G. 1.070, in a perspex container. Without Teepol added, in (a) the meniscus reaches to the bottom of the tank, with sufficient added in (b) the meniscus is virtually eliminated by comparison, and is probably similar to that normally experienced at a water/air interface.

In some cases, though this may be due to the presence of impurities, and only occurred at glass walls, it was found to be possible to cause the meniscus to be upwards above the interface level by adding Teepol, whereas it is normally below, as in the photographs.



a) Before adding Teepol.



b) After adding Teepol.

FIG. 6.7. EFFECT OF TEEPOL ON MENISCUS

6.4. Experiments to Investigate the Rayleigh-Taylor Instability  
When  $\frac{\partial j}{\partial x} \neq 0$

6.4.1. Small amplitude

The particular aim of this experiment was to create a situation where  $\underline{j}$  was imposed in a fluid, perpendicular to  $\underline{B}$ , exerting a vertical  $\underline{j} \times \underline{B}$  force which in some parts of the fluid was less than the stabilising gravity forces, and in other places was greater, giving a tendency towards instability. A tank similar to that sketched in fig. (5.7) was constructed in perspex, the central barrier being made of P.V.C. sheet, and filled with copper sulphate so that the depth above the top of the barrier was less than half the total depth. A liquid tight seal of thin plastic tube was run down the sides of the barrier to prevent current passing through and consequently generating rotational  $\underline{j} \times \underline{B}$  forces. Surface tension effects were cut to a minimum by treating the electrolyte with Teepol.

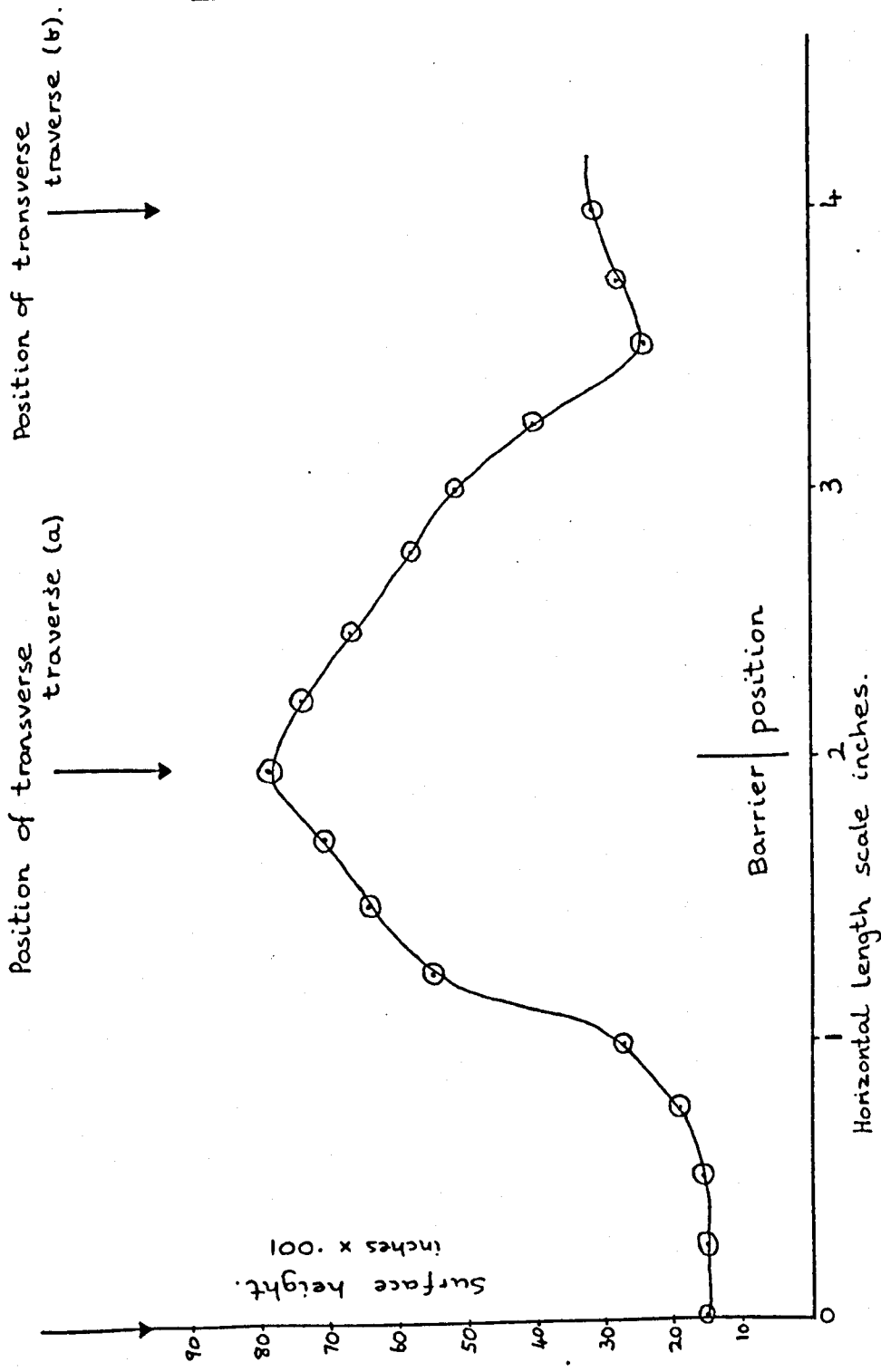
With a magnetic field of around  $0.4 - 0.5 \text{ Wb/m}^2$  applied in the 3" gap magnet, the current was slowly turned up. On the  $\underline{j} \times \underline{B}$  force reaching the level at which instability might be expected to occur above the obstacle, the surface was seen to be disturbed, but only when it had reached about 10% greater value did the fluid truly go unstable, with the large amplitude instability form described in 6.4.2.

If care was taken in slowly increasing the imposed current, it was found that just before the interface went unstable, motion was to be observed in the copper sulphate - revealed by the motion of small particles of impurities, and on careful observation of reflections of the interface, it could be seen to be disturbed in a way similar to that suggested in the theoretical investigation i.e. fig. (5.8). The fact that no such motion or disturbance

could be observed until the current was increased above the theoretical stability limit, suggests that the theoretical prediction is borne out, viz that a quasi-stable regime, where a disturbed fluid surface is maintained by a regular fluid motion pattern, exists between the states of true stability at rest and the Rayleigh-Taylor instability.

To show up the extent of surface disturbance involved, the A.C. depth probe was used to plot the contours of the surface, and this was found to be possible to achieve since once the motion was established it seemed to follow a fairly stable pattern, maintaining the interface disturbance steady over a period of some minutes. The results of this contour plot are to be found in fig. (6.8). In this width of tank there was only one peak, but in the larger tank in the Helmholtz coils, it was found possible to create 4 or 5 such quasi-stable motions side by side, as shown by the shadowy patches in fig. (6.9), although it was not possible to maintain them there for more than a few seconds due to spurious motions starting from the tank walls. The effect seemed to be easiest to achieve when using a more viscous upper fluid such as olive oil, and fig. (6.10c) taken as part of the experiment described in the next section shows typical side view of the disturbed but stationary interface.

Clearly the actual shape of the barrier, and pattern of electric current flow, will determine the exact pattern of secondary fluid flow and surface disturbance shape, but whether using a short or longer obstacle, the general motion seemed to be the same. It would be interesting to try to obtain some idea of the sort of fluid flow pattern involved, using hot film probes.



Experimental parameters.

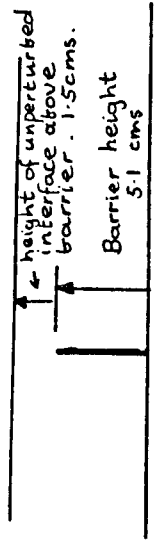
$B = 0.65 \text{ wb/m}^2$

$\rho_{\text{upper}} = 1.080$

$\rho_{\text{lower}} = 1.110$

total current per

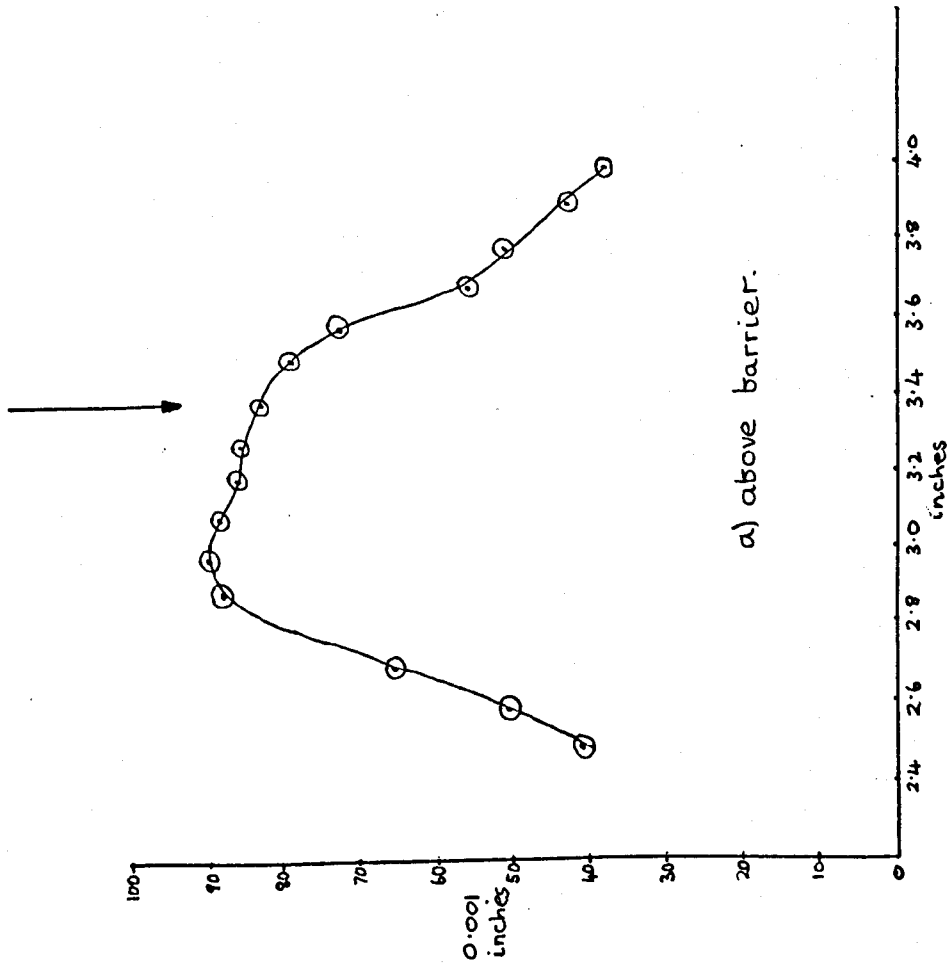
unit width =  $0.089 \text{ A/cm}$



(i) Longitudinal Traverse.

FIG. 6.8. SURFACE PROFILE PLOTTED USING RESISTIVE PROBE.

Longitudinal traverse



position of Longitudinal traverse

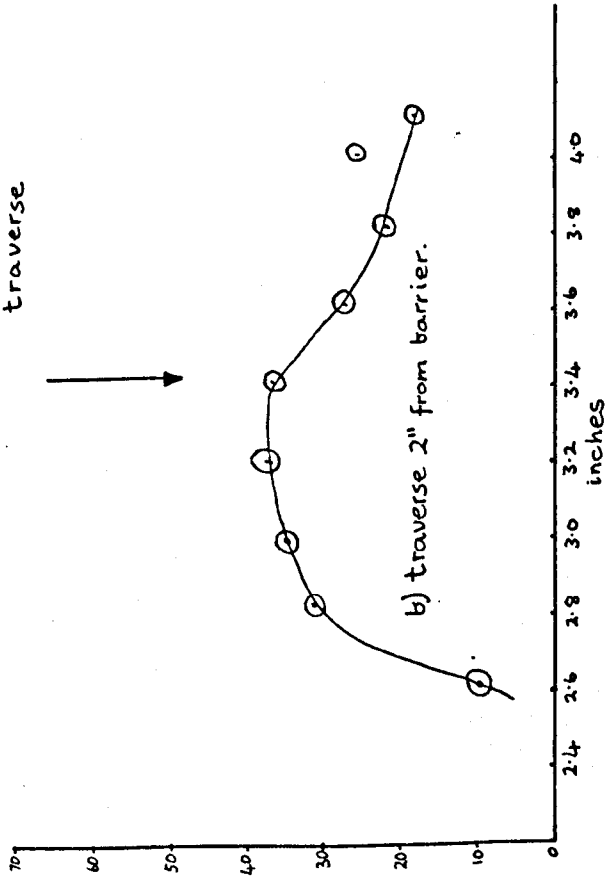


FIG. 6.8 . (ii) TRANSVERSE TRAVERSES.

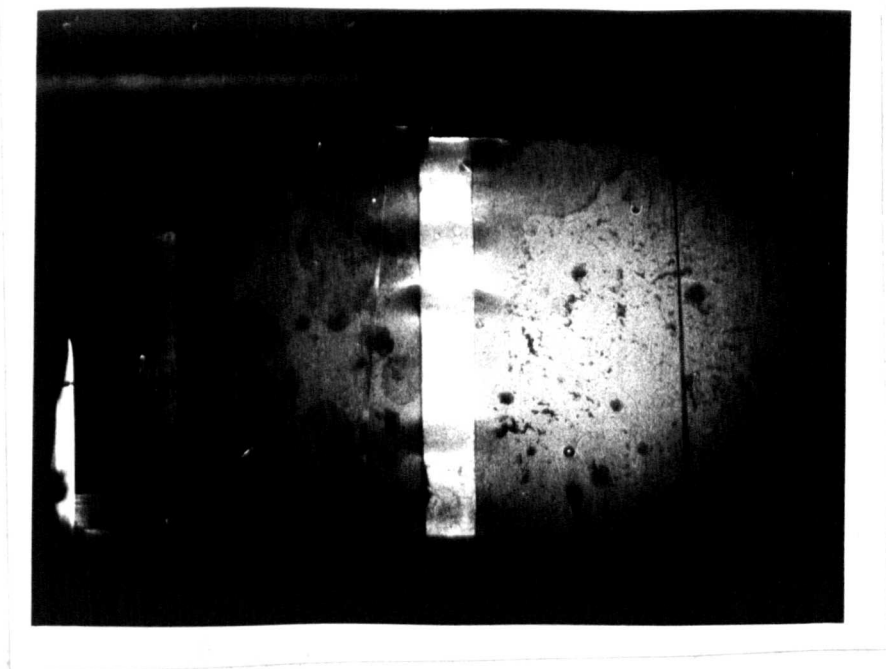


FIG. 6.9.  $\frac{\delta j}{\delta x} \neq 0$  INSTABILITY IN LARGE TANK.

All that could be deduced from observation of dust particle motion was that it was similar to that suggested in the theoretical section and shown in fig. (5.8).

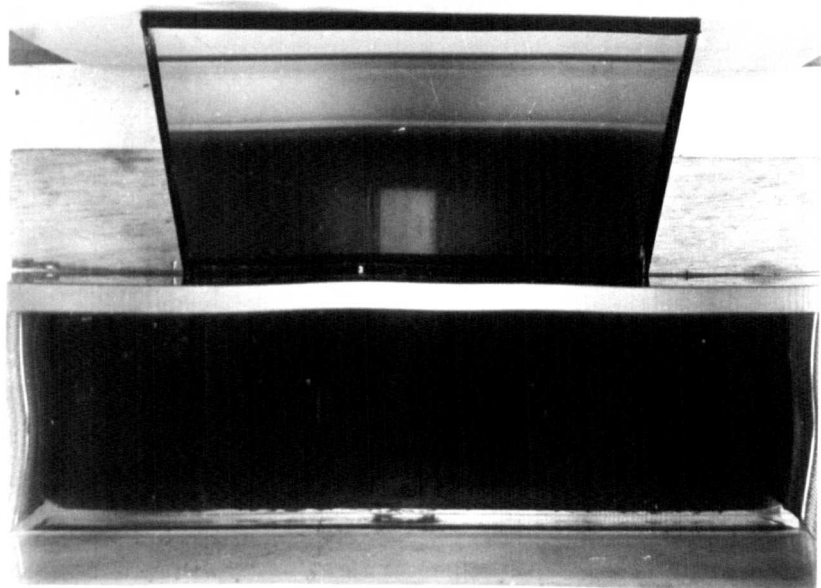
#### 6.4.2. Large amplitude motion

Not only was the quasi-stable regime of interest, but when the interface finally went truly unstable, the motion was of great interest at large amplitude.

This again appeared to be a characteristic motion, whether the obstacle to current was long or short, and whether the tank was narrow, and only able to take one peak, or wide enough to take a number side by side. The phenomenon was slowest, and most easily observed, when using a viscous upper liquid - a mixture of olive oil and carbon tetrachloride, and when no steps were taken to reduce surface tension.

A special experiment was mounted to take sequence photographs of the phenomenon.

A perspex tank 3" wide was placed in the gap of the 6" magnet, with a mirror at one side at  $45^\circ$  to the vertical, so that viewing from above revealed a plan and side elevation of the fluid in the tank. The motion was recorded using a Shackman auto camera, set to take a photograph once a second. Important stages in the sequence are shown in fig. (6.10). First the current is switched on with the generator in the constant current mode, set at a value sufficiently high to cause instability. Apparently what happens next is that initially the surface changes shape under the influence of surface tension, as described in 5.2.5., causing the meniscus to increase in size, and to reach down towards the floor of the tank where it is stepped up. At the onset of the instability proper this continues so that the position where the interface touches



a)  $t = 0$

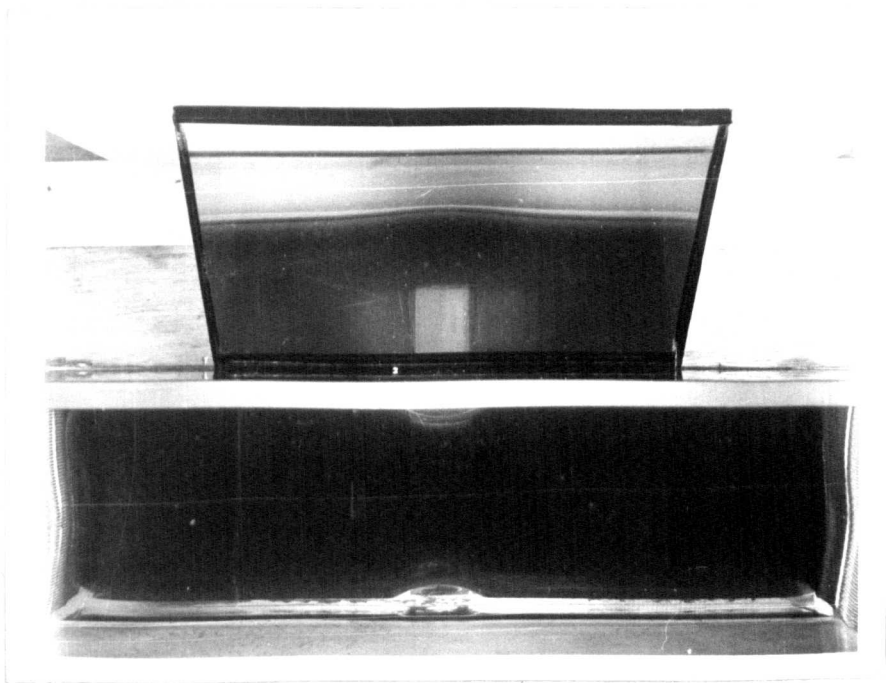
FIG. 6.10. SEQUENCE OF PHOTOGRAPHS TO  
SHOW BRIDGE INSTABILITY.

upper fluid s.g. = 1.152

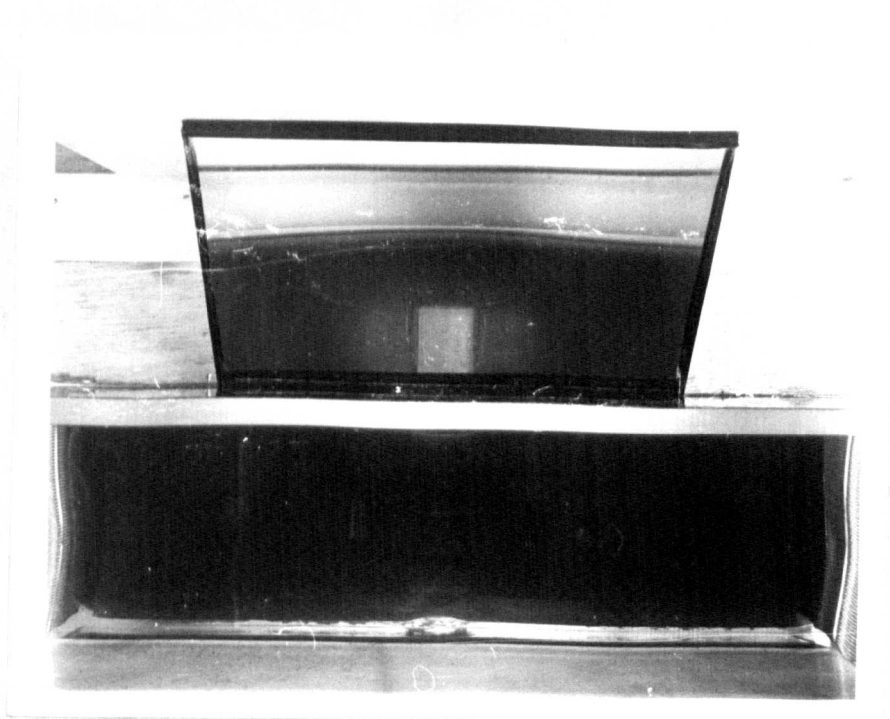
lower fluid s.g. = 1.162

mag. field =  $0.40 \text{ Wb/m}^2$  total current = 0.6 Amps

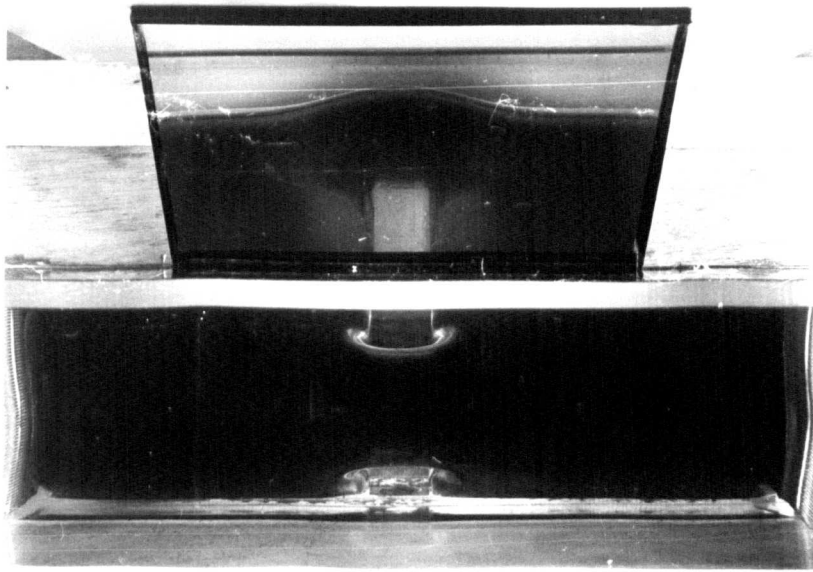
time after switch on =  $t$  secs.



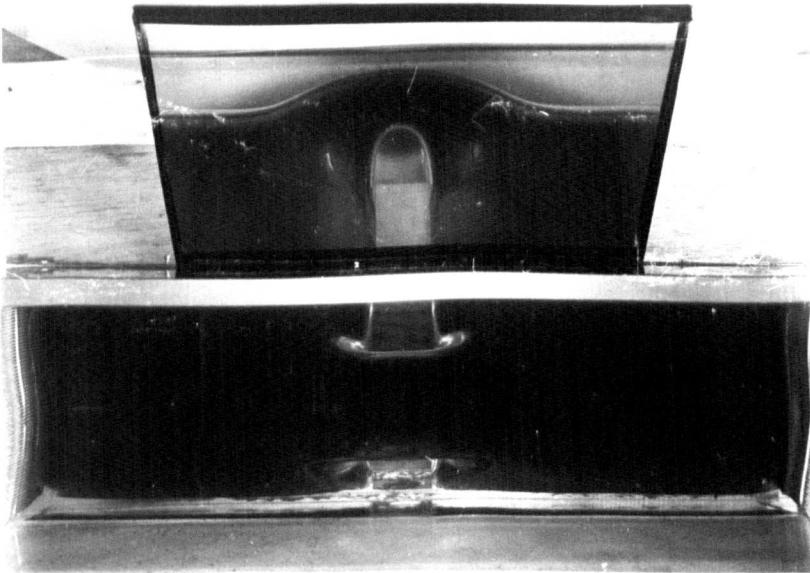
b)  $t = 4$



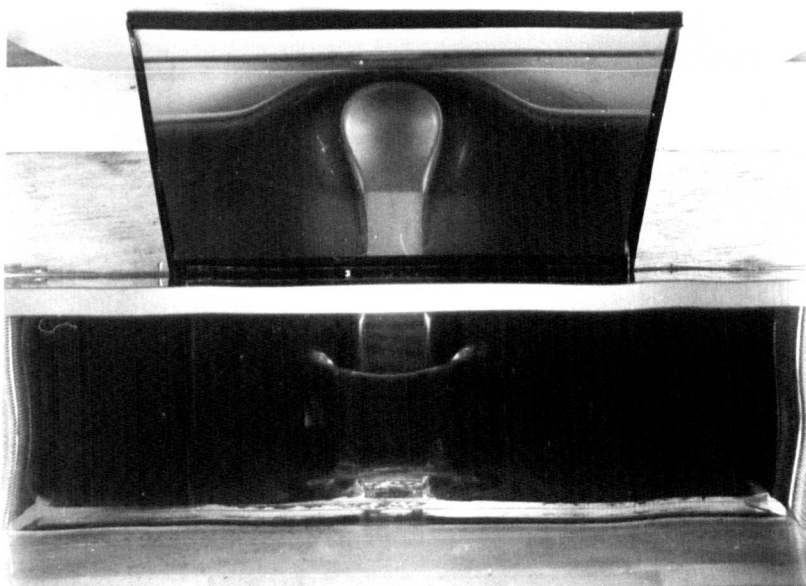
c)  $t = 8$



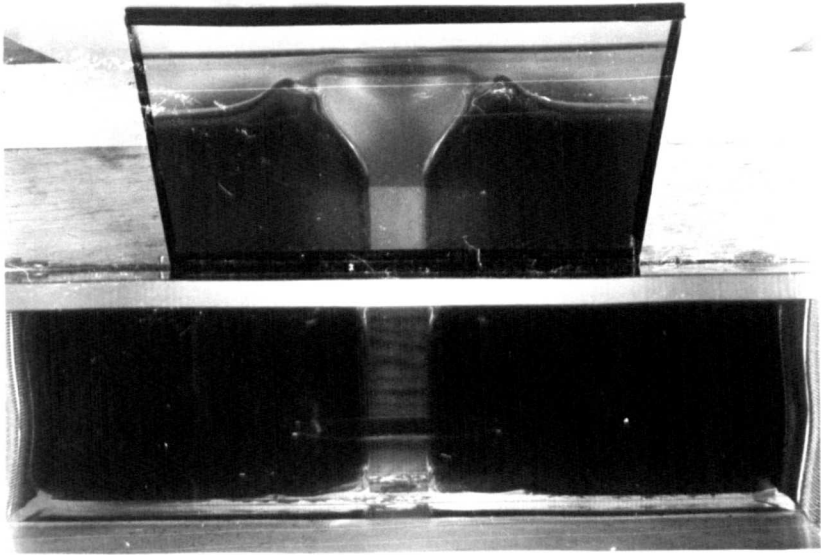
d)  $t=13$



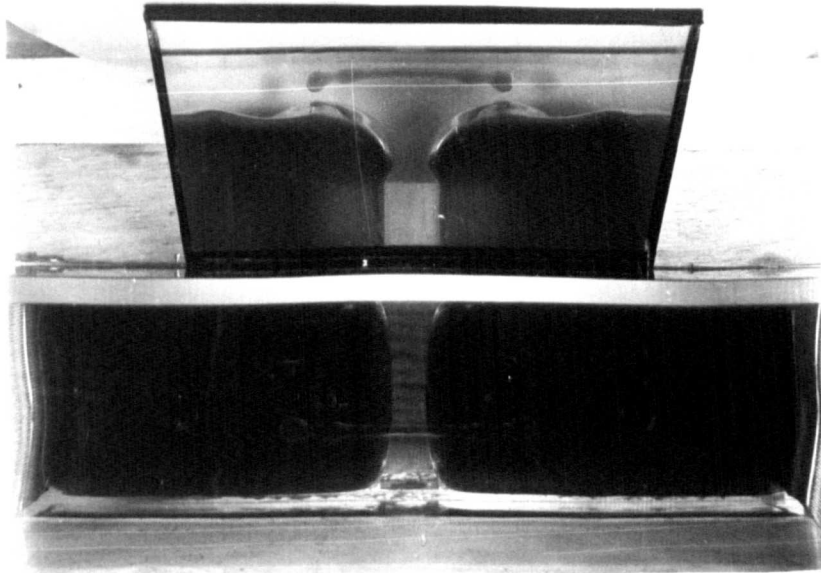
e)  $t=15$



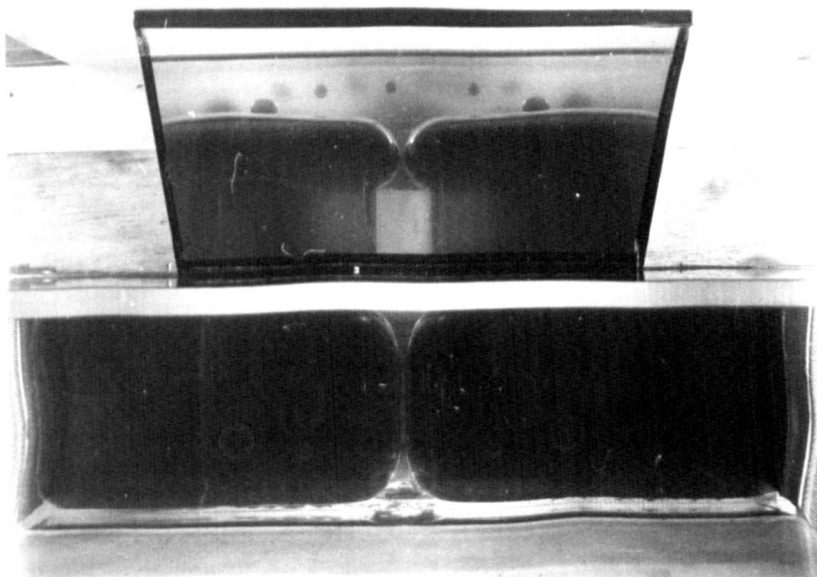
f)  $t=16$



g)  $t=17$



h)  $t=18$



i)  $t=26$

the wall of the tank reaches the corner as the surface meanwhile humps up and internal motion of the fluid occurs, tending to stabilise the interface. If the current was set at a suitable level this state could be maintained indefinitely as in 6.4.1. On allowing the instability to develop further, the interface intersection with the tank moves along the floor of the tank until it links with the interface on the other side, forming a circle of the lighter fluid right round the copper sulphate which now forms a 'bridge' between two bodies of stable electrolyte on either side of the humped floor. This bridge now carries all the current passing through the tank, and the  $\underline{j} \times \underline{B}$  force lifts the bridge bodily through the lighter fluid. Because of the nature of the M.H.D. Rayleigh-Taylor instability the fluid interface even in this bridge is stable to 'pinch' type modes of instability, and remains stable in shape. However, as it is lifted, two other effects occur. The ends are 'anchored' to the main bodies of fluid, so that the bridge arches upwards in the middle, and this permits fluid to run out down either end as if it were a hose pipe, since whilst the sausage shape as a whole is stable, there are no forces acting to prevent the fluid flowing under gravity down each side. The other effect is that distortion of current in the two main bodies of fluid produces rotational  $\underline{j} \times \underline{B}$  forces which induce motion such that the ends of the bridge are carried away from the middle and each other, thus stretching the bridge. As the bridge narrows in cross-section, its resistance increases and the current generator can no longer operate at constant current mode, but switches to constant voltage. The bridge finally becomes so narrow that it breaks, presumably under surface tension forces, and once the current path is broken the whole bridge breaks into bubbles which

float slowly back to the bottom. After some time, the two bodies of fluid meet again, coalesce, and if the current source is still on, the instability will repeat itself ad infinitum in a graceful and beautiful motion. At first sight this motion might be compared with the original pinch experiments of Northrup (1907), where a metallic conductor in a trough was made to pinch itself into two parts by the current passing through it, with no imposed field, and hence a similar intermittent current flow was obtained. However, in that case the pinch was due to the radially inward pressure gradient produced by interaction of the current and its own induced field, whereas in our case, using electrolyte, the current densities are not high enough for this effect to be at all significant, even just before the breaking of the bridge, so that the pinch mode in which the bridge appears to break must be due to surface tension forces. In the case of a wide tank where a number of these instabilities occur, side by side, the same arching motion is seen, but presumably the effect in this case is for the instability modes to grow until the troughs reach the floor of the tank, and then arch under to form the bridge or hose-pipe form, whence the motion is repeated as above.

#### 6.5. The Effect of B Varying with Height

In 5.3.4. it has been shown that if the interface between the two fluids is in a region where the horizontal magnetic field varies with height, an instability can occur with perturbations in a vertical plane parallel to the current vector in the conducting fluid (if the current is normal to the applied magnetic field).

The most interesting case to investigate practically is that where

$\frac{\partial B}{\partial z}$  is negative, in which case a current in the lower conducting fluid directed such that  $\mathbf{j} \times \mathbf{B}$  is downwards, will give rise to

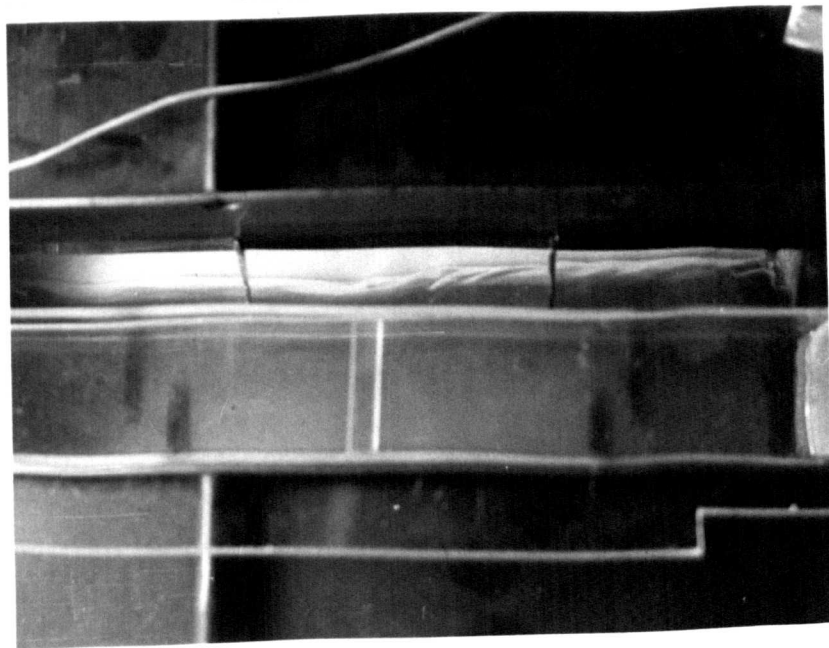
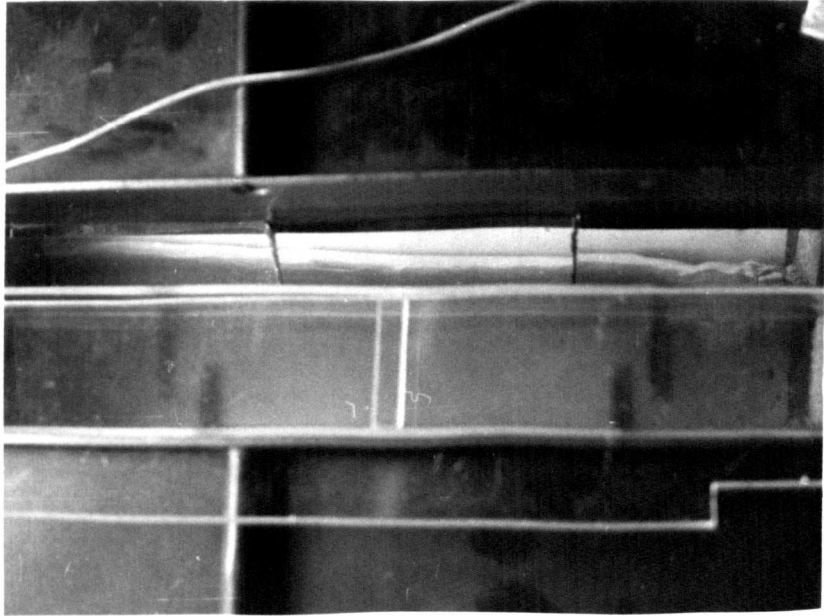
instability. This instability could not be confused experimentally

with the usual M.H.D. Rayleigh-Taylor instability which only occurs for upward  $\underline{j} \times \underline{B}$  forces.

The narrow tank was used in the narrow magnet with 3" pole gap, since this was capable of producing a decreasing horizontal field which reduced from  $1.2 \text{ Wb/m}^2$  to almost zero in approximately 10 cms height, the depth of the magnet coils i.e. use was made of the fringe field of the magnet. The tank was supported with the interface between the copper sulphate solution and the Genklene/white spirit mixture in the middle of the region of decreasing field, at the top side of the gap, where  $\frac{\partial B}{\partial z}$  is negative. With a field of more than  $1.0 \text{ Wb/m}^2$  and current of about  $100 \text{ mA/sq.cm}$ , the interface was seen to be perturbed in the expected mode, with one wavelength the length of the tank, although not purely sinusoidal. However the disturbance did not grow exponentially, but appeared to reach a maximum amplitude of a few millimetres, possibly because of other factors becoming important, such as the finite depth of the conducting liquid (about 4 cms.). The perturbation tended to oscillate slowly, as a progressive wave travelling along the trough. The absence of this perturbation when the tank was placed in the uniform part of the field, suggests that what was observed was in fact due to the effect predicted in 5.3.4.

Using a narrow, 2" wide, tank, with a strip mirror along one side at  $45^\circ$  to the vertical to enable the side profile to be viewed from above, photographs were taken of the instability, shown in fig. (6.11). The instability shows up as the wave-like surface profile seen in the mirror.

It is worth recording here that care should be taken in interpreting such observations lest the instability described in 5.3.4. be confused with an instability due to the purely magnetic



SIDE VIEW  
IN MIRROR

SURFACE  
VIEWED  
FROM  
ABOVE

FIG. 6.11 . INTERFACIAL INSTABILITY WHEN

$$\delta B \neq 0$$

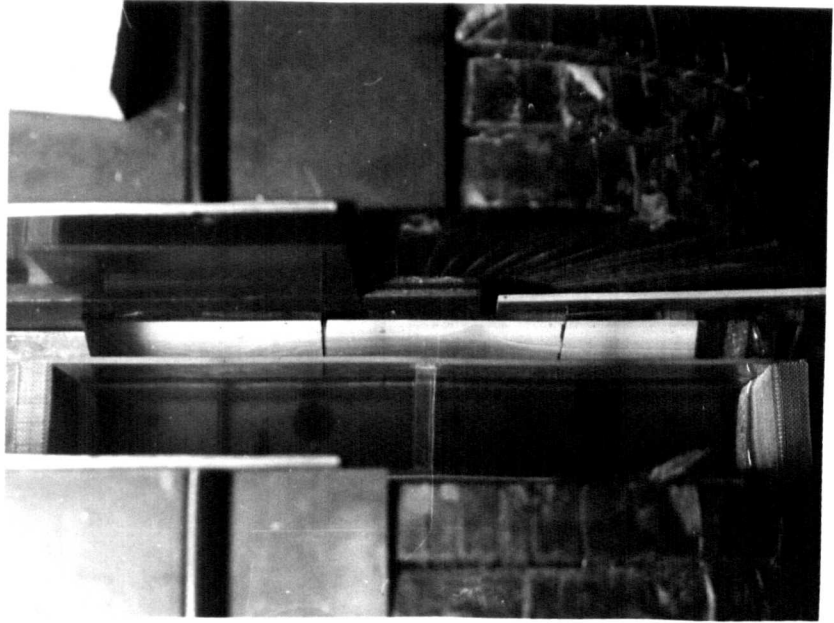
$$\delta z$$

upper S.G. 1.087

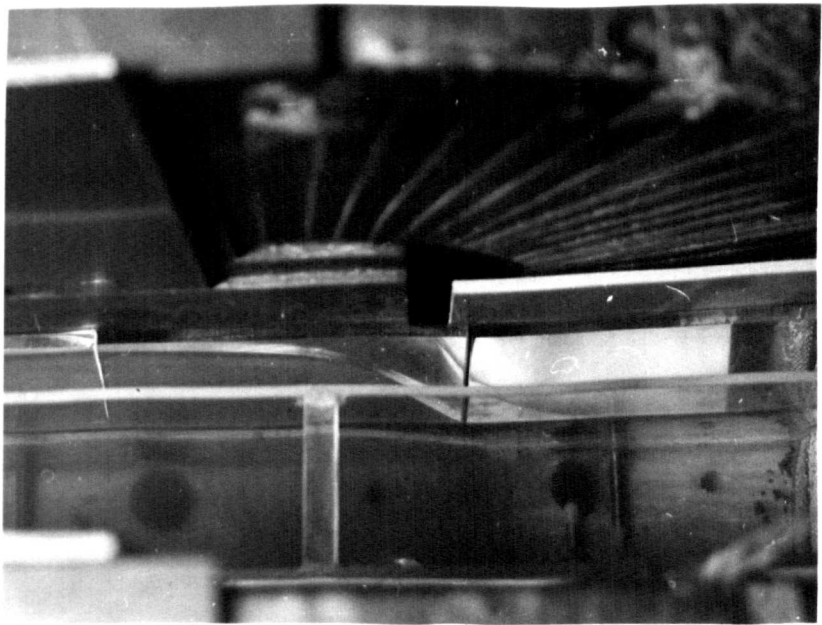
lower S.G. 1.095

field = 1.1 Wb/m<sup>2</sup>

current = 100 mA/cm<sup>2</sup>



(a)  $B \approx 0.3 \text{ Wb/m}^2$



(b)  $B \approx 1.1 \text{ Wb/m}^2$

FIG 6.12 EFFECT OF MAGNETIC FIELD ALONE ON FLUIDS OF DIFFERENT  $\mu$ .

upper S.G 1.087

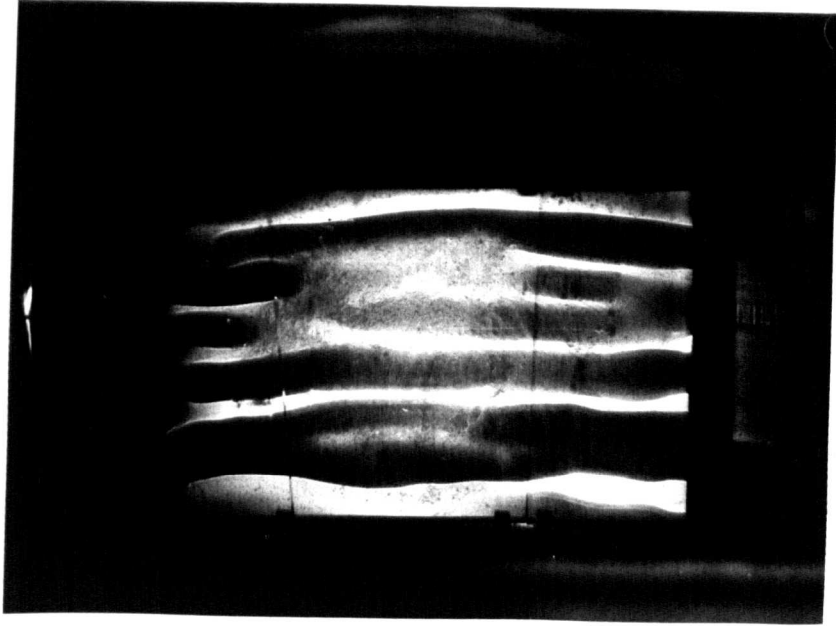
lower S.G 1.095

6.6. The Dependence of Instability Mode Orientation upon the Relative Orientation of Magnetic Field and Current Density

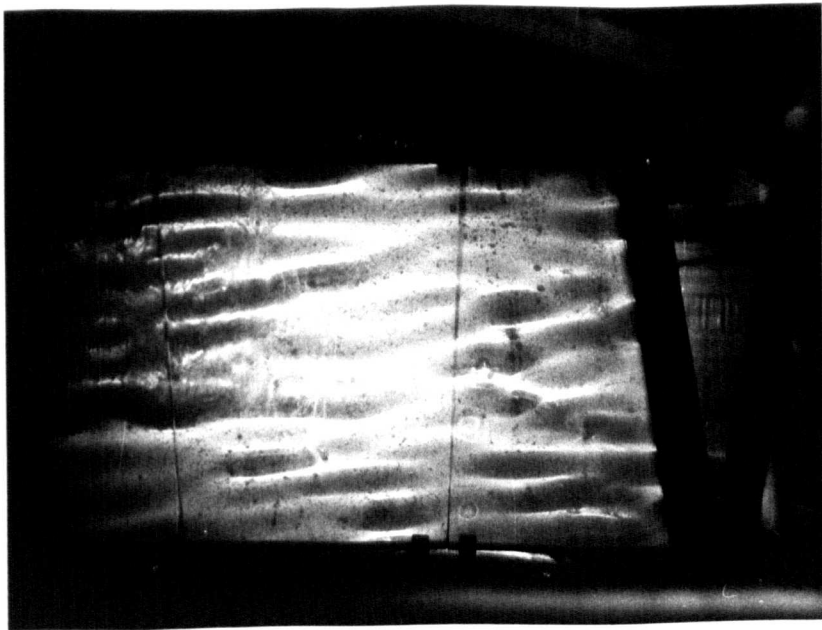
To verify experimentally the predictions of § 5.4, the second square tank (40cms x 40cms x 20cms deep) described in § 4.3.5, and shown in fig. (4.17) was used. The tank was used as for the wave experiments, with a flat floor, and with about 2.5 cms depth of each fluid, densities matched to within 1.5%. The orientation was set, the current gradually increased until instability started to occur, and when sufficient amplitude was attained a photograph was taken, using the viewing arrangement described in § 4.3.7. This was repeated for different orientations of the tank, and the required angles  $\theta$  and  $\beta$  (as defined in fig. (2.11) and § 5.6) were measured from the photographs. Since the surface tension could not be accurately measured, it was not considered worthwhile to measure the actual current value at which the instability first occurred, though it was noticeable that as the tank was swung towards the  $\beta = 0$  or  $\beta = \pi$  positions from the  $\beta = \frac{\pi}{2}$  (central) position, it required a considerably greater current to produce instability, as expected. In fact, at  $\beta = 0$  or  $\pi$ , the required current was so high that other spurious motion due to non-uniformity of current density was generated to the extent that it almost occluded the Rayleigh-Taylor instability.

Fig. (6.13) shows some photographs typical of those taken during the experiment, 6.13 (f) being the case where  $\beta = \frac{\pi}{4}$  and the Rayleigh-Taylor instability just shows as diagonal patches, whereas a spurious current-generated motion dominates in the corners.

Fig. (6.14) is a plot of  $\theta$  against  $\beta$  showing excellent agreement with the theoretical prediction. In a few cases, there was an ambiguity in the photograph, as if two sets of instabilities were

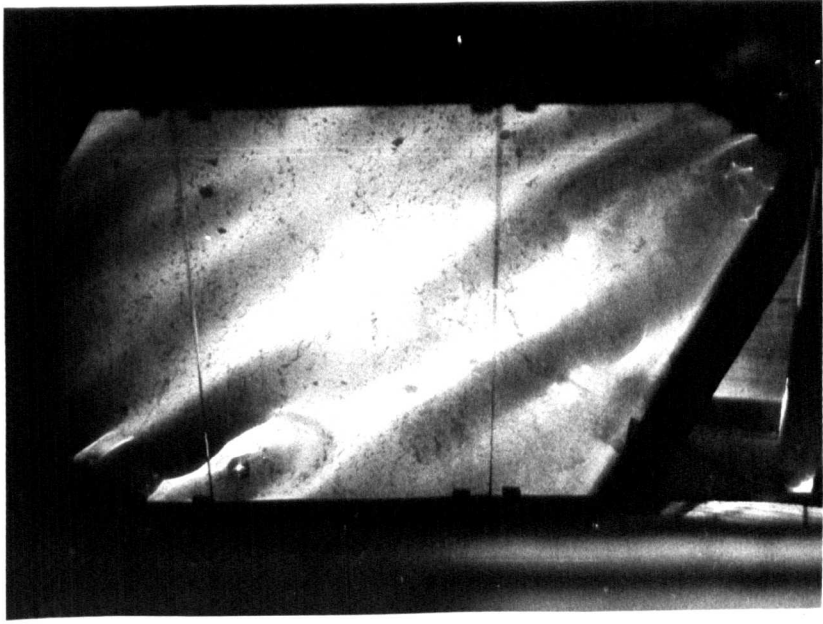


a)

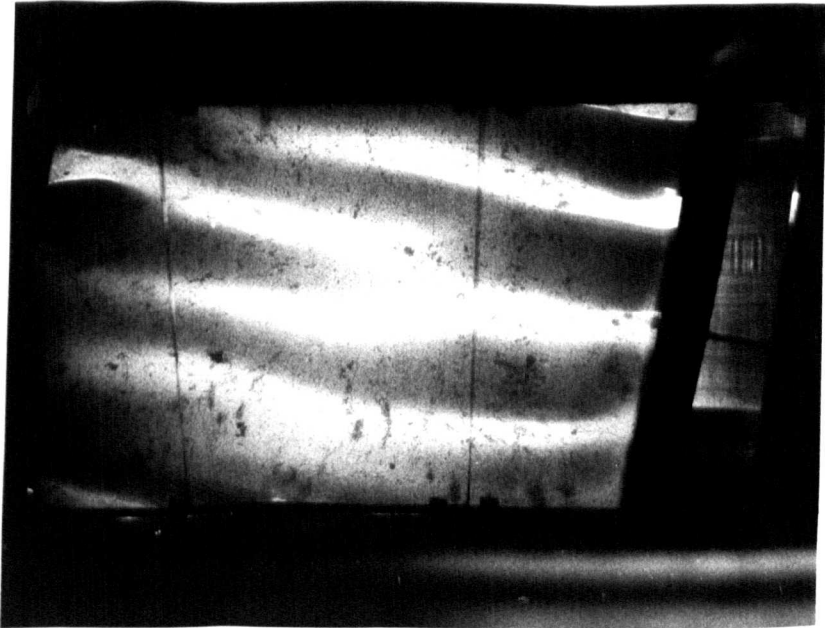


b)

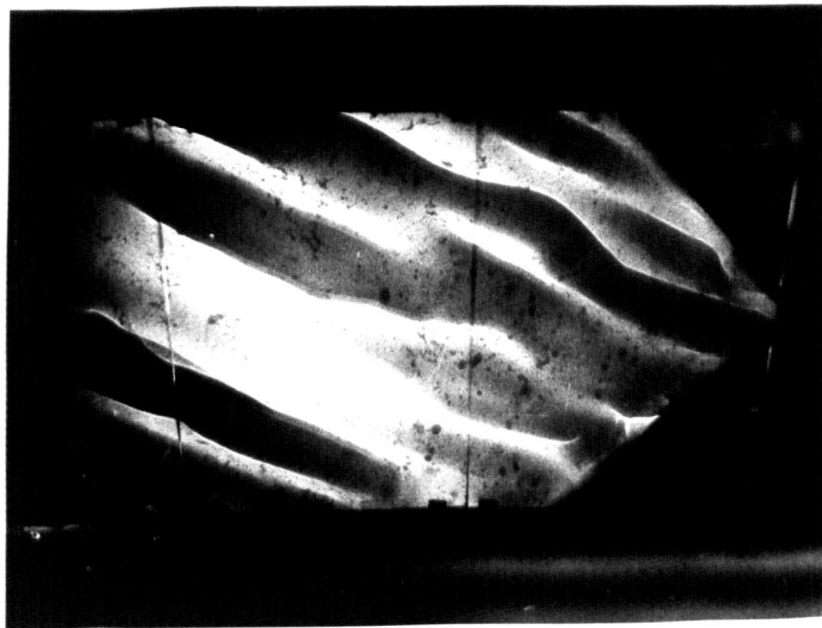
FIG. 6.13. TYPICAL PHOTOGRAPHS FROM ORIENTATION EXPERIMENT.



c)



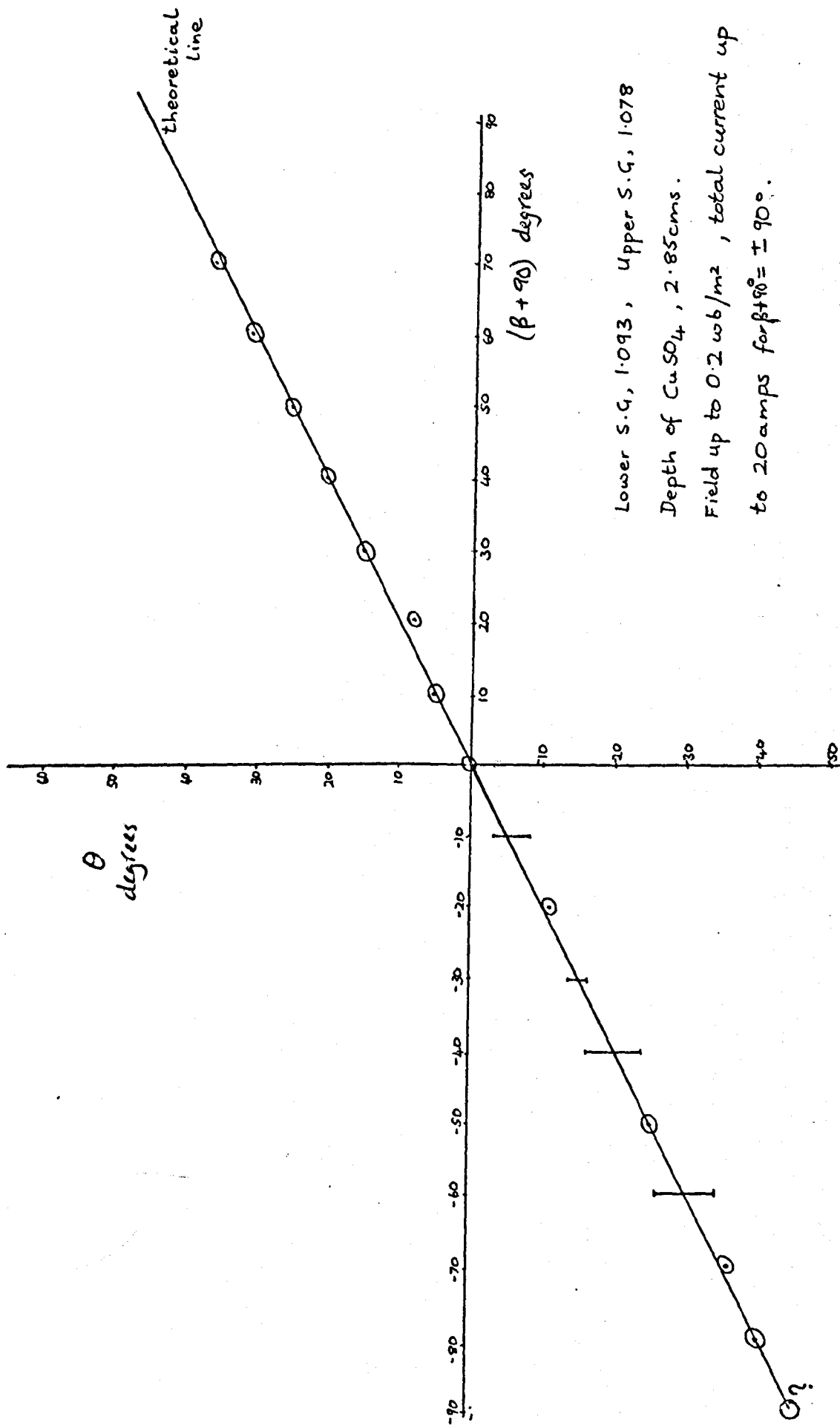
d)



e)



f)



Lower S.G. 1.093, Upper S.G. 1.078

Depth of  $\text{CuSO}_4$ , 2.85 cms.

Field up to 0.2 wb/m<sup>2</sup>, total current up to 20 amps for  $\beta \pm 90^\circ = \pm 90^\circ$ .

FIG.6.14. PLOTTED RESULTS MEASURED FROM PHOTOGRAPHS OF ORIENTATION OF INSTABILITY.

occurring at once, but in these cases, the average of  $\theta$  for the two sets lay on the predicted  $\theta = \frac{\beta}{2} + \frac{\pi}{4}$  line, such cases being represented in fig. (6.14) by a line joining the two possible interpretations.

7. CONCLUSIONS AND SUGGESTIONS FOR FURTHER WORK

a) Shercliff's (1969) theory of anisotropic surface waves under a vertical electromagnetic force was adjusted to accommodate those factors which might be important in the experimental demonstration of such waves in the laboratory. Surface tension was found to reduce significantly the influence of the anisotropic term in the dispersion relation, for a given applied  $\underline{j} \times \underline{B}$  force in the cases of both surface and long waves, thus making the experimental problem very much more difficult than suggested by the original solution ignoring surface tension. Viscosity was found to affect the anisotropy only for cases where viscous damping would prohibit experiments in the O.H.D. case anyway. Consideration of the dispersion of waves at the interface between a conducting and non-conducting fluid, closely matched in density, showed that in this situation the  $\underline{j} \times \underline{B}$  force required to produce noticeable anisotropy would be much less, but that too close a matching of densities would lead to greater domination by viscous and surface tension forces. Polar plots of phase and group velocity, and the shape of lines of constant phase for waves excited continuously at a point source, were produced for parameters corresponding to potential experimental conditions, suggesting that it should be possible to produce anisotropic wave patterns in the laboratory.

b) The practical problem of setting up a system to observe the anisotropic waves was found to be considerably magnified by the number of experimental variables involved, each of which had to be set within a narrow range relative to the other parameters to enable the experiments to be a success. After some laboratory

refraction due to the dispersion relation varying in space, the pattern of waves produced by an initial impulse disturbance at a point, and the pattern of waves resulting from the steady motion of an object or pressure disturbance across the surface, with and without surface tension considered. For each case the problem was solved analytically in principle, and numerical results were obtained and plotted by computer. In each case, the introduction of the anisotropic term removed any triviality of the O.H.D. counterpart, and required a more generalised solution which should contribute to the theory of waves in general. It also produced some interesting wave patterns which are worth demonstrating experimentally, and which could provide a useful visual aid for the teaching of the nature of anisotropic waves in other branches of physics, most of which do not permit direct observation.

e) Attempts were made on the experimental rig to demonstrate the above phenomena. Refraction was shown to occur as expected, but the other situations proved difficult to generate because of practical limitations. The unexpected problem of being hardly able to reflect waves at all in a two-fluid system raises the possibility of an interesting theoretical study into this question. Whilst the small scale of laboratory experiments within the confines of the magnet is a hindrance, it may nonetheless be concluded that the overall design of the rig is adequate to demonstrate these anisotropic wave phenomena, but that further work is needed on detailed design points. particularly of wave makers of one sort or another, to be able to gain really good results.

f) The stability equation for the M.H.D. Rayleigh-Taylor instability was obtained for modes in any direction, including the case where  $B$  varies in a vertical direction. Unsuccessful attempts

were made to produce an analytical solution of the case where  $j$  varies due to the variation in depth of the containing tank, but a heuristic understanding of the situation was obtained, predicting the possibility of a state of intermediate stability with an electrically driven flow maintaining a disturbed, but stationary, surface elevation.

g) The influence of  $j \times D$  forces on the shape of a free or interfacial surface, and vice versa, was considered in detail, and it was established that the surface cannot, except by surface tension, be supported in any shape other than normal to the prevailing body forces without there being motion in the fluid. The possibility of surface tension effects masking the onset of true instability in experiments was noted.

h) Since visual methods of observation are not very appropriate, various probes were developed to measure the growth rate of M.H.D. Rayleigh-Taylor instability, and to plot surface contours, bearing in mind the particular problems of working in an M.H.D. situation. Although not used for a particular experiment, these probes should be useful in any future quantitative measurements of the instability.

i) Qualitative observations were made photographically of the M.H.D. Rayleigh-Taylor instability when  $\frac{\partial j}{\partial x} \neq 0$  and when  $\frac{\partial B}{\partial z} \neq 0$ . For the former case, probe measurement of surface contours verified the existence of a quasi-stable state, with electrically driven flow producing a disturbed surface, as predicted theoretically. It would be of interest to try to examine this in more detail, using anemometry to measure the fluid velocity distribution. The large amplitude state of the instability in this case was observed to have an interesting arch structure, which was repeatable in every case and appeared

to be very well defined in shape until break-up finally occurred. Whilst theoretical analysis seems difficult, the phenomenon is of such a unique form that further understanding of the balance of forces involved would be valuable.

Experiments to measure the orientation of the unstable mode, varying the relative angle between imposed current and magnetic field, supported the theoretical predictions conclusively.

j) In general, it can be said that qualitative experimental evidence has concurred with the predictions of the theories of M.H.D. anisotropic surface wave propagation and the M.H.D. Rayleigh-Taylor instability.

8. REFERENCES

- Baker, R.C., 1965, Maximum growth rates of Rayleigh-Taylor instabilities due to an electromagnetic force. *Nature*, 207, 65-6.
- Batchelor, G.K., 1967, 'An Introduction to Fluid Dynamics', C.U.P.
- Chandrasekhar, S., 1961, 'Hydrodynamic and Hydromagnetic Stability'. Oxford, Clarendon Press.
- Devime, R., Karr, Marle, Duc, X.N., 1966, Evaluation des Effets de L'Instabilite De Rayleigh-Taylor et de la Diffusion Turbulente dans la Conversion en Veine Inhomogene. 'Electricity from M.H.D.', 3, 505. IAEA Vienna.
- Duc, X.N., 1968, Etude theorique et experimentale sur modele hydraulique des instabilites de Rayleigh-Taylor en magnetohydrodynamique. *Comptes Rendus, Acad.Sci., Paris*, 266 A, 738-740.
- Fussey, D.E., 1969, 'Magneto-Viscous effects in combustion plasma', Ph.D. thesis, University of Warwick.
- Hayes, W.D. 1970, Kinematic Wave Theory. *Proc.Roy.Soc.Lond.*, A320, 209-226.
- Hunt, J.C.R., 1967, Some aspects of Magnetohydrodynamics. Ph.D. thesis, University of Cambridge.
- Hunter, C., 1972, On the calculation of wave patterns. *J.Fluid Mech.*, 53, 637-646.
- Lamb, H., 1932, 'Hydrodynamics'. Cambridge University Press.
- Lemaire, A., 1963, Instabilite de Rayleigh-Taylor sous l'effet de forces electromagnetiques. Conference internationale sur les phenomenes d'ionisation dans les gaz. 4, 487-490.
- Lewis, D.J., 1950, The instability of liquid surfaces when accelerated in a direction parallel to their planes II. *Proc.Roy.Soc.Lond.*, A202, 81.
- Lighthill, M.J., 1964, Group Velocity. *J.Inst.Maths.Applics.*, 1, 1-28.
- Llowarch, W., 1961, 'Ripple tank studies of wave motion'. Oxford, Clarendon Press.
- McLachlan, N.W., 1947, 'Theory and application of Mathieu Functions'. Oxford, Clarendon Press.

Melcher, J.R., 1963, 'Field-Coupled Surface Waves!'. M.I.T.Press.

Murty, G.S., 1961, Instability of a conducting fluid slab carrying a uniform current in the presence of a homogeneous magnetic field.

Arkiv fur Fysik, 19, 499.

Northrup, E.F., 1907, Some newly observed manifestations of forces in the interior of an electric conductor. Phys.Rev., 24, 474-497.

Sax, N.I., 1963, 'Dangerous properties of industrial materials'  
Reinhold Publishing Corp. New York.

Shercliff, J.A., 1969, Anisotropic surface waves under a vertical magnetic force. J.Fluid Mech., 38, 353.

Shercliff, J.A., 1970, A note on the envelope construction for group velocity in dispersive anisotropic wave systems. J.Inst.Maths Applics., 6, 91-95.

Stoker, J.J., 1957, 'Water Waves'. Interscience, New York.

Ursell, F., 1960, Steady wave patterns on a non-uniform steady fluid flow. J.Fluid Mech., 9, 333-346.

Whitham, G.B., 1961, Group velocity and energy propagation for three-dimensional waves. Comm.Pure Appl.Maths., 14, 675-691.

## APPENDIX

### COMPUTER PROGRAMME LISTINGS

As mentioned in the introduction, it was not thought to be necessary to explain the working of the computer programmes in detail, being fairly straightforward algorithms of the relevant equations in the main text of the thesis. However, it is desirable to list them to enable any future use to be made of them and further results to be obtained. They are written in standard Fortran IV language, and were run on the I.C.L. 4100 machine at the University of Warwick Computer Unit.

ROOTS is a library subprogramme on the file of that machine which solves for the roots of a polynomial equation.

ORIGIN, MOVE, DRAW, WAY, are all subroutines in the 4100 software to control the digital plotter output. The plotter output is scaled for a 12" plotter, and some of the figures in the main part of the thesis are examples of output.

The following are the programmes listed, and the sections in the thesis where reference is made to each one :-

- |     |  |            |
|-----|--|------------|
| C2. | To solve the anisotropic surface wave dispersion equation and produce polar plots of phase velocity, group velocity and lines of constant phase. | ...(2.4.2) |
| C3. | As C2, but for the long wave dispersion equation   | ...(2.4.2) |
| C4. | To calculate and plot the phase and group velocity reflection characteristics.   | ...(3.2.3) |
| C5. | To plot the group rays from a line source, refracted by varying current density.   | ...(3.4.3) |
| C7. | As C5, but waves from a point source.  | ...(3.4.3) |
| F1. | To generate and plot out the wave patterns for the anisotropic 'ship-wave' problem.  | ...(3.5.4) |
| F2. | To generate and plot out the wave patterns for the anisotropic 'fish-line' problem.  | ...(3.5.5) |
| G2. | To use surface wave dispersion relation to plot lines of constant phase at a set time after an impulsive disturbance.                            | ...(3.3.2) |

JOB: ES/R104/C2;

DE  
OP

OPTIONS:

FORTRAN:

C 2

LIST:

LINE:15;

```

1* C      COMPREHENSIVE SURFACE WAVES DATA (DEEP FLUID), PHASE AND
2* C      GROUP VELOCITIES, CONSTANT PHASE LINES PLOTTED AND PRINTED, WITH
3* C      ANISOTROPY RATIO, PROGRAMME ACCOMODATES WAVES AT TWO-FLUID
4* C      INTERFACE
5*      DIMENSION C(21),CG(21),CT(21),CK(21),PHI(21),X(3,21),Y(3,21),
6*      THE(21)
7*      READ(7,50)ALFA,RO1,RO2,I,GAN
8* C      I=1 FOR UPWARD FORCE,2 FOR DOWNWARD
9*      50 FORMAT(F10.6,2F10.4,I1,F6.4)
10*      WRITE(2,51)ALFA,RO1,RO2
11*      51 FORIAT(5HALFA#,F10.6,6H RO1=,F10.4,6H RO2=,F10.4)
12*      READ(7,52)EGA
13* C      EGA IS OMEGA IN RADS PER SECOND
14*      EGAL=EGA
15*      DO 101 L=1,3
16*      CALL ORIGIN(0,0)
17*      CALL MOVE(0,2600)
18*      CALL ORIGIN(650,0)
19*      CALL DRAW(1600,0)
20*      CALL MOVE(0,0)
21*      CALL DRAW(0,2200)
22*      CALL MOVE(-20,100)
23*      CALL WAY(1,5)
24*      WRITE(9,70)
25*      70 FORMAT(11HJ DIRECTION)
26*      CALL MOVE(100,-30)
27*      CALL WAY(0,5)
28*      IF(L-2)201,202,203
29*      201 WRITE(9,71)
30*      71 FORIAT(28H B DIRECTION, PHASE VELOCITY)
31*      CALL MOVE(120,-60)
32*      GO TO 204
33*      202 WRITE(9,72)
34*      72 FORIAT(23H B DIRECTION, GROUP VEL)
35*      GO TO 204
36*      203 WRITE(9,73)
37*      73 FORIAT(33H B DIRECTION, CONSTANT PHASE LINE)
38*      204 CALL MOVE(0,0)
39*      101 CONTINUE
40*      DO 103 M=1,10
41*      EGA=EGAL*M/10,0
    
```

```

42* WRITE(2,53)EGA,GAM
43* 53 FORMAT(6HOMEGA=,F6.2,8H GAMMA=,F6.4)
44* 52 FORMAT(F6.2)
45* IF(I.EQ.1)WRITE(2,54)
46* IF(I.EQ.2)WRITE(2,55)
47* 54 FORMAT(12HUPWARD FORCE)
48* 55 FORMAT(14HDOWNWARD FORCE)
49* G=9.81
50* PI=3.14159262
51* TAW=ALFA/(R01*G)
52* WRITE(2,58)
53* 58 FORMAT(7X,5HTHETA,6X,1HC,8X,2HCG,7X,2HCK,7X,2HCT,5X,4HPHI,7X,2HX1
54* 1,7X,2HX2,7X,2HX3,7X,2HY1,7X,2HY2,7X,2HY3,3X,12HWAVE NO(C/M))
55* DO 100 J=1,21
56* THE(J)=PI*(J-1)/40,0
57* AB=R01*GAM*COS(THE(J))*2
58* IF(I.EQ.1)AB=-AB
59* A=-(Q*(R01-R02+AB)/((R01+R02)*EGA))
60* AC=-(R01*G*TAW*EGA/(R01+R02))
61* AP=-(A*A/9)
62* AQ=((A**3)/27,0)+AC/2,0
63* AZ=AP**3*AQ*AQ
64* C THE NEXT SECTION DEALS WITH SPECIAL CASES OF UNSTABLE AND
65* C NOMINALLY UNSTABLE DISPERSIONS
66* IF(I.EQ.2)GO TO 301
67* C THIS ELIHINATES DOWNWARD FORCE FROM OTHER TESTS
68* IF(A.GT.0.0)WRITE(2,56)J
69* IF(A.EQ.0.0)WRITE(2,57)J
70* 56 FORMAT(18HNOMINALLY UNSTABLE,I2)
71* 57 FORMAT(27HNOMINALLY NEUTRAL STABILITY,I2)
72* C TEST FOR VALUE OF Q
73* IF(AQ)301,302,303
74* C 301 STARTS BASIC CUBIC SOLUTION, NORMAL STABILITY
75* C 302 STARTS SPECIAL SOLUTION WHEN Q=0 (SEE CUBIC SOLUTION NOTES
76* C 303 STARTS SOLUTION WHEN Q POSITIVE.
77* 302 C(J)=SQRT(-3.0*AP)-(A/3)
78* WRITE(2,59)
79* 59 FORMAT(30X,3HQ=0)
80* GO TO 305
81* 303 WRITE(2,60)
82* 60 FORMAT(1H+,30X,16HQ GREATER THAN 0)
83* IF(AZ.LT.0.0)GO TO 304
84* C THIS TESTS FOR AZ LESS THAN 0. IF SO, REQUIRES SPECIAL SOLUTION
85* C TO START WITH, JOINING MAIN SOLUTION AT 307
86* C IF NOT THEN SITUATION IS UNSTABLE, SETS VALUES TO 0 AND REJOINING
87* C (AT306)BASIC PROGRAMME FOR LAST PART OF GROUP VELOCITY CALCULATIONS
88* WRITE(2,61)
89* 61 FORMAT(1H+,50X,8HUNSTABLE)
90* C(J)=0
91* CT(J)=0
92* CK(J)=0
93* PHI(J)=0
94* GO TO 306
95* 304 PHIL=PI-ATAN(SQRT(-AZ)/AQ)
96* WRITE(2,62)
97* 62 FORMAT(1H+,50X,12HSTILL STABLE)
98* GO TO 307
99* 301 IF(AZ)600,601,601
100* 601 U=(-AQ+SQRT(AZ))*0.33333333
101* V=(-AQ-SQRT(AZ))*0.33333333

```

```

102*      C(J)=U+V=A/3.0
103*      GO TO 305
104*      600 PHIL=ATAN(SQRT(-AZ)/(-AQ))
105*      307 C(J)=2*SQRT(-AP)*COS(PHIL/3.0)-(A/3.0)
106*      C      305 STARTS GROUP VELOCITY
107*      305 CK(J)=-A/2-1.2*AG/(C(J)**2)
108*      CT(J)=-G*GAN*SIN(2*THE(J))*R01/(2*EGA*(R01+R02))
109*      IF(L.EQ.1)CT(J)=-CT(J)
110*      PHI(J)=ATAN(CT(J)/CK(J))
111*      306 CG(J)=SQRT(CK(J)*CK(J)+CT(J)*CT(J))
112*      X(1,J)=C(J)*COS(THE(J))
113*      C      IN X(L,J) L=1 GIVES PHASE VEL LOCUS
114*      C      L=2 GIVES GROUP VEL LOCUS
115*      C      L=3 GIVES CONSTANT PHASE LOCUS
116*      Y(1,J)=C(J)*SIN(THE(J))
117*      X(2,J)=CG(J)*COS(THE(J)+PHI(J))
118*      Y(2,J)=CG(J)*SIN(THE(J)+PHI(J))
119*      X(3,J)=X(1,J)-C(J)*SIN(THE(J))*SIN(PHI(J))/COS(PHI(J))
120*      Y(3,J)=Y(1,J)+C(J)*COS(THE(J))*SIN(PHI(J))/COS(PHI(J))
121*      CN=EGA/(C(J)*2*PI)
122*      63  FORMAT(I4,13F9.5)
123*      100 WRITE(2,63)J,THE(J),C(J),CG(J),CK(J),CT(J),PHI(J),(X(L,J),L=1,3),
124*      1(Y(L,J),L=1,3),CN
125*      R=0
126*      IF(C(1).GT.0)R=C(21)/C(1)
127*      WRITE(2,64)R
128*      64  FORMAT(5X,17HANISOTROPY RATIO=,F8.4)
129*      DO 110 L=1,3
130*      IF(L.EQ.1)CALL MOVE(0,-5200)
131*      IF(L.EQ.2)CALL MOVE(0,2600)
132*      IF(L.EQ.3)CALL MOVE(0,2600)
133*      CALL ORIGIN(620,0)
134*      CALL MOVE(IFIX(X(L,1)*20000),0)
135*      DO 205 J=2,20
136*      ICX=X(L,J)*20000.0
137*      ICY=Y(L,J)*20000.0
138*      IF(ICX.GT.2000.OR.ICY.GT.2400)GO TO 110
139*      205 CALL DRAW(ICX,ICY)
140*      CALL DRAW(0,IFIX(Y(L,21)*20000))
141*      CALL MOVE(0,0)
142*      110 CONTINUE
143*      103 CONTINUE
144*      102 STOP
145*      END

```

```

CODELENGTH  990  WORDS
LOCAL WKSPCE 69  WORDS
DYN, ARRAYS  504  WORDS
DATA         0    WORDS

```

LABEL	ADDRESS	LABEL	ADDRESS	LABEL	ADDRESS
50	23	**	51	29	**
71	113	**	282	123	**
73	133	**	284	136	**
52	160	**	54	181	**
56	323	**	57	326	**
303	357	**	60	360	**
62	417	**	381	421	**
				70	90
				72	126
				101	142
				55	184
				302	334
				61	374
				601	425

RES/R104/C3

C3

TRAN:

```

ST;
* C COMPREHENSIVE LONG WAVES DATA, PHASE AND GROUP VELOCITIES;
* C CONSTANT PHASE LINES PLOTTED AND PRINTED, WITH WAVE NUMBERS
* C AND ANISOTROPY RATIO. ACCOMMODATES WAVES AT TWO-FLUID
* C INTERFACE
* C DIMENSION C(21), CG(21), CT(21), CK(21), PHI(21), X(3,21), Y(3,21),
1 THE(21), WN(21), HEWN1(21), HEWN2(21)
* C READ(7,50)ALFA,RO1,RO2,B,CUR
* C ALFA IS SURFACE TENSION (N/M)
* C RO1 IS LOWER DENSITY, RO2 IS UPPER IN SPECIFIC GRAVITY UNITS
* C B IS MAG FIELD IN W/SQ.M
* C CUR IS CURRENT DENSITY IN MILLIAMPS/SQ.CM -VE DENOTES UPWARD FORCE
* C H IS DEPTH IN M.
* C READ(7,500)IX
4* 500 FORMAT(I1)
* C READ(7,51)EGA
* C EGA IS FREQUENCY IN CYCLES/SEC
7* READ(7,52)IP
* C IP=1 SUPPRESSES GRAPH PLOTTING
9* 50 FORMAT(F10.6,2F10.4,F8.5,F6.3)
0* 51 FORMAT(F6.2)
1* 52 FORMAT(I1)
2* WRITE(2,53)ALFA,RO1,RO2,B,CUR, EGA,
3* 53 FORMAT(5HALFA=,F10.6,1H,4HR01=,F10.4,6H R02=,F10.4,1H,
4* 1,10HMAG.FIELD=,F8.5,27H CURRENT DENSITY(M/20CM)=,F8.3,
5* 2 9HFREQUENCY,F6.3,10HCYCLES/SEC)
6* IF(IX.EQ.1)GO TO 510
7* IF(IX.EQ.2)GO TO 511
8* IF(IX.EQ.3)GO TO 512
9* 510 READ(7,501)H1
10* WRITE(2,503)H1
11* GO TO 515
12* 511 READ(7,501)H2
13* WRITE(2,504)H2
14* GO TO 515
15* 512 READ(7,502)H1,H2
16* WRITE(2,505)H1,H2
17* 501 FORMAT(F6.2)
18* 502 FORMAT(2F6.2)
19* 503 FORMAT(3HH1=,F6.2,9H H2=LARGE)
20* 504 FORMAT(13HH1=LARGE, H2=,F6.2)
21* 505 FORMAT(3HH1=,F6.2,4H H2=,F6.2)
22* DO 106 KID=1,2
23* IF(KID.EQ.2)CUR=-CUR
24* 515 IF(CUR.GT.0.0)WRITE(2,54)
25* IF(CUR.LT.0.0)WRITE(2,55)
26* 54 FORMAT(14HDOWNWARD FORCE)
27* 55 FORMAT(12HUPWARD FORCE)
28* IF(IX.EQ.1)EX=H1/(RO1*100000.0)

```

```

49*      IF (IX.EQ.2) EX=H2/(R02*1000000.0)
50*      IF (IX.EQ.3) EX=H1*H2/((R01*H2+R02*H1)*1000000.0)
51*      G=9.81
52*      PI=3.14159
53*      DD=(R01-R02)*1000.0
54*      DS=(R01+R02)*1000.0
55*      DO 105 H=1,20
56*      OMEGA=2.0*PI*EGA*M*1/20.0
57*      WRITE(2,60) OMEGA
58*      60 FORMAT(1X,6HOMEGA=,F10.6)
59*      WRITE(2,56)
60*      56 FORMAT(7X,5HTHETA,6X,1HC,8X,2HCG,7X,2HCK,7X,2HCT,5X,3HPhi,7X,2HX1,
61*      17X,2HX2,7X,2HX3,7X,2HY1,7X,2HY2,7X,2HY3,3X,12HWAVE NO(C/M),2X,2HH,2
62*      2)
63*      DO 100 J=1,21
64*      THE(J)=PI*(J-1)/40.0
65*      GAM=8*CUR*10*COS(THE(J))**2
66*      IF (DD*G+GAM) 200,201,201
67*      200 WRITE(2,57) J
68*      57 FORMAT(12,20HPOTENTIALLY UNSTABLE)
69*      IP=1
70*      ID=200
71*      GO TO 100
72*      201 C(J)=SQRT((DD*G*EX+GAM*EX+SQRT(EX*EX*(DD*G+GAM)*(DD*G+GAM)+4.0*EX
73*      1*ALFA*OMEGA*OMEGA))/2.0)
74*      WN(J)= EGA/C(J)
75*      WNR=OMEGA/C(J)
76*      IF (IX.EQ.1.OR. IX.EQ.3) HEWN1(J)=WNR*H1/1000.0
77*      IF (IX.EQ.1) HEWN2(J)=100.0
78*      IF (IX.EQ.2.OR. IX.EQ.3) HEWN2(J)=WNR*H2/1000.0
79*      IF (IX.EQ.2) HEWN1(J)=100.0
80*      CK(J)=EX*WNR*(2.0*WNR*WNR*ALFA+DD*G+GAM)/OMEGA
81*      CT(J)=-(EX*WNR*R*CUR*10.0*SIN(THE(J)*2.0)/2.0*OMEGA)
82*      CG(J)=SQRT(CK(J)**2+CT(J)**2)
83*      PHI(J)=ATAN(CT(J)/CK(J))
84*      X(1,J)=C(J)*COS(THE(J))
85*      Y(1,J)=C(J)*SIN(THE(J))
86*      X(2,J)=CG(J)*COS(THE(J)+PHI(J))
87*      Y(2,J)=CG(J)*SIN(THE(J)+PHI(J))
88*      X(3,J)=X(1,J)+C(J)*SIN(THE(J))*SIN(PHI(J))/COS(PHI(J))
89*      Y(3,J)=Y(1,J)+C(J)*COS(THE(J))*SIN(PHI(J))/COS(PHI(J))
90*      WRITE(2,58) J,THE(J),C(J),CG(J),CK(J),CT(J),PHI(J),(X(L,J),L=1,3),
91*      1(Y(L,J),L=1,3),WN(J),HEWN1(J),HEWN2(J)
92*      58 FORMAT(14,15F9.5)
93*      100 CONTINUE
94*      R=J
95*      IF (ID.NE.200) R=C(21)/C(1)
96*      WRITE(2,59) R
97*      59 FORMAT(5X,17HANISOTROPY RATIO=,F8.4)
98*      105 CONTINUE
99*      106 CONTINUE
100*     102 STOP
101*     END

```

CODELENGTH	775	WORDS
LOCAL WKSPACE	6	WORDS
DYN. ARRAYS	630	WORDS
DATA	0	WORDS

&JOB:ES/R104/C41

&OPTIONS:

&TIME:20;

&FORTRAN;

C 4

&LIST;

```

1* C REFLECTION CHARACTERISTICS FOR DEEP FLUID MHD WAVES
2* SUBROUTINE WAVES(THETA,R01,R02,BE,CUR,EGA,C,CG,PHIB,WNR,ALFA)
3* G=9.81
4* PI=3.14159
5* GAM=BE*CUR*10.0/(C*R01)
6* AB=R01*GAM*COS(THETA)**2
7* A=-(G*(R01-R02+AB)/((R01+R02)*EGA))
8* AC=-(ALFA*EGA/(R01+R02))
9* AP=-(A*A/9)
10* AQ=((A**3)/27.0)*AC/2.0
11* AZ=AP**3+AQ*AQ
12* C THE NEXT SECTION DEALS WITH SPECIAL CASES OF UNSTABLE AND
13* C NOMINALLY UNSTABLE DISPERSIONS
14* IF(CUR.GT.0.0)GO TO 301
15* C THIS ELIMINATES DOWNWARD FORCE FROM OTHER TESTS
16* IF(A.GT.0.0)WRITE(2,56)
17* IF(A.EQ.0.0)WRITE(2,57)
18* 56 FORMAT(18H'NOMINALLY UNSTABLE')
19* 57 FORMAT(27H'NOMINALLY NEUTRAL STABILITY')
20* C TEST FOR VALUE OF Q.
21* IF(AQ)301,302,303
22* C 301 STARTS BASIC CUBIC SOLUTION,NORMAL STABILITY
23* C 302 STARTS SPECIAL SOLUTION WHEN Q=0 (SEE CUBIC SOLN. NOTES)
24* C 303 STARTS SOLUTION WHEN Q POSITIVE
25* 302 C=SQRT(-3.0*AP)-(A/3)
26* WRITE(2,58)
27* 58 FORMAT(25H ' IN CUBIC SOLUTION,Q=0)
28* GO TO 305
29* 303 WRITE(2,59)
30* 59 FORMAT(29H ' IN CUBIC SOLUTION Q G.T.0)
31* IF(AZ.LT.0.0)GO TO 304
32* C IF AZ L.T.0,REQUIRES SPECIAL SOLUTION TO START WITH,JOINING
33* C MAIN SOLN.AT 307. IF G T 0,SITUATION UNSTABLE
34* WRITE(2,60)
35* 60 FORMAT(50X,3HUNSTABLE)
36* GO TO 103
37* 304 PHIL=PI-ATAN(SQRT(-AZ)/AQ)
38* WRITE(2,61)
39* 61 FORMAT(50X,12HSTILL STABLE)
40* GO TO 307
41* 301 IF(AZ)600,601,602
42* 601 U=(-AQ+SQRT(AZ))*0.3333333
43* V=(-AQ-SQRT(AZ))*0.3333333
44* C=U+V-A/3.0

```

```

45*      GO TO 305
46*      600 PHIL=ATAN(SQRT(AZ)/(-AQ))
47*      307 C=2*SQRT(-AP)*COS(PHIL/3,0)-(A/3,0)
48* C      305 STARTS GROUP VELOCITY
49*      305 CK=A/2-1.5*AC/(C**2)
50*      CT=-Q*GAM*SIN(2*THETA)*RQ1/(2*EGA*(RQ1+RQ2))
51*      PHI=ATAN(CT/CK)
52*      PHI3=THETA+PHI
53*      CG=SQRT(CK*CK+CT*CT)
54*      WNR=EGA/C
55*      103 RETURN
56*      END

```

```

CODELENGTH 328 WORDS
LOCAL WKSPCE 52 WORDS
DYN. ARRAYS 0 WORDS
DATA 0 WORDS

```

LABEL	ADDRESS		LABEL	ADDRESS		LABEL	ADDRESS
56	137	**	57	140	**	302	148
303	167	**	59	170	**	60	184
61	199	**	301	203	**	601	207
307	246	**	305	264	**	103	327

```

57*      - FETCH ROOTS,3
58*      DIMENSION B(9),X1(8),X2(8),PLOT1(21),PLOT2(21)
59*      READ(7,50)ALFA,RO1,RO2,BE,CUR
60* C      ALFA IS SURFACE TENSION (N/M)
61* C      RO1 IS LOWER DENSITY,RO2 UPPER,IN SPECIFIC GRAVITY UNITS
62* C      BE IS MAG FIELD IN 4/SQ.M.
63* C      CUR IS CURRENT DENSITY IN MILLIA/SQ.CM -VE DENOTES UPWARDFOR
64*      READ(7,51) EGO
65* C      EGO IS FREQUENCY IN CYCLES/SEC
66* C      ZHETD IS WAVE NO.ANGLE TO BO,ALFDIS MIRROR ANGLE TO B(THETA BTAL
67*      50 FORMAT(F10.6,2F7.4,F8.5,F8.3)
68*      51 FORMAT(F6.2)
69*      WRITE(2,53)ALFA,RO1,RO2,BE,CUR,EGO
70*      53 FORMAT(16HSURFACE TENSION=F10.4,10HN/M RO1=F10.4,10H RO
71*      1,F11.4,19H MAG.FIELD=F8.4,25HNR/SQM,FCURRENT DENSITY=F
72*      2,3,16HMILLIAMPS/SQ.CM,,1H0,9HFREQUENCY,F6.3,10HCYCLES/SEC)
73*      IF(CUR.GT.0.0)WRITE(2,54)
74*      IF(CUR.LT.0.0)WRITE(2,55)
75*      54 FORMAT(14HDOWNWARD FORCE)
76*      55 FORMAT(12HUPWARD FORCE)
77*      S=6.0
78*      CALL MOVE(0,1200)
79*      CALL ORIGIN(1200,0)
80*      INP=0
81*      44 CALL DRAW(0,-1000)
82*      DO 10 I=1,19
83*      IAN=-90+10*(I-1)
84*      CALL MOVE(S,(6*IAN))
85*      CALL CENCH(1)
86*      CALL MOVE(-40,6*IAN)
87*      CALL WAY(0,3)
88*      40 WRITE(9,41)IAN
89*      41 FORMAT(I3)
90*      CALL MOVE(0,1000)
91*      CALL DRAW(0,0)
92*      CALL DRAW(-1000,0)
93*      DO 21 I=1,19
94*      IAN=-90+10*(I-1)
95*      CALL MOVE(6*IAN,0)
96*      CALL CENCH(1)
97*      CALL MOVE(6*IAN,-30)
98*      421 WRITE(9,41)IAN
99*      CALL MOVE(1000,0)
100*      CALL DRAW(0,0)
101*      CALL MOVE(100,2)
102*      CALL WAY(0,5)
103*      WRITE(9,42)
104*      42 FORMAT(18HANGLE OF INCIDENT
105*      CALL MOVE(40,200)
106*      CALL WAY(1,5)
107*      WRITE(9,43)
108*      43 FORMAT(19HANGLE OF REFLECTI
109*      IF(INP.GQ.1)GO TO 45
110*      CALL MOVE(-800,600)
111*      CALL WAY(0,20)
112*      CALL MOVE(-1000,1225)
113*      CALL WAY(0,5)
114*      WRITE(9,47)ALFA,RO1,RO2

```

```

115* 47 FORMAT(16HS IFFACE TENSION=,F8.4,17HM/M, UPPER S.G.,F7.4,13H LOW
116* 1ER S.G.,F7.4)
117* CALL MOVE(-1000,1175)
118* WRITE(9,48)CUR,RE,EO
119* 48 FORMAT(10HCHR,DENS.,F7.2,24HMILLIA/SQ.CH MAG FIELD=,F6.3,20HMB/S
120* 1Q.M. FREQUENCY=,F7.3,1H CYCLES/SEC)
121* CALL MOVE(0,2400)
122* CALL ORIGIN(1200,0)
123* CALL MOVE(-800,600)
124* CALL WAY(0,20)
125* CALL MOVE(600,-600)
126* CALL WAY(0,5)
127* WRITE(9,491)
128* 491 FORMAT(25HMIRROR ANGLE TO MAG FIELD)
129* DO 492 J=1,9
130* IALFD=-45+(J-1)*15
131* CALL MOVE(600,-(600+50*J))
132* CALL CENCH(J)
133* CALL MOVE(650,-(600+50*J))
134* 492 WRITE(9,493)IALFD
135* 493 FORMAT(13,84 DEGREES)
136* INP=1
137* CALL MOVE(0,0)
138* GO TO 44
139* 45 CALL MOVE(0,-2400)
140* CALL ORIGIN(1200,0)
141* R01=R01*1000.0
142* R02=R02*1000.0
143* DO 105 J=1,9
144* ALFD=-45+(J-1)*15
145* WRITE(2,56)ALFD
146* 56 FORMAT(26HMIRROR ANGLE TO MAG FIELD=,F6.1,7HDEGREES)
147* WRITE(2,80)
148* 80 FORMAT(1H0,7X,1HC,9X,5HTHETD,6X,5HRINCD,8X,2HWN,10X,2HCG,8X,5H GVI
149* 1D,8X,5HCHECK,9X,2HCR,8X,6HTHETAD,6X,5HREFLD,7X,4HNER,11X,3HCGR,6X
150* 2,4HGRD)
151* G=9.81
152* PI=3.14159
153* EGA=EG0*2*PI
154* ALF=PI*ALFD/180.0
155* GLO7=90
156* DO 104 ID=1,21
157* THETD=ALFD+180.0*(ID-1)/20.0
158* THETA=PI*THETD/180.0
159* CALL WAVES(THETA,R01,R02,8E,CUR,EGA,C,CG,PHIB,WNR,ALFA)
160* PHID=PHIB*180.0/PI
161* GVID=90.0-PHID+ALFD
162* RINCD=90.0-THETD+ALFD
163* WN=EG0/C
164* WK1=WNR*COS(THETA-ALF)
165* WK2=WNR*SIN(THETA-ALF)
166* N=8
167* IF(ALFA.EQ.0.00)N=4
168* DS=(R01+R02)
169* DD=(R01-R02)
170* BA=CUR*BE*10.0
171* Z8=ALFA*ALFA
172* Z6=.0*ALFA*DD*G
173* Z4=2.0*ALFA*BA*WK1*WK1*COS(ALF)*COS(ALF)+DD*DD*G*G
174* Z41=-2.0*ALFA*BA*WK1*SIN(ALF*2.0)

```

```

175* Z42=2.0*ALFA*BA*SIN(ALF)*SIN(ALF)
176* Z2=2.0*BA*G*DD*WK1*WK1*COS(ALF)*COS(ALF)-EGA**4.0*DS*DS
177* Z21=-2.0*BA*G*DD*WK1*SIN(ALF*2.0)
178* Z22=2.0*BA*G*DD*SIN(ALF)*SIN(ALF)
179* WK3=WK1*WK1
180* Z0=BA*BA*WK3**2.0*COS(ALF)**4.0
181* Z01=-4.0*BA*BA*WK1*WK3 *COS(ALF)**3.0*SIN(ALF)
182* Z02=3.0*BA*BA*WK1*WK1*SIN(2*ALF)*SIN(2*ALF)/2.0
183* Z03=-4.0*BA*BA*WK1*COS(ALF)*SIN(ALF)*SIN(ALF)*SIN(ALF)
184* Z04=BA*BA*SIN(ALF)*SIN(ALF)*SIN(ALF)*SIN(ALF)
185* B(9)=78
186* B(8)=0
187* B(7)=4.0*Z8*WK1*WK1+Z6+Z42
188* B(6)=241
189* B(5)=6.0*Z8*WK3**2.0+3.0*Z6*WK1*WK1+Z4+Z42*WK1*WK1*2.0+Z0+Z22
190* B(4)=241*WK1*WK1*2.0+Z03+Z21
191* B(3)=4.0*Z8*WK3**3.0+3.0*Z6*WK3**2.0+2.0*Z4*WK1*WK1+Z02*WK3**2.0+Z
192* 12+Z22*WK1*WK1+Z02
193* B(2)=741*WK3**2.0+Z21*WK1*WK1+Z01
194* B(1)=78*WK3**4.0+Z6*WK3**3.0+Z4*WK3**2.0+Z2*WK1*WK1+Z0
195* MAXIT=100
196* CALL ROOTS(N,B,MAXIT,X1,X2,PR,PT,BC,BI,WFND,EPS,NSW)
197* IN=0
198* DO 700 I=1,WFND
199* IF(X2(I),NE.0.00)GO TO 700
200* DIANE=ABS(X1(I)-WK21)
201* IF(DIANE,LT.0.10)ALT=X1(I)
202* IF(DIANE,LT.0.10)GO TO 700
203* WK2R=X1(I)
204* IN=IN+1
205* 700 CONTINUE
206* IF(IN,NE.1)WRITE(2,70)IN, ID
207* 70 FORMAT(1H0,3HIN=,I2,18HTOO MANY ROOTS, ID=,I2)
208* DREGS=-WK1/WK2R
209* IF(DREGS,LT.0.000)REFL=-ATAN(-DREGS)
210* IF(DREGS,GT.0.000)REFL=ATAN(DREGS)
211* REFLD=180.0*REFL/PI
212* IF(RINCD,GT.0.1.AND.REFLD,LT.0.0)REFLD=REFLD+180
213* IF(RINCD,LT.-0.1.AND.REFLD,GT.0.0)REFLD=REFLD-180
214* WNRZ=SQRT(WK1*WK1+WK2R*WK2R)
215* THETA=PI/2.0-ALF-REFL
216* CALL WAVES (THETA,R01,R02,DE,CUR,EGA,CR,CGR,PHIBR,WNR,ALFA)
217* PHIDR=PHIBR*180.0/PI
218* GVRD=90.0-ALFD-PHIDR
219* IF (GVID,LT.0.0.AND.GLOB,LT.0.0.AND.GVRD,GT.0.0)GVRD=GVRD-180
220* IF (GVID,GT.0.0.AND.GVRD,LT.0.0.AND.GLOB,GT.20.0)GVRD=GVRD+180
221* CHECK=WNR/WNRZ
222* WNEZ=WNR*0.5/PI
223* THETA=THETA*180.0/PI
224* WRITE(2,71)C,THETA,RINCD,WN,CG,GVID,CHECK,CR,THETA,REFLD,WNR,CGN
225* 1,GVRD
226* 71 FORMAT(13F12.6)
227* IF(ID,NE.1)GO TO 30
228* CALL MOVE(IFIX(S*RINCD),IFIX(S*REFLD))
229* 30 IF(ABS(GVID).GT.99.0)GO TO 31
230* CALL DRAW(IFIX(S*RINCD),IFIX(S*REFLD))
231* GO TO 33
232* 31 CALL MOVE(IFIX(S*RINCD),IFIX(S*REFLD))
233* 33 CALL CENCH(J)
234* PLOTI(ID)=GVID

```

```

235* PLOTR(I)=QVRD
236* GLOT=GVRD
237* 104 CONTINUE
238* CALL MOVE(0,2400)
239* CALL ORIGIN(1200,0)
240* CALL MOVL(IFIX(S*PLOTI(1)),IFIX(S*PLOTR(1)))
241* DO 32 I=2,21
242* CALL DRAW(IFIX(S*PLOTI(1)),IFIX(S*PLOTR(1)))
243* 32 CALL CENCH(I)
244* CALL MOVE(0,-2400)
245* CALL ORIGIN(1200,0)
246* 105 CONTINUE
247* CALL MOVE(0,4800)
248* CALL ORIGIN(1200,0)
249* 103 STOP
250* END

```

```

CODELENGTH 1241 WORDS
LOCAL WKSPE 159 WORDS
DYN, ARRAYS 134 WORDS
DATA 0 WORDS

```

LABEL	ADDRESS		LABEL	ADDRESS		LABEL	ADDRESS
50	24	**	51	27	**	53	33
55	60	**	44	79	**	40	116
421	170	**	42	205	**	43	223
48	272	**	491	314	**	492	314
45	364	**	56	393	**	80	399
70	902	**	71	1072	**	30	1092
33	1123	**	104	1139	**	32	1194
103	1237	**			**		

---

JOB:ES/R104/C5;  
 OP

OPTIONS:

FORTRAN:

*c5*

LINES:24001

```

LIST:
1* SUBROUTINE DERIVS (G0,G3,G2,X1,WK1,WK2,DX1DX,DX2DX,DKDX1,DKDX2,D2
2* 1X1,D2X2)
3* C THIS SUBROUTINE OBTAINS VARIOUS DERIVATIVES,5 INPUTS,6 OUTPUTS
4* WK=SQRT(WK1*WK1+WK2*WK2)
5* G=G0+G3*X1+G2*X1*X1
6* G1=G3+G2*X1*2.0
7* IF(ABS(WK1).LT.0.00001)GO TO 10
8* DKDX1=WK2*WK2*WK*WK*G1/(WK1*WK*WK+G*WK2*WK2*WK1)
9* C DKDX1 IS THE FIRST DERIVATIVE OF K1 WITH RESPECT TO X1
10* 11 DKDX2=WK2*WK2*WK*WK*G1/(WK2*WK*WK+G*(WK2*WK2*WK2-2.0*WK2*WK*WK))
11* IF(ABS(WK1).LT.0.00001)GO TO 12
12* C DKDX2 IS THE FIRST DERIVATIVE OF K1 WITH RESPECT TO X2
13* DX1DX=DKDX2/DKDX1
14* C DX1DX IS THE FIRST DERIVATIVE OF X1 WITH RESPECT TO X2 AND VICE
15* DX2DX=1.0/DX1DX
16* C DK1 AND DK2 ARE DERIVATIVES OF K W.R.T.X1 AND X2
17* 12 DK1=WK1*DKDX1/WK
18* DK2=WK1*DKDX2/WK
19* D2X1=((DKDX2*WK*WK+WK1*WK2*DK2+G*WK2*WK2*DKDX2+WK2*WK2*WK1*G1*D
20* 1X1DX)*(WK2*WK*WK+G*(WK2*WK2*WK2-2*WK2*WK*WK))-(WK1*WK*WK+G*WK1*WK2
21* 2*WK2)*(2*WK*WK2*DK2-G*4*WK*WK2*DK2+(WK2*WK2*WK2-2*WK2*WK*WK)*G1*DX
22* 31DX))/(WK2*WK*WK+G*(WK2*WK2*WK2-2*WK2*WK*WK))*(WK2*WK*WK+G*(WK2*W
23* 4K2*WK2-2*WK2*WK*WK))
24* IF(ABS(WK1).LT.0.00001)GO TO 13
25* C D2X2 IS THE SECOND DERIVATIVE OF X2 W.R.T. X1
26* D2X2=((2*WK*WK2*DK1+G1*(WK2*WK2*WK2-2*WK2*WK*WK)-G*4*WK2*WK*DK1)*
27* 1WK1*WK*WK+G*WK2*WK2*WK1)-(2*WK*WK1*DK1+WK*WK*DKDX1+G1*WK2*WK2*WK1
28* 2+G*WK2*WK2*DKDX1)*(WK2*WK*WK+G*(WK2*WK2*WK2-2*WK2*WK*WK)))/((WK*WK
29* 3*WK1+G*WK2*WK2*DK1)*(WK*WK*WK1+G*WK2*WK2*WK1))
30* GO TO 13
31* 10 DX1DX=0
32* DX2DX=1
33* DKDX1=1.0
34* D2X2=1.000
35* GO TO 11
36* 13 RETURN
37* END
  
```

CODELENGTH 388 WORDS  
 LOCAL WKSPACE 62 WORDS  
 DYN. ARRAYS 0 WORDS

```

38* C THIS PROGRAMME DETERMINES THE GROUP VELOCITY PROPAGATION RAYS AND TH
39* C VARIATION OF WAVE NUMBER ALONG THEM FOR MHD ANISOTROPIC SURFACE WAVES
40* C  $EGA**2 = k*(1 - (G1*X1 + G2)*K2**2/K**2)$  THIS IS OUR DISPERSION RELATION
41* C 1 IS THE J DIRECTION, 2 IS THE H DIRECTION
42* DIMENSION X1(20,20), X2(20,20), WK1(20,20), WK2(20,20)
43* G=9.31
44* PI=3.14159
45* READ(7,70) EGA, G0, G1, G2, SA, SB
46* C EGA IS FREQUENCY IN RADS/SEC, G1 AND G2 ARE CONSTANTS OF ANISOTROPY SIN
47* C THE DISPERSION RELATION, SA AND SB ARE CONSTANTS IN EQUATION OF LINE SOU
48* C  $X2 = SA*X1 + SB$ 
49* 70 FORMAT(6F12.6)
50* WRITE(2,80) EGA, G0, G1, G2
51* 80 FORMAT(4HEGA=, F12.6, 6HGAMMA=, F8.4, 4HPLUS, F8.4, 4H*X2=, F8.4, 6H*X1**2
52* 1)
53* WRITE(2,81) SA, SB
54* 81 FORMAT(20HLINESOURCE IS X2=X1*, F9.6, 4H + , F9.6)
55* THETA = -ATAN(SA)
56* SCM=0
57* DO 100 I=1,20
58* X22=I/20.0
59* IF (ABS(SA).GE.1.0) X11=(X22-SB)/SA
60* IF (ABS(SA).LT.1.0) X11=I/20.0
61* GUS=G0+G1*X11+G2*X11*X11
62* WK=EGA*EGA/(G*(1-COS(THETA)*COS(THETA)*GUS))
63* WK1(I,1)=WK*SIN(THETA)
64* WK2(I,1)=WK*COS(THETA)
65* X1(I,1)=X11
66* X2(I,1)=SA*X11+SB
67* DO 101 J=2,20
68* BX1=X1(I,J-1)
69* BX2=X2(I,J-1)
70* BKX1=BKX1+WK1(I,J-1)
71* WK2(I,J)=WK2(I,J-1)
72* PE=1
73* P=0.05
74* JAM=0
75* JIT=0
76* 100 CALL DERIVS (G0,G1,G2,BX1 ,BKX1 ,WK2(I,J-1),D1,D2,D3,D4
77* 1,D5,D6)
78* IF (D1/D2-1.00) 200,200,201
79* 200 AX2=BX2+P
80* AX1=BX1+P*(D1+D5*P/2.0)
81* AKX1=BKX1+P*D4
82* CALL DERIVS (G0,G1,G2,AX1 ,AKX1 ,WK2(I,J),DC1,DC2,DC3,DC4,D
83* 105,DC6)
84* IF (ABS(D1).LT.0.00001) GO TO 71
85* IF (ABS((DC1-D1-P*05)*100.0/D1)-1) 111,111,202
86* 71 IF (ABS(DC1).LT.0.00001) GO TO 111
87* IF (ABS((DC1-I*D5)*100.0/DC1)-1.0) 111,111,202
88* 202 P=P/2
89* JAM=JAM+1
90* JIT=JIT+1
91* IF (JIT.NE.10) GO TO 200
92* WRITE(2,21) I , J
93* 21 FORMAT(18HNOT CONVERGING, I=, I2, 3H J=, I2)
94* GO TO 100
95* 201 CONTINUE
96* IF (J.EQ.2) GO TO 401
97* IF (D2.LT.0.0.AND.X1(I,J-1).LT.X1(I,J-2)) P=-P

```

```

08* GO TO 301.
09* 401 IF (D2.LT.0.0)P=-P
100* 301 AX1=BX1+P
101* AX2=BX2+P*(D2+D6+P/2,0)
102* AKX1=BKX1+P*D3
103* CALL DERIVS (G0,G1,G2,AX1 ,AKX1 ,WK2(I,J),DC1,DC2,DC3,DC4,D
104* 105,DC6)
105* IF (ABS((DC2-D2-P*96)*100,0/D2)-1)111,111,203
106* 203 P=P/2
107* JIT=JIT+1
108* JAM=JAM+1
109* IF (JIT.NE.10)GO TO 301
110* WRITE(2,21)I,J
111* GO TO 100
112* 111 IF (P.LT.0.0)P=-P
113* PE=PE+P
114* IF (PE.GE.0.05) GO TO 110
115* IF (JAM.GE.20)GO TO 110
116* BX1=AX1
117* BX2=AX2
118* BKX1=AKX1
119* P=P*2.0
120* JIT=JIT-1
121* GO TO 109
122* 110 X1(I,J)=AX1
123* X2(I,J)=AX2
124* IF (SCM.LT.X1(I,J))SCM=X1(I,J)
125* IF (SCM.LT.X2(I,J))SCM=X2(I,J)
126* WK1(I,J)=AKX1
127* 101 CONTINUE
128* 100 CONTINUE
129* WRITE(2,23)
130* 23 FORMAT(4HX1..)
131* DO 103 J=1,20
132* 103 WRITE(2,22)(X1(I,J),I=1,20)
133* 22 FORMAT(20F9.4)
134* WRITE(2,24)
135* 24 FORMAT(4HX2..)
136* DO 104 J=1,20
137* 104 WRITE(2,22)(X2(I,J),I=1,20)
138* WRITE(2,25)
139* 25 FORMAT(5HWK1..)
140* DO 105 J=1,20
141* 105 WRITE(2,22)(WK1(I,J),I=1,20)
142* WRITE(2,26)
143* 26 FORMAT(5HWK2..)
144* DO 106 J=1,20
145* 106 WRITE(2,22)(WK2(I,J),I=1,20)
146* SC= 900.0/SCM
147* C SC IS A SCALING FACTOR PRODUCING MAX DISPLACEMENT FROM ORIGIN OF 6
148* CALL ORIGIN(250,0)
149* CALL DRAW(1400,0)
150* CALL MOVE(0,-800)
151* CALL DRAW(0,1400)
152* CALL MOVE(200,-100)
153* CALL WAY(0,10)
154* WRITE(2,90)
155* 90 FORMAT(15HX1, J DIRECTION)
156* CALL MOVE(-40,200)
157* CALL WAY(1,10)

```

```

158* WRITE(9,91)
159* 91 FORMAT(15HX2, B DIRECTION)
160* ICENT=IFIX(SC)
161* IHALF=IFIX(SC/2.0)
162* CALL MOVE(IHALF,0)
163* CALL GENCH(1)
164* CALL MOVE(IHALF,-30)
165* CALL WAY(0,5)
166* WRITE(9,92)
167* 92 FORMAT(10H0.5 METRES)
168* CALL MOVE(ICENT,0)
169* CALL GENCH(1)
170* CALL MOVE(ICENT,-30)
171* WRITE(9,93)
172* 93 FORMAT(10H1.0 METRES)
173* CALL MOVE(0,IHALF)
174* CALL GENCH(1)
175* CALL WAY(1,5)
176* CALL MOVE(-10,IHALF)
177* WRITE(9,92)
178* CALL MOVE(0,ICENT)
179* CALL GENCH(1)
180* CALL MOVE(-10,ICENT)
181* WRITE(9,93)
182* CALL MOVE(0,0)
183* CALL DRAW(IFIX(SC*X1(20,1)),IFIX(SC*X2(20,1)))
184* C SCW IS A SCALE FACTOR TO MAKE PHASE VELOCITY(WAVE NUMBER) ARROWS ABOUT
185* C ONE TENTH OF AN INCH LONG
186* DO 900 I=1,20
187* CALL MOVE(IFIX(SC*X1(I,1)),IFIX(SC*X2(I,1)))
188* DO 901 J=1,20
189* W=SQRT(WK1(I,J)*WK1(I,J)+WK2(I,J)*WK2(I,J))
190* SCW=7.5/W
191* CALL DRAW(IFIX(SC*X1(I,J)),IFIX(SC*X2(I,J)))
192* CALL MOVE(IFIX(SC*X1(I,J)-SCW*WK2(I,J)),IFIX(SC*X2(I,J)+SCW*WK1(I,
193* 1J)))
194* CALL DRAW(IFIX(SC*X1(I,J)+SCW*WK2(I,J)),IFIX(SC*X2(I,J)-SCW*WK1(I,
195* 1J)))
196* 901 CALL MOVE(IFIX(SC*X1(I,J)),IFIX(SC*X2(I,J)))
197* 900 CONTINUE
198* CALL MOVE(0,2200)
199* CALL ORIGIN(250,0)
200* CALL DRAW(1200,0)
201* CALL MOVE(0,0)
202* CALL DRAW(0,500)
203* CALL MOVE(0,IFIX(500*G0))
204* DO 9 M=1,20
205* 9 CALL DRAW((ICENT+M/20),IFIX(500*(G0+G1*M/20+G2*M*M/400)))
206* CALL MOVE (-100,600)
207* CALL DRAW (1800,600)
208* CALL MOVE (0,2000)
209* 8 STOP
210* END

```

CODELENGTH	1104	WORDS
LOCAL WKSPACE	103	WORDS
DYN. ARRAYS	3200	WORDS
DATA	0	WORDS

JOB:ES/R104/C7:

TIME:10:

OPTIONS:

FORTRAN:

C7

LIST:

```

1*      FUNCTION PHIL(THI,GAM)
2*      PHIL=THI+ATAN(GAM*SIN(2*THI)/(1+GAM*COS(THI)*COS(THI)))
3*      RETURN
4*      END

```

```

CODELENGTH  32      WORDS
LOCAL WKSPCE 12      WORDS
DYN, ARRAYS  0      WORDS
DATA         0      WORDS

```

```

5*      SUBROUTINE RAYS (GAM,N,T)
6*      DIMENSION T(25)
7*      PI=3.14159
8*      DO 10 J=1,N
9*      THI=PI*(J-1)/FLOAT(N*2)
10*     T(J)=THI
11*     11 T(J)=T(J)+THI-PHIL(T(J),GAM)
12*     IF (ABS(THI-PHIL(T(J),GAM)).GE.(PI/FLOAT(100*N))) GO TO 11
13*     10 CONTINUE
14*     IF (N.EQ.25) GO TO 12
15*     JA=1+N
16*     DO 13 J=JA,25
17*     13 T(J)=0
18*     12 RETURN
19*     END

```

```

CODELENGTH  118     WORDS
LOCAL WKSPCE 17     WORDS
DYN, ARRAYS  0     WORDS
DATA         0     WORDS

```

LABEL	ADDRESS	LABEL	ADDRESS	LABEL	ADDRESS
11	36	10	82	13	99
	**		**		**
	**		**		**

```

20* SUBROUTINE DERIVS (G0,G1,G2,X1,WK1,WK2,DX1DX,DX2DX,DKDX1,DKDX2,D2
21* 1X1,D2X2)
22* C THIS SUBROUTINE OBTAINS VARIOUS DERIVATIVES,5-INPUTS,6-OUTPUTS
23* WK=SQRT(WK1*WK1+WK2*WK2)
24* G=G0+G1*X1+G2*X1*X1
25* G1=G1+G2*X1
26* IF(ABS(WK1).LT,.00001)GO TO 10
27* DKDX1=WK2*WK2*WK*WK*G1/(WK1*WK*WK+G*WK2*WK2*WK1)
28* C DKDX1 IS THE FIRST DERIVATIVE OF K1 WITH RESPECT TO X1
29* 11 DKDX2=WK2*WK2*WK*WK*G1/(WK2*WK*WK+G*(WK2*WK2*WK2-2,.0*WK2*WK*WK))
30* IF(ABS(WK1).LT,.00001)GO TO 12
31* C DKDX2 IS THE FIRST DERIVATIVE OF K1 WITH RESPECT TO X2
32* DX1DX=DKDX2/DKDX1
33* C DX1DX IS THE FIRST DERIVATIVE OF X1 WITH RESPECT TO X2 AND DX2DX VICE
34* DX2DX=1.0/DX1DX
35* C DK1 AND DK2 ARE DERIVATIVES OF K W.R.T,X1 AND X2
36* 12 DK1=WK1*DKDX1/WK
37* DK2=WK1*DKDX2/WK
38* D2X1=((DKDX2*WK*WK+WK1*WK*2*DK2+G*WK2*WK2*DKDX2+WK2*WK2*WK1*G1*D
39* 1X1DY)*(WK2*WK*WK+G*(WK2*WK2*WK2-2*WK2*WK*WK))-(WK1*WK*WK+G*WK1*WK2
40* 2*WK1)*(2*WK*WK2*DK2-G*4*WK*WK2*DK2+(WK2*WK2*WK2-2*WK2*WK*WK)*G1*DX
41* 31DX))/((WK2*WK*WK+G*(WK2*WK2*WK2-2*WK2*WK*WK))*(WK2*WK*WK+G*(WK2*W
42* 4K2*WK2-2*WK2*WK*WK)))
43* IF(ABS(WK1).LT,.00001)GO TO 13
44* C D2X2 IS THE SECOND DERIVATIVE OF X2 W.R.T, X1
45* D2X2=((2*WK*WK2*DK1+G1*(WK2*WK2*WK2-2*WK2*WK*WK))-G*4*WK2*WK*DK1)*{
46* 1WK1*WK*WK+G*WK2*WK2*WK1)-(2*WK*WK1*DK1+WK*WK*DKDX1+G1*WK2*WK2*WK1
47* 2+G*WK2*WK2*DKDX1)*(WK2*WK*WK+G*(WK2*WK2*WK2-2*WK2*WK*WK)))/((WK*WK
48* 3*WK1+G*WK2*WK2*WK1)*(WK*WK*WK2+G*WK2*WK2*WK1))
49* GO TO 13
50* 10 DX1DX=0
51* DX2DX=1
52* DKDX1=1.0
53* D2X2=1.000
54* GO TO 11
55* 13 RETURN
56* END

```

```

CODELENGTH 388 WORDS
LOCAL WKSPACE 60 WORDS
DYN, ARRAYS 0 WORDS
DATA 0 WORDS

```

LABEL	ADDRESS	LABEL	ADDRESS	LABEL	ADDRESS
11	77	**	12	**	10
		**		**	372

```

57* DIMENSION TH(10), X1(20,20), X2(20,20), WK1(20,20), WK2(20,20)
58* READ(7,70) EGA, G0, G1, G2, A1, A2
59* 70 FORMAT(6F12.6)
60* N=17
61* GAM=G0+G1*A1+G2*A1*A1
62* CALL RAYS(GAM, N, TH)
63* JD=3*N-1
64* DO 100 J=1, JD
65* IF(J.LE.N) JE=J
66* IF(J.GT.N) JE=J-N+1
67* WK=EGA*EGA/(9.81*(1-COS(TH(JE))*COS(TH(JE))*GAM))
68* WK2(1, J)=WK*COS(TH(JE))
69* IF(J.LE.N) WK1(1, J)=WK*SIN(TH(JE))
70* IF(J.GT.N) WK1(1, J)=- (WK*SIN(TH(JE)))
71* X1(1, J)=A1
72* X2(1, J)=A2
73* WRITE(2,22) J
74* 22 FORMAT(3H J=,I2)
75* WRITE(2,23)
76* 23 FORMAT(45H I X1 X2 WK1 WK2 )
77* DO 101 I=1,19
78* P=0
79* PE=.05
80* AX1=X1(I, J)
81* AX2=X2(I, J)
82* AK1=WK1(I, J)
83* AK2=WK2(I, J)
84* 12 CALL DERIVS(G0, G1, G2, AX1, AK1, AK2, D1, D2, D3, D4, D5, D6)
85* JIT=0
86* IF(ABS(D1).GT,ABS(D2)) GO TO 10
87* 13 PED=PE*1/SQRT(1+D1*D1)
88* B2=AX2+PED
89* B1=AX1+PED*D1+PED*PED*D5/2.0
90* BK1=PED*D4+AK1
91* BK2=AK2
92* CALL DERIVS(G0, G1, G2, B1, BK1, BK2, DC1, DC2, DC3, DC4, DC5, DC6)
93* HOPB=ABS(D1+PED*D5-DC1)/ABS(DC1)
94* IF(HOPB,LT,0.01) GO TO 11
95* PE=PE/2.0
96* JIT=JIT+1
97* IF(JIT,LE,10) GO TO 13
98* 17 WRITE(2,20) J
99* 20 FORMAT(20HNOT CONVERGING, RAY ,I2)
100* DO 16 IY=1,19
101* WK1(IY+1, J)=0
102* WK2(IY+1, J)=0
103* X1(IY+1, J)=0
104* 16 X2(IY+1, J)=0
105* GO TO 100
106* 10 PED=PE*1/SQRT(1+D2*D2)
107* IF(J.GT,N) PED=- (PE*1/SQRT(1+D2*D2))
108* B1=PED+AX1
109* B2=AX2+PED*D2+PED*PED*D6/2.0
110* BK1=PED*D3+AK1
111* BK2=AK2
112* CALL DERIVS(G0, G1, G2, B1, BK1, BK2, DC1, DC2, DC3, DC4, DC5, DC6)
113* IF((ABS(D2+PED*D6-DC2)/ABS(DC2)),LT,0.01) GO TO 11
114* PE=PE/2.0
115* JIT=JIT+1
116* IF(JIT,LE,10) GO TO 10

```

```

117*      GO TO 17
118*      11 P=P*PP
119*      IF(P.GE.0.05)GO TO 14
120*      AX1=B1
121*      AX2=B2
122*      AK1=BK1
123*      AK2=BK2
124*      PE=.025
125*      GO TO 12
126*      14 WK1(I+1,J)=BK1
127*      WK2(I+1,J)=BK2
128*      X1(I+1,J)=B1
129*      X2(I+1,J)=B2
130*      WRITE(2,21)I,X1(I,J),X2(I,J),WK1(I,J),WK2(I,J)
131*      ILL=20
132*      IF(I.EQ.19)WRITE(2,21)ILL,X1(20,J),X2(20,J),WK1(20,J),WK2(20,J)
133*      21 FORMAT(I3,4F11.5)
134*      101 CONTINUE
135*      100 CONTINUE
136*      SCM=X2(20,1)
137*      IF(X1(20,N).GT.SCM)SCM=X1(20,N)
138*      IF(X1(20,JD).GT.SCM)SCM=X1(20,JD)
139*      SC=-750.0/SCM
140*      CALL ORIGIN(1200,0)
141*      CALL DRAW(1200,0)
142*      CALL MOVE(0,0)
143*      CALL DRAW(0,600)
144*      CALL MOVE(200,-100)
145*      CALL WAY(0,10)
146*      WRITE(9,90)
147*      90 FORMAT(15HX1, J DIRECTION)
148*      CALL MOVE(-40,200)
149*      CALL WAY(1,10)
150*      WRITE(9,91)
151*      91 FORMAT(15HX2, B DIRECTION)
152*      ICENT=IFIX(SC)
153*      IHALF=IFIX(SC/2.0)
154*      CALL MOVE(IHALF,0)
155*      CALL CENCH(1)
156*      CALL MOVE(IHALF,-30)
157*      CALL WAY(0,5)
158*      CALL MOVE(ICENT,0)
159*      CALL CENCH(1)
160*      CALL MOVE(ICENT,-30)
161*      WRITE(9,93)
162*      93 FORMAT(10H1.0 METRES)
163*      CALL MOVE(0,IHALF)
164*      CALL CENCH(1)
165*      CALL WAY(1,5)
166*      CALL MOVE(-10,IHALF)
167*      CALL MOVE(-10,ICENT)
168*      WRITE(9,93)
169*      CALL MOVE(0,ICENT)
170*      CALL CENCH(1)
171*      W=SQRT(WK1(1,1)*WK1(1,1)+WK2(1,1)*WK2(1,1))
172*      SCW=15.0/W
173*      DO 200 J=1,JD
174*      CALL MOVE(0,0)
175*      DO 201 I=1,20
176*      CALL DRAW(IFIX(SC*X1(I,J)),IFIX(SC*X2(I,J)))

```

```

177* CALL MOVE(IFIX(SC*X1(I,J)+SCW*WK2(I,J)),IFIX(SC*X2(I,J)-SCW*WK1(I,
178* 1J)))
179* CALL DRAW(IFIX(SC*X1(I,J)-SCW*WK2(I,J)),IFIX(SC*X2(I,J)+SCW*WK1(I,
180* 1J)))
181* 901 CALL MOVE(IFIX(SC*X1(I,J)),IFIX(SC*X2(I,J)))
182* 900 CONTINUE
183* CALL MOVE(0,1400)
184* CALL ORIGIN(1200,0)
185* CALL MOVE(1200,0)
186* CALL DRAW(-1200,0)
187* CALL MOVE(0,500)
188* CALL CENCH(1)
189* CALL MOVE(0,600)
190* CALL DRAW(0,0)
191* CALL MOVE(0,IFIX(500*G0))
192* DO 7 M=1,20
193* 9 CALL DRAW((ICENT*M/20),IFIX(500*(G0+G1*M/20,0+G2*M*M/400,0)))
194* CALL MOVE(0,IFIX(500*G0))
195* DO 8 M=1,20
196* 8 CALL DRAW(-(ICENT*M/20),IFIX(500*(G0-G1*M/20,0+G2*M*M/400,0)))
197* CALL MOVE(0,2000)
198* STO?
199* END

```

```

CODELENGTH 1084 WORDS
LOCAL WKSPCE 100 WORDS
DYN, ARRAYS 3220 WORDS
DATA 0 WORDS

```

LABEL	ADDRESS		LABEL	ADDRESS		LABEL	ADDRESS
70	20	**	22	169	**	23	175
13	235	**	17	305	**	20	308
10	367	**	11	459	**	14	485
101	544	**	100	549	**	90	648
93	709	**	901	898	**	900	920
8	1031	**			**		

OBJECTS/R104/F1:

OPTIONS:

F1

ORTRAN:

LIST:

```

1*   DIMENSION X(37),Y(37)
2*   REAL(7,20)GAM
3*   C GAM + = DOWNWARD FORCE
4*   C GAM - = UPWARD FORCE
5*   20 FOR IAT(F8.4)
6*   IF (GAM.EQ.0.000)ALFA=0.0
7*   IF(GAM.EQ.0.000) GO TO 12
8*   DO 102 J=1,8
9*   ALFA=30+15*J
10*  12 WRITE(2,21)GAM,ALFA
11*  21 FORMAT(7HGMMA= ,F8.4,6HALFA= ,F8.4)
12*  WRITE(2,23)
13*  23 FOR IAT(40H TED BETAD XI YI MAX )
14*  PI=3.14159
15*  ALF=ALFA*PI/180.0
16*  X(1)=1.0
17*  Y(1)=0.0
18*  AMX=1.0
19*  DO 100 I=1,36
20*  THETD=5*I-95-ALFA
21*  THE=THETD*PI/180.0
22*  A=1+GAM*COS(THE)*COS(THE)
23*  PHI=THE+ALF-ATAN(GAM*SIN(2*THE)/A)
24*  EL=COS(ALF+THE)*SQRT(A*A+GAM*GAM*SIN(2*THE)*SIN(2*THE))/(2*A)
25*  B=EL*SIN(PHI)/SQRT(1-EL*EL-2*EL*COS(PHI))
26*  BETA=ATAN(B/SQRT(1-B*B))
27*  BETAD=BETA*180/PI
28*  TED=THETD+ALFA
29*  TE=THE+ALF
30*  IF(I.EQ.1) GO TO 101
31*  T=(TI+TE)/2.0
32*  IF(I.EQ.2)X(I)=ABS(1.0/(1-SIN(BETA)*SIN(T)/(COS(BETA)*COS(T))))
33*  IF(I.EQ.2)GO TO 39
34*  X(I)=(X(I-1)+Y(I-1)*SIN(T)/COS(T))/(1-SIN(BETA)*SIN(T)/(COS(BETA)*
35*  COS(T)))
36*  30 Y(I)=(X(I)*SIN(BETA)/COS(BETA))
37*  IF(AMX.LT.X(I))AMX=X(I)
38*  IF(AMX.LT.Y(I))AMX=Y(I)
39*  101 TI=TE
40*  100 WRITE(2,22)TED,BETAD,X(I),Y(I),AMX
41*  22 FOR IAT(2F8.4,3F8.2)
42*  S=600.0/AMX
43*  WRITE(2,24)S
44*  24 FOR IAT(4H S= ,F8.4)
45*  CALL MOVE(0,1200)
46*  CALL ORIGIN(200,0)
47*  CALL MOVE(IFIX(S),0)

```

```

48* DO 200 I=2,36
49* 200 CALL DRAW(IFIX(S*X(I)),IFIX(S*Y(I)))
50* CALL MOVE(0,0)
51* CALL DRAW(IFIX(600*COS(ALF)),IFIX(600*SIN(ALF)))
52* CALL MOVE(0,0)
53* CALL DRAW(1600,0)
54* CALL MOVE(1250,0)
55*
56* CALL CENCH(7)
57* CALL MOVE(1260,10)
58* CALL WAY(0,5)
59* WRITE(9,50)
60* 50 FORMAT(14HSHIP DIRECTION)
61* CALL MOVE(1260,-30)
62* WRITE(9,51)GAM
63* 51 FORMAT(6HGAMMA=,F5.2)
64* CALL MOVE(1260,-70)
65* WRITE(9,52)ALFA
66* 52 FORMAT(5HALFA=,F5.1 )
67* 102 CALL MOVE(0,0)
68* STOP
69* END

```

```

CODELENGTH 575 WORDS
LOCAL WKSPACE 63 WORDS
DYN, ARRAYS 148 WORDS
DATA 0 WORDS

```

LABEL	ADDRESS		LABEL	ADDRESS		LABEL	ADDRESS
20	12	**	12	39	**	21	42
30	292	**	101	345	**	100	347
24	364	**	200	388	**	50	472
52	496	**	102	499	**		

---

JOBS/R104/F2

OPTIONS:

FORTRAN:

F2

LIST:

```

1*   DIMENSION BETA1(72),BETA2(72),CHI(72),X1(72),X2(72),Y1(72),Y2(72)
2*   READ(7,70)R01,R02,BE,CUR,ALFA
3*   70 FORMAT(5F12.6)
4*   WRITE(2,20)R01,R02,BE,CUR,ALFA
5*   20 FORMAT(1X,4H R01=,F12.6,6H R02=,F12.6,11H MAG FIELD,F12.6,10H CU
6*   1RRENT=,F12.6,16H SURFACE TENSION=,F12.6)
7* C DENSITY IN S.G. UNITS,MAG FIELD IN W/SO.M.,CURRENT IN MILLIA/SO.CM,
8* C SURFACE TENSION IN N.K.S.,VELOCITY IN M/S, ANGLES IN RADIANS
9* C CURRENT NEGATIVE = UPWARD FORCE
10*   PI=3.14159
11*   G=9.81
12*   AF=(R02-R01)*G/(R01+R02)
13*   B=(CUR*BE)/(100.0*(R01+R02))
14*   C=ALFA/(1000.0*(R01+R02))
15*   READ(7,71)UD,ALFIE
16*   71 FORMAT(2F12.6)
17*   DO 103 IU=1,3
18*   IF(IU.EQ.1)U=UD/5.0
19*   IF(IU.EQ.2)U=UD
20*   IF(IU.EQ.3)U=UD*5.0
21*   DO 104 IAN=1,7
22*   ALF=ALFIE*(IAN-1)
23*   ALFD=ALF*180.0/PI
24*   WRITE(2,21)U,ALFD
25*   21 FORMAT(1X,9HVELOCITY=,F12.6,20H ANGLE TO MAG FIELD=,F12.6)
26*   WRITE(2,24)
27*   24 FORMAT(55H      CHI          BETA 1          BETA 2          AK=      BK)
28*   NB=1
29*   NE=0
30*   SCM?=0
31*   SCH1=0
32*   DO 100 I=1,72
33*   CHI(I)=(I-1)*PI/72.0
34*   S=SIN(CHI(I)+ALF)*SIN(CHI(I)+ALF)
35*   B2=U*U*U*U*SIN(CHI(I))*SIN(CHI(I))*SIN(CHI(I))*SIN(CHI(I))
36*   IF(72.LT.(4*(A+B*S)*C)) GO TO 101
37*   AK=(U*U*SIN(CHI(I))*SIN(CHI(I))+SQRT(B2-4*(A+B*S)*C))/(2*C)
38*   BK=(U*U*SIN(CHI(I))*SIN(CHI(I))-SQRT(B2-4*(A+B*S)*C))/(2*C)
39*   ART=SQRT(A/AK+B*S/AK+C*AK)
40*   BRT=SQRT(A/BK+B*S/BK+C*BK)
41*   AD=(A/AK+B*S/AK-C*AK)/(2.0*ART*(U*COS(CHI(I))-B*SIN(2*(CHI(I)+ALF)
42*   1)/(AK*2.0*ART)))
43*   BD=(A/BK+B*S/BK-C*BK)/(2.0*BRT*(U*COS(CHI(I))-B*SIN(2*(CHI(I)+ALF)
44*   1)/(BK*2.0*BRT)))
45*   ADD=ATAN(AD)
46*   BDD=ATAN(BD)
47*   IF(ADD.GT.0.0)ADD=ADD-PI
    
```

```

48*      IF(NDB.LT.0.0)BDD=BDD+PI
49*      BETA1(I)=CHI(I)-ADD
50*      BETA2(I)=CHI(I)-BDD
51*      CHID=CHI(I)*180.0/PI
52*      BETD1=BETA1(I)*180.0/PI
53*      BETD2=BETA2(I)*180.0/PI
54*      IF(NB.EQ.0)X1(I)=1.0
55*      IF(NB.EQ.0)X2(I)=1.0
56*      IF(NB.EQ.0)GO TO 300
57*      AV=(CHI(I)+CHI(I-1))/2.0
58*      X1(I)=(Y1(I-1)-X1(I-1)*SIN(AV)/COS(AV))/(SIN(BETA1(I))/COS(BETA1(I
59*      1))-SIN(AV)/COS(AV))
60*      X2(I)=(Y2(I-1)-X2(I-1)*SIN(AV)/COS(AV))/(SIN(BETA2(I))/COS(BETA2(I
61*      1))-SIN(AV)/COS(AV))
62* 300  Y1(I)=X1(I)*SIN(BETA1(I))/COS(BETA1(I))
63*      Y2(I)=X2(I)*SIN(BETA2(I))/COS(BETA2(I))
64*      IF(NB.EQ.0)NB=I
65*      NE=I
66*      IF(3CM1.LT.ABS(X1(I)))SCM1=ABS(X1(I))
67*      IF(3CM1.LT.ABS(Y1(I)))SCM1=ABS(Y1(I))
68*      IF(3CM2.LT.ABS(X2(I)))SCM2=ABS(X2(I))
69*      IF(3CM2.LT.ABS(Y2(I)))SCM2=ABS(Y2(I))
70*      GO TO 102
71* 101  WRITE(2,23)CHI(I)
72* 23  FORMAT(F12.6,12)NOT POSSIBLE)
73*      GO TO 100
74* 102  WRITE(2,22)CHI(I),BETA1(I),BETA2(I),AK,BK,CHID,BETD1,BETD2
75* 22  FORMAT(5F12.4,10X,3F12.5)
76*      WRITE(2,25)X1(I),Y1(I),X2(I),Y2(I)
77* 25  FORMAT(1X,2F12.2,10X,2F12.5)
78* 100  CONTINUE
79*      IF(NB.EQ.0)GO TO 104
80*      SC1=600.0/SCM1
81*      SC2=600.0/SCM2
82*      CALL ORIGIN(1200,0)
83*      CALL MOVE(-1200,0)
84*      CALL WAY(0,6)
85*      WRITE(9,90)R01,P02,CUR,ALFA
86* 90  FORMAT(1X,F5.3,1X,F5.3,1X,F6.1,1X,F5.3)
87*      CALL MOVE(-1200,-100)
88*      WRITE(9,91)U,ALFD
89* 91  FORMAT(1X,F7.4,1X,F5.1)
90*      CALL MOVE(IFIX(X1(NB)*SC1),IFIX(Y1(NB)*SC1))
91*      DO 301 I=NB,NE
92* 301  CALL DRAW(IFIX(X1(I)*SC1),IFIX(Y1(I)*SC1))
93*      CALL MOVE(IFIX(X2(NB)*SC2),IFIX(Y2(NB)*SC2))
94*      DO 302 I=NB,NE
95* 302  CALL DRAW(IFIX(X2(I)*SC2),IFIX(Y2(I)*SC2))
96*      CALL MOVE(0,0)
97*      CALL CENCH(1)
98*      CALL MOVE(0,1000)
99* 104  CONTINUE
100* 103  CONTINUE
101*      STOP
102*      END

```

```

CODELENGTH 289  WORDS
LOCAL HRSPACE 103  WORDS
DYN. ARRAYS 1008  WORDS

```

&JOB:ES/R104/G2

SWOP

OPTIONS:

REPORTS:

G 2

LIST:

RTIME:40

1\* FETCH ROOTS,3

```

2*   DIMENSION EGA(10,21),WK(10,21),X(10,21),Y(10,21),Z1(5),Z2(5),
3*   IB(6),BC(6),BI(6),PR(5),PT(5),EGA1(10,21),WK1(10,21),X1(10,21),
4*   Y1(10,21),WK2(10,21),EGA2(10,21),X2(10,21),Y2(10,21),KD(10,21)
5* C THIS PROGRAMME PLOTS LINES OF CONSTANT PHASE IN THE INITIAL VALUE
6* C PROBLEM
7*   READ(7,70)RO1,RO2,ALFA,CUR,BE,T
8*   70 FORMAT(6F10,4)
9* C RO IN G.G. UNITS, CUR IN MILLIAMPS/SQ. CM., OTHERS IN MKS
10*  WRITE(2,20)RO1,RO2,ALFA,CUR,BE,T
11*  20 FORMAT(6F10,4)
12*  PI=3.14159
13*  GAM=10.0*CUR*BE
14*  G=9.81
15*  GIM=G*(RO2-RO1)*1000.0
16*  DS=(RO2+RO1)*1000.0
17*  DO 100 I=1,10
18*  PHAS=PI*I
19*  WRITE(2,24)PHAS
20*  24 FORMAT(6HPHASE=,F10,5)
21*  WRITE(2,25)
22*  25 FORMAT(1X,10BTHETA NO, FREQ 1 W/NO,1 X1 Y1 FREQ,2 W/
23*  1VE NO,2 X2 Y2 FREQ,3 WAVE NO,3 X3 Y3)
24*  DO 101 J=1,21
25*  X(I,J)=0
26*  X1(I,J)=0
27*  X2(I,J)=0
28*  Y(I,J)=0
29*  Y1(I,J)=0
30*  Y2(I,J)=0
31*  THE=(J-1)*PI/40,0
32*  N=5
33*  B(6)=T*T*ALFA*ALFA/DS
34*  B(5)=0
35*  B(4)=-2*T*T*ALFA*(GIM+GAM*COS(THE)*COS(THE))/DS
36*  B(3)=-4*PHAS*PHAS*ALFA
37*  B(2)=T*T*(GIM+GAM*COS(THE)*COS(THE))*2/DS
38*  B(1)=-4*PHAS*PHAS*(GIM+GAM*COS(THE)*COS(THE))
39*  MAXIT=100
40*  CALL ROOTS(N,B,MAXIT,Z1,Z2,PR,PT,BC,BI,NEND,EPS,NSW)

```

```

41* IF (ISW.EQ.2)WRITE(2,26)
42* 26 FORMAT(14HNOT CONVERGING)
43* KN=1
44* WK(I,J)=0
45* WK1(I,J)=0
46* WK2(I,J)=0
47* DO 102 K=1,NFND
48* IF(Z2(K).NE.0,0)GO TO 102
49* IF(Z1(K).LE.0,0)GO TO 102
50* IF(KN.EQ.0)WK(I,J)=Z1(K)
51* IF(KN.EQ.1)WK1(I,J)=Z1(K)
52* IF(KN.EQ.2)WK2(I,J)=Z1(K)
53* KN=KN+1
54* 102 CONTINUE
55* IF((KN.EQ.0).OR.(KN.GT.3))WRITE(2,21)I,J,K,KN
56* 21 FORMAT(17HURONG NO OF ROOTS,4I3)
57* KD(I,J)=0
58* IF(KM.NE.KN)KD(I,J)=1
59* KM=KN
60* IF(KN.EQ.0)GO TO 101
61* IF(WK(I,J).EQ.0,0)GO TO 113
62* EGA(I,J)=(GIM*WK(I,J)+GAM*WK(I,J)*COS(THI)*COS(THI)+ALFA*WK(I,J)*
63* 13.0)/DS
64* X(I,J)=T*(GIM*COS(THI)+2*GAM*COS(THI)-GAM*COS(THI)**3+3*ALFA*COS(
65* 1THI)*WK(I,J)*WK(I,J))/(2*EGA(I,J)*DS)
66* Y(I,J)=T*(GIM*SIN(THI)-GAM*COS(THI)*COS(THI)*SIN(THI)+3*ALFA*SIN(
67* 1THI)*WK(I,J)*WK(I,J))/(2*EGA(I,J)*DS)
68* 113 IF(WK1(I,J).EQ.0,0)GO TO 114
69* EGA1(I,J)=(GIM*WK1(I,J)+GAM*WK1(I,J)*COS(THI)*COS(THI)+ALFA*WK1(I
70* 1J)**3.0)/DS
71* X1(I,J)=T*(GIM*COS(THI)+2*GAM*COS(THI)-GAM*COS(THI)**3+3*ALFA*COS
72* 1THI)*WK1(I,J)*WK1(I,J))/(2*EGA1(I,J)*DS)
73* Y1(I,J)=T*(GIM*SIN(THI)-GAM*COS(THI)*COS(THI)*SIN(THI)+3*ALFA*SIN
74* 1THI)*WK1(I,J)*WK1(I,J))/(2*EGA1(I,J)*DS)
75* 114 IF(WK2(I,J).EQ.0,0)GO TO 115
76* EGA2(I,J)=(GIM*WK2(I,J)+GAM*WK2(I,J)*COS(THI)*COS(THI)+ALFA*WK2(I
77* 1J)**3.0)/DS
78* X2(I,J)=T*(GIM*COS(THI)+2*GAM*COS(THI)-GAM*COS(THI)**3+3*ALFA*COS
79* 1THI)*WK2(I,J)*WK2(I,J))/(2*EGA2(I,J)*DS)
80* Y2(I,J)=T*(GIM*SIN(THI)-GAM*COS(THI)*COS(THI)*SIN(THI)+3*ALFA*SIN
81* 1THI)*WK2(I,J)*WK2(I,J))/(2*EGA2(I,J)*DS)
82* 115 IF(WK(I,J).EQ.0,0)WRITE(2,23)THE,KN
83* IF(WK(I,J).EQ.0,0)GO TO 116
84* WRITE(2,27)THE,KN,EGA(I,J),WK(I,J),X(I,J),Y(I,J)
85* 116 IF(WK1(I,J).NE.0,0)WRITE(2,28)EGA1(I,J),WK1(I,J),X1(I,J),Y1(I,J)
86* IF(WK2(I,J).NE.0,0)WRITE(2,29)EGA2(I,J),WK2(I,J),X2(I,J),Y2(I,J)
87* 23 FORMAT(1X,F6.4,I2)
88* 27 FORMAT(1X,F6.4,I2,F9.3,F7.2,2F9.4)
89* 28 FORMAT(42X,F9.3,F7.2,2F9.4)
90* 29 FORMAT(75X,F9.3,F7.2,2F9.4)
91* 101 CONTINUE
92* 100 CONTINUE
93* CALL ORIGIN(500,0)
94* CALL DRAW(0,3000)
95* CALL MOVE(0,2000)
96* CALL DRAW(1000,2000)
97* CALL MOVE(1000,1000)
98* CALL DRAW(0,1000)
99* CALL MOVE(0,0)
100* CALL DRAW(1000,0)

```

```

101*      IAN=0
102*      DO 107 I=1,10
103*      DO 106 J=1,20
104*      IF((IK(I,J).EQ.0,0)GO TO 106
105*      AX=X(I,J)
106*      AY=Y(I,J)
107*      IF(SQRT(AX*AX+AY*AY).LT.0.001)GO TO 104
108*      IF(SQRT(AX*AX+AY*AY).LT.0.01)GO TO 105
109*      IF(SQRT(AX*AX+AY*AY).GT.1.00)GO TO 106
110*      IF((J.EQ.1).OR.(KD(I,J).EQ.1).OR.(IAN.NE.1))GO TO 103
111*      IAN=1
112*      CALL DRAW(IFIX(AX*1000),(2000+IFIX(AY*1000)))
113*      GO TO 106
114*      103 CALL MOVE(IFIX(AX*1000),(2000+IFIX(AY*1000)))
115*      IAN=1
116*      GO TO 106
117*      105 IF((J.EQ.1).OR.(KD(I,J).EQ.1).OR.(IAN.NE.2))GO TO 108
118*      IAN=2
119*      CALL DRAW(IFIX(AX*100000),(1000+IFIX(AY*100000)))
120*      GO TO 106
121*      108 CALL MOVE(IFIX(AX*100000),(1000+IFIX(AY*100000)))
122*      IAN=2
123*      GO TO 106
124*      104 IF((J.EQ.1).OR.(KD(I,J).EQ.1).OR.(IAN.NE.3))GO TO 109
125*      IAN=3
126*      CALL DRAW(IFIX(AX*1000000),IFIX(AY*1000000))
127*      GO TO 106
128*      109 CALL MOVE(IFIX(AX*1000000),IFIX(AY*1000000))
129*      IAN=3
130*      106 CONTINUE
131*      DO 136 J=1,20
132*      IF((IK1(I,J).EQ.0,0)GO TO 136
133*      AX=X1(I,J)
134*      AY=Y1(I,J)
135*      IF(SQRT(AX*AX+AY*AY).LT.0.001)GO TO 134
136*      IF(SQRT(AX*AX+AY*AY).LT.0.01)GO TO 135
137*      IF(SQRT(AX*AX+AY*AY).GT.1.0)GO TO 136
138*      IF((J.EQ.1).OR.(KD(I,J).EQ.1).OR.(IAN.NE.1))GO TO 133
139*      IAN=1
140*      CALL DRAW(IFIX(AX*1000),(2000+IFIX(AY*1000)))
141*      GO TO 136
142*      133 CALL MOVE(IFIX(AX*1000),(2000+IFIX(AY*1000)))
143*      IAN=1
144*      GO TO 136
145*      135 IF((J.EQ.1).OR.(KD(I,J).EQ.1).OR.(IAN.NE.2))GO TO 138
146*      IAN=2
147*      CALL DRAW(IFIX(AX*100000),(1000+IFIX(AY*100000)))
148*      GO TO 136
149*      138 CALL MOVE(IFIX(AX*100000),(1000+IFIX(AY*100000)))
150*      IAN=2
151*      GO TO 136
152*      134 IF((J.EQ.1).OR.(KD(I,J).EQ.1).OR.(IAN.NE.3))GO TO 139
153*      IAN=3
154*      CALL DRAW(IFIX(AX*1000000),IFIX(AY*1000000))
155*      GO TO 136
156*      139 CALL MOVE(IFIX(AX*1000000),IFIX(AY*1000000))
157*      IAN=3
158*      136 CONTINUE
159*      DO 146 J=1,20
160*      IF((IK2(I,J).EQ.0,0)GO TO 146

```

```

161*      AX=Y2(I,J)
162*      AY=Y2(I,J)
163*      IF(BORT(AX*AX+AY*AY),LT,0,001)GO TO 144
164*      IF(BORT(AX*AX+AY*AY),LT,0,01)GO TO 145
165*      IF(BORT(AX*AX+AY*AY),GT,1,0)GO TO 146
166*      IF((J,EQ,1).OR.(KD(I,J),EQ,1).OR.(IAN,NE,1))GO TO 143
167*      IAN=1
168*      CALL DRAW(IFIX(AX*1000),(2000+IFIX(AY*1000)))
169*      GO TO 146
170*  143 CALL MOVE(IFIX(AX*1000),(2000+IFIX(AY*1000)))
171*      IAN=1
172*      GO TO 146
173*  145 IF((J,EQ,1).OR.(KD(I,J),EQ,1).OR.(IAN,NE,2))GO TO 148
174*      IAN=2
175*      CALL DRAW(IFIX(AX*100000),(1000+IFIX(AY*100000)))
176*      GO TO 146
177*  148 CALL MOVE(IFIX(AX*100000),(1000+IFIX(AY*100000)))
178*      IAN=2
179*      GO TO 146
180*  144 IF((J,EQ,1).OR.(KD(I,J),EQ,1).OR.(IAN,NE,3))GO TO 149
181*      IAN=3
182*      CALL DRAW(IFIX(AX*1000000),IFIX(AY*1000000))
183*      GO TO 146
184*  149 CALL MOVE(IFIX(AX*1000000),IFIX(AY*1000000))
185*      IAN=3
186*  146 CONTINUE
187*  107 CONTINUE
188*      STOP
189*      END

```

```

CODELENGTH 1951 WORDS
LOCAL WKSPCE 83 WORDS
DYN; ARRAYS 5326 WORDS
DATA 0 WORDS

```

LABEL	ADDRESS	**	LABEL	ADDRESS	**	LABEL	ADDRESS
70	48	**	20	54	**	24	83
26	289	**	102	405	**	21	428
114	838	**	115	1027	**	116	1060
27	1091	**	28	1098	**	29	1101
100	1107	**	103	1285	**	105	1301
104	1361	**	109	1404	**	106	1418
135	1559	**	138	1602	**	134	1618
130	1679	**	143	1799	**	145	1615
144	1877	**	149	1918	**	146	1932
		**			**		